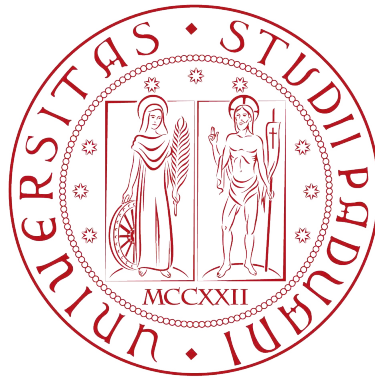


UNIVERSITÀ DEGLI STUDI DI PADOVA

DEPARTMENT OF MATHEMATICS "TULLIO LEVI-CIVITA"
DOCTORAL PROGRAM IN MATHEMATICS
CURRICULUM: COMPUTATIONAL MATHEMATICS
(COHORT XXXV)



PH.D. THESIS

**Close approaches and the border of stable secular
motions in the Restricted 3-Body Problem**

Coordinator:

Prof. Giovanni Colombo

Supervisor:

Prof. Christos Efthymiopoulos

Candidate:

Mattia Rossi

ACADEMIC YEAR 2021-2022

To my loved ones

Pure mathematics and physics are becoming ever more closely connected, though their methods remain different. One may describe the situation by saying that the mathematician plays a game in which he himself invents the rules while the physicist plays a game in which the rules are provided by Nature, but as time goes on it becomes increasingly evident that the rules which the mathematician finds interesting are the same as those which Nature has chosen. It is difficult to predict what the result of all this will be. Possibly, the two subjects will ultimately unify, every branch of pure mathematics then having its physical application, its importance in physics being proportional to its interest in mathematics.

Paul Adrien Maurice Dirac

The Relation between Mathematics and Physics

ABSTRACT

The central goal of the present thesis consists in proposing a novel threshold, in the context of the restricted three-body problem, capable to discriminate between the regime of motion governed by the classic secular theory and the rest of regimes, which are mainly influenced either by close encounters or by resonant interactions of the test particle (e.g. asteroid) with the primary perturber (e.g. Jupiter). This goal is reached operating on the following fronts:

i) We explore at the beginning the possibility to take into account suitable regularization methods in the vicinity of the gravitational singularities: we introduce a Hamiltonian extension of the Kustaanheimo-Stiefel regularization to the elliptic restricted N -body problem by means of a symplectic reduction of the extended phase space. After a short review of the state of the art on regularization techniques, we develop the theory for $N = 3$ and test it numerically. In particular, we provide an implementation of the theory in the propagation of the orbits having close encounters with the primary perturber. This is shown to usefully improve the performance of numerical integrations when needed, regardless the complexity of the three-body model considered (planar/spatial, circular/elliptic).

ii) We pass to the machinery of Hamiltonian canonical perturbation theory and present a closed-form approach (i.e. without expanding in powers of the eccentricities) without use of relegation for particles with non-crossing trajectories exterior to the primary perturber's trajectory, including those highly eccentric.

iii) At this point, we address the question of identifying and topologically characterizing the long-term (secular) stability regions in appropriate sections of the phase space via different numerical stability maps. We discuss, then, the applicability of the above closed-form method as a criterion for estimating the boundary of such domains for orbits further than Jupiter's when the planet is assumed on a circular orbit and compare the result to other existent heuristic criteria.

iv) As a side result from the above analysis, the aforementioned stability maps reveal a much richer orbital architecture consisting in an "ornamental

structure" of manifolds generated by the planet connected in a series of arches that spread throughout the whole Solar System. We then investigate the implications of these structures for small body dynamics. As a pivotal case, we consider the well-known open problem of the observed asymmetry in the number and phase-space distribution of Trojan asteroids around Jupiter's equilateral equilibrium points L_4 and L_5 in our solar system. We discuss possible links of this problem to a detected asymmetry in the heteroclinic intersections between the unstable and stable manifolds of the Lyapunov orbits around the Lagrangian points L_1 , L_2 and L_3 . We show how these intersections influence the inflow of particles to the Trojan region, and propose a plausible trapping mechanism of the bodies under an approximately adiabatic process of planetary migration.

SOMMARIO

Lo scopo principale della presente tesi consiste nel proporre, nell'ambito del problema dei tre corpi ristretto, una nuova definizione del limite che discrimina tra il regime di moto governato dalla teoria secolare classica e gli altri tipi di regime, in cui questi ultimi risultano essenzialmente influenzati o dalla presenza di incontri ravvicinati o da interazioni risonanti della particella di massa trascurabile (p.e. un asteroide) con il perturbatore primario (p.e. Giove). Tale obiettivo viene raggiunto operando sui seguenti fronti:

i) Esploriamo all'inizio la possibilità di tenere conto di opportuni metodi di regolarizzazione in prossimità delle singolarità gravitazionali: si introduce così un'estensione hamiltoniana della regolarizzazione di Kustaanheimo-Stiefel al problema ellittico ristretto degli N corpi mediante una riduzione simplettica dello spazio delle fasi esteso. Dopo una breve rassegna dello stato dell'arte sulle tecniche di regolarizzazione, la teoria viene sviluppata per $N = 3$ e testata numericamente. In particolare forniamo un'implementazione della teoria nella propagazione di orbite aventi incontri ravvicinati con il perturbatore primario. Tale implementazione si dimostra migliorativa in termini di accuratezza delle prestazioni numeriche durante l'integrazione laddove necessario, indipendentemente dalla complessità del modello a tre corpi considerato (piano/spaziale, circolare/ellittico).

ii) Passiamo ora al contesto della teoria perturbativa canonica hamiltoniana e presentiamo un approccio in forma chiusa (cioè senza espandere nelle potenze delle eccentricità) senza l'uso dell'algoritmo di "relegation" per particelle con traiettorie non intersecanti esterne alla traiettoria del perturbatore primario, comprese quelle altamente eccentriche.

iii) A questo punto ci si prefigge di identificare e caratterizzare topologicamente le regioni di stabilità a lungo termine (secolari) in sezioni appropriate dello spazio delle fasi tramite diverse mappe di stabilità numerica. Discutiamo l'applicabilità del metodo come criterio per stimare la frontiera dei suddetti domini per orbite lontane da quella di Giove quando il pianeta è assunto in orbita circolare e confrontiamo il risultato con altri criteri euristici esistenti.

iv) In qualità di risultato complementare, le suddette mappe di stabilità

rivelano un'architettura orbitale assai più ricca costituita da una "struttura ornamentale" di varietà generate dal pianeta e collegate in una serie di archi che si estendono per l'intero Sistema Solare. Indaghiamo così le implicazioni di queste strutture riguardo alla dinamica dei corpi minori. Come caso di riferimento consideriamo il noto problema aperto nel nostro sistema solare relativo all'asimmetria osservata nel numero e nella distribuzione nello spazio delle fasi degli asteroidi troiani attorno ai punti di equilibrio equilateri di Giove L_4 ed L_5 . Si discutono i possibili collegamenti di questo fenomeno con un'asimmetria rilevata che interessa le intersezioni eterocline tra le varietà stabili e instabili delle orbite periodiche di Lyapunov attorno ai punti lagrangiani L_1 , L_2 ed L_3 . Mostriamo come tali intersezioni influenzino il flusso di particelle nella regione troiana e proponiamo un meccanismo plausibile di intrappolamento dei corpi in presenza di un processo di migrazione planetaria approssimativamente adiabatico.

CONTENTS

1	Introduction	1
1.1	Non-linear dynamical systems	1
1.1.1	General definitions	1
1.1.2	Non-integrability and chaotic systems	3
1.1.3	Poincaré maps and spectral stability of periodic orbits	4
1.1.4	Hyperbolic dynamics	6
1.2	Hamiltonian dynamical systems	11
1.2.1	Hamilton's equations of motion	11
1.2.2	Conservation properties of Hamiltonian systems	12
1.2.3	Canonical transformations	12
1.2.4	Action-angle variables and Liouville-Arnold theorem	15
1.2.5	Perturbations of integrable systems	17
1.3	The N -body problem	21
1.3.1	Kepler's problem	21
1.3.2	The planetary N -body problem	25
1.3.3	The restricted three-body problem	26
1.4	Goal and structure of the thesis	35
2	Hamiltonian regularization theory in the restricted three-body problem	39
2.1	The nature of the singularities in the N -body problem	39
2.2	Motivations	41
2.3	Kustaanheimo-Stiefel regularization of the elliptic restricted three-body problem	42
2.3.1	Formulation in the rotating-pulsating frame	42
2.3.2	The space of redundant variables	43
2.3.3	The modified Lagrangian	47
2.3.4	Rotational invariance of the modified Lagrangian	48
2.3.5	The regularized Hamiltonian	50
2.3.6	Projection of the solutions of the regularized Hamiltonian	51
2.3.7	Implementation procedure	55

2.3.8	The advantage of the regularization: a numerical test . . .	56
3	Closed-form perturbation theory for external orbits in the restricted three-body problem without relegation	63
3.1	Introduction	63
3.2	The closed-form method for the outermost R3BP	68
3.2.1	Multipole expansion of the perturbation	68
3.2.2	Canonical form of the Hamiltonian	68
3.2.3	Poisson structure and book-keeping	71
3.2.4	Iterative normalization algorithm	76
3.3	Numerical tests	88
3.3.1	Computer-algebraic implementation of the normalization algorithm	88
3.3.2	Semi-analytic orbit propagations in the Sun-Jupiter R3BP	90
4	Numerical detection of the secular stability domain in the Sun-Jupiter system	97
4.1	State of the art on stability analysis and purposes	97
4.2	Preliminaries on chaos indicators	100
4.2.1	Variational dynamics	100
4.2.2	Finite time chaos indicators	101
4.3	FLI cartographies of the Sun-Jupiter planar CR3BP	102
4.3.1	The semi-major axis's maximum variation indicator . . .	104
4.4	Semi-analytical determination of the domain of secular motions	108
4.4.1	Order and size of the optimal remainder in the planar CR3BP	108
4.4.2	Semi-analytical determination of the domain of secular motions	110
5	Manifolds in the Solar System: an application to the L_4/L_5 asymmetry of Trojan asteroids	115
5.1	On Trojan asteroids and the asymmetry problem	115
5.2	Heteroclinic dynamics at co-orbital resonance	118
5.2.1	On the computation of invariant manifolds	118
5.2.2	The stable manifold of PL_3	122
5.2.3	The asymmetric distribution of heteroclinic intersections	124
5.3	Non-stationary case: Jupiter's migration	126
5.3.1	Extension of the model	126
5.3.2	Trapping of particles at L_4/L_5	130
6	Summary of new results and perspectives	133
A	Derivation of the f-dependent elliptic restricted three-body problem Hamiltonian in the rotating-pulsating frame	137
A.1	Time-dependent Lagrangian	138
A.2	The true anomaly as independent variable	142

B	Disturbing function for external orbits in the restricted three-body problem in terms of the orbital elements	145
C	Computation of Poisson bracket's intermediate derivatives	147
D	Example of normalization for a μ^2 quadrupole expansion	149
E	Normalization algorithm as pseudo-code	155
	Bibliography	159
	Acknowledgements	167

LIST OF FIGURES

1.1	Example of Poincaré surface of section	4
1.2	Dynamics originating at hyperbolic equilibria	10
1.3	Foliation of invariant tori for $n = 2$	16
1.4	Elliptical orbit and its geometric parameters	23
1.5	Orbit of the 2BP in 3D	23
1.6	The co-rotating synodic reference frame	28
1.7	Tisserand’s parameters for a Jupiter-family comet	29
1.8	Zero-velocity surfaces of the spatial CR3BP	30
1.9	Lagrangian points of the CR3BP and zero-velocity curves in the planar case	32
1.10	Types of orbits in the planar CR3BP	36
2.1	Physical orbit in the Sun-Jupiter ER3BP integrated backward and forward in true anomaly	58
2.2	Projections on the coordinate planes of the right bottom panel of Fig. 2.1	59
2.3	Convergence profile of the error decay in the bilinear form preser- vation in Fig. 2.1	60
3.1	Representation of the R3BP in the barycentric frame (or equiva- lently in Jacobi variables) with $\ R\ > \ r_1\ $	69
3.2	First example (ER3BP) of semi-analytic vs. direct Cartesian prop- agation	91
3.3	Second example (ER3BP) of semi-analytic vs. direct Cartesian propagation	92
3.4	Third example (ER3BP) of semi-analytic vs. direct Cartesian propagation	93
3.5	Fourth example (planar CR3BP) of semi-analytic vs. direct Carte- sian propagation	94
3.6	Fifth example (planar CR3BP) of semi-analytic vs. direct Carte- sian propagation	94

3.7	Sixth example (planar CR3BP) of semi-analytic vs. direct Cartesian propagation	95
4.1	Short-period ($\tau = 50T_J$) FLI cartographies of the Sun-Jupiter system	104
4.2	Long-period ($\tau = 1000T_J$) FLI cartography of the Sun-Jupiter system and binary plot for the semi-major axis' criterion	106
4.3	Comparison as in bottom panel of Fig. 4.2 on a larger region of the long-time FLI map.	107
4.4	Histograms of the break-up times and corresponding distances for the binary plot in Fig. 4.2	107
4.5	Trend of the size of the remainder for the three examples in the planar CR3BP of §3.3.2	109
4.6	Size of the remainder vs. short-period FLI map for the Sun-Jupiter planar CR3BP in the semi-plane $a/a_J > 1$	112
5.1	Distribution of Trojans and their inclinations in the L_4/L_5 swarms	117
5.2	Pericentric Poincaré sections of the Sun-Jupiter planar CR3BP for increasing value of the Jacobi integral	120
5.3	Characteristic curves of PL_3 as functions of the Jacobi integral .	123
5.4	Representations of $W^s(PL_3)$ in the Sun-Jupiter-asteroid system on the (φ_1, I_1) and (a, e) planes.	123
5.5	Poincaré section of the heteroclinic connections between $W^s(PL_3)$ and $W^u(PL_1), W^u(PL_2)$ in the surroundings of L_4/L_5	124
5.6	Poincaré map iterations of a neighborhood of PL_2 in a higher energetic section than the one of Fig. 5.5	127
5.7	Continuation of the Poincaré map iterations of Fig. 5.6	128
5.8	Poincaré section as in Fig. 5.6-5.7 for initial data close and transverse to $W^s(PL_2)$	129
5.9	Sketch of the Trojan dynamics during the giant planets' migration phase	129
5.10	Illustration of a hypothetical proposed trapping mechanism in the Trojan regions	131
5.11	Temporary number of bodies inside the L_4/L_5 resonant-like domain during Jupiter's migration	132

INTRODUCTION

This thesis is devoted to the inspection of different regimes of motion in the so-called *restricted three-body problem* (R3BP), a widely studied model in the framework of the gravitational N -body problem in celestial mechanics. The applications of such model are countless: in our case, for example, the minor body typically represents an asteroid (or minor planet) orbiting either in the outer reaches of the Solar System, like the trans-Neptunian ones, or in a neighborhood of Jupiter. In extrasolar planetary systems, the model describes the motion of a small planet under the gravitational influence of a star and of another giant planet in the same system.

By its very nature, the topic is advantageously contextualized in the environment of the Hamiltonian dynamical systems theory (H. Poincaré, [86]), whose formalism is founded on the use of a special class of infinitely differentiable transformations, called canonical or symplectic. These diffeomorphisms allow to carry out perturbative treatments in a convenient way, leading to formal series solutions to the equations of motion known in literature as the method of *Hamiltonian normal forms*.

Hamiltonian mechanics turns out to be the right setting for the study of the R3BP also because of its elegant symplectic geometric interpretation and adequacy in describing reversible dynamics: locally, Hamiltonian structures are equivalent to symplectic ones (Poincaré lemma) and physical properties, like energy conservation over time, are naturally embedded in the Hamiltonian formalism.

In this chapter we summarize some basic notions of the theory of dynamical systems as well as its Hamiltonian formulation, with emphasis on the N -body problem and on aspects particularly relevant to our study. Finally, we expose the structure and the goal of the present dissertation.

1.1 Non-linear dynamical systems

1.1.1 General definitions

Definition 1.1.1. A (smooth) dynamical system is a triple (G, M, Φ) s.t.:

- M is a smooth manifold called *phase space*;
- $G = \mathbb{R}$ (continuous time) or $G = \mathbb{Z}$ (discrete time);
- Φ is a free differentiable action of the group G on M .

Specifically, in the continuous case a dynamical system is represented by an ordinary differential equation of the form

$$\dot{x} = X(x), \quad x \in M, \quad (1.1)$$

where $X: M \rightarrow TM$ is a smooth vector field and $TM = \bigsqcup_{x \in M} T_x M$ denotes the tangent bundle of M ; the map $\Phi: \mathbb{R} \times M \rightarrow M$ is called the *flow* of X , such that $\Phi(t, x_0)$ denotes the value at current time t of the solution which at initial time $t = 0$ is equal to x_0 .

Likewise, it is also possible to consider phenomena evolving in discrete time, whose associated mathematical law, that is a function, is iteratively repeated. The resulting dynamical system is thus obtained by the relationship

$$x_n = \Psi^n(x_0), \quad x_0, x_n \in M, \quad n \in \mathbb{Z}, \quad (1.2)$$

where $\Psi: M \rightarrow M$ is a diffeomorphism and

$$\Psi^n = \begin{cases} \Psi \circ \dots \circ \Psi & n \text{ times, } n > 0 \\ \Psi^{-1} \circ \dots \circ \Psi^{-1} & |n| \text{ times, } n < 0 \end{cases}.$$

Analogously, we can define now $\Phi: \mathbb{Z} \times M \rightarrow M$ by setting $\Phi(n, x_0) := \Psi^n(x_0)$. Finally, we remind that Φ is a differentiable action in the sense that it satisfies the following properties:

- (i) $\Phi(0, \cdot) = \text{id}_M$;
- (ii) $x \mapsto \Phi(t, x)$ is a diffeomorphism $\forall t \in G$;
- (iii) $\Phi(t, \Phi(s, \cdot)) = \Phi(t + s, \cdot) \forall t, s \in G$.

For practical purposes, we work in local coordinates and shall assume from now on that $M = D \subseteq \mathbb{R}^d$ and mostly $G = \mathbb{R}$.

Definition 1.1.2. The *orbit* (or *integral curve*) of a point $x \in D$ is the set $\mathcal{O}_x = \{\Phi(t, x) : t \in \mathbb{R}\}$. The set of all orbits is called *phase portrait*.

Remark 1.1.1. Given $X \in C^\infty(D; \mathbb{R}^d)$, Cauchy theorem about the existence and uniqueness of the solution in a neighborhood of $t = 0$ to (1.1) with initial condition $x(0) = x_0$ holds. In addition, as already understood, we assume to extend this $\forall t \in \mathbb{R}$, so that the phase portrait forms a partition of D .

1.1.2 Non-integrability and chaotic systems

In general (1.1) is non-linear and the corresponding solutions cannot be provided easily. Usually it is not possible to find a global analytic formula accounting for all orbits, but not even local solutions valid in open domains of the phase space and given under, e.g., the form of convergent series in a small parameter.

These observations about the solvability of a system are encompassed by the notion of *non-integrability*. This roughly refers to the incapability of determining all the solutions explicitly, or characterizing them in terms of invariant objects embedded in the phase space. More specifically, we can give the following two broad definitions of integrability:

Operational: The solutions as functions of time can be expressed in terms of quadratures, that is simple arithmetic operations ($+$, $-$, \cdot , $:$), radicals ($\sqrt{\cdot}$) or integration and inversion of elementary functions ($\int \cdot$, \cdot^{-1}).

Geometric: There exists an embedded Φ -invariant foliation in the phase space (e.g. invariant tori in integrable Hamiltonian systems, see §1.2.4).

The second definition is intimately related to the existence of conserved quantities along the flow, that act as constraints for the orbits (Remark 1.1.2).

Definition 1.1.3. A *first integral* of $\dot{x} = X(x)$ is a smooth function $f: D \rightarrow \mathbb{R}$ which is constant on all the solutions of (1.1), i.e. $f(\Phi(t, x)) = f(x) \forall t \in \mathbb{R}$ and $x \in D$.

Remark 1.1.2. Every time we provide a first integral, the problem is reduced from dimension d to dimension $d - 1$. So if $\exists f_1, \dots, f_{d-1}$ independent first integrals, the level sets have dimension $d - (d - 1) = 1$, which are the orbits of the differential equation.

Non-integrability is a necessary condition for *chaos*.

Definition 1.1.4. We call a dynamical system **chaotic** [6] whenever

- (i) it is *topologically transitive*, namely $\forall U, V \subseteq D$ open, $\exists t \in \mathbb{R}$ s.t. $\Phi(t, U) \cap V \neq \emptyset$;
- (ii) it has a dense set of periodic orbits;
- (iii) it is sensitive to initial conditions.

Banks et al. in [6] proved that (iii) is redundant, that is the first two conditions (i) and (ii) imply the third one. However, it is precisely the picture that we practically bear in mind: depending on the rate of separation $\lambda > 0$ (Lipschitz constant), given initial conditions s.t. $\|x_1 - x_0\| < \varepsilon$, we have

$$\|\Phi(t, x_1) - \Phi(t, x_0)\| \leq e^{\lambda|t|} \|x_1 - x_0\| , \quad (1.3)$$

so in principle the dynamics becomes unpredictable for $|t|$ large enough. Then, we customarily associate chaos to the worst case: *exponential separation* in time of orbits of close initial data.

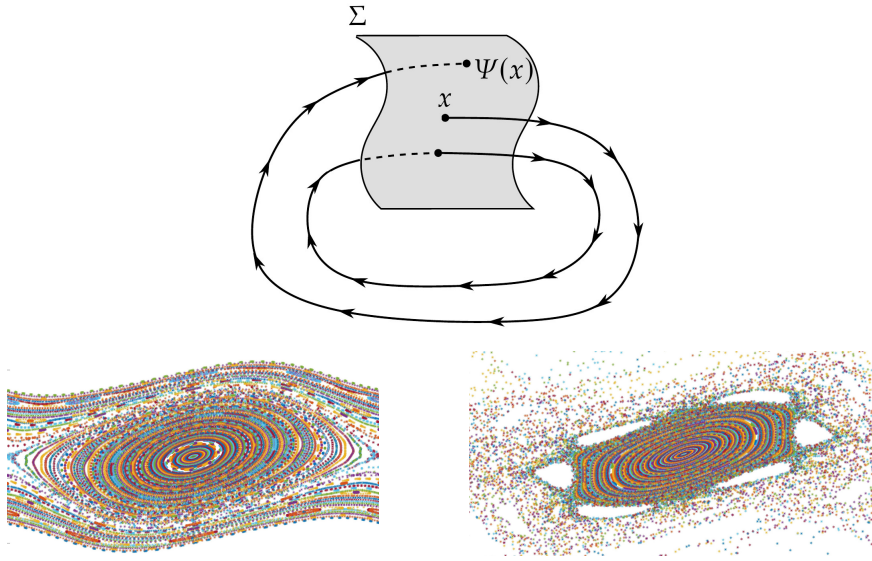


Figure 1.1: Example of Poincaré surface of section. **Top panel:** schematic illustration of the transversal intersection of Φ with Σ . **Bottom panels:** example of numerical computation for the classic (Chirikov–Taylor) standard map [15, 16], with Σ given by a coordinate plane, for two different values of the perturbing parameter; in the picture on the right we have more chaos, represented by apparently randomly distributed points, as opposed to regular motions leading to points distributed along closed invariant curves.

1.1.3 Poincaré maps and spectral stability of periodic orbits

An effective technique to explore the phase space of a dynamical system consists in reducing the study of the flow of the differential equation (1.1) to the study of the iterations of a discrete map, called *Poincaré map*, defined in a subspace of dimension $d - 1$, called accordingly *Poincaré section*. Poincaré sections are used, in particular, to visualize the complicated topology of non-integrable systems. Basically, we consider $\Sigma^{d-1} \subseteq D$: $\forall x \in \Sigma, \exists t(x)$ such that $\Phi(t(x), x) \in \Sigma$, returning always “on the same side” of Σ (Fig. 1.1); viz. $\bigcup_{x \in \Sigma} \mathcal{O}_x$ is replaced by $\bigcup_{n \in \mathbb{Z}} \Psi^n(x)$, where $\Psi(x) := \Phi(t(x), x)$.

Periodic orbits (i.e. $\exists T \neq 0: \Phi(t + T, x) = \Phi(t, x) \forall t \in \mathbb{R}$) appear as fixed points of Ψ . In particular, it is possible to map the analysis of local properties of stability of a periodic orbit to the stability of the corresponding fixed point in the Poincaré map.

Definition 1.1.5. A fixed point $\bar{x} \in D$ for (1.2) is said to be:

- *attractive* if there exists a neighborhood V of \bar{x} s.t. for all $x \in V$ $\lim_{n \rightarrow +\infty} \Phi(n, x) = \bar{x}$, whereas *repulsive* if $\lim_{n \rightarrow -\infty} \Phi(n, x) = \bar{x}$.
- (Lyapunov) *stable* if for every neighborhood U of \bar{x} there exists a neighborhood U_0 of \bar{x} s.t. $\Phi(n, U_0) \subseteq U \forall n \geq 0$.
- *asymptotically stable* if it is stable and attractive.
- (Lyapunov) *unstable* if it is not stable.

The same definitions apply straightforwardly to periodic orbits. We have the following.

Proposition 1.1.1. *A periodic orbit of a given flow is attractive (resp. Lyapunov stable, asymptotically stable, Lyapunov unstable) if and only if the corresponding fixed point of any associated Poincaré map is attractive (resp. Lyapunov stable, asymptotically stable, Lyapunov unstable).*

Proposition (1.1.1) states the equivalence claimed above. Such study is usually carried out by classic Lyapunov-Floquet's theory [29]:

Theorem 1.1.1 (LYAPUNOV'S SPECTRAL THEOREM). *Let \bar{x} be a fixed point of (1.2) and $D\Psi(\bar{x})$ the Jacobian matrix of Ψ computed at \bar{x} .*

- (i) *If all the eigenvalues of $D\Psi(\bar{x})$ have absolute value < 1 , then \bar{x} is asymptotically stable.*
- (ii) *If at least one eigenvalue of $D\Psi(\bar{x})$ has absolute value > 1 , then \bar{x} is Lyapunov unstable.*

At first glance this seems unpractical because in general an analytic expression for Ψ is not available. However, there is a way to calculate its linearization starting from the linearization of Φ , through the so-called monodromy matrix.

Definition 1.1.6. Let $\mathcal{O}_{\bar{x}}$ a periodic orbit of period $T \neq 0$. Then the Jacobian matrix $D\Phi(T, \bar{x})$ of the mapping $x \mapsto \Phi(t, x)$ at (T, \bar{x}) is called *monodromy matrix* of $\mathcal{O}_{\bar{x}}$ related to the point \bar{x} .

Since $D\Phi$ is supposed to fulfil the *variational equation*

$$\frac{d}{dt}D\Phi(t, x) = DX(\Phi(t, x))D\Phi(t, x), \quad (1.4)$$

in which $DX = \partial X / \partial x$, the monodromy matrix $D\Phi(T, \bar{x})$ is the solution of (1.4) at time T along the periodic orbit $\mathcal{O}_{\bar{x}}$ with initial condition $D\Phi(0, \bar{x}) = \mathbb{I}$.

We can now enunciate the result on the link between monodromy matrixes and linearizations of Poincaré maps, recalling that $\text{Spec}(A)$ indicates the collection of the eigenvalues of the operator A (its spectrum).

Proposition 1.1.2. *Let $\mathcal{O}_{\bar{x}}$ a periodic orbit, $D\Phi(T, \bar{x})$ its monodromy matrix and $D\Psi(\bar{x})$ the linearization of a Poincaré map Ψ at \bar{x} . Then*

$$\text{Spec}(D\Phi(T, \bar{x})) = \text{Spec}(D\Psi(\bar{x})) \cup \{1\}.$$

The eigenvalues of the monodromy matrix are called *Floquet multipliers* and their logarithms are called *Floquet exponents*. The Floquet multipliers give a measure of the rate by which the flow expands or contracts the orbits close to the periodic orbit. The existence of the eigenvalue 1 implies that there is always a direction of neither expansion nor contraction, which is, clearly, the one tangent to the orbit itself.

Remark 1.1.3. When DX is constant along the periodic orbit, (1.4) has constant coefficients and thus

$$\text{Spec}(D\Phi(T, \bar{x})) = e^{\text{Spec}(TDX(\bar{x}))}.$$

1.1.4 Hyperbolic dynamics

Equilibrium points are the simplest solutions to (1.1) and are found as critical points of the vector field $X(x)$. Among all of them, those of hyperbolic or partially hyperbolic origin are, in general, sources of chaos and exhibit the richest and most interesting local dynamics, characterized by intricate structures stemming from such equilibria that have the structure of differentiable manifolds.

Definition 1.1.7. An *equilibrium point* for (1.1) (that is $x = c \in D$ s.t. $X(c) = 0$) is called

- *hyperbolic* if all the eigenvalues of the Jacobian matrix DX have non-zero real part.
- *partially hyperbolic* if the Jacobian matrix DX has both eigenvalues with zero and non-zero real part.

As for fixed points in §1.1.3, around equilibria one performs the linearization of the system in order to make the investigation easier and try to deduce relevant properties of the full dynamics or at least of the approximate one. So we look at

$$\dot{y} = DX(c)y, \quad y = x - c. \quad (1.5)$$

We assume $DX(c)$ diagonalizable, so, by standard theory of linear ODEs,¹ the system has three invariant vector spaces, called *stable*, *unstable* and *center space* (resp. $E^s(c)$, $E^u(c)$, $E^c(c)$).

This strategy turns out to be extremely powerful with hyperbolic equilibrium points thanks to the two following fundamental results.

Theorem 1.1.2 (GROBMAN–HARTMAN THEOREM). *Let $c \in D$ be an hyperbolic equilibrium point. Then there exists a neighborhood U of c in D , a neighborhood V of $0 \in \mathbb{R}^d$ and a homeomorphism $h: U \rightarrow V$ such that*

- (i) $h(c) = 0$,
- (ii) $h(\Phi(t, c)) = e^{tDX(c)}h(c)$,

for all $x \in U_0 \subseteq U$ neighborhood of c and $t \in]-\varepsilon, \varepsilon[$, $\varepsilon > 0$ small enough.

The upshot is that the phase portraits around hyperbolic equilibrium points appear locally as deformations of the portraits of their linearized system. Nevertheless, h is only continuous and out of U there is no information about the global evolution. Luckily, we can benefit from the so-called *stable manifold theorem* about the existence and regularity of the sets

$$\begin{aligned} W^s(c) &= \left\{ x \in D : \lim_{t \rightarrow +\infty} \Phi(t, x) = c \right\} \\ W^u(c) &= \left\{ x \in D : \lim_{t \rightarrow -\infty} \Phi(t, x) = c \right\} \end{aligned} \quad (1.6)$$

which represent a non-linear generalization of $E^s(c)$, $E^u(c)$, called respectively and consequently *stable* and *unstable manifold* of c .

¹Ordinary Differential Equation

Theorem 1.1.3 (LOCAL STABLE MANIFOLD THEOREM). *Given c hyperbolic equilibrium point, let E^s, E^u be the stable and unstable spaces of the linearization (1.5) at c . Then $\exists U$ neighborhood of c s.t.:*

(i) $W_{loc}^s := W^s|_U, W_{loc}^u := W^u|_U$ are smooth invariant connected embedded submanifolds of D with $T_c W_{loc}^s = E^s, T_c W_{loc}^u = E^u$;

(ii) $\exists a_s, a_u \in (0, 1)$ and $b > 0$ s.t.

$$\begin{aligned} x \in W_{loc}^s, \zeta \in T_x W_{loc}^s &\implies \|D\Phi(t, x)\zeta\| \leq b a_s^t \|\zeta\| \\ x \in W_{loc}^u, \zeta \in T_x W_{loc}^u &\implies \|D\Phi(-t, x)\zeta\| \leq b a_u^{-t} \|\zeta\| \end{aligned}$$

for all $t > 0$.

Proof (sketch). Being a crucial result in this section and later on in the present thesis, let us quickly sketch part of the proof of (i) following essentially the reference [83]. We wish to show that there exists a positively invariant set W_{loc}^s such that, given $x \in W_{loc}^s$, we have $\lim_{t \rightarrow +\infty} \Phi(t, x) = 0$. For the regularity and connectedness of W_{loc}^s , as well as its tangency to E^s , the reader can refer to [17]. We set $c = 0$ (equivalent to the simple translation in (1.5) for $c \neq 0$, so that the equilibrium point is located always at the origin). Since we work locally, it is not restrictive to assume the vector field X of the form

$$X(x) = Ax + f(x), \quad A := DX(0), \quad (1.7)$$

where $f: \mathbb{R}^d \rightarrow \mathbb{R}^d$ is a smooth function at least of quadratic order close to 0, viz.

$$f(0) = \frac{\partial f}{\partial x}(0) = 0.$$

The idea is to consider the space of curves that approach 0 with a certain exponential rate. In particular, for each $z \in E^s$ we will consider the set of such curves that begin at $z + w$ for some $w \in E^c \oplus E^u$. We do not assume a priori that these curves are trajectories of the ODE. Then, we will define an integral operator on this space whose fixed points are solutions of (1.1) under (1.7). Lastly, an application of the Banach contraction mapping theorem completes the proof.

Let $B := A|_{E^s}$ and $C := A|_{E^c \oplus E^u}$. Let $-\alpha$ be the maximum value of $\operatorname{Re} \lambda$ for the eigenvalues λ of B and fix constants $0 < \gamma < \beta < \alpha$ such that all the eigenvalues of B lie strictly to the left of $-\beta$ and all eigenvalues of C lie strictly to the right of $-\gamma$. Notably, we can set a matrix norm on \mathbb{R}^d with the property that

$$\|e^{Bt}\| \leq e^{-\beta t}, \quad \|e^{-Ct}\| \leq e^{\gamma t},$$

for all $t \geq 0$.

We work in the space of all smooth curves for positive times approaching 0 with exponential rate at least ξ :

$$\mathcal{X} := \left\{ x \in C^\infty([0, \infty[; \mathbb{R}^d) \mid \|x\|_\xi := \sup_{t \geq 0} |x(t)| e^{\xi t} < \infty \right\}.$$

This is a complete metric space (alias Banach space) with distance given by $\delta(x, y) = \|x - y\|_\xi$. Fixing $z \in E^s$, we consider the subspace $\mathcal{X}_z = \{x \in \mathcal{X} \mid x^s(0) = z\}$, where $x^s \in E^s$ and $x^{cu} \in E^c \oplus E^u$ for the components of x lying in the stable and center-unstable subspaces, so that $x = x^s + x^{cu}$. Having established \mathcal{X}_z , we define an integral operator on it whose fixed points are trajectories of the system. According to the method of variation of constants for inhomogeneous linear ODEs, we have, integrating from 0 to t ,

$$x(t) = e^{At}x(0) + \int_0^t e^{A(t-s)}f(x(s))ds .$$

Now by decomposing $f = f^s + f^{cu}$ for $f^s \in E^s$, $f^{cu} \in E^c \oplus E^u$, we see that $x(t)$ is a solution to (1.1)-(1.7) if and only if

$$\begin{aligned} x^s(t) &= e^{Bt}x^s(0) + \int_0^t e^{B(t-s)}f^s(x(s))ds \\ x^{cu}(t) &= e^{C(t-T)}x^{cu}(T) + \int_T^t e^{C(t-s)}f^{cu}(x(s))ds \end{aligned}$$

for every $T \geq 0$. Note that, owing to the choices above, by letting $T \rightarrow \infty$,

$$\left| e^{C(t-T)}x^{cu}(T) \right| \leq \left\| e^{C(t-T)} \right\| |x(T)| \leq e^{-\gamma(t-T)} \|x\|_\xi e^{-\xi T} = e^{-\gamma t} \|x\|_\xi e^{(\gamma-\xi)T} \longrightarrow 0 .$$

Hence, we can introduce

$$(\mathcal{P}x)(t) := e^{Bt}x^s(0) + \int_0^t e^{B(t-s)}f^s(x(s))ds - \int_t^\infty e^{C(t-s)}f^{cu}(x(s))ds$$

and $x = \mathcal{P}x$ if and only if x solves the ODE in question.

Now we show that \mathcal{P} maps \mathcal{X}_z to itself, and that it is a contraction. First we observe that because the non-linear part f of the vector field X is C^∞ with Jacobian matrix at the equilibrium $Df(0) = 0$, it is Lipschitz on small neighborhoods of 0, and the Lipschitz constant can be selected arbitrarily small by making the neighborhood small enough: $\forall \varepsilon > 0$ there exists $r > 0$ such that if $|x|, |y| \leq r$ then $|f(x) - f(y)| \leq \varepsilon|x - y|$. By definition, $|x(t) - y(t)| \leq \delta(x, y)e^{-\xi t}$

for all $t \geq 0$, and write $\Delta^s(x, y) := |x^s(0) - y^s(0)|$. Then

$$\begin{aligned}
|(\mathcal{P}x)(t) - (\mathcal{P}y)(t)| &\leq \|e^{Bt}\| |x^s(0) - y^s(0)| + \int_0^t \|e^{B(t-s)}\| |f^s(x(s)) - f^s(y(s))| ds \\
&\quad + \int_t^\infty \|e^{C(t-s)}\| |f^{cu}(x(s)) - f^{cu}(y(s))| ds \\
&\leq e^{-\beta t} \Delta^s(x, y) + \int_0^t e^{-\beta(t-s)} \varepsilon |x(s) - y(s)| ds \\
&\quad + \int_t^\infty e^{-\gamma(t-s)} \varepsilon |x(s) - y(s)| ds \\
&\leq e^{-\beta t} \Delta^s(x, y) + \varepsilon \delta(x, y) \left(\int_0^t e^{-\beta(t-s)} e^{-\xi s} ds \right. \\
&\quad \left. + \int_t^\infty e^{-\gamma(t-s)} e^{-\xi s} ds \right) \\
&= e^{-\beta t} \Delta^s(x, y) + \varepsilon \delta(x, y) \left(\frac{e^{-\xi t} - e^{-\beta t}}{\beta - \xi} - \frac{e^{-\xi t}}{\gamma - \xi} \right) \\
&\leq \left(\Delta^s(x, y) + \frac{\varepsilon(\beta - \gamma)}{(\beta - \xi)(\xi - \gamma)} \delta(x, y) \right) e^{-\xi t}.
\end{aligned}$$

Writing $L := (\beta - \gamma)/((\beta - \xi)(\xi - \gamma))$ and recalling the definition of $\|\cdot\|_\xi$, this gives

$$\|\mathcal{P}x - \mathcal{P}y\|_\xi \leq \Delta^s(x, y) + \varepsilon L \delta(x, y).$$

Given $x \in \mathcal{X}$, by putting $y = 0$ we realize that

$$\|\mathcal{P}x\|_\xi \leq |x^s(0)| + \varepsilon L \|x\|_\xi < \infty,$$

and so \mathcal{P} maps \mathcal{X} to itself. Moreover, if $x \in \mathcal{X}_z$ then it is evident from the definition of $(\mathcal{P}x)(t)$ that $\mathcal{P}x \in \mathcal{X}_z$ as well. Finally, if $x, y \in \mathcal{X}_z$ for some $z \in E^s$, then $\Delta^s(x, y) = 0$ and the estimate above yields

$$\delta(\mathcal{P}x, \mathcal{P}y) \leq \varepsilon L \delta(x, y).$$

By choosing r small enough we can guarantee that $\varepsilon L < 1$ and hence \mathcal{P} is a contraction. Thus it has a unique fixed point $\bar{x} \in \mathcal{X}_z$. This is an orbit of (1.1)-(1.7) which approaches 0 exponentially (with at least rate ξ) and has $\bar{x}^s(0) = z$, so we work out a function

$$\psi: \mathbb{B}_r(0) \cap E^s \longrightarrow E^c \oplus E^u$$

such that $\psi(z) = x^{cu}(0)$ and whose graph is the local stable manifold, namely $W_{\text{loc}}^s = \text{Graph } \psi$. By construction, W_{loc}^s has the properties of invariance and convergence claimed at the very beginning. \square

Remark 1.1.4.

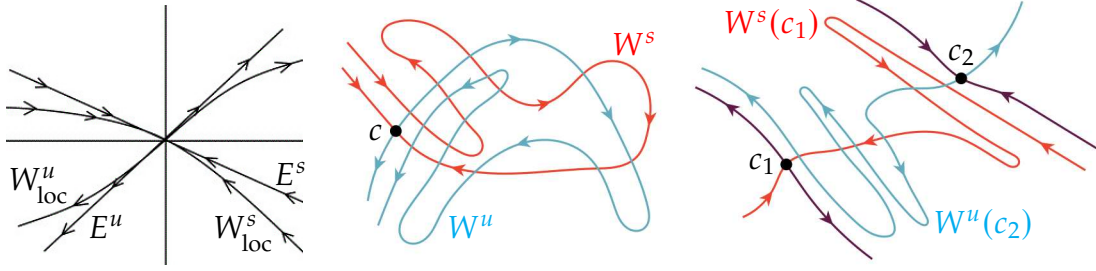


Figure 1.2: Dynamics originating at hyperbolic equilibria. **Left panel:** illustration of statement (i) of Theorem 1.1.3. **Middle panel:** intersection between W^s and W^u spreading from an hyperbolic equilibrium point c (homoclinic). **Right panel:** intersection between $W^s(c_1)$ and $W^u(c_2)$ emanating from two different hyperbolic equilibrium points c_1, c_2 (heteroclinic).

- (i) From the knowledge of W^s_{loc}, W^u_{loc} we can recover the global manifolds W^s, W^u considering respectively $\bigcup_{t \leq 0} \Phi(t, W^s_{loc})$ and $\bigcup_{t \geq 0} \Phi(t, W^u_{loc})$. Analogous characteristics of these sets are encapsulated in the global variant of Theorem 1.1.3, although these in general are slightly weaker (for example W^s, W^u are only immersed and not embedded in the phase space, thus their overall structure may be way more complicated than W^s_{loc}, W^u_{loc} , like the presence of accumulation points).
- (ii) The geometric structure of the stable and unstable manifolds becomes even more complex when they have transverse intersections, especially *homoclinic points* (Fig. 1.2, middle panel) or *heteroclinic points* (Fig. 1.2, right panel).

When the equilibrium point is partially hyperbolic, we still have the same configuration described in Fig. 1.2, but also another object, called *center manifold* W^c , as in the following theorem.

Theorem 1.1.4 (CENTER MANIFOLD THEOREM). *Consider the differential equation (1.1) with vector field expressed by (1.7). Suppose now that $f \in C^k(\mathbb{R}^d; \mathbb{R}^d)$ and let the origin be a partially hyperbolic equilibrium point. Then, there exists a C^{k-1} manifold W^c tangent at 0 to the center space E^c .*

Remark 1.1.5.

- (i) The center manifold is, generally, locally invariant: $\forall x \in W^c \exists I$ neighborhood of $t = 0$ such that $\Phi(t, x) \in W^c$ for any $t \in I$, i.e. a solution supported by W^c can exit from the manifold at some given time.
- (ii) Contrary to W^s and W^u , W^c is not necessarily unique.

Remark 1.1.6. The stable, unstable and center manifolds can be defined also for periodic orbits and even higher dimensional invariant sets under a condition of hyperbolicity resembling the one in Definition 1.1.7.

1.2 Hamiltonian dynamical systems

1.2.1 Hamilton's equations of motion

Consider a phase space $D \subseteq \mathbb{R}^d$ open of even dimension $d = 2n$ equipped with coordinates $x = (q, p)$, $q = (q_i)_{i=1, \dots, n}$, $p = (p_i)_{i=1, \dots, n}$. The dynamical system (1.1) with vector field

$$X = X_H := \mathbb{J} \nabla H = \left(\frac{\partial H}{\partial p}, -\frac{\partial H}{\partial q} \right), \quad (1.8)$$

where

$$\mathbb{J} = \begin{pmatrix} 0_n & \mathbb{I}_n \\ -\mathbb{I}_n & 0_n \end{pmatrix} \quad (1.9)$$

is the $2n \times 2n$ symplectic unit and $H \in C^\infty(D)$, is called *Hamiltonian*. The ODEs

$$\dot{q}_i = \frac{\partial H}{\partial p_i}, \quad \dot{p}_i = -\frac{\partial H}{\partial q_i}, \quad i = 1, \dots, n \quad (1.10)$$

are *Hamilton's (canonical) equations*. The coordinates (q, p) are called *canonical* (and usually the p_i are said to be the *conjugate momenta* of the *generalized positions* q_i). $H(q, p)$ is called the *Hamiltonian*. The integer n is referred to as the number of *degrees of freedom* (d.o.f). As in Remark 1.1.1, we assume to have a *Hamiltonian flow* Φ_H associated to (1.8) defined $\forall t \in \mathbb{R}$.

Remark 1.2.1. The Hamiltonian H may also explicitly depend on time t ($H = H(q, p, t)$). Then, the system (1.10) is called non-autonomous and of $n + 1/2$ d.o.f. However, it is possible to treat non-autonomous systems as autonomous ones (§1.1) by formally extending the phase space D . In practice, one appends one more dimension to $q_{n+1} := t$:

$$D' = \left\{ (q_1, \dots, q_n, q_{n+1}, p_1, \dots, p_n, p_{n+1}) \mid (q_1, \dots, q_n, p_1, \dots, p_n) \in D, q_{n+1}, p_{n+1} \in \mathbb{R} \right\},$$

so that now $q = (q_i)_{i=1, \dots, n+1}$, $p = (p_i)_{i=1, \dots, n+1}$, and consider Hamilton's equations induced by

$$H': D' \longrightarrow \mathbb{R} \\ (q, p) \longmapsto H'(q, p) := H(q_1, \dots, q_n, p_1, \dots, p_n, q_{n+1}) + p_{n+1}. \quad (1.11)$$

In particular $\dot{q}_{n+1} = 1$, thus Hamilton's equations associated to H' do not depend on the cyclic coordinate² p_{n+1} and we can ignore the corresponding equation \dot{p}_{n+1} . The solutions of these ODEs with $q_{n+1}(0) = 0$ provide the solutions $q_1(t), \dots, q_n(t), p_1(t), \dots, p_n(t)$ to Hamilton's equations with Hamiltonian $H(q_1, \dots, q_n, p_1, \dots, p_n, t)$.

²A coordinate is said to be *cyclic* when it does not appear explicitly in the Hamiltonian.

1.2.2 Conservation properties of Hamiltonian systems

Let us focus on the Hamiltonian system (1.10). Denote by \mathcal{L}^{2n} the $2n$ -dimensional Lebesgue measure of a measurable set $E \subseteq D$:

$$\mathcal{L}^{2n}(E) = \int_E dq_1 \dots dq_n dp_1 \dots dp_n .$$

Proposition 1.2.1. *The Hamiltonian flow Φ_H preserves the measure of the phase space, that is for every Lebesgue measurable set $E \subseteq D$*

$$\mathcal{L}^{2n}(E) = \mathcal{L}^{2n}(\Phi_H(t, E))$$

$\forall t \in \mathbb{R}$.

This assertion is a direct consequence of the transport theorem for general ODEs (1.1). Under the assumptions of Remark 1.1.1, the theorem states that

$$\frac{d}{dt} \int_{\Phi(t, E)} dx_1 \dots dx_d = \int_{\Phi(t, E)} \operatorname{div} X(x) dx_1 \dots dx_d \quad (1.12)$$

for every \mathcal{L}^d -measurable set $E \subseteq D$. Since $\operatorname{div} X_H(q, p) \equiv 0$, $\mathcal{L}^{2n}(\Phi_H(t, E))$ is constant over time.

Autonomous Hamiltonian systems preserve another quantity along the flow, which is the Hamiltonian itself, i.e., the energy. An immediate computation yields indeed

$$\frac{d}{dt} H(q(t), p(t)) = \sum_{j=1}^n \left(\frac{\partial H}{\partial q_j} \dot{q}_j + \frac{\partial H}{\partial p_j} \dot{p}_j \right) = \sum_{j=1}^n \left(\frac{\partial H}{\partial q_j} \frac{\partial H}{\partial p_j} - \frac{\partial H}{\partial p_j} \frac{\partial H}{\partial q_j} \right) = 0 , \quad (1.13)$$

hence $H(q(t), p(t)) = H(q(0), p(0))$. This is no longer true for non-autonomous Hamiltonians $H(q, p, t)$, where $\dot{H} = \partial H / \partial t$, but, in virtue of Remark 1.2.1, the extended Hamiltonian H' is a constant of motion of the flow in the extended phase space.

1.2.3 Canonical transformations

A change of variables can be useful to simplify the study of the solutions to (1.10) and may bring out possible symmetries. The characterization of the transformations of the phase space that maintain the canonical structure in (1.8) is a fundamental aspect of Hamiltonian mechanics.

We consider C^∞ -diffeomorphisms between $D, \tilde{D} \subseteq \mathbb{R}^{2n}$ s.t.

$$\begin{aligned} w: D &\longrightarrow \tilde{D} \\ (q, p) &\longmapsto w(q, p) = (\tilde{q}, \tilde{p}) \end{aligned} \quad (1.14)$$

We denote synthetically $y = (\tilde{q}, \tilde{p})$, $\tilde{q} = u(q, p)$, $\tilde{p} = v(q, p)$, so that $y = w(x)$, $w = (u, v)$.³

³Again, on the basis of Remark 1.2.1, we do not tackle separately time-dependent transformations.

The mapping (1.14) conjugates the equation made up of (1.1)-(1.8) to $\dot{y} = Y(y)$, where

$$Y(y) = Dw(x)X_H(x)\Big|_{x=w^{-1}(y)} \quad (1.15)$$

and $Dw(x)$ is the Jacobian matrix of w .

Definition 1.2.1. The transformation (1.14) is called *canonical* or *symplectic* if for every Hamiltonian $H(q, p)$, the vector field (1.15) conjugated to (1.8) is still Hamiltonian for the Hamilton's function $\tilde{H}(\tilde{q}, \tilde{p})$ obtained as

$$\tilde{H}(\tilde{q}, \tilde{p}) = H(u^{-1}(\tilde{q}, \tilde{p}), v^{-1}(\tilde{q}, \tilde{p})) .$$

Remark 1.2.2. Canonical transformations satisfy Proposition 1.2.1, namely they preserve the measure of the phase space.

Remark 1.2.3. When $X = X_H = \mathbb{J}\nabla H$, let us consider the restriction $\Phi_H|_{D_h}$ of the Hamiltonian flow Φ_H to a regular set $D_h := H^{-1}(h)$, $h \in \mathbb{R}$, of H . Let $\Sigma_h \subset D_h$ be a section of $\Phi_H|_{D_h}$ and suppose that the orbit of a point of Σ_h returns to Σ_h , so that there exists a Poincaré map Ψ (§1.1.3) relative to Σ_h . Then Σ_h inherits a symplectic structure with respect to which Ψ is symplectic.

The following are some equivalent criteria to check whether a mapping w is canonical.

Proposition 1.2.2. *The following are equivalent. The map (1.14) is canonical if and only if*

(i) *the Poisson bracket*

$$\begin{aligned} \{\cdot, \cdot\}: C^\infty(D) \times C^\infty(D) &\longrightarrow C^\infty(D) \\ (f, g) &\longmapsto \{f, g\} = \nabla f \cdot \mathbb{J}\nabla g = \frac{\partial f}{\partial q} \cdot \frac{\partial g}{\partial p} - \frac{\partial f}{\partial p} \cdot \frac{\partial g}{\partial q} \end{aligned} \quad (1.16)$$

are preserved by $y = w(x)$, i.e.

$$\{f, g\}_{q,p}(x) = \{\tilde{f}, \tilde{g}\}_{\tilde{q},\tilde{p}}(w(x)) , \quad (1.17)$$

for every $f(x) = \tilde{f}(w(x))$, $g(x) = \tilde{g}(w(x)) \in C^\infty(D)$. Particularly, (1.17) holds if and only if the elementary Poisson brackets

$$\{q_i, p_j\} = \delta_{ij} , \quad \{q_i, q_j\} = \{p_i, p_j\} = 0 , \quad i, j = 1, \dots, n , \quad (1.18)$$

are preserved by w .

(ii)

$$Dw(x)\mathbb{J}Dw(x)^T = \mathbb{J} \quad \forall x \in D . \quad (1.19)$$

(iii) *the Liouville 1-form (or tautological 1-form)*

$$\begin{aligned} \theta: D &\longrightarrow (\mathbb{R}^{2n})^* \\ (q, p) &\longmapsto \theta(q, p) = p \cdot dq = \sum_{i=1}^n p_i dq_i \end{aligned} \quad (1.20)$$

is preserved by w , viz. there exists a differentiable function $f(q, p)$ s.t.

$$v \cdot du = p \cdot dq - df ; \quad (1.21)$$

in other words, the differential form $p \cdot dq - v \cdot du$ is closed, or equivalently locally exact.

Remark 1.2.4. The Hamiltonian flow $\Phi_H(t, x)$ satisfies (1.21), i.e. it is canonical.

Remark 1.2.5. The pair $(C^\infty(D), \{\cdot, \cdot\})$ forms an associative commutative algebra, called *Poisson algebra*, and has the structure of a Lie algebra satisfying Leibniz rule

$$\{f, gh\} = \{f, g\}h + g\{f, h\} \quad \forall f, g, h \in C^\infty(D) .$$

Moreover, for every fixed $g \in C^\infty(D)$, we can define the operator

$$\begin{aligned} \mathcal{L}_g : C^\infty(D) &\longrightarrow C^\infty(D) \\ f &\longmapsto \mathcal{L}_g f := \{f, g\} \end{aligned} \quad (1.22)$$

which is the *Lie derivative* related to the Hamiltonian vector field $X_g = (-\partial g / \partial q, \partial g / \partial p)$ of Hamiltonian g .

A useful technique to construct canonical transformations, which naturally emerges from the condition on the preservation of the Liouville 1-form (Proposition (1.2.2)), consists in assigning f and consequently determining u, v so that the condition (1.21) be true. Briefly, given a function $f(q, p)$, it can be shown [60] that the system

$$\tilde{p}_i = -\frac{\partial F}{\partial \tilde{q}_i}(q, \tilde{q}), \quad p_i = \frac{\partial F}{\partial q_i}(q, \tilde{q}), \quad i = 1, \dots, n \quad (1.23)$$

under the invertibility condition

$$\det \frac{\partial^2 F}{\partial q \partial \tilde{q}}(q, \tilde{q}) \neq 0 \quad (1.24)$$

defines, after inversion, a canonical transformation $(\tilde{q}, \tilde{p}) = w(q, p)$, where $F(\tilde{q}, q) := f(q, U(q, \tilde{q}))$ for $U(q, \tilde{q})$ the inverse of u with respect to p , that is

$$u(q, U(q, \tilde{q})) = \tilde{q} .$$

Functions of mixed variables $F(q, \tilde{q})$ fulfilling the requirement (1.24) are called *generating functions of the 1st kind*.

The argument can be repeated for other choices of independent variables, namely with respect to (q, \tilde{p}) (*generating functions of the 2nd kind*), (p, \tilde{q}) (*generating functions of the 3rd kind*), (p, \tilde{p}) (*generating functions of the 4th kind*).

A class of maps particularly relevant for canonical perturbation theory is represented by *near-identity transformations*. For instance, all functions of the form $F(q, \tilde{p}) = \tilde{p} \cdot q + \varepsilon S(q, \tilde{p})$, for $|\varepsilon|$ small enough, are generating functions

of the second kind. They give rise to a family of canonical transformations by inversion of

$$\tilde{q}_i = q_i + \varepsilon \frac{\partial S}{\partial \tilde{p}_i}, \quad p_i = \tilde{p}_i + \varepsilon \frac{\partial S}{\partial q_i}, \quad i = 1, \dots, n, \quad (1.25)$$

which, for $\varepsilon = 0$, correspond to the identity. Near-identity canonical transformations produced in the framework of the Lie method [23, 45] are discussed in §1.2.5.

1.2.4 Action-angle variables and Liouville-Arnold theorem

We have already introduced the notion of integrability in §1.1.2 for general ODEs. For Hamiltonian systems in particular, the geometric description of integrability is encapsulated in the celebrated theorem by Liouville and Arnold⁴ [3], which exploits the existence of n independent integrals of motion in involution to find the orbits of the differential system (1.10).

Theorem 1.2.1 (LIOUVILLE-ARNOLD THEOREM). *Let H be an autonomous Hamiltonian of n d.o.f. If*

- *H possesses a set of n first integrals $\mathcal{I} = (\mathcal{I}_1, \dots, \mathcal{I}_n)$ which are independent, that is*

$$\text{rk} \left(\frac{\partial \mathcal{I}}{\partial x} \right) = n; \quad (1.26)$$

- *\mathcal{I}_i are mutually in involution, that is*

$$\{\mathcal{I}_i, \mathcal{I}_j\} = 0, \quad i, j = 1, \dots, n; \quad (1.27)$$

- *the level surfaces*

$$M_{\widehat{\mathcal{J}}} = \left\{ (q, p) \in D \mid \mathcal{I}_i(q, p) = \widehat{\mathcal{J}}_i, i = 1, \dots, n \right\}, \quad (1.28)$$

for $\widehat{\mathcal{J}} \in \mathbb{R}^n$, are compact and connected;

then there exists a symplectic map

$$w: \bigcup_{\mathcal{J} \in \mathcal{S}} M_{\mathcal{J}} \longrightarrow \mathbb{T}^n \times \mathcal{A} \\ (q, p) \longmapsto (\varphi, I), \quad (1.29)$$

where \mathcal{S} is a neighborhood of $\widehat{\mathcal{I}}$, such that (1.28) is diffeomorphic to $\mathbb{T}^n := \mathbb{R}^n / (2\pi\mathbb{Z}^n)$ and $H \circ w^{-1}(\varphi, I) = \widetilde{H}(I)$.

⁴and actually Jost [49]

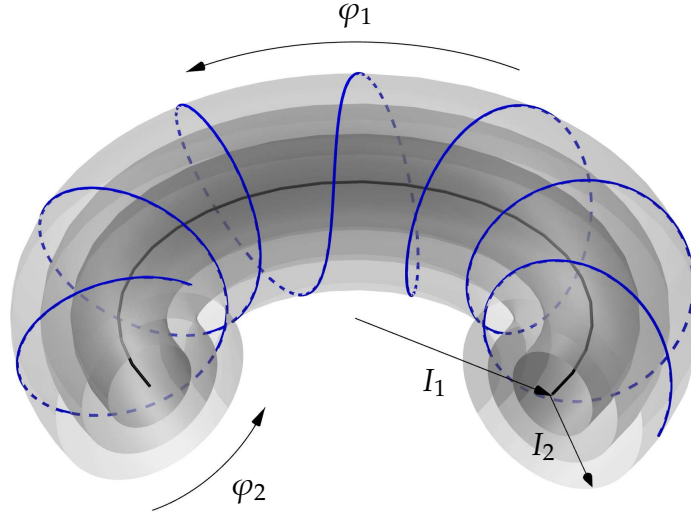


Figure 1.3: Schematic illustration of a foliation of invariant tori for $n = 2$ and increasing I_2 immersed in \mathbb{R}^3 . The constant action vector $I = (I_1, I_2)$ identifies the torus (in gray scale, for similar values of I_1) on which the orbits lie (blue), while the two angles $\varphi = (\varphi_1, \varphi_2)$ parametrize the motion around it. The innermost torus of the family degenerates into a circle (black arc), viz. a periodic orbit.

The canonical variables φ, I are called respectively *angles* and *actions*. The solution of Hamilton's equations for the Hamiltonian $\tilde{H}(I)$ are trivial:

$$I(t) = I_0, \quad \varphi(t) = \varphi_0 + \omega(I_0)t, \quad \omega(I) := \frac{\partial \tilde{H}}{\partial I}(I), \quad (1.30)$$

which indicate that the temporal evolution of each I_i is constant, while the one of each φ_i is linear modulo 2π with frequency ω_i . The resulting orbit spirals on the torus \mathbb{T}^n (a schematic representation is portrayed in Fig. 1.3). Unless all the frequencies ω_i have pairwise rational ratio, the orbits are called *quasi-periodic* and densely wrap around the invariant torus supporting them, called *non-resonant*; this is equivalent to

$$k \cdot \omega = 0 \iff k = 0, k \in \mathbb{Z}^n. \quad (1.31)$$

On the other hand, if there exist one or more combinations of integers k_i such that

$$k_1\omega_1 + \dots + k_n\omega_n = 0, \quad \sum_{i=1}^n |k_i| \neq 0, \quad (1.32)$$

the torus is called *resonant*. The commensurability between frequencies induces orbits lying on tori of dimension lower than n : if m independent relations of the form (1.32) exist, the corresponding orbits lie in a $(n - m)$ -dimensional torus.

Remark 1.2.6. In the case $m = n - 1$ the orbits become 1-dimensional tori, i.e., periodic orbits.

1.2.5 Perturbations of integrable systems

A variety of phenomena in nature are described by models representing, mathematically, a special class of non-integrable systems, called *quasi-integrable*. Given a phase space $\mathbb{T}^n \times \mathcal{A}$, $\mathcal{A} \subseteq \mathbb{R}^n$, endowed with action-angle variables (φ, I) and standard symplectic form $d\varphi \wedge dI$, quasi-integrable systems are defined by Hamiltonian functions of the form

$$H(\varphi, I) = H_0(I) + \varepsilon H_1(\varphi, I; \varepsilon), \quad (1.33)$$

where ε is a small parameter. The Hamiltonian H_0 , depending only on the actions, is Liouville–Arnold integrable and it is called the *integrable approximation* to the system (1.33). The orbits of H_0 deviate from the orbits of H by a quantity of order $|\varepsilon|$ in a time of order unity and by a quantity of order unity in a time of order $1/|\varepsilon|$. The function H_1 is called the *perturbation*, usually parametrically dependent on ε and assumed analytic for $|\varepsilon|$ small enough.

Remark 1.2.7. The easiest formulation of perturbation theory holds when one assumes the maximum regularity for H_0 and H_1 . Typically, passing to a complexification of the domains, we suppose that H_0, H_1 are holomorphic functions in a complex neighborhood of $\mathbb{T}^n \times \mathcal{A}$, so they admit a convergent expansion in Fourier series with harmonics exponentially decaying as their order increases (for details, see [32]).

Although cases of strong chaos are possible to encounter, nearly integrable models (1.33) are the most common case in Solar System dynamics. For such systems, quite precise approximations of the orbits can be found using the perturbative method of *Hamiltonian normal forms* [26].

A normal form is a Hamiltonian yielding a dynamics which only approximates the true one, but is simpler to control. The normalized Hamiltonian is obtained by implementing a sequence of conveniently chosen canonical transformations of the form

$$(\tilde{\varphi}, \tilde{I}) = w(\varphi, I) \quad (1.34)$$

such that, after one application of (1.34) to (1.33), the new conjugated Hamiltonian displays the dependence on the angles at higher order in ε (for instance at order 2):

$$\tilde{H}(\tilde{\varphi}, \tilde{I}) = \tilde{Z}(\tilde{\varphi}, \tilde{I}; \varepsilon) + \varepsilon^2 \tilde{H}_2(\tilde{\varphi}, \tilde{I}; \varepsilon). \quad (1.35)$$

The term $\tilde{Z}(\tilde{\varphi}, \tilde{I}; \varepsilon) = H_0(\tilde{I}) + \varepsilon \tilde{H}_1(\tilde{\varphi}, \tilde{I})$, called the *normal form*, yields a dynamics on which we have control. The term $\tilde{R}(\tilde{\varphi}, \tilde{I}; \varepsilon) = \varepsilon^2 \tilde{H}_2(\tilde{\varphi}, \tilde{I}; \varepsilon)$, called the *remainder*, is an order of magnitude less in size than the normal form. Iterating the procedure via (1.34) one expects in principle to push the perturbation to higher orders in ε at every step. However, in general this process cannot be done endlessly: it is necessary to stop at some optimal order, depending on ε and on the properties of the system (see, for example, [26]).

By “control” we mean, for instance, that one could be interested in eliminating only some of the angles at first order (this is quite customary in celestial mechanics when we distinguish between “fast” and “slow” angles, see Chapter 3).

Transformations (1.34) leading to (1.35) or variants are feasible by means of essentially two methods taking advantage of near-identity canonical mappings: the method of the generating functions (1.25) and the method of Lie series. We hereby illustrate the latter.

The canonicity of the Hamiltonian flow (Remark 1.2.4) allows to produce transformations ε -close to the identity. Consider the flow Φ_χ of a *generating Hamiltonian* $\chi(\varphi, I)$ (or *Lie generating function*) at time $t = \varepsilon$ with initial datum $(\tilde{\varphi}, \tilde{I})$

$$(\varphi, I) = \Phi_\chi(\varepsilon, (\tilde{\varphi}, \tilde{I}))$$

and denote by $(\varphi(t), I(t))$ the corresponding solutions of Hamilton's equations. The canonical transformation at issue is the map

$$(\tilde{\varphi}, \tilde{I}) \longmapsto (\varphi, I) = (\varphi(\varepsilon), I(\varepsilon)). \quad (1.36)$$

Consider, now, the Hamiltonian (1.33) which is to be normalized. From the relationships

$$\begin{aligned} \frac{d}{dt}H(\varphi(t), I(t)) &= \{H, \chi\} = \mathcal{L}_\chi H \\ \frac{d^j}{dt^j}H(\varphi(t), I(t)) &= \{\dots \{\{H, \chi\}, \chi\}, \dots, \chi\} = \mathcal{L}_\chi^j H \end{aligned} \quad (1.37)$$

where \mathcal{L}_χ is the operator defined as in (1.22), using a Maclaurin expansion of $H(\varphi(t), I(t))$ we get the representation

$$\begin{aligned} \tilde{H}(\tilde{\varphi}, \tilde{I}) &= H(\varphi(\varepsilon), I(\varepsilon)) = \sum_{j \geq 0} \frac{\varepsilon^j}{j!} \frac{d^j}{dt^j} H(\varphi(t), I(t)) \Big|_{t=0} = \sum_{j \geq 0} \frac{\varepsilon^j}{j!} \mathcal{L}_\chi^j H(\tilde{\varphi}, \tilde{I}) \\ &= H(\tilde{\varphi}, \tilde{I}) + \varepsilon \{H, \chi\}(\tilde{\varphi}, \tilde{I}) + \frac{\varepsilon^2}{2} \{\{H, \chi\}, \chi\}(\tilde{\varphi}, \tilde{I}) + \dots \\ &= \exp(\varepsilon \mathcal{L}_\chi) H(\tilde{\varphi}, \tilde{I}), \end{aligned} \quad (1.38)$$

in which $\exp(\varepsilon \mathcal{L}_\chi)$ is the *Lie series operator*, namely

$$\begin{aligned} \exp(\varepsilon \mathcal{L}_\chi) &: C^\omega(\mathbb{T}^n \times \mathcal{A}) \longrightarrow C^\omega(\mathbb{T}^n \times \mathcal{A}) \\ \exp(\varepsilon \mathcal{L}_\chi) &= \sum_{j \geq 0} \frac{\varepsilon^j}{j!} \mathcal{L}_\chi = \text{id}_{\mathbb{T}^n \times \mathcal{A}} + \varepsilon \mathcal{L}_\chi + \frac{\varepsilon^2}{2} \mathcal{L}_\chi \circ \mathcal{L}_\chi + \dots \end{aligned} \quad (1.39)$$

where $C^\omega(\mathbb{T}^n \times \mathcal{A})$ indicates the set of real analytic functions on the phase space; thus, the expressions of (1.36) are

$$\varphi = \exp(\varepsilon \mathcal{L}_\chi) \tilde{\varphi}, \quad I = \exp(\varepsilon \mathcal{L}_\chi) \tilde{I}. \quad (1.40)$$

Remark 1.2.8. The equality between the left- and the last right-hand side in (1.38) implies that the series expansion in ε of the transformed Hamiltonian may be calculated by applying the exponential operator of the Lie series directly to the Hamiltonian itself with no need of making a substitution of variables.

This is a special case of the so-called Gröbner exchange theorem [37], according to which

$$f(\varphi, I) \Big|_{\varphi=\exp(\varepsilon \mathcal{L}_\chi)\tilde{\varphi}, I=\exp(\varepsilon \mathcal{L}_\chi)\tilde{I}} = \exp(\varepsilon \mathcal{L}_\chi) f \Big|_{\varphi=\tilde{\varphi}, I=\tilde{I}}$$

for any $f \in C^\omega(\mathbb{T}^n \times \mathcal{A})$.

We now explicitly determine χ such that \tilde{H} has the form (1.35). If H has the form (1.33), (1.38) becomes

$$\tilde{H} = H_0 + \varepsilon H_1 + \varepsilon \{H_0, \chi\} + \varepsilon^2 \{H_1, \chi\} + \frac{\varepsilon^2}{2} \{\{H_0, \chi\}, \chi\} + \mathcal{O}(\varepsilon^3), \quad (1.41)$$

implicitly assuming hereafter that the right-hand side is a function of $(\tilde{\varphi}, \tilde{I})$. Split now H_1 in a normal form part and a part to eliminate: $H_1 = Z_1 + h_1$. \tilde{H} will assume the desired form if there exists an analytic function χ s.t.

$$H_1 + \{H_0, \chi\} = Z_1. \quad (1.42)$$

Equation (1.42) is known in literature as *the homological equation*. To solve (1.42) we exploit the quasi-periodicity of H and expand h_1 in Fourier series in light of Remark 1.2.7 as

$$h_1(\tilde{\varphi}, \tilde{I}) = \sum_{k \in \mathbb{Z}^n} c_k(\tilde{I}) e^{ik \cdot \tilde{\varphi}}, \quad i = \sqrt{-1}. \quad (1.43)$$

We then look for a solution χ to (1.42) of the same form

$$\chi(\tilde{\varphi}, \tilde{I}) = \sum_{k \in \mathbb{Z}^n} d_k(\tilde{I}) e^{ik \cdot \tilde{\varphi}}, \quad (1.44)$$

so that in the left-hand side of (1.42) we get

$$h_1(\tilde{\varphi}, \tilde{I}) - \omega_0(\tilde{I}) \cdot \frac{\partial \chi}{\partial \tilde{\varphi}}(\tilde{\varphi}, \tilde{I}) = \sum_{k \in \mathbb{Z}^n} (c_k(\tilde{I}) - ik \cdot \omega_0(\tilde{I}) d_k(\tilde{I})) e^{ik \cdot \tilde{\varphi}} = 0,$$

where $\omega_0(\tilde{I}) := \partial H_0(\tilde{I}) / \partial \tilde{I}$. Hence

$$d_k(\tilde{I}) = \frac{c_k(\tilde{I})}{ik \cdot \omega_0(\tilde{I})}, \quad k \in \mathbb{Z}^n \setminus \{0\}. \quad (1.45)$$

Equation (1.45) has a caveat: for the solution to exist, all denominators $k \cdot \omega_0$ must satisfy the condition $k \cdot \omega_0 \neq 0$ and for practical computations we usually exclude also the harmonics satisfying $k \cdot \omega_0 \simeq 0$. Strictly speaking, to every $k \in \mathbb{Z}^n \setminus \{0\}$ there is an associated locus

$$\mathcal{R}_k = \{\tilde{I} \in \mathcal{A} : k \cdot \omega_0(\tilde{I}) = 0\} \quad (1.46)$$

called *resonant module*: the Fourier coefficients of χ can be defined only when \mathcal{A}' does not intersect any resonant module. This restriction, known as the *problem of small divisors* is fundamental in normal form theory. Customarily, there are two ways to sort this situation out (cf. [69]).

- (i) By Remark 1.2.7, the Fourier coefficients of h_1 decay exponentially. Then we can choose to decompose h_1 into two parts, one $h_1^{\geq K}$ with $|k| \geq K$ and $h_1^{< K}$ with $|k| < K$, for K large enough ($|k| = |k_1| + \dots + |k_n|$ is the order of the Fourier harmonic $k = (k_1, \dots, k_n)$). We then set

$$\chi(\tilde{\varphi}, \tilde{I}) = - \sum_{k \in \mathbb{Z}^n, |k| < K} i \frac{c_k(\tilde{I})}{k \cdot \omega_0(\tilde{I})} \exp(ik \cdot \tilde{\varphi}), \quad (1.47)$$

accepting a remainder $\varepsilon h_1^{\geq K}$ in the series after normalization. Since χ contains only a finite number of harmonics, it is possible to find an open domain \mathcal{A}_K in the action space, such that the denominators in (1.47) do not vanish for any $\tilde{I} \in \mathcal{A}_K$. The domain \mathcal{A}_K is said to be *non-resonant up to order K* (cf. [69]).

- (ii) A second strategy consists in selecting a point $\tilde{I}^* \in \mathcal{A}$ expanding H in power series of the small quantity $\delta \tilde{I} = \tilde{I} - \tilde{I}^*$. In this way H_0 can be redefined as $H_0 = \omega_* \delta \tilde{I}$, where $\omega_* = \omega_0(\tilde{I}^*)$. This implies that the frequencies in all small divisors do not depend on the actions, hence, with the correct choice of resonant module, χ can be defined in an open ball around \tilde{I}^* (see Remark 3.2.3 in Chapter 3 for a concrete application).

Remark 1.2.9. The notorious Kolmogorov-Arnold-Moser (KAM) theorem [5, 50, 72] examines the existence of quasi-periodic orbits in (1.33) when $\varepsilon > 0$ is sufficiently small. Under suitable hypotheses, the theorem states that some of the non-resonant invariant tori of the unperturbed problem of Hamiltonian H_0 survive as deformed invariant tori (*KAM tori*), whose union fills locally a region in phase space of density $1 - \mathcal{O}(\sqrt{\varepsilon})$ as ε goes to zero. While the dynamics on this set trivializes (being conjugated to a linear quasi-periodic translation on \mathbb{T}^n with a Diophantine frequency vector), in its complement (which asymptotically represents a small region of measure $\mathcal{O}(\sqrt{\varepsilon})$) the dynamics can be very complicated, exhibiting, in many cases, “random motions”⁵ or *Arnold diffusion* [4].

In the case of a system with 2 d.o.f, any trajectory evolves on an 3-dimensional iso-energetic surface, thus a KAM torus divides the phase space in two non-communicating parts, ensuring non-linear stability for all the orbits confined in the interior of an invariant KAM torus. On the contrary, in systems with more than 2 d.o.f. the invariant tori do not isolate the orbits in their interior and the non-linear stability of such orbits has to be analyzed by other methods (like Nekhoroshev’s theorem [74]).

The above normalization scheme in question can be iterated r times performing a composition $\mathcal{S}_{\chi^{(r)}}$ of Lie series to eliminate the dependence on $\tilde{\varphi}$ at higher orders in ε , where

$$\mathcal{S}_{\chi^{(r)}} = \exp(\varepsilon^r \mathcal{L}_{\chi_r}) \dots \circ \exp(\varepsilon^2 \mathcal{L}_{\chi_2}) \circ \exp(\varepsilon \mathcal{L}_{\chi_1}), \quad (1.48)$$

⁵Not in literal sense, i.e. a dynamics generated according to some probability distribution over time (stochastic process), but in the sense of §1.1.2, i.e. so highly unpredictable to be de facto assimilated to a random process.

$\chi^{(r)} = \{\chi_j\}_{j=1,\dots,r}$. We then end up with a normal form of order ε^r with a remainder of order $\mathcal{O}(\varepsilon^{r+1})$.

Remark 1.2.10. Several variations to this perturbative treatment have been proposed so far and a flourishing literature exists also in the case of resonance dynamics (refer to e.g. [69]). A novel alternative in the framework of the three-body problem is presented in Chapter 3.

1.3 The N -body problem

1.3.1 Kepler's problem

The *two-body problem* (2BP) (or *Kepler's problem*) consists in the motion of two point masses m_0 and m_1 moving under their mutual gravitational attraction in \mathbb{R}^3 equipped with the usual Euclidean metric and an inertial reference frame $OXYZ$. Denoting respectively with R_0, R_1 the two position vectors, and by $r = R_1 - R_0$ their relative position, the force on the mass m_1 (planet) by m_0 (Sun) is given by Newton's law:

$$F = -\mathcal{G} \frac{m_0 m_1}{\|r\|^3} r \quad (1.49)$$

where $\mathcal{G} = 6.6726 \cdot 10^{-11} \text{ Nm}^2 \text{ kg}^{-2}$ is the universal constant of gravitation. The heliocentric vector r fulfils the second-order differential equation

$$\ddot{r} = -\frac{\mathcal{G}(m_0 + m_1)}{\|r\|^3} r. \quad (1.50)$$

Passing to the Hamiltonian formalism giving rise to (1.50), i.e. fixing a co-moving frame $Oxyz$ centered at one of the two masses, say m_0 , so that $r = (x, y, z)$, the two-body problem possesses five independent scalar first integrals (Equation (1.26)) in the six-dimensional phase space $D = (\mathbb{R}^3 \setminus \{0\}) \times \mathbb{R}^3$, three out of which are in involution (Equation (1.27)). Therefore Kepler's problem is completely integrable. The integrals are:

- three components of the *angular momentum* (per unit of mass)

$$\mathcal{M} = (\mathcal{M}_x, \mathcal{M}_y, \mathcal{M}_z) = r \times \dot{r} = (y\dot{z} - z\dot{y}, z\dot{x} - x\dot{z}, x\dot{y} - y\dot{x}). \quad (1.51)$$

An orbit with angular momentum \mathcal{M} lies constantly in a fixed plane, called the *orbital plane*, normal to \mathcal{M} ;

- the *energy* (per unit of mass)

$$\mathcal{E} = \frac{1}{2} \|\dot{r}\|^2 - \frac{\mathcal{G}(m_0 + m_1)}{\|r\|} = \frac{1}{2} (\dot{x}^2 + \dot{y}^2 + \dot{z}^2) - \frac{\mathcal{G}(m_0 + m_1)}{\sqrt{x^2 + y^2 + z^2}}. \quad (1.52)$$

- the *Runge-Lenz vector*

$$\mathcal{L} = (\mathcal{L}_x, \mathcal{L}_y, \mathcal{L}_z) = \dot{r} \times \mathcal{M} - \mathcal{G}(m_0 + m_1) \frac{r}{\|r\|}, \quad (1.53)$$

that represents the constancy of the direction of the *pericenter* (or *periapsis*), the position of closest approach between the two bodies.

As pointed out, only five of these integrals are independent: they can be chosen as $\mathcal{M}_x, \mathcal{M}_y, \mathcal{M}_z, \mathcal{E}, \mathcal{L}_x$. Three can be chosen in involution, $\|\mathcal{M}\|, \mathcal{E}$ and, for example, \mathcal{M}_z .

The Keplerian trajectories are either bounded or unbounded conic sections where m_0 occupies one of the foci and are described by the *polar orbit equation*:

$$\|r(t)\| = \frac{\mathfrak{p}}{1 + e \cos f(t)}, \quad (1.54)$$

where $\mathfrak{p} = \|\mathcal{M}\|^2 / (\mathcal{G}(m_0 + m_1))$ is the conic parameter, $e \geq 0$ the *eccentricity* and $f \in \mathbb{T}$ the *true anomaly*, the angle identifying the actual position of the particle at time t along the orbit since the pericenter (usually coinciding with $f = 0$). Depending on the eccentricity we have either a circle ($e = 0$), an ellipse ($0 < e < 1$), a parabola ($e = 1$), a hyperbola ($e > 1$). In the present thesis we are interested in elliptic motions ($e < 1$, see Fig. 1.4). The ellipse's *semi-major axis* is $a = -\mathcal{G}(m_0 + m_1) / (2\mathcal{E})$, with $\mathcal{E} < 0$; the *semi-minor axis* is $b = a\sqrt{1 - e^2}$. The distance to the pericenter Π is equal to $a(1 - e)$, the distance to the *apocenter* (or *apoapsis*) A is equal to $a(1 + e)$.

Besides the true anomaly, another convenient angle to express the position of the orbiting body in time is the *eccentric anomaly* E (see Fig. 1.4). We have the identities

$$\cos f = \frac{\cos E - e}{1 - e \cos E}, \quad \sin f = \frac{\sqrt{1 - e^2} \sin E}{1 - e \cos E} \quad (1.55)$$

and

$$\|r\| = a(1 - e \cos E). \quad (1.56)$$

The relationship between E and the time t is given by *Kepler's equation* [20]:

$$E - e \sin E = M, \quad M := n(t - t_0), \quad (1.57)$$

where M is called *mean anomaly*,

$$n = \sqrt{\mathcal{G}(m_0 + m_1)} a^{-3/2} \quad (1.58)$$

the *mean motion* and t_0 is the time of passage from the periapsis.

The orientation of the ellipse with respect to $Oxyz$ requires to define three additional angles (Fig. 1.5). The the inclination $i \in [0, \pi[$ of the orbital plane with respect to the x - y plane is given by

$$i = \arccos \left(\frac{\mathcal{M}_z}{\|\mathcal{M}\|} \right).$$

If $i \neq 0$ the orbit intersects the reference plane in two points, called respectively the *ascending node*, where the body passes from negative to positive z , and the *descending node*, where the body goes from positive to negative z . We then

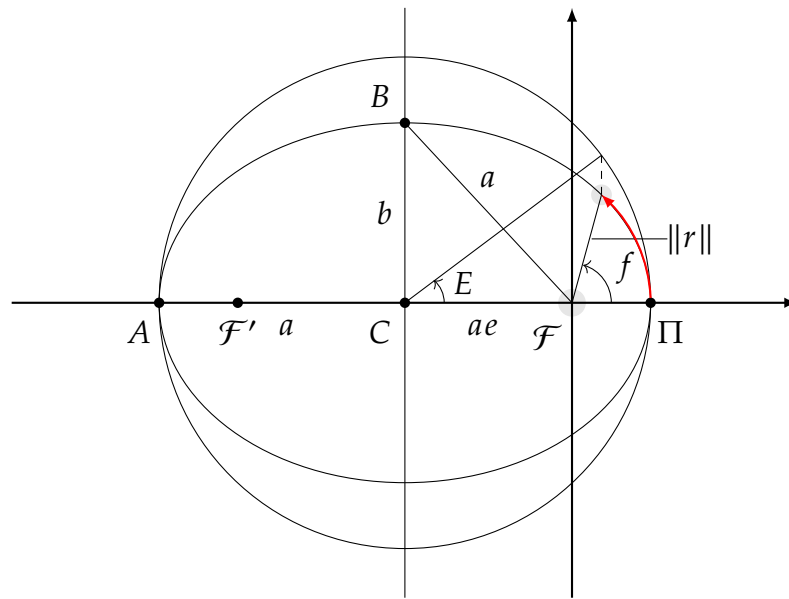


Figure 1.4: Elliptical orbit and its geometric parameters (semi-major axis $a = \overline{CA} = \overline{C\Pi} = \overline{FB}$, eccentricity $e = \overline{CF}/\overline{C\Pi}$, semi-minor axis $b = \overline{CB}$): m_0 is positioned at focus $\mathcal{F} \equiv O$, at distance ae from the center C , while \mathcal{F}' denotes the empty one; m_1 moves on the ellipse counterclockwise from the pericenter Π towards the apocenter A (red arc spanned by the true anomaly f) and E denotes the eccentric anomaly.

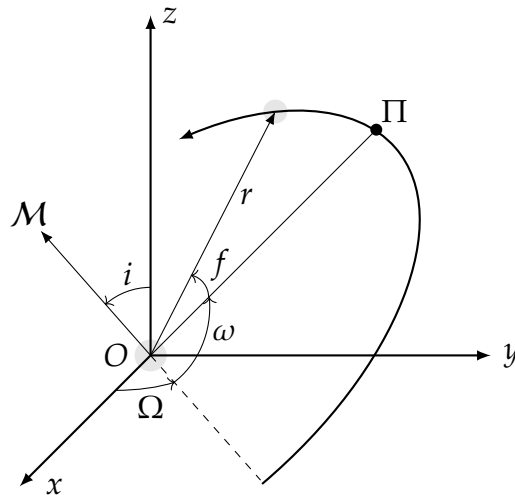


Figure 1.5: Orbit of the 2BP in the 3D $Oxyz$ reference frame. The ellipse is oriented in space through the longitude of the ascending node Ω , the argument of pericenter ω and the inclination i . The intersection between the dotted line (intersection between the orbital plane and the reference plane $x-y$) and the path of m_1 reckoned counterclockwise (direction of the arrow) determines the ascending node.

define the *longitude of the ascending node* $\Omega \in \mathbb{T}$, and the *argument of pericenter* $\omega \in \mathbb{T}$ (see Fig. 1.5).

The variables $a, e, i, \omega, \Omega, M$ (or f), called *orbital elements*, completely define the position and velocity of m_1 with respect to m_0 , that is the mapping

$$\begin{aligned} (\mathbb{R}^3 \setminus \{0\}) \times \mathbb{R}^3 &\longrightarrow]0, +\infty[\times]0, 1[\times]0, \pi[\times \mathbb{T}^3 \\ (x, y, z, \dot{x}, \dot{y}, \dot{z}) &\longmapsto (a, e, i, \omega, \Omega, M) \end{aligned} \quad (1.59)$$

is a bijection (see [73]). The transformation from the elements to the state vector (r, \dot{r}) is given by

$$r = \mathcal{R} \begin{pmatrix} a(\cos E - e) \\ a\sqrt{1-e^2} \sin E \\ 0 \end{pmatrix}, \quad \dot{r} = \mathcal{R} \begin{pmatrix} -\frac{na \sin E}{1-e \cos E} \\ \frac{na\sqrt{1-e^2} \cos E}{1-e \cos E} \\ 0 \end{pmatrix}, \quad (1.60)$$

where

$$\mathcal{R} = \begin{pmatrix} c\Omega c\omega - s\Omega ci s\omega & -c\Omega s\omega - s\Omega ci c\omega & s\Omega si \\ s\Omega c\omega + c\Omega ci s\omega & -s\Omega s\omega + c\Omega ci c\omega & -c\Omega si \\ si s\omega & si c\omega & ci \end{pmatrix}, \quad (1.61)$$

$c \cdot, s \cdot$ are abbreviations for $\cos \cdot, \sin \cdot$ and the dependence on M is obtained through E via (1.57).

In the cases $i = 0$ and $e = 0$ two singularities appear: in the former the line of nodes is not well-defined, and so Ω, ω are, while in the latter the periapsis is not unique (circular orbit), hence ω, M are undefined. To deal with the case, we consider angles

$$\varpi := \omega + \Omega, \quad \lambda := M + \omega + \Omega, \quad (1.62)$$

named respectively *longitude of the pericenter* and *mean longitude*. In particular, λ is well-defined if $e = 0, i \neq 0$, and absent from the transformation (1.60) if $i = e = 0$.

The Hamiltonian formulation of Kepler's problem

$$\mathcal{H}_{\text{E2BP}}(r, p) = \frac{1}{2} \|p\|^2 - \frac{\mathcal{G}(m_0 + m_1)}{\|r\|} = -\frac{\mathcal{G}(m_0 + m_1)}{2a} < 0, \quad (1.63)$$

with $p = \dot{r}$, is Liouville-Arnold integrable, so we can derive action-angle variables from it. Their expressions are

$$\begin{aligned} L &= \sqrt{\mathcal{G}(m_0 + m_1)a}, & \ell &= M, \\ G &= L\sqrt{1-e^2}, & g &= \omega, \\ H &= G \cos i, & h &= \Omega, \end{aligned} \quad (1.64)$$

called *Delaunay variables* (or *Delaunay elements*). We have $G = \|\mathcal{M}\|$ and $H = \mathcal{M}_z$. $\mathcal{H}_{\text{E2BP}}$ in these new variables reads

$$\mathcal{H}_{\text{E2BP}}(r(\ell, g, h, L, G, H), p(\ell, g, h, L, G, H)) = -\frac{\mathcal{G}^2(m_0 + m_1)^2}{2L^2}. \quad (1.65)$$

Delaunay variables become singular when $e = 0$ or $i = 0$. Thus, we need the *modified Delaunay variables*:

$$\begin{aligned} \Lambda &= L, & \lambda &= M + \omega, \\ \Gamma &= \Lambda(1 - \sqrt{1 - e^2}), & \gamma &= -\omega, \\ Z &= \Gamma(1 - \cos i), & \zeta &= -\Omega. \end{aligned} \quad (1.66)$$

The singularities now correspond to the fact that the angles γ and ζ are multi-valued whenever their corresponding actions are null. This is bypassed by the use of Cartesian-like variables known as *Poincaré variables*:

$$\begin{aligned} \Lambda, & & \lambda, \\ \xi &= \sqrt{2\Gamma} \cos \gamma, & \eta &= \sqrt{2\Gamma} \sin \gamma, \\ v &= \sqrt{2Z} \cos \zeta, & \vartheta &= \sqrt{2Z} \sin \zeta. \end{aligned} \quad (1.67)$$

1.3.2 The planetary N -body problem

The Hamiltonian of the planetary N -body problem (NBP) is given by

$$\mathcal{H}_{\text{NBP}}(r_0, \dots, r_{N-1}, p_0, \dots, p_{N-1}) = \frac{1}{2} \sum_{i=0}^{N-1} \frac{\|p_i\|^2}{2m_i} - \mathcal{G} \sum_{0 \leq i < j \leq N-1} \frac{m_i m_j}{\|r_i - r_j\|}, \quad (1.68)$$

where $(r_i, p_i) \in \mathbb{R}^6$, $i = 0, \dots, N-1$, are barycentric conjugate variables and $m_0 \gg m_i$, $i = 1, \dots, N-1$. This problem for $N \geq 3$ is not integrable.

Assigning m_0 as the mass of the central star, the perturbative parameter of the problem is

$$\mu = \max_{i=1, \dots, N-1} \mu_i,$$

where $\mu_i = m_i/m_0 \ll 1$.

We reduce the d.o.f. by 3 passing to heliocentric coordinates Q_i and extend canonically the change of variables to construct the new momenta P_i :

$$\begin{aligned} Q_0 &= r_0, & Q_i &= r_i - r_0, & i &= 1, \dots, N-1, \\ p_0 &= P_0 - \sum_{j=1}^{N-1} P_j, & p_i &= P_i, & i &= 1, \dots, N-1. \end{aligned}$$

In particular $P_0 = \sum_{j=0}^{N-1} p_j$ is the total linear momentum and since it is conserved we can limit ourselves to study the dynamics corresponding to $P_0 = 0$. The heliocentric Hamiltonian of the planetary N -body problem then reads

$$\begin{aligned} \mathcal{H}_{\text{HelNBP}}(Q_1, \dots, Q_{N-1}, P_1, \dots, P_{N-1}) &= \sum_{i=1}^{N-1} \left(\frac{1}{2} \left(\frac{1}{m_0} + \frac{1}{m_i} \right) \|P_i\|^2 - \mathcal{G} \frac{m_0 m_i}{\|Q_i\|} \right) \\ &+ \sum_{1 \leq i < j \leq N-1} \left(\frac{P_i \cdot P_j}{m_0} - \mathcal{G} \frac{m_i m_j}{\|Q_i - Q_j\|} \right) \end{aligned} \quad (1.69)$$

on the collisionless domain

$$D = \{(Q_1, \dots, Q_{N-1}, P_1, \dots, P_{N-1}) \in \mathbb{R}^{6(N-1)} : Q_i \neq 0 \forall i, Q_i \neq Q_j \forall i, j\}. \quad (1.70)$$

The first summation in (1.69) is a sum of $N - 1$ decoupled 2BP (1.63) each multiplied by \bar{m}_i with masses m_0, m_i and re-scaled gravitational constant $\mathcal{G}\bar{m}_i^2$, where $\bar{m}_i = m_0 m_i / (m_0 + m_i)$ is the reduced mass. Keplerian action-angle variables (like Delaunay elements, etc.) thus can be introduced in a suitable domain far from collisions in a similar manner as at the end of §1.3.1.

1.3.3 The restricted three-body problem

A simplified version of the N -body problem, yet interesting and highly non-trivial, is the so called *restricted N -body problem* (RNBP), in which we analyze the motion of a body of negligible mass under the gravitational forces of the Sun and of $N - 2$ planets in given orbits, typically assumed to be circular or elliptic. Basically we focus on the dynamics of a single massless body under the effect of $N - 2$ uncoupled elliptic 2BP, whose Hamilton's function in heliocentric variables is written as

$$\mathcal{H}_{\text{RNBP}}(Q, P, t) = \frac{\|P\|^2}{2} - \frac{\mathcal{G}m_0}{\|Q\|} - \mathcal{G} \sum_{i=1}^{N-2} m_i \left(\frac{1}{\Delta_i(t)} - \frac{Q \cdot Q_i(t)}{\|Q_i(t)\|^3} \right), \quad (1.71)$$

for $(Q, P) \in \mathbb{R}^6$ position-momentum couple of the particle, $\Delta_i(t) = \|Q - Q_i(t)\|$, $i = 1, \dots, N - 2$, and $Q_i(t)$ the i -th given heliocentric two-body motion whose magnitude is computed according to (1.54) and $p_i = a_i(1 - e_i^2)$. The structure of the Hamiltonian $\mathcal{H}_{\text{RNBP}}$ is also the one of a quasi-integrable system: the first two addenda give the Keplerian part, while the rest represents a small perturbation, since, under the planetary model assumption, it is proportional to $m_i \ll m_0$.

Remark 1.3.1. The Hamiltonian (1.71) is non-autonomous. However, introducing the planetary mean motions n_i of the 2BPs involved: one then introduces mean anomalies $M_i = n_i t$ and conjugate momenta J_i , $i = 1, \dots, N - 2$, (1.71) can be extended to a formally autonomous model

$$\begin{aligned} \mathcal{H}'_{\text{RNBP}}(Q, M_1, \dots, M_{N-2}, P, J_1, \dots, J_{N-2}) \\ = \mathcal{H}_{\text{RNBP}}(Q, P, M_1, \dots, M_{N-2}) + \sum_{i=1}^{N-2} n_i J_i. \end{aligned}$$

It is trivial to check that the equations of motion for Q and P under $\mathcal{H}'_{\text{RNBP}}$ are identical with those under $\mathcal{H}_{\text{RNBP}}$.

The case $N = 3$, named *restricted three-body problem* (R3BP hereafter), is a cornerstone model extensively studied which carries a highly non-trivial

dynamics.

The Hamiltonian of the R3BP is provided by (1.71) after setting $N = 3$:

$$\mathcal{H}_{\text{R3BP}}(Q, P, t) = \frac{\|P\|^2}{2} - \frac{\mathcal{G}m_0}{\|Q\|} - \mathcal{G}m_1 \left(\frac{1}{\Delta(t)} - \frac{Q \cdot Q_1(t)}{\|Q_1(t)\|^3} \right), \quad (1.72)$$

where, to ease notation, we drop labels for quantities referring to the test particle \mathcal{P} of null mass $m \equiv m_2 = 0$ and simply put $\Delta = Q - Q_1$. The two massive bodies \mathcal{P}_0 and \mathcal{P}_1 with masses $m_0 > m_1$ are called respectively *primary* (or *central mass*) and *secondary* (or *primary perturber*) (together simply the *primaries*). The perturbative part dependent on m_1 in (1.72) is the *disturbing function of the R3BP* and is responsible for all the interesting dynamical peculiarities of the problem; for this reason it lends itself to several manipulations, like series expansion (see [13] and Chapter 3) in order to decompose the various perturbing effects.

Let us select now as Keplerian orbit performed by \mathcal{P}_0 and \mathcal{P}_1 a circular trajectory: this is called the *Circular Restricted 3-Body Problem* (CR3BP). The study of the CR3BP is simplified by passing to a suitably defined rotating frame. Consider:

- a non-inertial, called also *synodic*, Cartesian reference frame centered at the barycenter of the system (that we keep denoting by $Oxyz$), and rotating at uniform speed so that its x axis contains \mathcal{P}_0 and \mathcal{P}_1 for all times t , hence x - y coincides with the orbital plane of the Keplerian motion (Fig. 1.6);
- a unit of time so that the revolution period of the \mathcal{P}_0 - \mathcal{P}_1 2BP is $T_1 = 2\pi$ and thus the angular speed is $n_1 = 1$;
- the primary and the secondary particles have masses respectively $m_0 = 1 - \mu$ and $m_1 = \mu$, with

$$\mu = \frac{m_1}{m_0 + m_1} \in]0, 1/2] \quad (1.73)$$

the mass parameter (or reduced mass), such that the unit of mass is given by $m_0 + m_1 = 1$;

- \mathcal{P}_0 and \mathcal{P}_1 located on the x axis with coordinates $\mathcal{P}_0(-\mu, 0, 0)$ and $\mathcal{P}_1(1 - \mu, 0, 0)$, which in turn determine the unit of distance $\overline{\mathcal{P}_0\mathcal{P}_1} = 1$.

In the above units we have $\mathcal{G} = 1$. The resulting Hamiltonian in symplectic variables

$$(x, y, z), (p_x, p_y, p_z) \in (\mathbb{R}^3 \setminus \{(-\mu, 0, 0), (1 - \mu, 0, 0)\}) \times \mathbb{R}^3, \\ dx \wedge dp_x + dy \wedge dp_y + dz \wedge dp_z,$$

becomes autonomous:

$$\mathcal{H}(x, y, z, p_x, p_y, p_z) = \frac{p_x^2 + p_y^2 + p_z^2}{2} + p_x y - p_y x - \frac{1 - \mu}{d_0} - \frac{\mu}{d_1}, \quad (1.74)$$

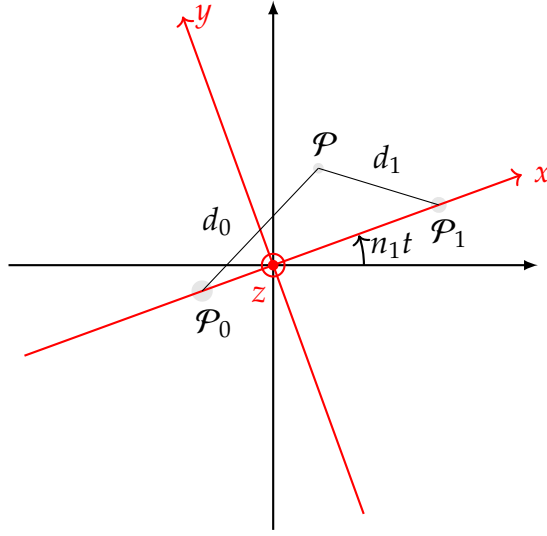


Figure 1.6: The co-rotating synodic reference frame (in red) rotating at radial frequency n_1 with outgoing z axis showing the configuration of the CR3BP; the inter-distances are indicated by $d_0 = \overline{\mathcal{P}_0\mathcal{P}}$ and $d_1 = \overline{\mathcal{P}_1\mathcal{P}}$.

where

$$\begin{aligned} d_0 &= \|\mathcal{P} - \mathcal{P}_0\| = \sqrt{(x + \mu)^2 + y^2 + z^2} \\ d_1 &= \|\mathcal{P} - \mathcal{P}_1\| = \sqrt{(x - 1 + \mu)^2 + y^2 + z^2} \end{aligned} \quad (1.75)$$

denote the distances of $\mathcal{P}(x, y, z)$ from \mathcal{P}_0 and \mathcal{P}_1 .

No smooth global first integrals exist besides the Hamiltonian itself, usually called, in terms of the velocity $(\dot{x}, \dot{y}, \dot{z})$, *Jacobi integral*:

$$E_J = \mathcal{H} \Big|_{p_x=\dot{x}-y, p_y=\dot{y}+x, p_z=\dot{z}} = \frac{1}{2}(\dot{x}^2 + \dot{y}^2 + \dot{z}^2) + \mathcal{U}(x, y, z), \quad (1.76)$$

in which

$$\mathcal{U}(x, y, z) = -\frac{1}{2}(x^2 + y^2) + \mathcal{V}(x, y, z) = -\frac{1}{2}(x^2 + y^2) - \frac{1-\mu}{d_0} - \frac{\mu}{d_1} \quad (1.77)$$

is the *effective potential*. The *Jacobi constant* is defined as $C_J = -2E_J$. Its importance is twofold: on one hand, although the CR3BP is not Liouville-Arnold integrable (§1.3.2), the first integral can be exploited to obtain some relevant information and restrictions about the dynamics; on the other hand, in dynamical astronomy C_J is historically well-known to be useful in the study of orbits of small particles under the influence of a planet (e.g. Jupiter in our solar system, cf. [73]). In particular, due to the conservation of the Jacobi constant, the quantity

$$\mathcal{T}(a, e, i) = \frac{1}{a} + 2\sqrt{a(1-e^2)} \cos i \quad (1.78)$$

called *Tisserand's parameter* (see [10] for a review) remains approximately constant before and after the encounter of the small particle with the planet (Fig.

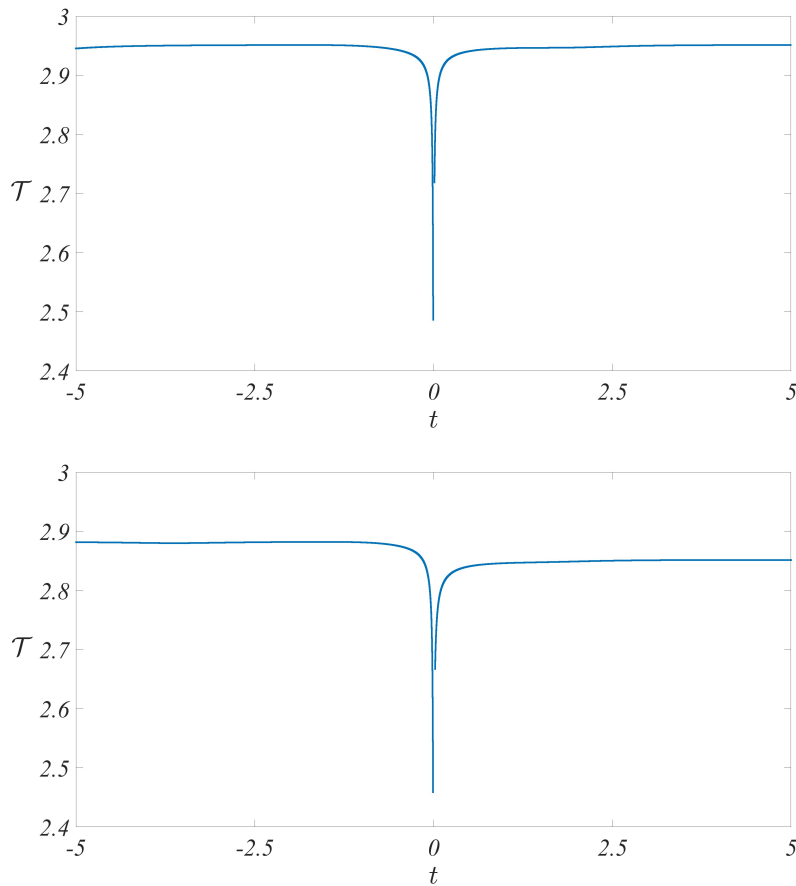


Figure 1.7: Tisserand's parameter for a small body in the circular and elliptic Sun-Jupiter R3BP with close encounter at $t = 0$ ($\mu = 9.536433730801362 \cdot 10^{-4}$). The initial conditions are $x(0) = 1.0009678077067754$, $y(0) = 0$, $z(0) = 0$, $p_x(0) = 0.2$, $p_y(0) = 1.8$, $p_z(0) = 0.6$, then the orbit is propagated backward and finally forward in time to get a full deflection. **Top panel:** zero Jupiter's eccentricity (CR3BP). **Bottom panel:** Jupiter's eccentricity equal to 0.0489 (ER3BP).

1.7). In Jupiter's case, \mathcal{T} is frequently applied to distinguish asteroids (typically $\mathcal{T} > 3$) from Jupiter-family comets (typically $2 < \mathcal{T} < 3$).

In reality, although (1.78) is only an approximation to the Jacobi constant and is derived by assuming that Jupiter is in a circular orbit (CR3BP), the quantity \mathcal{T} is still an approximate constant of the motion in the case where the eccentricity of Jupiter is taken with its actual nonzero value, i.e. considering an *Elliptic Restricted 3-Body problem* (ER3BP, see §2.3.1). An example is shown in Fig. 1.7.

As claimed above, (1.76) constrains the phase space: to be precise, a solution $(x(t), y(t), z(t), p_x(t), p_y(t), p_z(t))$ of Hamilton's equations associated to (1.74) characterized by a value $\bar{E}_J \in \mathbb{R}$ of E_J is forced to project for any time t in the portion of space:

$$\mathcal{A}(\bar{E}_J) = \{(x, y, z) \in \mathbb{R}^3 \setminus \{(-\mu, 0, 0), (1 - \mu, 0, 0)\} : \mathcal{U}(x, y, z) \leq \bar{E}_J\}, \quad (1.79)$$

called *admissible region*. Its complement $\mathbb{R}^3 \setminus \mathcal{A}(\bar{E}_J)$ is the *forbidden region*. The

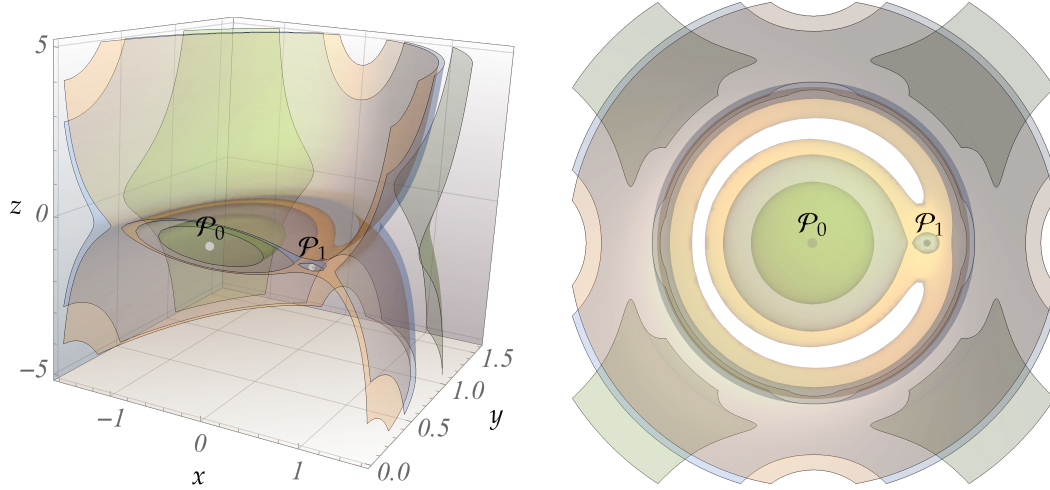


Figure 1.8: Zero-velocity surfaces of the spatial CR3BP. **Left panel:** cross-section of three zero-velocity surfaces around the primary and secondary for $\mu = 0.01$ (close to the mass parameter of the Earth-Moon system) in the regimes described in text. The green surface is obtained for $\bar{E}_J = -2$ and delimits the realm of motions only around \mathcal{P}_0 or exterior to \mathcal{P}_0 - \mathcal{P}_1 ; the blue one surrounds the two disconnected realms of motions around \mathcal{P}_0 and \mathcal{P}_1 or the external realm and is obtained for $\bar{E}_J = -1.587$; the orange one creates a channel opening allowing transits between the realms of the two bodies and transits which go outwards and is obtained for $\bar{E}_J = -1.51$. **Right panel:** top view of the three-dimensional zero-velocity surfaces projected onto the x - y plane and plotted with low opacity to visualize the self-contained lobes for the three different values of \bar{E}_J at issue. The admissible regions are the set of points enclosed by the lobes around \mathcal{P}_0 , \mathcal{P}_1 or outside the double paraboloid-like shapes.

boundary of the admissible region $\partial\mathcal{A}(\bar{E}_J)$ is defined by the equation

$$\mathcal{U}(x, y, z) = \bar{E}_J \quad (1.80)$$

and therefore the trajectory $(x(t), y(t), z(t))$ can hit $\partial\mathcal{A}(\bar{E}_J)$ when the kinetic part in (1.76) is equal to zero, i.e. when $\dot{x} = \dot{y} = \dot{z} = 0$. For this reason the surfaces defined by (1.80) are called *zero-velocity surfaces* (in the spatial case, otherwise when the dynamics develops only in two dimensions in the orbital plane, that is considering a planar CR3BP, they are usually known as *zero-velocity curves*). The topology of the admissible region, highly dependent on the value of \bar{E}_J , is important to properly understand the dynamics taking place: we have the following three scenarios.

- (i) $\mathcal{A}(\bar{E}_J)$ corresponds to the whole physical space $\mathbb{R}^3 \setminus \{(-\mu, 0, 0), (1-\mu, 0, 0)\}$ if $\bar{E}_J \geq \max_{(x,y,z)} \mathcal{U}(x, y, z)$; for these large values, the energy integral does not actually constrain the path $(x(t), y(t), z(t))$.
- (ii) For suitably small values of \bar{E}_J , the admissible region is made up of three disconnected components (Fig.1.8), in particular the region of the motions

which are satellite of \mathcal{P}_0 , the region of the motions which are satellite of \mathcal{P}_1 and the region of motions which are external to the binary system \mathcal{P}_0 - \mathcal{P}_1 . Any motion of energy \bar{E}_J with $(x(0), y(0), z(0))$ in the region of the satellites of \mathcal{P}_0 will never visit the region of satellites of \mathcal{P}_1 . To have an orbit which transits between the two regions one has to consider larger values.

- (iii) For lower values of \bar{E}_J , the admissible region asymptotically shrinks to two disconnected components and eventually one: the realm of motions around \mathcal{P}_0 and the external one, with the second one eventually taking over (Fig.1.8).

We can even better characterize $\mathcal{A}(\bar{E}_J)$ by looking at the critical points of the effective potential, the *Lagrangian points*.

Proposition 1.3.1. *For any value of $\mu \in]0, 1/2]$, the effective potential $\mathcal{U}(x, y, z)$ has five critical points:*

$$L_1(x_{L_1}, 0, 0), \quad L_2(x_{L_2}, 0, 0), \quad L_3(x_{L_3}, 0, 0),$$

which are saddle points for \mathcal{U} and are named collinear points, where

$$x_{L_3} < -\mu < x_{L_1} < 1 - \mu < x_{L_2}$$

and $x_{L_1}, x_{L_2}, x_{L_3}$ are found as the solutions of

$$(1 - \mu) \frac{x + \mu}{|x + \mu|^3} + \mu \frac{x - 1 + \mu}{|x - 1 + \mu|^3} = x;$$

$$L_4(x_{L_4}, y_{L_4}, 0), \quad L_5(x_{L_5}, y_{L_5}, 0),$$

which are local (and absolute) maxima for \mathcal{U} and are named equilateral points, with

$$x_{L_4} = x_{L_5} = \frac{1}{2} - \mu, \quad y_{L_4} = -y_{L_5} = \frac{\sqrt{3}}{2}.$$

The indices attributed to L_1, L_2, L_3 and L_4, L_5 reflect the ordering of the corresponding value of the value of the effective potential, i.e.

$$\begin{aligned} \mathcal{U}(x_{L_5}, y_{L_5}, z_{L_5}) = \mathcal{U}(x_{L_4}, y_{L_4}, z_{L_4}) &> \mathcal{U}(x_{L_3}, y_{L_3}, z_{L_3}) \\ &> \mathcal{U}(x_{L_2}, y_{L_2}, z_{L_2}) > \mathcal{U}(x_{L_1}, y_{L_1}, z_{L_1}). \end{aligned}$$

This gives further information on the topology of the zero-velocity curves/surfaces (Fig. 1.9).

Besides, one can promptly realize that these configurations, complemented by $\dot{x}_{L_j} = \dot{y}_{L_j} = \dot{z}_{L_j} = 0, j = 1, \dots, 5$, are equilibria for the Lagrange's equations of motion.⁶ The corresponding orbits in the inertial reference frame will be circular periodic orbits and the mutual distances d_0, d_1 in (1.75) remain constant in time. It comes natural then to inspect the motion in the vicinity of equilibrium

⁶Or equivalently for the Hamilton's equations with $p_{x_{L_j}} = -y_{L_j}, p_{y_{L_j}} = x_{L_j}, p_{z_{L_j}} = 0, j = 1, \dots, 5$.

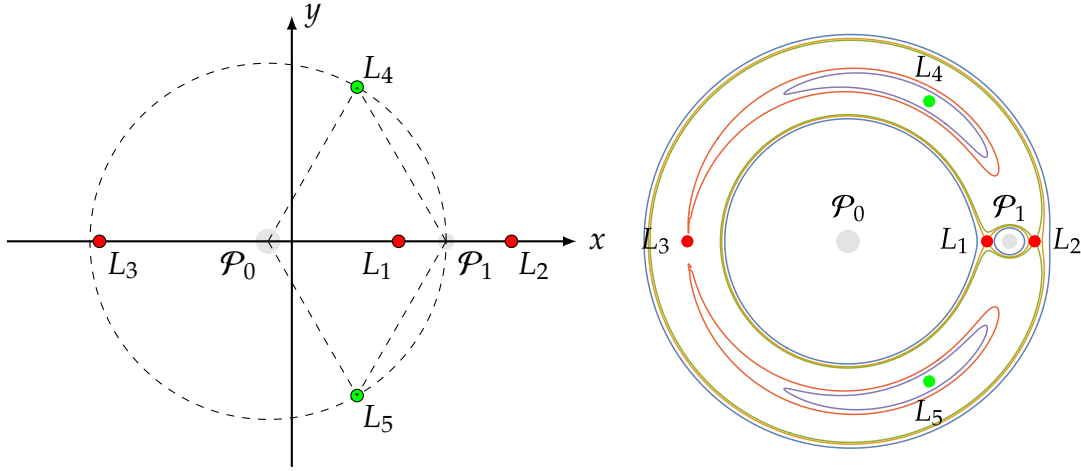


Figure 1.9: Lagrangian points of the CR3BP and zero-velocity curves in the planar case. **Left panel:** location of the five Lagrangian critical points. The red dots stand for the collinear points, being aligned along the x axis, while the green ones stand for the equilateral points, since they have same distance from \mathcal{P}_0 and \mathcal{P}_1 equal to $\overline{\mathcal{P}_0\mathcal{P}_1} = 1$, thus they are positioned on one of the vertices of two equilateral triangles. **Right panel:** zero-velocity curves for the planar CR3BP. The iso-lines are computed for $\mu = 0.01$ in ascending order of Jacobi energy $\bar{E}_J \in \{-1.6, -1.5838, -1.5772, -1.5050, -1.50\}$, where $-1.6 < \mathcal{U}(x_{L_1}, y_{L_1})$ (blue contour), $-1.5838 = \mathcal{U}(x_{L_1}, y_{L_1})$ (ocher contour), $-1.5772 = \mathcal{U}(x_{L_2}, y_{L_2})$ (green contour), $-1.5050 = \mathcal{U}(x_{L_3}, y_{L_3})$ (red contour), $\mathcal{U}(x_{L_3}, y_{L_3}) < -1.50 < \mathcal{U}(x_{L_4}, y_{L_4})$ (violet contour). For $\mathcal{U}(x_{L_4}, y_{L_4}) = \mathcal{U}(x_{L_5}, y_{L_5})$, the two violet “tadpoles” shrink to L_4, L_5 and from this value on all motions are permitted. The global picture gives an intuition on how the topology of the admissible/forbidden region changes around the Lagrangian points along with \bar{E}_J . For clear symmetry reasons, the spatial analogues behave accordingly.

positions, namely to study their linear stability.

Let us linearize the equations of motion at $L_j, j = 1, \dots, 5$. We limit ourselves to the investigation in the planar case. Combining Hamilton's equations of (1.74) (dropping the couple (z, p_z)), the coordinates $x(t), y(t)$ of \mathcal{P} solve

$$\ddot{x} - 2\dot{y} = -\frac{\partial \mathcal{U}}{\partial x}(x, y), \quad \ddot{y} + 2\dot{x} = -\frac{\partial \mathcal{U}}{\partial y}(x, y),$$

or

$$\begin{cases} \dot{x} = v_x \\ \dot{y} = v_y \\ \dot{v}_x = 2v_y - \frac{\partial \mathcal{U}}{\partial x}(x, y) \\ \dot{v}_y = -2v_x - \frac{\partial \mathcal{U}}{\partial y}(x, y) \end{cases} . \quad (1.81)$$

The Jacobian matrix of the vector field defined by the right-hand sides of (1.81) reads

$$A(x, y, v_x, v_y) = \begin{pmatrix} 0 & 0 & 1 & 0 \\ 0 & 0 & 0 & 1 \\ -\frac{\partial^2 \mathcal{U}}{\partial x^2} & -\frac{\partial^2 \mathcal{U}}{\partial x \partial y} & 0 & 2 \\ -\frac{\partial^2 \mathcal{U}}{\partial y \partial x} & -\frac{\partial^2 \mathcal{U}}{\partial y^2} & -2 & 0 \end{pmatrix} \quad (1.82)$$

and we need to find eigenvalues and eigenvectors at each point $(x_{L_j}, y_{L_j}, 0, 0)$, $j = 1 \dots, 5$. We have the following.

Proposition 1.3.2. *For $0 < \mu < \mu_R$ the equilateral equilibrium points L_4, L_5 are linearly stable with purely imaginary eigenvalues*

$$\lambda_{1,2} = \pm i \sqrt{\frac{1 + \sqrt{1 - 27\mu + 27\mu^2}}{2}}, \quad \lambda_{3,4} = \pm i \sqrt{\frac{1 - \sqrt{1 - 27\mu + 27\mu^2}}{2}},$$

where

$$\mu_R = \frac{9 - \sqrt{69}}{18} \approx 0.038$$

is the Routh's critical value.

The collinear equilibrium points L_1, L_2, L_3 have linearization matrix (1.82) with eigenvalues

$$\lambda_{1,2} = \pm \sqrt{\frac{\sqrt{(\alpha_1 + \alpha_2 + 4)^2 - 4\alpha_1\alpha_2} - \alpha_1 - \alpha_2 - 4}{2}},$$

$$\lambda_{3,4} = \pm i \sqrt{\frac{\sqrt{(\alpha_1 + \alpha_2 + 4)^2 - 4\alpha_1\alpha_2} + \alpha_1 + \alpha_2 + 4}{2}},$$

where

$$\alpha_1 = -1 - \frac{2(1-\mu)}{|x_{L_j} + \mu|^3} - \frac{2\mu}{|x_{L_j} - 1 + \mu|^3},$$

$$\alpha_2 = \frac{1-\mu}{|x_{L_j} + \mu|^3} + \frac{\mu}{|x_{L_j} - 1 + \mu|^3} - 1, \quad j = 1, 2, 3,$$

which are pairwise opposite real and opposite purely imaginary, i.e. they are partially hyperbolic equilibria (Definition 1.1.7) with $\dim E^s = 1$, $\dim E^u = 1$, $\dim E^c = 2$ (§1.1.4).

For details on Proposition 1.3.2 see, for example, [73]. In the case of the Sun-Jupiter system, the class of minor bodies orbiting nearby L_4 and L_5 are called (Jupiter's) *Trojan asteroids*. Relative to Jupiter, these objects librate in tadpole-shaped regions co-orbital with Jupiter with average semi-major axis of about 5.2 AU around one of the equilateral points, either 60° ahead of the planet or 60° behind. Their study has a long history in the literature, especially regarding their chaotic nature (cf., e.g., [58, 59, 70, 88]). The topic is treated in Chapter 5 in relation to the question of the asymmetry in their distribution around the two regions of L_4 and L_5 .

Linear stability results are applicable in very small domains, where the linearization of the system is a valid approximation. More general results can be formulated only by the use of non-linear stability theorems (Remark 1.2.9) or by numerical analysis of the orbits.

We conclude the subsection with a short recap on interesting types of orbits in the planar CR3BP and hyperbolic structures stemming from the collinear Lagrangian points (cf. Fig. 1.10). We can give the following classification:

- If $\bar{E}_{J_{L_3}} < \bar{E}_J < \bar{E}_{J_{L_4}}$, the motion in the proximity of L_4/L_5 is energetically allowed to take place surrounding the equilateral points only (although it is not energetically restricted to do so); however, if $\bar{E}_J < \bar{E}_{J_{L_3}}$ the orbits necessarily surround all the three points L_3, L_4, L_5 , thus this distinction raises two different kinds of motion in the neighborhood of the equilateral points, known as *tadpole orbits* (the former) and *horseshoe orbits* (the latter). Their dynamics is characterized, in the linear approximation, by a decomposition of two different contributions: the slow motion, associated to the motion of a *guiding center* around the position of equilibrium, with long period $\approx 2\pi/|\operatorname{Im} \lambda_{3,4}|$ and $\lambda_{3,4}$ as in Proposition 1.3.2 for L_4/L_5 , known as *synodic libration*, and the fast one, attributed to the short period motion of the particle around the guiding center.
- Families of periodic orbits associated to linearized centers around L_4, L_5 and central invariant structures due to the partially hyperbolic character around L_1, L_2, L_3 , still persisting in the original non-linear extension. There are also other groups of periodic orbits not associated with a particular Lagrangian point: resonant orbits, i.e. the ratio between the Keplerian period of \mathcal{P} around the primary and the Keplerian period of

the secondary around the primary is a rational number, or \mathcal{P}_1 -centered orbits, originating from the secondary body's dynamical neighborhood. Notably, among these collections we mention

- the *Lyapunov orbits* of L_1, L_2 or L_3 (which extend to *halo orbits* in the 3D case), indicated respectively by PL_1, PL_2, PL_3 and existing for any $\bar{E}_j \in]\bar{E}_{L_j}, \bar{E}_{L_j} + \epsilon[$, $j = 1, 2, 3$, $\epsilon = \epsilon(\mu) > 0$;
 - the *short and long period orbits* stemming from L_4 and L_5 .
- L_1, L_2, L_3 are partially hyperbolic equilibria for (1.81) (§1.1.4), therefore for any value of the reduced mass $\mu \in [0, 1/2[$, besides a two-dimensional differentiable center manifold W^c tangent at each L_j , $j = 1, 2, 3$, to its center space E^c which gives birth to the Lyapunov orbits, there exist smooth stable and unstable manifolds W^s, W^u made of two tubes, on both sides of the Lyapunov orbit, locally diffeomorphic to cylinders $\mathbb{S}^1 \times \mathbb{R}$ (\mathbb{S}^1 denoting the unit circle). Instead, the global structure, as it happens for stable and unstable manifolds in non-integrable systems, may be very complicated due to the presence of folds and lobes, and its projections are essentially visualized by integrating numerically the flow backward and forward. Moreover, the stable and unstable manifolds of PL_1 and PL_2 intersect transversely, providing orbits which are homoclinic to PL_1 , to PL_2 , or heteroclinic orbits, i.e. orbits which in the future converge to one Lyapunov orbit and in the past to a different one (§1.1.4). This has considerable implications in space mission design by cleverly maneuvering the spacecraft (see e.g. [18, 36]). Indeed, such a geometry enables one to move
 - from the realm of motions around L_1 , following W^s of PL_1 , close to PL_1 ;
 - from a neighborhood of PL_1 to a neighborhood of PL_2 following a heteroclinic orbit;
 - from PL_2 to the external region following W^u of PL_2 .

We note that all results regarding the existence and stability of the Lagrangian fixed points can be extended from the circular to the elliptic R3BP using a “pulsating and non-uniformly rotating” reference system (see Appendix A). In that case, the equilibria correspond to periodic orbits in the uniformly rotating system of reference whose angular velocity is equal to the mean motion of the primary perturber. On the other hand, the Lyapunov families of the CR3BP generalize to 2D-hyperbolic tori in the ER3BP (see [76] and references therein).

1.4 Goal and structure of the thesis

From what was exposed in these introductory paragraphs, it becomes clear that the challenging dynamical phenomenology of the R3BP gives rise to a necessity for methods of study based on an interplay between analytical and numerical

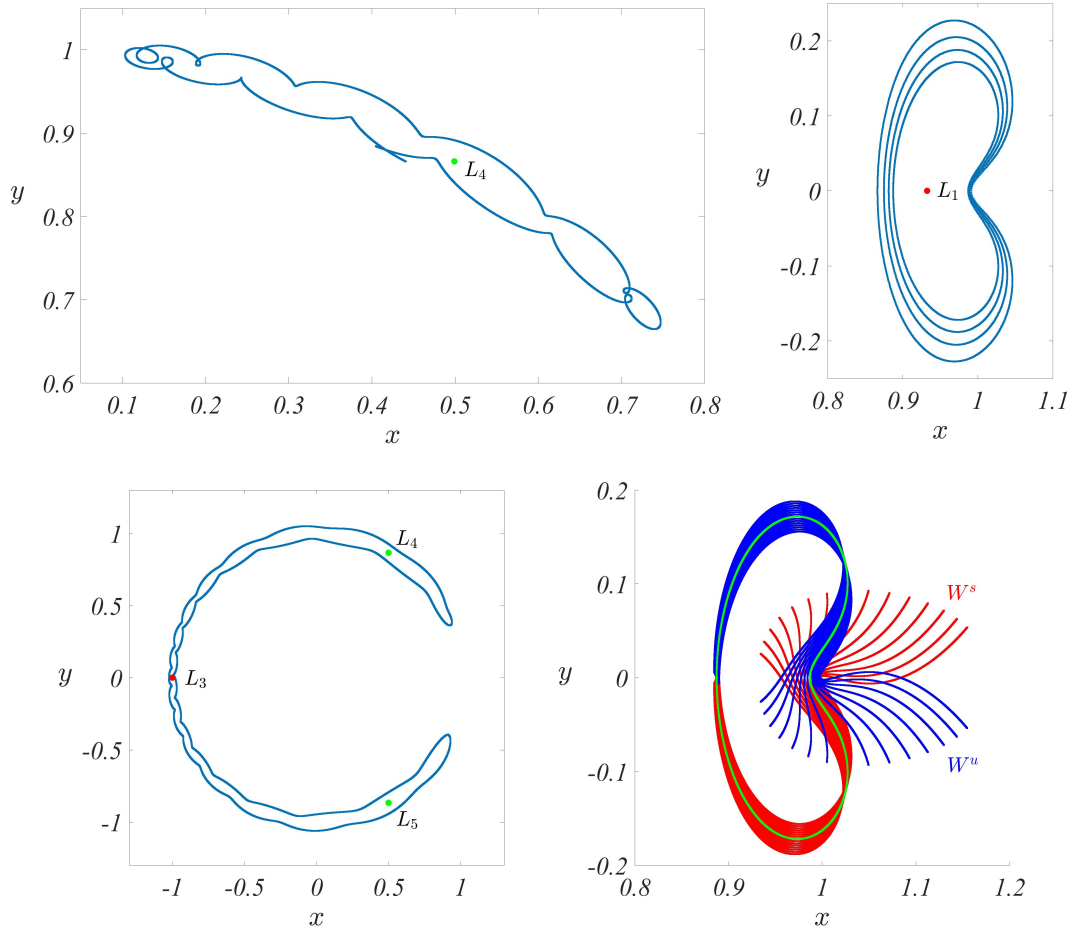


Figure 1.10: Some orbits of the planar CR3BP for $\mu = 9.536433730801362 \cdot 10^{-4}$ (Sun-Jupiter system). **Top left panel:** tadpole orbit around L_4 integrated with $\bar{E}_J = -1.4996$ s.t. $\bar{E}_{J_{L_3}} < \bar{E}_J < \bar{E}_{J_{L_4}}$. The initial conditions are $(x(0), y(0), p_x(0), p_y(0)) = (0.44075, 0.86597, -0.908, 0.46215)$. **Top right panel:** collection of PL_1 Lyapunov orbits for decreasing energy values starting from $\bar{E}_J = -1.498943763343622$. **Bottom left panel:** horseshoe orbit embracing L_3, L_4, L_5 for $\bar{E}_J = -1.500518632470854 < \bar{E}_{J_{L_3}}$ and initial conditions $(x(0), y(0), p_x(0), p_y(0)) = (-1.02445, 0, 0, -0.98413)$. **Bottom right panel:** orbits in the branches of the stable (red) and unstable (blue) tube manifolds relative to PL_1 (green) at energy $\bar{E}_J = -1.498943763343622$. In the vicinity of the Lyapunov orbit we can appreciate the local topology of the projection of the manifolds W^s and W^u , which are diffeomorphic to cylinders.

approaches.

In view of the above, we now state the main goal of the thesis, which is the development of semi-analytical methods allowing to clearly separate between two regimes, namely i) one in which the test particle remains always far from close encounters with the primary perturber, called hereafter the *regime of secular motion*, and ii) another in which short-period effects introduced by the interaction with the primary perturber dominate the dynamics. The methods developed in the present thesis aim also to provide a clear way to identify semi-analytically the border between these two regimes, and to predict whether particular initial conditions lead to one or the other regime of motion.

The here developed methods are compared with the results of numerical simulations. In particular:

In *Chapter 2* we revisit the Kustaanheimo-Stiefel (KS) regularization of the spatial elliptic restricted three-body problem by adopting a simple geometric Hamiltonian approach introduced in a recent paper [9], and report consequent numerical results. We start from the Lagrangian of the system in a suitable rotating and pulsating frame and then we apply the classic KS transformation. By exploiting its rotational symmetries and a precise condition on the initial data, we are able to move to the Hamiltonian formulation and subsequently perform a local geometric regularization analogous to the circular case, even if in the elliptic problem there is no conservation of the Jacobi constant. In particular, we prove a theorem on the projection of the regularized to the original solutions, also when the primaries perform an elliptic motion. Finally we test the theoretical apparatus numerically on selected orbits of the Sun-Jupiter system, providing evidence of the benefits in terms of the computational cost.

Chapter 3 proposes a closed-form (i.e. without expansion in the orbital eccentricities) scheme the derivation of a secular normal form in the restricted three-body problem when the massless particle is in an orbit exterior to the one of the primary perturber. Starting with a multipole expansion of the barycentric (Jacobi-reduced) Hamiltonian, we carry out a sequence of normalizations in Delaunay variables by Lie series, leading to a secular Hamiltonian model without use of relegation. To this end, we introduce a book-keeping analogous to the one proposed in [11] for test particle orbits interior to the one of the primary perturber, but here adapted, instead, to the case of exterior orbits. We give numerical examples of the performance of the method in both the planar circular and the spatial elliptic restricted three-body problem, for parameters pertinent to the Sun-Jupiter system. In particular, we demonstrate the method's accuracy in terms of reproducibility of the orbital elements' variations far from mean-motion resonances.

Chapter 4 contains the core result of the present work. It begins with the geometric visualization of suitable projections in phase space of regions subject to different regimes of motion when Jupiter is retained as the source of the perturbation. These sets are made of several components which include trajectories either crossing Jupiter's orbit or protected from collision. By means of stability (e.g. FLI [56]) maps, we classify the regimes at issue and portray, in addition, the fractal-like boundary of the region inhabited by weakly chaotic orbits exterior to Jupiter. As a fundamental outcome of the perturbative method

in Chapter 3, we show how, using as criterion the size of the series' remainder, we reach to obtain an accurate semi-analytical estimate of the boundary (in the space of orbital elements) where the secular Hamiltonian model arrived at after eliminating the particle's fast degree of freedom provides a valid approximation of the true dynamics.

Chapter 5 explores motions far from the secular regime. These are driven by invariant manifolds associated to periodic orbits originating at the collinear fixed points. In this respect, we analyze the distribution in phase space of heteroclinic intersections (with various other periodic orbits) of the two opposite branches of the stable and unstable manifolds of the short-period family of unstable periodic orbits emanating from the Lagrangian point L_3 for different energy values. We observe an asymmetry in the distribution of the intersections. We examine possible correlations of this asymmetry with the well-known open problem of the L_4/L_5 asymmetry for Jupiter's Trojans. In particular, following the scenario discussed in [70], we examine the captures and escapes of Trojans as driven by the invariant manifolds when Jupiter's migratory motion is taken into account.

Chapter 6 contains the conclusions of the present work and gives some perspectives on possible future extensions.

HAMILTONIAN REGULARIZATION THEORY IN THE RESTRICTED THREE-BODY PROBLEM

In this chapter we systematize and extend in the Hamiltonian setting the theory of local geometric regularization of gravitational singularities in the spatial restricted three-body problem. We develop the theory in detail in the case of the ER3BP resuming the research documented in [92], so that the planar or circular problems (for which a canonical structure, albeit quite different, exists) are naturally included and become just a particular case.

2.1 The nature of the singularities in the N -body problem

As a consequence of Newton's law of gravitation (1.49), according to which the forces acting between particles tend to infinity when the distance between them approaches zero, at collision the corresponding equations of motion show singularities. However, the wording "singularity" as synonym of "collision" in this context is not strictly rigorous, since, quite surprisingly for N not too small, it has been shown that the N -body problem admits also other types of mathematical singularities and this fact is far from being trivial. Although it is true that singularities that are not collisions are fairly rare to encounter and physically represent limit cases in Newtonian mechanics, let us clarify the matter at introductory level.

If we select initial conditions $(Q_1^{(0)}, \dots, Q_{N-1}^{(0)}, P_1^{(0)}, \dots, P_{N-1}^{(0)}) \in D$ for the Hamiltonian (1.69) at time $t = 0$, where D is the non-collision configuration set (1.70), then by Remark 1.1.1 we have in principle a unique real smooth solution, that we can also assume analytic operating in the Hamiltonian environment (§1.2.5), to the Hamilton's equations defined only on a maximal time interval $]t_-, t_+[$. For example indeed, it is easy to come up with choices of initial data so

that, for smaller or larger times, the orbits of the Hamiltonian vector field exit D (i.e. binary or simultaneous multiple collisions occur). Thus, depending on $(Q_1^{(0)}, \dots, Q_{N-1}^{(0)}, P_1^{(0)}, \dots, P_{N-1}^{(0)})$, we can have either a solution getting singular at $t_- > -\infty$ or $t_+ < +\infty$ or a regular one, whose time extremes therefore extend to infinity ($t_- = -\infty, t_+ = +\infty$).

Due to the symmetry of the problem, let us reduce ourselves to the study of the problem on the interval $[0, t_*[$, where $t_* \in \mathbb{R}_{>0}$ is a singularity time.

Definition 2.1.1. We say that a singularity time t_* is due to a *collision* if

$$\lim_{t \rightarrow t_*^-} Q(t) \in \mathbb{R}^{3(N-1)}$$

where $Q(t) = (Q_1(t), \dots, Q_{N-1}(t))$ and, correspondingly, t_* is the *collision time*. If Q has no limit, or it is unbounded when $t \rightarrow t_*^-$, we say that the singularity is a *pseudo-collision* or a *non-collision singularity*.

If we introduce the distance function

$$\rho: \mathbb{R}^{3(N-1)} \longrightarrow [0, +\infty[$$

$$\rho(Q) = \min_{1 \leq i < j \leq N-1} \{ \|Q_i\|, \|Q_j\|, \|Q_i - Q_j\| \} \quad , \quad (2.1)$$

the following holds [77].

Theorem 2.1.1 (PAINLEVÉ THEOREM). *If $(Q(t), P(t))$, $P(t) = (P_1(t), \dots, P_{N-1}(t))$, is an analytic solution of the Hamilton's equations associated to (1.69) defined on maximal interval $[0, t_*[$, then at t_* there is a singularity of the solution if and only if*

$$\lim_{t \rightarrow t_*^-} \rho(Q(t)) = 0 .$$

The theorem, in practice, states that at singularity times at least a single or mutual distance vanishes. This is particularly helpful to dynamically picture and characterize non-collision singularities, which, thanks to the result below by von Zeipel [108], are non-local behaviors as opposed to collision ones, and highly counter-intuitive [71]. Such wild configurations require indeed infinitely large velocities, hence physically incompatible with classical mechanics¹. So, essentially, pseudo-collisions happen when some particles scatter together with others zeroing their inter-distance (and thus the global limit, in the sense of Definition 2.1.1, does not exist).

Theorem 2.1.2 (VON ZEIPEL THEOREM). *If a non-collision singularity occurs at time t_* , then*

$$\lim_{t \rightarrow t_*^-} \rho(Q(t)) = 0 \quad \text{and} \quad \lim_{t \rightarrow t_*^-} \max_{1 \leq i < j \leq N-1} \{ \|Q_i\|, \|Q_j\|, \|Q_i - Q_j\| \} = +\infty .$$

How likely are pseudo-collision singularities? As anticipated, not so much.² They can be even impossible. Coming indeed to our interests, where we mainly consider $N = 3$, another assertion by Painlevé allow us to worry only about gravitational collision singularities.

¹But technically admissible in special relativity.

²Actually the set of initial conditions leading to discontinuities in general is (Lebesgue) negligible [93].

Theorem 2.1.3. *For $N = 3$ let $(Q_1(t), Q_2(t), P_1(t), P_2(t))$ be a solution of the heliocentric three-body problem equations defined on $[0, t_*[$. Then the singularity is due to a collision.*

Non-collision singularities are so hard to produce that, historically, Painlevé just conjectured that in the N -body problem with $N \geq 4$ there can exist non-collision singularities. Only in recent years the conjecture has been positively solved by Xia [106] for $N \geq 5$ and later on completed by Xue [107] for $N = 4$.

In conclusion, from now on, it will be implicit that by singularity we mean collision singularity and, in the restricted case where the motion of the planets is elliptic/circular Keplerian, only a binary collision with one of the primaries at a time is possible (and this motivates our focus on local regularization techniques in contrast to global ones, which aim to regularize all the singularities at once). Besides, even though pointwise exact collisions in finite time are, like said above, rather infrequent, in practical numerical computations we need to handle orbits passing by arbitrarily close to them, since $\rho(Q) \approx 0$, and thereby numerical schemes are inevitably affected. This translates into paying attention not just to the mere discontinuity points, but also to small balls of positions around them. Therefore, close approaches are definitely prevalent and regularization methods are almost indispensable both for better accuracy and to save computational time.

2.2 Motivations

The regularization of the gravitational singularities, appeared at the beginning of the XXth century, has become in the last decades an extremely useful technique to deal with the numerical integration of the N -body problems. Particularly two kinds of regularization techniques are widely known: a geometric one, which basically aims to modify the equations of motion such that they are defined and regular even on the singularities, and a solution-based one, whose goal consists in an analytic continuation of the original solution through the singular point. In this chapter we focus precisely on the former.

A special case of utmost importance, and central for this thesis, is represented by the restricted three-body problem, originally in its circular and then elliptic variant. In his celebrated paper [57] Levi-Civita performed a local regularization³ of the planar CR3BP, which relies on the conservation of the Jacobi integral (1.76), through the introduction of canonical transformations and a time reparametrization that nowadays are known, after his name, as Levi-Civita (LC) regularization. The issue for the spatial CR3BP was solved by Kustaanheimo and Stiefel in the mid-1990s [51, 52]. The latter procedure is more complicated than the LC one since it exploits a projection map from a space of four redundant variables to the three-dimensional Cartesian space. Both LC and KS regularizations are *iso-energetic*, since they exploit the existence

³The global one is mainly due to Birkhoff [8].

of a global first integral, that is the Jacobi constant. On the contrary, much less attention has been devoted to the geometric regularization of the ER3BP, which is complicated by the absence of any known integral of motion. The most relevant references in this regard remain [99, 100] for the planar setting and [2, 98, 104] for the full one, which date back more or less to the same years. In both cases the main idea consists in generalizing the respective circular counterpart, but unlike the former, whose complete extension has been carried out resulting in a system of integro-differential equations [100], the latter has been addressed by Waldvogel, Stiefel and Arenstorf in their works [2, 98] by transferring to the elliptic problem directly the global regularization theory, thus leaving the door open for a further insight on the local case, especially on a possible alternative derivation in view of the Hamiltonian formalism.

Although a local treatment represents a sort of sub-case of a simultaneous removal of the two centers of attraction, it is more profitable for the sake of definition simplicity and resulting numerical implementation to rely to switching single body-centered regularizations rather than a full one, therefore our focus is still meaningful, especially in virtue of §2.1. In light of such situation a reasonable interest in accomplishing these purposes follows quite naturally. In particular our goal here translates into obtaining a simpler construction of the KS formulation for the spatial ER3BP drawing the inspiration from the paper [9] about the CR3BP.

We hereby present a step-by-step construction of the regularization with a final rigorous statement on the projection of the regularized solutions onto the original ones, and related proof, which can be recognized as a symplectic reduction of the KS phase space; secondarily, after a short description of the algorithmic procedure employed, we perform numerical explorations in a neighborhood of \mathcal{P}_1 and outlines quantitatively the gain as regards computational effort.

2.3 Kustaanheimo-Stiefel regularization of the elliptic restricted three-body problem

2.3.1 Formulation in the rotating-pulsating frame

The ER3BP is defined by the motion of a body \mathcal{P} of negligible mass in the gravitation field of two massive bodies \mathcal{P}_0 and \mathcal{P}_1 , which trace this time an elliptic Keplerian path. As usual, the simplifying assumptions on the units correspond to setting

- $m_0 = 1 - \mu$ and $m_1 = \mu$ for the masses, where μ is given by (1.73);
- $T_1 = 2\pi$ for the period of the elliptic motion (thus $\mathcal{G} = 1$);
- $a_1 = 1$ for the semi-major axis of the elliptic motion.

The Hamiltonian of the problem is conveniently expressed in a rotating-pulsating Cartesian frame $Oxyz$ [99] with the classic simplification of explicit dependence

on the true anomaly $f_1 \in \mathbb{T}$ of the elliptic motion of \mathcal{P}_1 taken as independent variable [95] (in which, henceforth, we shall drop the subscript “1” for the sake of notational simplicity and clarity in treating this angle as a variable). In such a reference system, the bodies $\mathcal{P}_0, \mathcal{P}_1$ have coordinates $(-\mu, 0, 0), (1 - \mu, 0, 0)$ respectively. By denoting with $(x, y, z), (p_x, p_y, p_z)$ the coordinates of \mathcal{P} and their conjugate momenta, the Hamiltonian in question reads

$$\begin{aligned} \mathcal{H}(x, y, z, p_x, p_y, p_z, f) = & \frac{1}{2}(p_x^2 + p_y^2 + p_z^2) + p_x y - x p_y \\ & - \frac{1}{1 + e_1 \cos f} \left(\frac{1 - \mu}{d_0} + \frac{\mu}{d_1} - \frac{1}{2} e_1 \cos f (x^2 + y^2 + z^2) \right), \end{aligned} \quad (2.2)$$

where d_0, d_1 are given by (1.75) and $0 \leq e_1 < 1$ is the eccentricity of \mathcal{P}_0 - \mathcal{P}_1 . The derivation of (2.2) is detailed in Appendix A.

Even though the Hamiltonian (2.2) is the object of the KS regularization, for reasons that will be clear after introducing the KS machinery, our starting point is represented by the Lagrangian in $Oxyz$ (see Appendix A):

$$\begin{aligned} L(x, y, z, x', y', z', f) = & \frac{1}{2}((x')^2 + (y')^2 + (z')^2) + x y' - x' y \\ & + \frac{1}{1 + e_1 \cos f} \left(\frac{1 - \mu}{d_0} + \frac{\mu}{d_1} + \frac{1}{2} (x^2 + y^2 - z^2 e_1 \cos f) \right), \end{aligned} \quad (2.3)$$

where the superscript denotes the derivative with respect to f .

The origin of the coordinate axes is now moved to one of the two targeted singular positions, say, hereafter, the secondary body’s location $\mathcal{P}_1(1 - \mu, 0, 0)$:⁴

$$(x - 1 + \mu, y, z) = q. \quad (2.4)$$

Then (2.3) becomes

$$\begin{aligned} \tilde{L}(q, q', f) = & \frac{1}{2} \|q'\|^2 + q' \times (0, 0, 1) \cdot q \\ & + \frac{1}{1 + e_1 \cos f} \left[(1 - \mu) \left(\frac{1}{\|q + (1, 0, 0)\|} + q_1 \right) \right. \\ & \left. + \frac{\mu}{\|q\|} + \frac{1}{2} (q_1^2 + q_2^2 - q_3^2 e_1 \cos f) \right], \end{aligned} \quad (2.5)$$

where the addenda $q' \times (0, 0, 1) \cdot (1 - \mu, 0, 0)$ and $(1 - \mu)^2 / (2(1 + e_1 \cos f))$ are dropped because they do not contribute to the Lagrange’s equations.

2.3.2 The space of redundant variables

Following [9] and reprising their argument to the elliptic problem, we introduce the *Kustaanheimo-Stiefel space map* as a projection from a space of redundant

⁴The local regularization at the primary body \mathcal{P}_0 could be introduced following the same scheme. We here focus on the regularization at \mathcal{P}_1 because it is particularly relevant for applications to the motion of asteroids, comets and space-flight dynamics.

variables u_1, u_2, u_3, u_4 to a space of Cartesian variables q_1, q_2, q_3 :

$$\begin{aligned} \pi: \mathbb{R}^4 &\longrightarrow \mathbb{R}^3 \\ u = (u_1, u_2, u_3, u_4) &\longmapsto \pi(u) = (q_1, q_2, q_3) = q \end{aligned} \quad (2.6)$$

where

$$(q_1, q_2, q_3, 0) = A(u)u \quad (2.7)$$

and

$$A(u) = \begin{pmatrix} u_1 & -u_2 & -u_3 & u_4 \\ u_2 & u_1 & -u_4 & -u_3 \\ u_3 & u_4 & u_1 & u_2 \\ u_4 & -u_3 & u_2 & -u_1 \end{pmatrix} \quad (2.8)$$

is a matrix that plays a central role in the KS regularization. In particular, $A(u)$ fulfills the two properties below.

- (i) It is a linear homogeneous function of u_1, u_2, u_3, u_4 .
- (ii) It satisfies

$$A(u)A^T(u) = A^T(u)A(u) = \|u\| \mathbb{I}, \quad (2.9)$$

hence $\|u\|^2 = d_1$.

Remark 2.3.1. The two properties above are necessary to move forward and are peculiar of $n \times n$ matrices only with $n = 1, 2, 4, 8$, as discovered by Hurwitz in one of his number theory result [48]; the lack of this result for $n = 3$ thus gives reason to pass to a four-dimensional space. Particularly, the KS map can be rephrased equivalently using quaternions \mathbb{H} :

$$\begin{aligned} \pi: \mathbb{H} \cong \mathbb{R}^4 &\longrightarrow \mathbb{IH} \cong \mathbb{R}^3 \\ w = w_1 + w_2\mathbf{i} + w_3\mathbf{j} + w_4\mathbf{k} &\longmapsto \pi(w) = \bar{w}\mathbf{i}w \end{aligned}$$

with $\mathbf{i}^2 = \mathbf{j}^2 = \mathbf{k}^2 = \mathbf{ijk} = -1$, $\bar{w} = w_1 + w_2\mathbf{i} + w_3\mathbf{j} + w_4\mathbf{k}$ and $\mathbb{IH} = \{w \in \mathbb{H} \mid \text{Re } w = 0\}$.

We apply now (2.7) to (2.5) exploiting (2.9) and the relationship by simple differentiation

$$(q'_1, q'_2, q'_3, 0) = \left(\frac{\partial \pi}{\partial u}(u)u', 0 \right) = 2A(u)u' - 2(0, 0, 0, l(u, u')), \quad (2.10)$$

in which

$$l(u, u') := u_4u'_1 - u_3u'_2 + u_2u'_3 - u_1u'_4 \quad (2.11)$$

is the *bilinear form* appearing in the usual KS regularization, that has a very important and fundamental role in the regularizing procedure, as it will be appreciated subsequently.

$$\begin{aligned} \mathcal{L}(u, u', f) &= \tilde{L} \left(\pi(u), \frac{\partial \pi}{\partial u}(u)u', f \right) = 2 \|u\|^2 \|u'\|^2 - 2l^2(u, u') + b(u) \cdot u' \\ &\quad + \frac{1}{1 + e_1 \cos f} \left[(1 - \mu) \left(\frac{1}{\|\pi(u) + (1, 0, 0)\|} + \pi_1(u) \right) \right. \\ &\quad \left. + \frac{\mu}{\|u\|^2} + \frac{1}{2} (\pi_1^2(u) + \pi_2^2(u) - \pi_3^2(u) e_1 \cos f) \right], \end{aligned} \quad (2.12)$$

for

$$b(u) = 2A^T(u)\Lambda A(u)u, \quad \Lambda = \begin{pmatrix} 0 & -1 & 0 & 0 \\ 1 & 0 & 0 & 0 \\ 0 & 0 & 0 & 0 \\ 0 & 0 & 0 & 0 \end{pmatrix} \in \text{Skew}(4) \quad (2.13)$$

and $\text{Skew}(4)$ is the vector space of 4×4 (real) skew-symmetric matrices. The computation is straightforward, the only contribution that needs a little work is

$$\frac{\partial \pi}{\partial u} u' \times (0, 0, 1) \cdot \pi;$$

recall that, thanks to the representation theorem of skew-symmetric operators, $\forall v \in \mathbb{R}^3$ and $\omega = (\omega_1, \omega_2, \omega_3) \in \mathbb{R}^3$, $\exists! \bar{\Lambda} \in \text{Skew}(3)$ such that

$$\omega \times v = \bar{\Lambda} v, \quad \bar{\Lambda} = \begin{pmatrix} 0 & -\omega_3 & \omega_2 \\ \omega_3 & 0 & -\omega_1 \\ -\omega_2 & \omega_1 & 0 \end{pmatrix},$$

thence setting $\omega = (0, 0, 1)$,

$$\frac{\partial \pi}{\partial u} u' \times (0, 0, 1) = -\bar{\Lambda} \frac{\partial \pi}{\partial u} u'.$$

Therefore re-adding the fourth dimension and performing the scalar product it yields

$$\begin{aligned} -\bar{\Lambda} \frac{\partial \pi}{\partial u} u' \cdot \pi &= -\left(\bar{\Lambda} \frac{\partial \pi}{\partial u} u', 0 \right) \cdot (\pi, 0) = -\Lambda \begin{pmatrix} \frac{\partial \pi}{\partial u} u' \\ 0 \end{pmatrix} \cdot (\pi, 0) \\ &= -\Lambda(2Au' - 2(0, 0, 0, 1)) \cdot Au. \end{aligned}$$

Then

$$-\Lambda \left(2Au' - 2 \begin{pmatrix} 0 \\ 0 \\ 0 \\ 1 \end{pmatrix} \right) \cdot Au = -2\Lambda Au' \cdot Au = 2u' \cdot A^T \Lambda Au = b(u) \cdot u'.$$

The first task consists in proving the specific invariance of Lagrange's equations under the transformation at issue. In practice, the solutions of Lagrange's equations for $\mathcal{L}(u, u', f)$, which we write using the operator notation

$$[\mathcal{L}]_i(u, u', u'', f) = \frac{d}{df} \frac{\partial \mathcal{L}}{\partial u'_i} - \frac{\partial \mathcal{L}}{\partial u_i} = 0, \quad i = 1, 2, 3, 4, \quad (2.14)$$

have to be compared with the solutions of Lagrange's equations for $\tilde{\mathcal{L}}(q, q', f)$, denoted by

$$\langle \tilde{\mathcal{L}} \rangle_j(q, q', q'', f) = \frac{d}{df} \frac{\partial \tilde{\mathcal{L}}}{\partial q'_j} - \frac{\partial \tilde{\mathcal{L}}}{\partial q_j} = 0, \quad j = 1, 2, 3. \quad (2.15)$$

With the following statement it turns out that this requirement is fulfilled as soon as the solution $u(f) \neq 0$ for all $f \in \mathbb{T}$.

Proposition 2.3.1. *If $u(f)$ is a solution of Lagrange's equations associated to $\mathcal{L}(u, u', f)$ with initial condition $u(0) \neq 0$, then $q(f) = \pi(u(f))$ is a solution of Lagrange's equations associated to $\tilde{L}(q, q', f)$ as soon as $u(f) \neq 0$.*

Proof. For any smooth curve $u(f)$, reminding that

$$\mathcal{L}(u, u', f) = \tilde{L}\left(\pi(u), \frac{\partial \pi}{\partial u}(u)u', f\right),$$

as well as

$$\frac{\partial q'}{\partial u'} = \frac{\partial \pi}{\partial u},$$

one gets from the chain rule

$$\frac{\partial \mathcal{L}}{\partial u'_i} = \sum_{j=1}^3 \frac{\partial \tilde{L}}{\partial q'_j} \frac{\partial q'_j}{\partial u'_i} = \sum_{j=1}^3 \frac{\partial \tilde{L}}{\partial q'_j} \frac{\partial \pi_j}{\partial u_i}$$

and

$$\begin{aligned} \frac{d}{df} \frac{\partial \mathcal{L}}{\partial u'_i} &= \sum_{j=1}^3 \frac{d}{df} \frac{\partial \tilde{L}}{\partial q'_j} \frac{\partial \pi_j}{\partial u_i} + \sum_{j=1}^3 \frac{\partial \tilde{L}}{\partial q'_j} \frac{d}{df} \frac{\partial \pi_j}{\partial u_i} \\ &= \sum_{j=1}^3 \frac{d}{df} \frac{\partial \tilde{L}}{\partial q'_j} \frac{\partial \pi_j}{\partial u_i} + \sum_{j=1}^3 \frac{\partial \tilde{L}}{\partial q'_j} \sum_{k=1}^4 \frac{\partial^2 \pi_j}{\partial u_i \partial u_k} u'_k, \\ \frac{\partial \mathcal{L}}{\partial u_i} &= \sum_{j=1}^3 \frac{\partial \tilde{L}}{\partial q'_j} \frac{\partial \pi_j}{\partial u_i} + \sum_{j=1}^3 \frac{\partial \tilde{L}}{\partial q'_j} \sum_{k=1}^4 \frac{\partial^2 \pi_j}{\partial u_i \partial u_k} u'_k, \end{aligned}$$

for $i = 1, 2, 3, 4$. As a consequence we have

$$\begin{aligned} [\mathcal{L}](u(f), u'(f), u''(f), f) \\ = \left(\frac{\partial \pi}{\partial u}(u(f)) \right)^T \langle \tilde{L} \rangle \left(\pi(u(f)), \frac{d}{df} \pi(u(f)), \frac{d^2}{df^2} \pi(u(f)), f \right) \end{aligned}$$

where $[\mathcal{L}] \in \mathbb{R}^4$, $\langle \tilde{L} \rangle \in \mathbb{R}^3$ are the vectors of components respectively $[\mathcal{L}]_i$, $\langle \tilde{L} \rangle_j$.

Since by assumption $[\mathcal{L}]_i(u(f), u'(f), u''(f), f) = 0$, the vector

$$\langle \tilde{L} \rangle \left(\pi(u(f)), \frac{d}{df} \pi(u(f)), \frac{d^2}{df^2} \pi(u(f)), f \right)$$

is for any f in the kernel of the matrix $(\partial \pi(u(f))/\partial u)^T$. We claim that the kernel of $(\partial \pi(u(f))/\partial u)^T$ contains only $(0, 0, 0)$ if $u \neq 0$. In fact, an element (α, β, γ) is in the kernel of $(\partial \pi(u(f))/\partial u)^T$ if and only if its components satisfy the system:

$$\begin{cases} u_1 \alpha + u_2 \beta + u_3 \gamma = 0 \\ -u_2 \alpha + u_1 \beta + u_4 \gamma = 0 \\ -u_3 \alpha - u_4 \beta + u_1 \gamma = 0 \\ u_4 \alpha - u_3 \beta + u_2 \gamma = 0 \end{cases},$$

which admits the unique solution $\alpha = \beta = \gamma = 0$ as long as at least one of the components of u is different from zero.

This implies $\langle \tilde{L} \rangle (\pi(u(f)), d\pi(u(f))/df, d^2\pi(u(f))/df^2, f) = 0$ and $q(f) = \pi(u(f))$ is a solution of the Lagrange's equations of \tilde{L} . \square

2.3.3 The modified Lagrangian

The second matter to tackle regards the Legendre transform (necessary to deduce in the next §2.3.5 the corresponding transformed Hamiltonian and then proceed with the development):

$$\frac{\partial \mathcal{L}}{\partial u'} = \left(\frac{\partial \mathcal{L}}{\partial u'_1}, \frac{\partial \mathcal{L}}{\partial u'_2}, \frac{\partial \mathcal{L}}{\partial u'_3}, \frac{\partial \mathcal{L}}{\partial u'_4} \right) = 4 \|u\|^2 u' - 4(\Omega u \cdot u')\Omega u + b(u), \quad (2.16)$$

where

$$\Omega = \begin{pmatrix} 0 & 0 & 0 & 1 \\ 0 & 0 & -1 & 0 \\ 0 & 1 & 0 & 0 \\ -1 & 0 & 0 & 0 \end{pmatrix} \in \text{Skew}(4) \quad (2.17)$$

is an ad hoc permutation matrix coming from the bilinear form term ($l(u, u') = \Omega u \cdot u'$), which is not invertible with respect to the generalized velocities, because the Hessian matrix

$$\mathcal{H}_{u'} = \left(\frac{\partial^2 \mathcal{L}}{\partial u'_i \partial u'_j} \right), \quad i, j \in \{1, 2, 3, 4\}, \quad (2.18)$$

is identically singular, indeed

$$\begin{aligned} \det \mathcal{H}_{u'} &= \det \begin{pmatrix} 4 \|u\|^2 - 4u_4^2 & 4u_3u_4 & -4u_2u_4 & 4u_1u_4 \\ 4u_3u_4 & 4 \|u\|^2 - 4u_3^2 & 4u_2u_3 & -4u_1u_3 \\ -4u_2u_4 & 4u_2u_3 & 4 \|u\|^2 - 4u_2^2 & 4u_1u_2 \\ 4u_1u_4 & -4u_1u_3 & 4u_1u_2 & 4 \|u\|^2 - 4u_1^2 \end{pmatrix} \\ &= 256 \|u\|^6 (\|u\|^2 - \|u\|^2) = 0. \end{aligned}$$

This criticality is due to the presence of the degenerate quadratic form in u' variables $2 \|u\|^2 \|u'\|^2 - 2l^2(u, u')$ in (2.12), that makes the implicit function theorem not applicable.

To overcome the degeneracy we proceed as in [9]: it is profitable to change the Lagrangian just by adding two times the square of the bilinear form (so that $-2l^2$ vanishes). Such artifice precisely allows to restore the invertibility, thereby

$$\begin{aligned} \mathcal{L}(u, u', f) &= \mathcal{L}(u, u', f) + 2l^2(u, u') = 2 \|u\|^2 \|u'\|^2 + b(u) \cdot u' \\ &+ \frac{1}{1 + e_1 \cos f} \left[(1 - \mu) \left(\frac{1}{\|\pi(u) + (1, 0, 0)\|} + \pi_1(u) \right) \right. \\ &\quad \left. + \frac{\mu}{\|u\|^2} + \frac{1}{2} (\pi_1^2(u) + \pi_2^2(u) - \pi_3^2(u) e_1 \cos f) \right] \quad (2.19) \end{aligned}$$

is the *modified Lagrangian* and in fact, introducing the KS momenta $U = (U_1, U_2, U_3, U_4)$ conjugate to $u = (u_1, u_2, u_3, u_4)$, the relationship

$$U = \frac{\partial \mathcal{L}}{\partial u'}(u, u') = 4 \|u\|^2 u' + b(u) \quad (2.20)$$

is non-degenerate (thus invertible) in u' for $u \neq 0$.

2.3.4 Rotational invariance of the modified Lagrangian

The sum of the quadratic expression $2l^2(u, u')$ of course alters $\mathcal{L}(u, u', f)$ and again one has to make sure that such action is legitimized under appropriate conditions (until now $u(f) \neq 0$ always). Let then the investigation begin by realizing the well known remarkable symmetry property of the KS transformation.

Proposition 2.3.2. *The modified Lagrangian $\mathcal{L}(u, u', f)$ is invariant under the one-parameter family of transformations involving the redundant coordinates*

$$\begin{aligned} S_\theta: \mathbb{R}^4 &\longrightarrow \mathbb{R}^4 \\ u &\longmapsto S_\theta u' \end{aligned} \quad (2.21)$$

where $S_\theta \in SO(4)$ is the four-dimensional rotation matrix

$$S_\theta = \begin{pmatrix} \cos \theta & 0 & 0 & -\sin \theta \\ 0 & \cos \theta & \sin \theta & 0 \\ 0 & -\sin \theta & \cos \theta & 0 \\ \sin \theta & 0 & 0 & \cos \theta \end{pmatrix}, \quad (2.22)$$

whose orbits define the fibers of the projection π , i.e. $\pi(S_\theta u) = \pi(u)$ for all $\theta \in \mathbb{T}$. More precisely

$$\mathcal{L}(S_\theta u, S_\theta u', f) = \mathcal{L}(u, u', f). \quad (2.23)$$

Proof. First off

$$(\pi(S_\theta u), 0) = A(S_\theta u)S_\theta u = A(u)S_\theta^T S_\theta u = A(u)u = (\pi(u), 0),$$

and

$$b(S_\theta u) = 2A^T(S_\theta u)\Lambda A(S_\theta u)S_\theta u = 2S_\theta A^T(u)\Lambda A(u)u = S_\theta b(u).$$

So

$$\mathcal{L}(S_\theta u, S_\theta u', f) = \mathcal{L}(u, u', f),$$

using the above results and the properties of orthogonal matrices. \square

This fact implies that there exists, by Noether's theorem, a conserved quantity

$$J(u, u') = \frac{\partial \mathcal{L}}{\partial u'} \cdot \frac{d}{d\theta} S_\theta u \Big|_{\theta=0} = -4 \|u\|^2 l(u, u') - b(u) \cdot \Omega u = -4 \|u\|^2 l(u, u')$$

which is an autonomous first integral for the Lagrangian (2.19). For convenience the final constant of motion is given by

$$\mathcal{J}(u, u') = \|u\|^2 l(u, u'). \quad (2.24)$$

If the bilinear form is cleverly zeroed out at $f = 0$ (by proper initial conditions), it will keep taking zero value for further f (since we only consider time intervals such that $\|u\| \neq 0$), so the extra factor $2l^2$ would become a vanishing contribution to the Lagrange's equations.

According to such idea, the bilinear form assumes the meaning of non-holonomic constraint⁵ to be respected along the motion and the final claim, whose proof in the proposition below resolves completely the issue, that is the Lagrange's equations associated to \mathcal{L} have the same solutions of the Lagrange's equations associated to \mathcal{L} .

Proposition 2.3.3. *If $u(f)$ is a solution of the Lagrange's equations of $\mathcal{L}(u, u', f)$ with initial data $u(0), u'(0)$ satisfying $u(0) \neq 0$ and $l(u(0), u'(0)) = 0$, then it is also a solution of the Lagrange's equations of $\mathcal{L}(u, u', f)$ as long as $u(f) \neq 0$.*

Proof. Consider a solution $u(f)$ of the \mathcal{L} -equations with $u(0) \neq 0$ and $l(u(0), u'(0)) = 0$. As long as $u(f) \neq 0$, by (2.24), $l(u(f), u'(f)) = 0$. Moreover

$$\frac{d}{df} l(u(f), u'(f)) = l(u'(f), u'(f)) + l(u(f), u''(f)) = l(u(f), u''(f)).$$

Now $u(f)$ solves the Lagrange's equations for \mathcal{L} too, in fact, referring to the previous notation (2.14), for any $i = 1, 2, 3, 4$,

$$\begin{aligned} [\mathcal{L}]_i &= [\mathcal{L} - 2l^2]_i = [\mathcal{L}]_i - 2 \left(\frac{d}{df} \frac{\partial}{\partial u'_i} l^2(u, u') - \frac{\partial}{\partial u_i} l^2(u, u') \right) \\ &= [\mathcal{L}]_i - 4 \left[\frac{d}{df} \left(l(u, u') \frac{\partial}{\partial u'_i} l(u, u') \right) - l(u, u') \frac{\partial}{\partial u_i} l(u, u') \right] \end{aligned}$$

and when evaluated along the curve $u(f)$

$$\begin{aligned} [\mathcal{L}]_i(u(f), u'(f), u''(f), f) &= [\mathcal{L}]_i(u(f), u'(f), u''(f), f) \\ &- 4 \left(l(u(f), u''(f)) \frac{\partial}{\partial u'_i} l(u(f), u'(f)) + l(u(f), u'(f)) \frac{d}{df} \frac{\partial}{\partial u'_i} l(u(f), u'(f)) \right. \\ &\quad \left. - l(u(f), u'(f)) \frac{\partial}{\partial u_i} l(u(f), u'(f)) \right) = 0, \end{aligned}$$

owing to $l(u(f), u''(f)) = l(u(f), u'(f)) = 0$. □

⁵We remind that non-holonomic constraints acting on mechanical systems are constraints on the velocities that are not derivatives of constraints in positions.

2.3.5 The regularized Hamiltonian

The corresponding singular, i.e. non-regularized, Hamiltonian enters now by performing the Legendre transform:

$$\mathcal{K}(u, U, f) = U \cdot g(u, U) - \mathcal{L}(u, g(u, U), f), \quad (2.25)$$

where

$$u' = g(u, U) = \frac{U - b(u)}{4 \|u\|^2}$$

is the inverse of U with respect to u' ; more explicitly we have

$$\begin{aligned} \mathcal{K}(u, U, f) = & \frac{1}{8 \|u\|^2} \|U - b(u)\|^2 \\ & - \frac{1}{1 + e_1 \cos f} \left[(1 - \mu) \left(\frac{1}{\|\pi(u) + (1, 0, 0)\|} + \pi_1(u) \right) \right. \\ & \left. + \frac{\mu}{\|u\|^2} + \frac{1}{2} (\pi_1(u)^2 + \pi_2(u)^2 - \pi_3(u)^2 e_1 \cos f) \right] \quad (2.26) \end{aligned}$$

and the bilinear equality $l(u, u') = 0$ straightforwardly translates in the Hamiltonian formalism as $l(u, U) = 0$ for $u \neq 0$, because

$$l(u, u') = l(u, g(u, U)) = \frac{1}{4 \|u\|^2} l(u, U) - \frac{1}{4 \|u\|^2} l(u, b(u)),$$

but $l(u, b(u)) = \Omega u \cdot b(u) = 0$ identically, hence we have $l(u, u') = 0$ if and only if $l(u, U) = 0$.

With all this in hand it is useful to work with an autonomous extension of the transformed Hamiltonian \mathcal{K} . So we append one more degree of freedom to form the extended phase space $T^*((\mathbb{R}^4 \setminus C) \times \mathbb{T})$, where $T^* \cdot$ denotes the cotangent bundle of \cdot , and

$$C = \{(0, 0, 0, 0)\} \cup \left\{ \left(0, u_2, \pm \sqrt{1 - u_2^2}, 0 \right), u_2 \in \mathbb{R} \right\} \quad (2.27)$$

is the collision set in KS coordinates, with the extra couple of variables $(\phi, \Phi) \in \mathbb{T} \times \mathbb{R}$ and standard symplectic form $du \wedge dU + d\phi \wedge d\Phi$ ($du \wedge dU = \sum_{i=1}^4 du_i \wedge dU_i$), in such a way to build the autonomous transformed Hamiltonian

$$\widehat{\mathcal{K}}(u, \phi, U, \Phi) = \mathcal{K}(u, U, \phi) + \Phi, \quad (2.28)$$

and consider the solutions $u(f), U(f), \phi(f), \Phi(f)$ of the Hamilton's equations of (2.28) such that, for given initial value f_0 of the true anomaly, satisfy

$$u(f_0) = u_0, \quad U(f_0) = U_0, \quad \phi(f_0) = f_0, \quad \Phi(f_0) = -\mathcal{K}(u_0, U_0, f_0).$$

At this point we perform a rescaling similar to the one in the Levi-Civita regularization, and define the regularized Hamiltonian

$$\begin{aligned} \mathcal{K}(u, \phi, U, \Phi) &= \|u\|^2 \widehat{\mathcal{K}}(u, \phi, U, \Phi) = \frac{1}{8} \|U - b(u)\|^2 \\ &\quad - \frac{1}{1 + e_1 \cos \phi} \left[(1 - \mu) \|u\|^2 \left(\frac{1}{\|\pi(u) + (1, 0, 0)\|} + \pi_1(u) \right) + \mu \right. \\ &\quad \left. + \frac{1}{2} \|u\|^2 (\pi_1^2(u) + \pi_2^2(u) - \pi_3^2(u) e_1 \cos \phi) + \frac{(1 - \mu)^2}{2} \|u\|^2 \right] + \Phi \|u\|^2 . \end{aligned} \quad (2.29)$$

Remark 2.3.2.

- For $e_1 = 0$, the action Φ is a constant of motion and the Hamiltonian (2.29) is identical to the KS Hamiltonian of the CR3BP, as represented in [9] with $\Phi = -E$.
- $\mathcal{K}(u, \phi, U, \Phi)$ is invariant under the same one-parameter family of transformations defined by (2.21) and (2.22), hence $\mathcal{J}(u, g(u, U)) = l(u, U)$ is a first integral also for the Hamilton's equations of $\mathcal{K}(u, \phi, U, \Phi)$.
- Hamiltonian (2.29) is regular at $u = 0$.

2.3.6 Projection of the solutions of the regularized Hamiltonian

Let us prove that the solutions of the Hamilton's equations of the regularized Hamiltonian (2.29) project on the Hamilton's solutions of the Hamiltonian (2.2) of the ER3BP. Similarly to the classic LC and KS techniques we need an independent variable redefinition, which for the ER3BP is obtained by introducing the fictitious true anomaly s such that:

$$s'(f) = \frac{1}{\|u(f)\|^2}, \quad s(f_0) = 0, \quad (2.30)$$

whose inverse is precisely $\partial\mathcal{K}/\partial\Phi$. Thereby we state our result.

Theorem 2.3.1. *The solutions $(u(s), \phi(s), U(s), \Phi(s))$ of Hamilton's equations related to $\mathcal{K}(u, \phi, U, \Phi)$ with initial conditions satisfying*

- (i) $u(0) \neq 0$,
- (ii) $l(u(0), U(0)) = 0$,
- (iii) $\mathcal{K}(u(0), \phi(0), U(0), \Phi(0)) = 0$

project, for s in a neighborhood of $s = 0$, via the true anomaly reparametrization:

$$f(s) = f_0 + \int_0^s \|u(\sigma)\|^2 d\sigma, \quad (2.31)$$

the transformation (2.7) and the translation (2.4), onto solutions $(x(f), y(f), z(f), p_1(f), p_2(f), p_3(f))$ of the Hamilton's equations of Hamiltonian (2.2).

Proof. In light of what already derived in the previous subsections, we only need to prove the equivalence between the solutions associated to the transformed Hamilton's function $\widehat{\mathcal{K}}$ and the regularized function \mathcal{K} . Given the initial conditions u_0, U_0, f_0 , let us consider the solution $(\tilde{u}(s), \tilde{\phi}(s), \tilde{U}(s), \tilde{\Phi}(s))$ of the Hamilton's equations of \mathcal{K} with

$$\tilde{u}(0) = u_0, \quad \tilde{U}(0) = U_0, \quad \tilde{\phi}(0) = f_0, \quad \tilde{\Phi}(0) = -\mathcal{K}(u_0, U_0, f_0),$$

and s in a neighborhood of $s = 0$ such that $\|\tilde{u}(s)\| > 0$; in particular we have

$$\mathcal{K}(\tilde{u}(s), \tilde{\phi}(s), \tilde{U}(s), \tilde{\Phi}(s)) = 0$$

for all s . Next, consider

$$f(s) = f_0 + \int_0^s \|\tilde{u}(\sigma)\|^2 d\sigma,$$

which is invertible (since in the neighborhood of $s = 0$ we have $\|\tilde{u}(s)\| > 0$), and $(u(f), \phi(f), U(f), \Phi(f))$ defined by

$$u(f) = \tilde{u}(s(f)), \quad U(f) = \tilde{U}(s(f)), \quad \phi(f) = \tilde{\phi}(s(f)), \quad \Phi(f) = \tilde{\Phi}(s(f)).$$

We claim that $(u(f), \phi(f), U(f), \Phi(f))$ are the solutions of the Hamilton's equations of $\widehat{\mathcal{K}}$ with initial conditions

$$(u(f_0), \phi(f_0), U(f_0), \Phi(f_0)) = (u_0, f_0, U_0, -\mathcal{K}(u_0, U_0, f_0)).$$

In fact, for $i \in \{1, 2, 3, 4\}$, we have

$$\begin{aligned} \frac{du_i}{df} &= \frac{ds}{df} \frac{d\tilde{u}_i}{ds} \Big|_{s=s(f)} \\ &= \frac{1}{\|\tilde{u}(s(f))\|^2} \left[\frac{\partial}{\partial U_i} \left(\|u\|^2 \widehat{\mathcal{K}} \right) \right] \Big|_{(u, U, \phi, \Phi) = (\tilde{u}(s), \tilde{\phi}(s), \tilde{U}(s), \tilde{\Phi}(s)), s=s(f)} \\ &= \left[\frac{\partial}{\partial U_i} \widehat{\mathcal{K}} \right] (\tilde{u}(s(f)), \tilde{\phi}(s(f)), \tilde{U}(s(f)), \tilde{\Phi}(s(f))) \\ &= \left[\frac{\partial}{\partial U_i} \widehat{\mathcal{K}} \right] (u(f), \phi(f), U(f), \Phi(f)), \end{aligned}$$

as well as

$$\begin{aligned} \frac{d\phi}{df} &= \frac{ds}{df} \frac{d\tilde{\phi}}{ds} \Big|_{s=s(f)} \\ &= \frac{1}{\|\tilde{u}(s(f))\|^2} \left[\frac{\partial}{\partial \Phi} \left(\|u\|^2 \widehat{\mathcal{K}} \right) \right] \Big|_{(u, U, \phi, \Phi) = (\tilde{u}(s), \tilde{\phi}(s), \tilde{U}(s), \tilde{\Phi}(s)), s=s(f)} \\ &= \frac{\partial \widehat{\mathcal{K}}}{\partial \Phi} = 1 \end{aligned}$$

and

$$\begin{aligned}
\frac{dU_i}{df} &= \frac{ds}{df} \frac{d\tilde{U}_i}{ds} \Big|_{s=s(f)} \\
&= -\frac{1}{\|\tilde{u}(s(f))\|^2} \left[\frac{\partial}{\partial u_i} \left(\|u\|^2 \widehat{\mathcal{K}} \right) \right] \Big|_{(u,U,\phi,\Phi)=(\tilde{u}(s),\tilde{\phi}(s),\tilde{U}(s),\tilde{\Phi}(s)), s=s(f)} \\
&= -\left[\frac{\partial}{\partial u_i} \widehat{\mathcal{K}} \right] (\tilde{u}(s(f)), \tilde{\phi}(s(f)), \tilde{U}(s(f)), \tilde{\Phi}(s(f))) \\
&= -\left[\frac{\partial}{\partial u_i} \widehat{\mathcal{K}} \right] (u(f), \phi(f), U(f), \Phi(f)) ,
\end{aligned}$$

where to obtain the second equality we used $\widehat{\mathcal{K}}(\tilde{u}(s), \tilde{\phi}(s), \tilde{U}(s), \tilde{\Phi}(s)) = 0$. Finally, we also have

$$\begin{aligned}
\frac{d\Phi}{df} &= \frac{ds}{df} \frac{d\tilde{\Phi}}{ds} \Big|_{s=s(f)} \\
&= -\frac{1}{\|\tilde{u}(s(f))\|^2} \left[\frac{\partial}{\partial \phi} \left(\|u\|^2 \widehat{\mathcal{K}} \right) \right] \Big|_{(u,U,\phi,\Phi)=(\tilde{u}(s),\tilde{\phi}(s),\tilde{U}(s),\tilde{\Phi}(s)), s=s(f)} \\
&= -\left[\frac{\partial}{\partial \phi} \widehat{\mathcal{K}} \right] (\tilde{u}(s(f)), \tilde{\phi}(s(f)), \tilde{U}(s(f)), \tilde{\Phi}(s(f))) \\
&= -\left[\frac{\partial}{\partial \phi} \widehat{\mathcal{K}} \right] (u(f), \phi(f), U(f), \Phi(f)) .
\end{aligned}$$

□

Remark 2.3.3. The correspondence between the initial conditions of the solutions to the Hamilton's equations with regularized Hamiltonian \mathcal{K}

$$(u_1(0), u_2(0), u_3(0), u_4(0), \phi(0), U_1(0), U_2(0), U_3(0), U_4(0), \Phi(0))$$

and the Cartesian set

$$(x(f_0), y(f_0), z(f_0), p_x(f_0), p_y(f_0), p_z(f_0))$$

is clearly not of type one-to-one, leading to many possible real solutions all of them acceptable. It turns out that to close the problem one has some freedom on $u(0)$ to exploit, provided the conditions on the initial bilinear form and energy level of Theorem 2.3.1, for example by simply zeroing out $u_3(0)$ or $u_4(0)$. We exhibit two possible local inversions in §2.3.7.

As in the CR3BP, it is always possible to canonically extend the KS map to conjugate momenta that matches the solutions of the $\widehat{\mathcal{K}}$ -equations with those of the $\widehat{\mathcal{H}}$ -equations, with $\widehat{\mathcal{H}} = \mathcal{H} + \Phi$ autonomous version of (2.2), by considering the bilinear form-induced restriction and taking the quotient space by its characteristic foliation, i.e. the foliation by the orbits of the free circle

action (2.21) (because, like π , $l(S_\theta u, S_\theta U) = l(u, U)$, as for any bilinear form in general). Let

$$\Gamma = \{(u, \phi, U, \Phi) \in T^*((\mathbb{R}^4 \setminus C) \times \mathbb{T}) : l(u, U) = 0\} ,$$

be the constrained phase space of (2.28). The mapping

$$\begin{aligned} \Pi : (\mathbb{R}^4 \setminus \{(0, 0, 0, 0)\}) \times \mathbb{R}^4 &\longrightarrow \mathbb{R}^3 \\ (u, U) &\longmapsto \Pi(u, U) = \bar{p} = (p_x, p_y - 1 + \mu, p_z) \end{aligned} \quad (2.32)$$

where

$$(\bar{p}, 0) = (\bar{p}_1, \bar{p}_2, \bar{p}_3, 0) = \frac{1}{2 \|u\|^2} A(u)U , \quad (2.33)$$

together with (2.6) induce a symplectic correspondence between Γ/\mathcal{S} , that denotes the quotient of Γ by the group action of $\mathcal{S} = \langle S_\theta : \theta \in \mathbb{T} \rangle < SO(4)$, and the Cartesian phase space of $\widehat{\mathcal{H}}$, namely

$$\begin{aligned} \bar{\pi} : \Gamma/\mathcal{S} &\longrightarrow T^*(\mathbb{R}^3 \setminus \{(-1, 0, 0), (0, 0, 0)\}) \times \mathbb{T} \\ (u, \phi, U, \Phi) &\longmapsto \bar{\pi}(u, \phi, U, \Phi) = (q, \phi, \bar{p}, \Phi) \end{aligned} \quad (2.34)$$

with $\bar{\pi}(u, \phi, U, \Phi) = (\pi(u), \phi, \Pi(u, U), \Phi)$, is canonical. Indeed (2.34) preserves the elementary Poisson brackets, because the only non-trivial verifications rest on

$$\begin{aligned} \{\bar{p}_1, \bar{p}_2\} &= \frac{\pi_3(u)}{2 \|u\|^6} l(u, U) , \\ \{\bar{p}_1, \bar{p}_3\} &= -\frac{\pi_2(u)}{2 \|u\|^6} l(u, U) , \\ \{\bar{p}_2, \bar{p}_3\} &= \frac{\pi_1(u)}{2 \|u\|^6} l(u, U) , \end{aligned}$$

which are all zero on Γ/\mathcal{S} . Notice, however, that this can be done only a posteriori, once Γ is identified by Theorem (2.3.1) and the earlier construction.

In the language of symplectic geometry, the argument rephrases more formally as follows. The bilinear relation $l(u, U) = 0$ defines a 9-dimensional manifold in the augmented phase space $T^*((\mathbb{R}^4 \setminus C) \times \mathbb{T})$ interpreted as properly fixing the value of the moment map of the (Hamiltonian) \mathcal{S} action of the KS transformation; by standard symplectic reduction,⁶ the symplectic form $du \wedge dU + d\phi \wedge d\Phi$ determines a symplectic form on the quotient Γ/\mathcal{S} , hence we get a symplectic submanifold $(\Gamma/\mathcal{S}, (du \wedge dU + d\phi \wedge d\Phi)|_{\Gamma/\mathcal{S}})$. Finally, as showed above, the KS transformation induces a symplectic diffeomorphism between Γ/\mathcal{S} and $T^*(\mathbb{R}^3 \setminus \{(-1, 0, 0), (0, 0, 0)\}) \times \mathbb{T}$; the regularization is achieved by changing time via (2.30) on a fixed zero energy surface of the Hamiltonian (2.28) and extending this function through the pre-images of the collisions (cf. [109] and references therein for more details on the geometry of the KS).

⁶This is the content of Marsden-Weinstein-Meyer theorem [64, 67], stating that on a symplectic manifold (M, η) with a Hamiltonian action of a compact Lie group G and associated moment map $\mathcal{M} : M \rightarrow \mathfrak{g}^*$, where \mathfrak{g} is the Lie algebra of G , if $0 \in \mathfrak{g}^*$ is a regular value of \mathcal{M} such that G acts freely on $\overline{M} := \mathcal{M}^{-1}(0)$, then \overline{M}/G is a symplectic manifold with symplectic structure induced by η .

2.3.7 Implementation procedure

We take advantage of the canonical extension at the end of §2.3.6 and rely to the following roadmap to conduct the regularization numerically.

- (i) **Initial conditions.** Pick a Cartesian datum $(x_0, y_0, z_0, f_0, p_{x,0}, p_{y,0}, p_{z,0}, \Phi_0)$ s.t. $(x_0, y_0, z_0) \notin \{(-\mu, 0, 0), (1 - \mu, 0, 0)\}$ with the choice

$$\Phi_0 = -\mathcal{H}(x_0, y_0, z_0, p_{x,0}, p_{y,0}, p_{z,0}, f_0)$$

for the $\widehat{\mathcal{H}}$ -equations.

- (ii) **Transformed initial conditions.** Find u_0, U_0 using the bilinear form relation plus the possible closing relationship $u_{4,0} = 0$ (Remark 2.3.3) and the following atlas of local inversions of the map $\bar{\pi}$ [9]

$$\begin{aligned} \bar{\pi}_-^{-1} : T^*((\mathbb{R}^3 \setminus \{(q_1, 0, 0) : q_1 \geq 0, q_1 = -1\}) \times \mathbb{T}) &\longrightarrow \Gamma \\ \bar{\pi}_+^{-1} : T^*((\mathbb{R}^3 \setminus \{(q_1, 0, 0) : q_1 \leq 0\}) \times \mathbb{T}) &\longrightarrow \Gamma \end{aligned} \quad (2.35)$$

s.t.

$$\begin{aligned} \bar{\pi}_-^{-1}(q, \phi, \bar{p}, \Phi) &= \left(\pi_-^{-1}(q), \phi, 2A(\pi_-^{-1}(q))^T(\bar{p}, 0), \Phi \right) \\ \bar{\pi}_+^{-1}(q, \phi, \bar{p}, \Phi) &= \left(\pi_+^{-1}(q), \phi, 2A(\pi_+^{-1}(q))^T(\bar{p}, 0), \Phi \right), \end{aligned} \quad (2.36)$$

where

$$\begin{aligned} \pi_-^{-1}(q) &= \left(\frac{q_2}{\sqrt{2(d - q_1)}}, \sqrt{\frac{d - q_1}{2}}, 0, \frac{q_3}{\sqrt{2(d - q_1)}} \right) \\ \pi_+^{-1}(q) &= \left(\sqrt{\frac{d + q_1}{2}}, \frac{q_2}{\sqrt{2(d + q_1)}}, \frac{q_3}{\sqrt{2(d + q_1)}}, 0 \right) \end{aligned} \quad (2.37)$$

and $d = \sqrt{q_1^2 + q_2^2 + q_3^2}$.

- (iii) **Fictitious true anomaly span.** Given a certain true anomaly frame $[f_0, f_{\max}]$ of interest, select a suitable integration interval $[0, s_{\max}]$ according to the fact that the parametric motion typically “slows down” while approaching the singularity due to the rescaling (2.30), therefore tune properly $s_{\max} \gtrsim f_{\max} - f_0$ based on the case under consideration.

- (iv) **Solutions in redundant variables.** Integrate the regularized \mathcal{K} -ODEs.

(v) **Original solutions.** Retrieve the original \mathcal{H} -solutions:

$$\begin{cases} x_k = u_{1,k}^2 - u_{2,k}^2 - u_{3,k}^2 + u_{4,k}^2 + 1 - \mu \\ y_k = 2u_{1,k}u_{2,k} - 2u_{3,k}u_{4,k} \\ z_k = 2u_{3,k}u_{1,k} + 2u_{4,k}u_{2,k} \\ p_{x,k} = \frac{1}{2\|u_k\|^2}(u_{1,k}U_{1,k} - u_{2,k}U_{2,k} - u_{3,k}U_{3,k} + u_{4,k}U_{4,k}) \\ p_{y,k} = \frac{1}{2\|u_k\|^2}(u_{2,k}U_{1,k} + u_{1,k}U_{2,k} - u_{4,k}U_{3,k} - u_{3,k}U_{4,k}) + 1 - \mu \\ p_{z,k} = \frac{1}{2\|u_k\|^2}(u_{3,k}U_{1,k} + u_{4,k}U_{2,k} + u_{1,k}U_{3,k} + u_{2,k}U_{4,k}) \end{cases} \quad (2.38)$$

at sample points $f_k \approx f(s_k)$, $k = 1, 2, \dots, K$, given by (2.31).

2.3.8 The advantage of the regularization: a numerical test

In order to assess the effectiveness of KS regularization of the ER3BP near the singularity at \mathcal{P}_1 for numerical integrations, we consider a fictitious simple scenario which is nevertheless representative (for the choice of the initial conditions) of realistic close encounters in the Solar System, such as the close encounters of small objects (such as a comet) with Jupiter, in the Sun-Jupiter ER3BP (here identified by the values $\mu = 9.536433730801362 \cdot 10^{-4}$, $e_1 = 0.0489$). Precisely we consider the case, critical for the numerical integrations, of fast close encounters where “fast” means that the close encounter does not produce a temporary capture through the Lagrangian points L_1 , L_2 (see §A.1). We emphasize that fast close encounters are observed for celestial bodies in the Solar System (see for example [40, 42] where the dynamics of comet 67P Churyumov-Gerasimenko, target of the recent Rosetta mission, is discussed in detail), and are used in astrodynamics to accelerate spacecrafts.

In this subsection we consider a model example numerically integrated with an explicit fixed step numerical integrator of the Runge-Kutta family (Luther’s method [61], RK6 for brevity) to analyze possible gains in the use of the KS regularization. The choice of using an explicit fixed step integrator is motivated by the need to avoid any interference of a variable step strategy with the regularization, which automatically performs the reduction of the step size by adopting a fictitious independent variable. We also remark that, even if the RK6 integrator is not symplectic, it does not produce a relevant energy loss since fast close encounters occur in small time intervals.

In this regard, we choose orbits with initial conditions characterized by a high initial energy $\mathcal{E} > \mathcal{E}_{L_4} := J(x_{L_4}, y_{L_4}, z_{L_4}, x'_{L_4}, y'_{L_4}, z'_{L_4}, f_0)$, where J is the

f -dependent Jacobi “integral”⁷

$$J(x, y, z, x', y', z', f) = \frac{1}{2} \left((x')^2 + (y')^2 + (z')^2 \right) - \frac{1}{1 + e_1 \cos f} \left(\frac{1 - \mu}{d_0} + \frac{\mu}{d_1} + \frac{1}{2} (x^2 + y^2 - z^2 e_1 \cos f) \right), \quad (2.39)$$

having, in the vicinity of the secondary body, an important deflection of the trajectory with respect to the solutions of the Kepler problem defined by the Sun. Moreover, we consider orbits which are non-planar with Jupiter’s orbit. An efficient way to analyze the effect of the regularization on the fast close encounters is to consider the initial conditions already at their minimum distance from Jupiter, with $\mathcal{E} > \mathcal{E}_{L_4}$, with inclination different from 0, and then to numerically integrate the orbit by first running a backward integration up to a sufficiently large distance (at least $d_1 = \|\mathcal{P} - \mathcal{P}_1\| > 1 = \|\mathcal{P}_1 - \mathcal{P}_0\|$) and then, at $f = -2n\pi$ with $n \in \mathbb{N} \setminus \{0\}$ in principle at will, we switch to a forward integration lasting exactly twice the number of iterations of the previous operation, so that the upshot produces almost equal-length branches before and after the encounter (blue and red lines in top panels of Fig. 2.1). More details on the choice of the initial conditions are given in the captions of Fig. 2.1; the physical parameters are drawn from [1]. In such a way, we appreciate the whole dynamics with the deviation caused by the planet.

In Fig. 2.1 and 2.2 we illustrate the particle’s orbit: we set initial values so that the planetary flyby is of hyperbolic gravity-assist type and the heliocentric paths before and after the encounter are almost Keplerian ellipses.

In Table 2.1 we compare the numerical integration of the close encounter represented in Fig. 2.1 and 2.2 using both the Cartesian and the KS regularized equations of motion, for different values of the integration steps. Precisely, using as initial condition the point of closest approach, we integrate the equations of motion forward and backward for about $|\Delta f| \approx 0.5$, since $\Delta f \approx 1$ represents the interval of the true anomaly in which the close encounter takes place. We compare both the conservation of the extended Hamiltonians $\widehat{\mathcal{H}}$, $\widehat{\mathcal{K}}$ and the value of $\|r\|$, $r = (x, y, z)$, at the end of the numerical integration. Since the numerical integration of the Cartesian equations of motion is carried out with a fixed step Δf , while the numerical integration of the regularized equations of motion is realized with a fixed fictitious time Δs , in order to compare the outputs of the two numerical integrations at the same values of f we add a further step to the Cartesian numerical integration in order to reach the final value of f obtained with the KS numerical integration. We note the sharp advantage of the KS algorithm in terms of computational efficiency, providing a sharp reduction of the number of iterations needed to maintain a high level of accuracy in the representation of the trajectory around \mathcal{P}_1 .

We finally argue that, to maximize the computational efficiency in a long simulation, one should implement as usual a switching tool which works with the \mathcal{H} -equations out of a ball centered at \mathcal{P}_1 , say the body’s Hill sphere, and the

⁷We recall that, instead of (1.76), J is not a first integral for the eccentricities $e_1 > 0$; therefore the choice $\mathcal{E} > \mathcal{E}_{L_4}$ provides only a trial initial condition for having a fast close encounter.

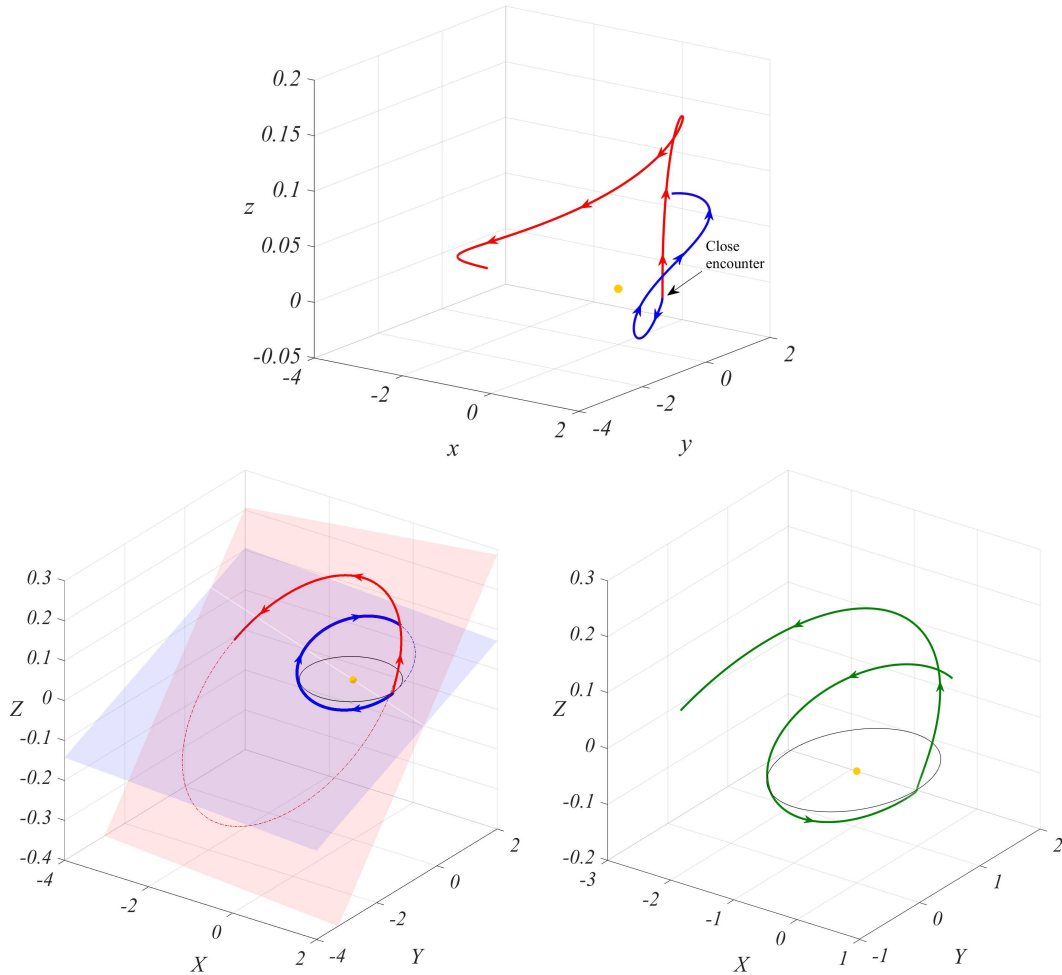


Figure 2.1: Physical orbit in the Sun-Jupiter ER3BP (reported in convenient aspect ratio for visual clarity) integrated backward and forward in true anomaly following the arrow heads for $x_0 = 1 - \mu + 1.921451079855507 \cdot 10^{-3}$ (≈ 0.01 AU of altitude), $y_0 = z_0 = f_0 = 0$, $p_{x,0} = 0.2$, $p_{y,0} = 1.8$, $p_{z,0} = 0.6$. The yellow dot symbolizes the Sun, whereas the black thin style curve represents Jupiter's elliptic motion. **Top panel:** Cartesian version (backward in blue overlapping the forward in red) traced in the rotating-pulsating frame $Oxyz$. **Left bottom panel:** Cartesian backward (blue) and forward (red) trajectory in the inertial barycentric frame $OXYZ$ with osculating heliocentric ellipses belonging to mutually inclined planes. **Right bottom panels:** KS integration of the inertial trajectory in the forward case.

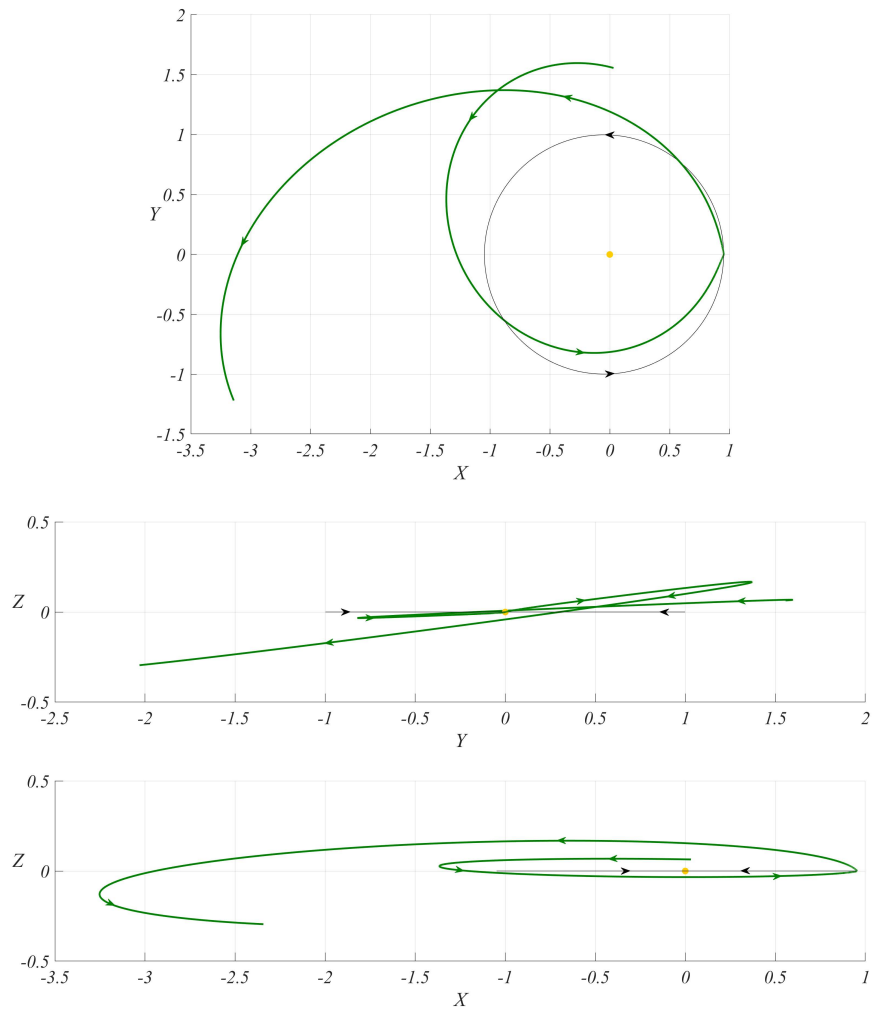


Figure 2.2: Projections on the coordinate planes of the right bottom panel of Fig. 2.1 on equal axis aspect ratio.

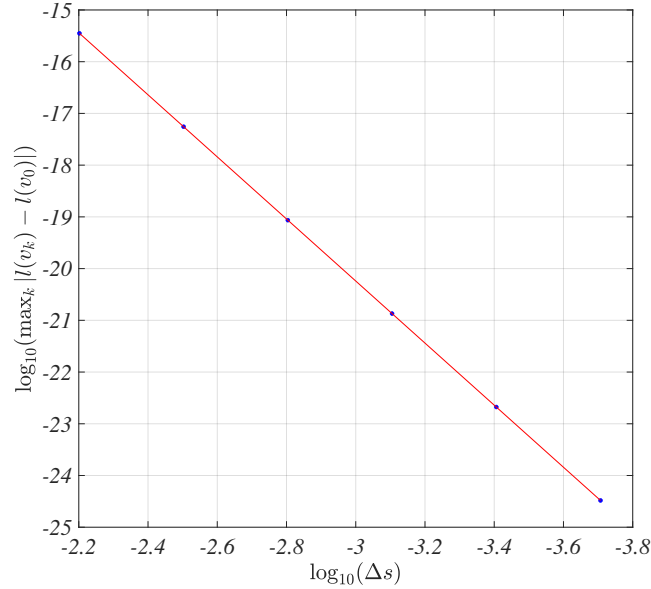


Figure 2.3: Logarithmic scale convergence profile of the maximum committed error in the bilinear form preservation along the forward motion in Fig. 2.1. Here $v := (u, U)$ and the discretization is $v_k \approx v(s_k)$ for $s_k = k\Delta s, k = 0, \dots, K$. The blue dots correspond to the worst errors found for five consecutive reductions starting from $\Delta s = 2\pi \cdot 10^{-3}$, halving each time the value (reversed horizontal axis). The best linear fitting returns the red straight interpolant with slope $\beta = 6.0000334$ and intercept $\alpha = -2.2403447$.

\mathcal{K} -equations once inside. This is exactly the strategy adopted with numerical propagations throughout the thesis whenever needed.

As conclusive remark, since \mathcal{K} and l are smooth functions in a neighborhood of \mathcal{P}_1 , we get that the invariances given by $\mathcal{K}(u, \phi, U, \Phi) = 0, l(u, U) = 0$ are numerically satisfied with high precision, and eventually the machine precision is quickly reached after lowering Δs by about a factor of a hundredth (in a convergence profile, the rate of decay reflects the accuracy of the method, i.e. $O(\Delta s^6)$, as illustrated in Fig. 2.3).

Δf (Cart.)	$\ r(-0.506682)\ $	$\ r(0.496131)\ $	# iter.
$2\pi \cdot 10^{-6}$	0.8553075048550535	0.9760051057296899	240244
$2\pi \cdot 10^{-5}$	0.8553075048542582	0.9760051057288172	24026
$2\pi \cdot 10^{-4}$	0.8553060796173549	0.9760054080001320	2404
$2\pi \cdot 10^{-3}$ (*)	0.8248588821498852	0.9897100124542644	241
Δs (KS reg.)	$\ r(f(-3.7\pi))\ $	$\ r(f(3.5\pi))\ $	# iter.
$\pi \cdot 10^{-4}$	0.8553075048550521	0.9760051057296942	109000
$\pi \cdot 10^{-3}$	0.8553075048550521	0.9760051057296942	10900
$\pi \cdot 10^{-2}$	0.8553075048550522	0.9760051057296968	1090
$\pi \cdot 10^{-1}$	0.8553075050607468	0.9760051591505222	109

Δf (Cart.)	$ \widehat{\mathcal{H}}(-0.506682) $	$ \widehat{\mathcal{H}}(0.496131) $
$2\pi \cdot 10^{-6}$	$1.0417562295 \cdot 10^{-18}$	$1.0277827090 \cdot 10^{-18}$
$2\pi \cdot 10^{-5}$	$9.3757489321 \cdot 10^{-13}$	$7.9843639352 \cdot 10^{-13}$
$2\pi \cdot 10^{-4}$	$1.1893484533 \cdot 10^{-7}$	$8.5748939646 \cdot 10^{-7}$
$2\pi \cdot 10^{-3}$ (*)	$8.0281428133 \cdot 10^{-2}$	0.10590853333
Δs (KS reg.)	$ \widehat{\mathcal{K}}(-3.7\pi) $	$ \widehat{\mathcal{K}}(3.5\pi) $
$\pi \cdot 10^{-4}$	$1.3746151644 \cdot 10^{-27}$	$1.3290033656 \cdot 10^{-28}$
$\pi \cdot 10^{-3}$	$1.3738069068 \cdot 10^{-21}$	$1.3119148531 \cdot 10^{-22}$
$\pi \cdot 10^{-2}$	$1.3654070424 \cdot 10^{-15}$	$1.1227698042 \cdot 10^{-16}$
$\pi \cdot 10^{-1}$	$1.2545211218 \cdot 10^{-9}$	$3.0569361253 \cdot 10^{-10}$

Table 2.1: Comparison of Cartesian with KS integrations for four consecutively increased step sizes in a small neighborhood of $f = s = 0$ (close approach). The propagations are performed backward in time up to $f(-3.7\pi) = -0.506682$, then forward up to $f(3.5\pi) = 0.496131$, according to choices of s such that the true anomaly interval is almost symmetric with respect to the origin and nodes are multiple integers of every Δs considered. For each case the step size is adapted in order to evaluate the singular and regularized solution at same corresponding times. The asterisk in the last Cartesian experiment indicates failure of the adopted numerical method (explicit RK6) to compute the orbit accurately. The computations are performed using a quadruple-precision floating-point format in FORTRAN 2008. **Top panel:** norm of the solutions and total number of iterations. **Bottom panel:** degree of conservation of the singular extended Hamiltonians, where $\widehat{\mathcal{H}}(0) = \widehat{\mathcal{K}}(0) = 0$.

CLOSED-FORM PERTURBATION THEORY FOR EXTERNAL ORBITS IN THE RESTRICTED THREE-BODY PROBLEM WITHOUT RELEGATION

This chapter aims to develop a semi-analytic algorithm that models the secular dynamics of bodies with orbits external to the one of the primary perturber of the R3BP using a sophisticated ad hoc version of the normal form theory recalled in §1.2.5. The content, jointly with the results of the next chapter, is partly available in [89] and entirely in [91].

3.1 Introduction

As opposed to the usual (Laplace-Lagrange) theory, closed-form perturbation theory [78] provides a framework for series calculations in perturbed Keplerian problems without expansions in powers of the bodies' orbital eccentricities. This is mainly motivated by the necessity to construct secular models for sufficiently eccentric orbits, like those of many asteroids, in our solar system, or the planets in extrasolar planetary systems.

The efficiency of the usual series methods of expansion in the orbital eccentricities is limited by the fact that the inversion of Kepler's equation in powers of the eccentricity converges only up to the so-called Laplace limit $e_L \approx 0.66274$ [28]. Generally, such convergence slows down way before this value (around $e \sim 0.3 - 0.4$ in many applications). In order to address this issue, closed form perturbation theory aims to solve in "closed-form" the homological equation by which the Lie generating function is computed at every perturbative step (see for example [23, 26]). The process is far from being priceless: a major obstruction appears when the kernel of the homological equations contains addenda beyond the Keplerian terms. The most common such addendum ([78]) is the centrifugal term $-\nu H$, where ν is the angular frequency in a frame co-rotating with the primary perturber, and H is the Delaunay action equal to

the particle's angular momentum in the direction of the axis of rotation. In the case of a planet's orbiter, ν is equal to the planet's rotation frequency, and the problem appears for all non-axisymmetric terms (tesseral harmonics) of the planet's multipole potential. In the R3BP, instead, ν represents the mean motion of the primary perturber (e.g. Jupiter in the Sun-Jupiter system), while the problem appears in a similar way after introducing a multipole expansion of the disturbing function in the particle's Hamiltonian.

An algorithm to overcome the above issue, called the *relegation algorithm*, has been proposed in works by Deprit, Palacián and collaborators [12, 24, 53, 79, 94]. Briefly, given a quasi-integrable Hamiltonian $H = H_0 + \varepsilon H_1$, where ε is a small parameter, suppose that $H_0 = H'_0 + H''_0$, where, in a domain in phase space we have that H'_0 yields the dominant contribution to the Hamiltonian flow of H_0 versus the H''_0 term. In usual perturbation theory, we seek to partly normalize the perturbation H_1 via a sequence of canonical transformations defined by generating functions $\chi^{(r)}$, $r = 1, 2, \dots$ satisfying a homological equation of the form $\{H_0, \chi^{(r)}\} + h_1^{(r)} = 0$, where $\{\cdot, \cdot\}$ denotes the Poisson bracket between two functions of the canonical variables and $h_1^{(r)}$ is a term in the Hamiltonian to be normalized. In the relegation technique, we use instead the equation $\{H'_0, \chi^{(r)}\} + h_1^{(r)} = 0$, i.e., letting only the dominant function H'_0 in the kernel of the homological equation. Such a choice stems mostly from motives of algorithmic convenience. For example, identifying H'_0 with the Keplerian term (when ν is small) leads to a homological equation that can be solved in closed form (we set, instead, $H'_0 = -\nu H$ when ν is large). However, all Poisson brackets of $\chi^{(r)}$ with the part H''_0 left out of the kernel lead to terms which need to be "relegated", i.e., pushed to normalization in subsequent steps. For reasons explained in detail in [96], only a finite number of relegation steps can be performed before reaching a point beyond which the scheme generates divergent sequences of terms (see also [94]). This implies that the process necessarily stops after some steps, leading to a finite, albeit possibly quite small remainder.

Relegation is a technique particularly suitable to the limiting situation of a strongly hierarchical problem, when the integrable part H_0 depends on a frequency vector involving n frequencies $\omega = (\omega_1, \dots, \omega_n)$ out of which one, say ω_i for some i with $1 \leq i \leq n$ is significantly larger in absolute value than the rest. In particular, the harmonics $\cos(k \cdot \varphi)$ in the Hamiltonian whose normalization can be 'relegated' should satisfy $|k_i \omega_i| \gg |k_j \omega_j|$, $j = 1, \dots, n$, $j \neq i$, for every integer $k_i, k_j \in \mathbb{Z} \setminus \{0\}$ (assuming also the non-resonant condition $k \cdot \omega \neq 0$, $k = (k_1, \dots, k_n)$). For example, as explained in [96] in the simple case with $n = 2$ and $\omega_2 \gg \omega_1$, the generating function $\chi^{(N)}$ produced after N relegation steps contains terms with coefficients growing as a geometric sequence with ratio $k_1 \omega_1 / k_2 \omega_2$. Thus, relegation is limited to those terms for which the above ratio is smaller than unity. This includes most harmonics of low Fourier order in the Hamiltonian perturbation when $\omega_2 \gg \omega_1$, but only few when the two frequencies become comparable in size. Hence, by construction, relegation has limited applicability in this latter, non-hierarchical, case.

Variants of the relegation technique have been discussed in literature to

address perturbed Keplerian problems in which the gravitational potential is due to an extended body expanded in spherical harmonics (e.g. [53, 62]). To address the non-hierarchical case, a technique similar to the one of the present paper is discussed in [53], referring to the averaging of the tesseral harmonics in the case of the Earth's artificial satellites. In the case of the R3BP, instead, Cavallari and Efthymiopoulos [11] discuss a relegation-free algorithm for the elimination of short-period terms in the particle's Hamiltonian, when the orbit of the particle (e.g. an asteroid) is totally interior to the orbit of the primary perturber (e.g. Jupiter). We are aware of no relegation-free algorithm proposed in literature which addresses, instead, the case when the particle's orbit is exterior to the orbit of the primary perturber. Providing such an algorithm, discussing some of its important differences with past-proposed algorithms, as well as checking its limits of applicability (addressed in more detail later in Chapter 4), constitutes the primary goal of the present chapter.

The R3BP has already been defined in §1.3.3. The starting point for our analysis in the sequel is the Hamiltonian of the model, obtained after reduction via Jacobi coordinates (R, P) .¹ Adopting the usual notation for labels as before, we keep referring to the primary (or central body) as \mathcal{P}_0 and to the secondary (or primary perturber) as \mathcal{P}_1 . Expressing time through the secondary's mean anomaly $M_1 = n_1 t$, where n_1 is the mean motion of the secondary, and canonically conjugating M_1 with a dummy action variable J_1 allows to express the Hamiltonian as

$$\mathcal{H}(R, M_1, P, J_1) = \frac{\|P\|^2}{2} - \frac{\mathcal{G}m_0}{\|R + \mu r_1(M_1)\|} - \frac{\mathcal{G}m_1}{\|R - (1 - \mu)r_1(M_1)\|} + n_1 J_1, \quad (3.1)$$

where \mathcal{G} is the gravitational constant and

$$\mu = \frac{m_1}{m_0 + m_1} \in]0, 1/2]$$

is the mass parameter;

$$r_1(M_1) = a_1 \left(\cos E_1(M_1) - e_1, \sqrt{1 - e_1^2} \sin E_1(M_1), 0 \right) \quad (3.2)$$

is the elliptic revolution of $\mathcal{P}_0 - \mathcal{P}_1$ around their barycenter with eccentricity e_1 and semi-major axis a_1 , in which the dependence of the system's eccentric anomaly $E_1 \in \mathbb{T}$ on the mean anomaly $M_1 \in \mathbb{T}$ is given through Kepler's equation according to standard two-body problem setting; $(R = (X, Y, Z), P = (P_X, P_Y, P_Z)) \in T^*(\mathbb{R}^3 \setminus \{-\mu r_1, (1 - \mu)r_1\})$ is the position-momentum couple of \mathcal{P} and the phase space is endowed with standard symplectic form $dP_X \wedge dX + dP_Y \wedge dY + dP_Z \wedge dZ + dJ_1 \wedge dM_1$.

We make use then of Delaunay elements (1.64) (ℓ, g, h, L, G, H) adapted to the

¹In the R3BP problem the Jacobi transformation is implemented when $\|R\| > \|r_1\|$.

restricted case, defined by

$$\begin{aligned} L &= \sqrt{\mathcal{G}m_0a} , & \ell &= M , \\ G &= L\sqrt{1-e^2} , & g &= \omega , \\ H &= G \cos i , & h &= \Omega , \end{aligned} \quad (3.3)$$

where $a, e, i, M, \Omega, \omega$ stand for the semi-major axis, the eccentricity, the inclination, the mean anomaly, the longitude of the ascending node, the argument of pericenter of the particle.

A key ingredient of the method proposed below is the following: similarly as in [11], we introduce a book-keeping symbol σ with numerical value equal to 1, whose role is to organize the perturbative scheme so as to successively normalize terms of similar order of smallness, treating together all small quantities of the problem, i.e.,

- the eccentricities e, e_1 (when $e_1 \neq 0$),
- the mass ratio μ ,
- the semi-major axis fluctuation δL around the mean L_* for a particular particle trajectory.

The book-keeping symbol acts by assigning powers σ^1 and σ^{ν_1} (for e and e_1), σ^ν (for μ), σ^ν (for δL) respectively, for non-zero natural numbers ν, ν_1 defined below, to all the terms in the original Hamiltonian as well as in the Hamiltonian produced after every normalization step. Given this baseline, we arrive (in §3.2) at the following result: we demonstrate that, for $k_\mu, k_{\text{mp}} \in \mathbb{N} \setminus \{0\}$ with $k_\mu > 1$, the combination of expansions of (3.1) up to μ^{k_μ} and $(\|r_1\|/\|R\|)^{k_{\text{mp}}}$ is canonically conjugate by $\nu(k_\mu - 1)$ near-identity transformations to a secular model, obtained as a normal form with respect to the fast angles ℓ, M_1

$$\mathcal{H}(\ell, g, h, M_1, \delta L, G, H, J_1) = \mathcal{H}_0(g, h, \delta L, G, H, J_1) + \mathcal{R}(\ell, g, h, M_1, \delta L, G, H) , \quad (3.4)$$

with

$$\mathcal{H}_0 = n_*\delta L + n_1J_1 + \sum_{l=\nu}^{\nu k_\mu - 1} \sum_{p \in \mathbb{Z}^2} c_{l,p}(\delta L, e, i; \mu, L_*, a_1, e_1) \cos(p_1g + p_2h)\sigma^l , \quad (3.5)$$

$$\begin{aligned} \mathcal{R} = \sum_{s \in \mathbb{Z}^4} d_{\nu k_\mu, s}(E_1, \delta L, e, i; \mu, L_*, a_1, e_1) \cos(s_1f + s_2g + s_3h + s_4E_1)\sigma^{\nu k_\mu} \\ + \mathcal{O}\left(\sigma^{\nu k_\mu + 1}; \left(\frac{\|r_1\|}{\|R\|}\right)^{k_{\text{mp}} + 1}\right) . \end{aligned} \quad (3.6)$$

The dependencies $f = f(\ell, \delta L, G)$ for the true anomaly, $e = e(\delta L, G)$ and $i = i(G, H)$ are implied in all the above expressions; $c_{l,p}, d_{\nu k_\mu, s}$ are real coefficients. A crucial point is the way by which the positive integers $\nu = \nu(e_*, \mu) \geq 1$,

$\nu_1 = \nu_1(e_*, e_1) \geq 1$ are chosen. As detailed below, these integers, which regulate the book-keeping scheme, are suitably tuned on the basis of a selected reference value $e_* \in]0, 1[$:

$$\nu = \left\lceil \frac{\log_{10} \mu}{\log_{10} e_*} \right\rceil, \quad \nu_1 = \left\lceil \frac{\log_{10} e_1}{\log_{10} e_*} \right\rceil, \quad (3.7)$$

where $\lceil \cdot \rceil$ is the ceiling function. The normalizing scheme leading to (3.4) is local: knowing that the semi-major axis is preserved under the flow of the (secular) normal form, we introduce the splitting $L = L_* + \delta L$, where $L_* = \sqrt{\mathcal{G}m_0 a_*} \gg \delta L$, $n_* = \sqrt{\mathcal{G}m_0 a_*}^{-3/2}$ is a targeted reference value for the semi-major axis a_* , and expand the Hamiltonian in powers of δL , rendering δL the new action variable canonically conjugated to the particle's mean anomaly.

Given the above, the normalization algorithm provides a sequence of Lie generating functions $\chi_{\nu+j-1}^{(j)} = \mathcal{O}(\sigma^{\nu+j-1})$, $j = 1, \dots, \nu(k_\mu - 1)$, which yields the Lie canonical transformation allowing to recursively normalize all terms depending on the angles f and E_1 in the Hamiltonian. The normalizing transformations are possible to define for values of the frequencies n_* (mean motion of the particle at the semi-major axis a_*) and n_1 far from mean-motion resonances (see Remark 3.2.3). Furthermore, the generating functions are computed as solutions of a homological equation of the form

$$\{\mathcal{Z}_0, \chi_{\nu+j-1}^{(j)}\} + \mathcal{R}_{\nu+j-1, \nu+j-1}^{(j-1)} = \mathcal{O}(\sigma^{\nu+j-1}), \quad (3.8)$$

where $\mathcal{Z}_0 = n_* \delta L + n_1 J_1$ and $\mathcal{R}_{\nu+j-1, \nu+j-1}^{(j-1)} \sim \sigma^{\nu+j-1}$ collects the trigonometric monomials of $\mathcal{O}(\sigma^{\nu+j-1})$ depending on at least one of the two anomalies. The key to obtaining a closed-form solution for (3.8) is, precisely, the appropriate choice of a $\mathcal{O}(\sigma^{\nu+j-1})$ remainder left in the second hand of the equation. In words, we do not seek for an exact cancellation of the terms $\mathcal{R}_{\nu+j-1, \nu+j-1}^{(j-1)}$, but only for an approximate cancellation, leading to a remainder, which, however, is of higher order in book-keeping, and, hence, possible to reduce at subsequent steps.

The presentation is structured as follows. §3.2 presents step-by-step the algorithm that gives rise to (3.5) and (3.6), supplemented with the formulas for the Poisson algebra in Keplerian elements used in all closed-form computations. §3.3 is devoted to a numerical investigation of the method's accuracy for an asteroid in the Sun-Jupiter system, first in the spatial ER3BP, and then in the planar CR3BP.

3.2 The closed-form method for the outermost R3BP

3.2.1 Multipole expansion of the perturbation

Referring to section 3.1, let \mathcal{H} be given in barycentric Cartesian coordinates as in (3.1):

$$\mathcal{H} = \frac{\|P\|^2}{2} + n_1 J_1 - \mathcal{G} m_0 \mathcal{R}, \quad (3.9)$$

Assuming $\|r_1\|/\|R\| < 1$, we carry out a multipole expansion of the function $\mathcal{R}(R, M_1)$ in powers of the ratio $\|r_1\|/\|R\| < 1$:

$$\begin{aligned} \mathcal{R} &= \frac{1}{\|R + \mu r_1\|} + \frac{\mu}{1 - \mu} \frac{1}{\|R + (1 - \mu)r_1\|} \\ &= \frac{1}{\|R\|} \left(\sum_{l=0}^{\infty} \binom{-1/2}{l} \left(\frac{2\mu r_1 \cdot R}{\|R\|^2} + \mu^2 \left(\frac{\|r_1\|}{\|R\|} \right)^2 \right)^l \right. \\ &\quad \left. + \frac{\mu}{1 - \mu} \sum_{l=0}^{\infty} \binom{-1/2}{l} \left(-\frac{2(1 - \mu)r_1 \cdot R}{\|R\|^2} + (1 - \mu)^2 \left(\frac{\|r_1\|}{\|R\|} \right)^2 \right)^l \right) \\ &= \frac{1}{1 - \mu} \frac{1}{\|R\|} + \mathcal{O} \left(\left(\frac{\|r_1\|}{\|R\|} \right)^2 \right). \end{aligned} \quad (3.10)$$

where, for $\beta \in \mathbb{R}$

$$\binom{\beta}{l} = \frac{\beta(\beta - 1) \cdots (\beta - l + 1)}{l!}$$

indicates the generalized binomial coefficient (equal to 1 for $l = 0$).

Remark 3.2.1. For $l = 1$ in (3.10) the coefficients of the dipole term $(r_1 \cdot R)/\|R\|^3$ in the two sums in the right-hand side of the equation cancel each other exactly. Thus, no dipole term appears in the disturbing function. This is a consequence of the choice of Jacobi coordinates.

3.2.2 Canonical form of the Hamiltonian

Performing an extra series expansion in powers of $\mu < 1$ yields the standard nearly-integrable form

$$\mathcal{H} = \mathcal{H}_0 + \mu \mathcal{H}_1, \quad (3.11)$$

where the Keplerian part reads

$$\mathcal{H}_0 = \frac{\|P\|^2}{2} - \frac{\mathcal{G} m_0}{\|R\|} + n_1 J_1 \quad (3.12)$$

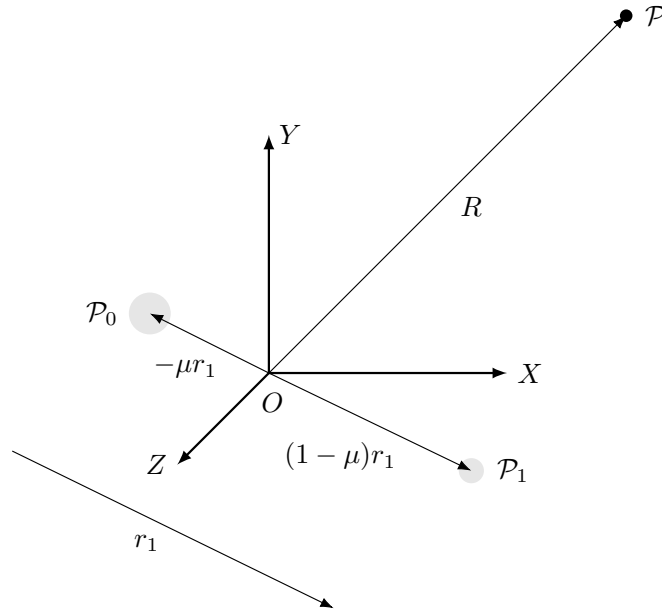


Figure 3.1: Representation of the R3BP in the barycentric frame (or equivalently in Jacobi variables) with $\|R\| > \|r_1\|$.

and the disturbing function becomes

$$\mathcal{H}_1 = -\frac{\mathcal{G}m_0}{\|R\|} \left(\sum_{l=0}^{\infty} \mu^l + \sum_{l=1}^{\infty} \mu^{l-1} \binom{-1/2}{l} \left(\frac{2r_1 \cdot R}{\|R\|^2} + \mu \left(\frac{\|r_1\|}{\|R\|} \right)^2 \right)^l + \sum_{l=1}^{\infty} (1-\mu)^{l-1} \binom{-1/2}{l} \left(-\frac{2r_1 \cdot R}{\|R\|^2} + (1-\mu) \left(\frac{\|r_1\|}{\|R\|} \right)^2 \right)^l \right). \quad (3.13)$$

We now move to Delaunay action-angle variables (3.3) by replacing into (3.11) the relationships

$$\mathcal{H}_0 = -\frac{\mathcal{G}m_0}{2a} + n_1 J_1, \quad (3.14)$$

$$\|R\| = \frac{a(1-e^2)}{1+e \cos f}, \quad (3.15)$$

$$r_1 \cdot R = a_1 \|R\| \left((\cos E_1 - e_1) (\cos h \cos(g+f) - \sin h \sin(g+f) \cos i) + \sqrt{1-e_1^2} \sin E_1 (\sin h \cos(g+f) + \cos h \sin(g+f) \cos i) \right) \quad (3.16)$$

as well as (3.2) for the vector r_1 . We get

$$\mathcal{H} = -\frac{\mathcal{G}m_0}{2a} + n_1 J_1 + \mu \mathcal{H}_1(f, g, h, E_1, a, e, i; \mu, a_1, e_1). \quad (3.17)$$

Remark 3.2.2. Only the square of the norm $\|r_1\|^2 = r_1 \cdot r_1$ is required in (3.13), while the norm $\|R\|$ appears only in the denominator of the above equation, in powers equal to or higher than quadratic. Then equations (3.15) and (3.2), respectively dependent on f and E_1 , lead to a representation of the disturbing function as a sum of trigonometric polynomials depending on harmonics of the form $\cos(s_1 f + s_2 g + s_3 h + s_4 E_1)$. This is a key ingredient of the closed-form method, i.e., working with the angles f and E_1 , instead of the mean anomalies M, M_1 , no series reversion of Kepler's equation is used throughout the whole perturbative scheme.

In order to avoid relegation, our method discussed below works locally, by constructing a model for the secular Hamiltonian valid for a particle's semi-major axis varying as $a = a_* + \delta a(t)$, i.e., by a small quantity δL around some reference value a_* . By standard secular theory, we have the estimate $\delta a = \mathcal{O}(\mu)$ far from mean-motion resonances. Formally, introducing the new canonical variable δL as

$$L = L_* + \delta L = \sqrt{\mathcal{G}m_0 a_*} + \frac{1}{2} \sqrt{\frac{\mathcal{G}m_0}{a_*}} \delta a + \mathcal{O}(\delta a^2). \quad (3.18)$$

and expanding the Hamiltonian in powers of the quantity δL around L_* , we obtain

$$\begin{aligned} \mathcal{H} &= -\frac{\mathcal{G}^2 m_0^2}{2L_*^2} \sum_{l=0}^{\infty} \binom{-2}{l} \left(\frac{\delta L}{L_*}\right)^l + n_1 J_1 + \mu \sum_{l=0}^{\infty} \frac{1}{l!} \left. \frac{\partial^l \mathcal{H}_1}{\partial L^l} \right|_{L=L_*} \delta L^l \\ &= n_* \delta L + n_1 J_1 + \mu \left(\mathcal{H}_1|_{\delta L=0, \mu=0} + \left. \frac{\partial \mathcal{H}_1}{\partial \delta L} \right|_{\delta L=0, \mu=0} \delta L \right) + \mathcal{O}(\mu^2, \delta L^2), \end{aligned} \quad (3.19)$$

where a constant term $-\mathcal{G}^2 m_0^2 / (2L_*^2)$ was dropped from the expansion. The constant $n_* = \mathcal{G}^2 m_0^2 / L_*^3$ is equal to the particle's mean motion under Keplerian orbit at the semi-major axis a_* . Other useful rewritings of \mathcal{H}_1 depending on the elements are exposed in Appendix B.

Remark 3.2.3. The choice of the reference value a_* determines the kind of divisors appearing in the normalization procedure. In the present paper, we deal only with the “non-resonant” case, in which the frequencies n_* and n_1 satisfy no-commensurability condition. For example, to be far from any resonance we may require that n_* and n_1 satisfy a Diophantine condition

$$|k_* n_* + k_1 n_1| > \frac{\gamma}{|k|^\tau}, \quad \forall k = (k_*, k_1) \in \mathbb{Z}^2 \setminus \{0\} \quad (3.20)$$

with $|k| = |k_*| + |k_1|$ and some suitable $\gamma > 0, \tau > 1$.

However, the algorithm presented below can be readily extended to cases of mean-motion resonance. We leave the details for a future work, noting only that in resonant cases we have the estimate $\delta L = \mathcal{O}(\mu^{1/2})$, instead of $\mathcal{O}(\mu)$. The effect of approaching close to a mean-motion resonance with the present series is seen, instead, as a rise in the value of the series' remainder, caused by (non-zero) small divisors in the series (as visible, for example, in Fig. 4.6 discussed in §4.4.2).

3.2.3 Poisson structure and book-keeping

Poisson bracket formulas

All steps of closed-form perturbation theory involve Poisson brackets between differentiable functions of the form $F(\ell, g, h, M_1, \delta L, G, H, J_1) \in C^\infty(\mathbb{T}^4 \times D)$, $D \subset \mathbb{R}^4$ being an open set, whose dependence on the variables ℓ , M_1 , G and H is given in implicit form through the functions $f(\ell, \delta L, G)$, $e(\delta L, G)$, $E_1(M_1, e(\delta L, G))$, $\iota_c(G, H) = \cos i(G, H)$, $\iota_s(G, H) = \sin i(G, H)$, $\eta(\delta L, G) = \sqrt{1 - e(\delta L, G)^2}$, $\|r_1\|(M_1) = a_1(1 - e_1 \cos E_1(M_1))$, and $\phi_1(M_1) = E_1(M_1, e(\delta L, G)) - M_1$. The Poisson bracket between two functions F_1, F_2 of the above form is computed by the formulas

$$\begin{aligned} \{F_1, F_2\} = & \frac{dF_1}{d\ell} \frac{dF_2}{d\delta L} + \frac{dF_1}{dg} \frac{dF_2}{dG} + \frac{dF_1}{dh} \frac{dF_2}{dH} + \frac{dF_1}{dM_1} \frac{dF_2}{dJ_1} \\ & - \frac{dF_1}{d\delta L} \frac{dF_2}{d\ell} - \frac{dF_1}{dG} \frac{dF_2}{dg} - \frac{dF_1}{dH} \frac{dF_2}{dh} - \frac{dF_1}{dJ_1} \frac{dF_2}{dM_1} \end{aligned} \quad (3.21)$$

implemented to the closed-form version of the functions F_1, F_2 . The closed-form version of a function F is defined as:

$$F = F(f, g, h, E_1, \delta L, e, \eta, \iota_c, \iota_s, J_1). \quad (3.22)$$

The derivatives in the canonical variables of a function F as in (3.21) are computed by the chain rule formulas

$$\frac{dF}{d\ell} = \frac{\partial F}{\partial f} \frac{\partial f}{\partial \ell}, \quad (3.23)$$

$$\frac{dF}{dg} = \frac{\partial F}{\partial g}, \quad (3.24)$$

$$\frac{dF}{dh} = \frac{\partial F}{\partial h}, \quad (3.25)$$

$$\frac{dF}{dM_1} = \left(\frac{\partial F}{\partial E_1} + \frac{\partial F}{\partial \|r_1\|} \frac{d\|r_1\|}{dE_1} + \frac{\partial F}{\partial \phi_1} \right) \frac{dE_1}{dM_1} - \frac{\partial F}{\partial \phi_1}, \quad (3.26)$$

$$\frac{dF}{d\delta L} = \frac{\partial F}{\partial f} \frac{\partial f}{\partial \delta L} + \frac{\partial F}{\partial \delta L} + \frac{\partial F}{\partial e} \frac{\partial e}{\partial \delta L} + \frac{\partial F}{\partial \eta} \frac{\partial \eta}{\partial \delta L}, \quad (3.27)$$

$$\frac{dF}{dG} = \frac{\partial F}{\partial f} \frac{\partial f}{\partial G} + \frac{\partial F}{\partial e} \frac{\partial e}{\partial G} + \frac{\partial F}{\partial \eta} \frac{\partial \eta}{\partial G} + \frac{\partial F}{\partial \iota_c} \frac{\partial \iota_c}{\partial G} + \frac{\partial F}{\partial \iota_s} \frac{\partial \iota_s}{\partial G}, \quad (3.28)$$

$$\frac{dF}{dH} = \frac{\partial F}{\partial \iota_c} \frac{\partial \iota_c}{\partial H} + \frac{\partial F}{\partial \iota_s} \frac{\partial \iota_s}{\partial H}, \quad (3.29)$$

$$\frac{dF}{dJ_1} = \frac{\partial F}{\partial J_1}, \quad (3.30)$$

where

$$\frac{\partial f}{\partial \ell} = \frac{(1 + e \cos f)^2}{\eta^3}, \quad (3.31)$$

$$\frac{d\|r_1\|}{dE_1} = a_1 e_1 \sin E_1, \quad (3.32)$$

$$\frac{dE_1}{dM_1} = \frac{a_1}{\|r_1\|}, \quad (3.33)$$

$$\frac{\partial f}{\partial \delta L} = \frac{1}{L} \left(\frac{2 \sin f}{e} + \frac{\sin(2f)}{2} \right) = \frac{1}{L_*} \left(\frac{2 \sin f}{e} + \frac{\sin(2f)}{2} \right) \left(1 - \frac{\delta L}{L_*} \right) + \mathcal{O}(\delta L^2), \quad (3.34)$$

$$\frac{\partial e}{\partial \delta L} = \frac{\eta^2}{eL} = \frac{\eta^2}{eL_*} \left(1 - \frac{\delta L}{L_*} \right) + \mathcal{O}(\delta L^2), \quad (3.35)$$

$$\frac{\partial \eta}{\partial \delta L} = -\frac{\eta}{L} = -\frac{\eta}{L_*} \left(1 - \frac{\delta L}{L_*} \right) + \mathcal{O}(\delta L^2), \quad (3.36)$$

$$\begin{aligned} \frac{\partial f}{\partial G} &= -\frac{1}{\eta L} \left(\frac{2 \sin f}{e} + \frac{\sin(2f)}{2} \right) \\ &= -\frac{1}{\eta L_*} \left(\frac{2 \sin f}{e} + \frac{\sin(2f)}{2} \right) \left(1 - \frac{\delta L}{L_*} \right) + \mathcal{O}(\delta L^2), \end{aligned} \quad (3.37)$$

$$\frac{\partial e}{\partial G} = -\frac{\eta}{eL} = -\frac{\eta}{eL_*} \left(1 - \frac{\delta L}{L_*} \right) + \mathcal{O}(\delta L^2), \quad (3.38)$$

$$\frac{\partial \eta}{\partial G} = \frac{1}{L} = \frac{1}{L_*} \left(1 - \frac{\delta L}{L_*} \right) + \mathcal{O}(\delta L^2), \quad (3.39)$$

$$\frac{\partial \iota_c}{\partial G} = -\frac{\iota_c}{\eta L} = -\frac{\iota_c}{\eta L_*} \left(1 - \frac{\delta L}{L_*} \right) + \mathcal{O}(\delta L^2), \quad (3.40)$$

$$\frac{\partial \iota_s}{\partial G} = -\frac{1 - \iota_s^2}{\eta L \iota_s} = -\frac{1 - \iota_s^2}{\eta L_* \iota_s} \left(1 - \frac{\delta L}{L_*} \right) + \mathcal{O}(\delta L^2), \quad (3.41)$$

$$\frac{\partial \iota_c}{\partial H} = \frac{1}{\eta L} = \frac{1}{\eta L_*} \left(1 - \frac{\delta L}{L_*} \right) + \mathcal{O}(\delta L^2), \quad (3.42)$$

$$\frac{\partial \iota_s}{\partial H} = -\frac{\iota_c}{\eta L \iota_s} = -\frac{\iota_c}{\eta L_* \iota_s} \left(1 - \frac{\delta L}{L_*} \right) + \mathcal{O}(\delta L^2). \quad (3.43)$$

A sketch of the derivation of the above formulas can be found in Appendix C. They are strictly valid with $e \in]0, 1[$, $i \in]0, \pi[$. However, several cancellations lead to no singular behavior of the Poisson bracket formulas arising throughout the various perturbative steps also when $e = 0$ or $i = 0$.

Book-keeping: Hamiltonian

We introduce in the series a book-keeping symbol σ (see [26] for an introduction to the book-keeping technique), with numerical value $\sigma = 1$, whose role is to provide a grouping of all the various terms in the series according to their

“order of smallness”. Hence, a group of terms with common factor σ^l , $l \in \mathbb{Z}$, indicates a term considered as of the “ l -th order of smallness”.

Since in our series there are several small quantities, we introduce a book-keeping scheme allowing to simultaneously deal with all small quantities while maintaining the closed-form character of the series. To this end, we make the following substitutions, called “book-keeping rules”, within the initial Hamiltonian:

- BK-Rule 1: $e \rightsquigarrow \sigma^1 e = \sigma e$ (not applicable to the quantity e^2 within $\eta = \sqrt{1 - e^2}$),
- BK-Rule 2: $\eta \rightsquigarrow \sigma^0 \eta = \eta$,
- BK-Rule 3: $\mu \rightsquigarrow \sigma^\nu \mu$, with ν as in (3.7),
- BK-Rule 4: $e_1 \rightsquigarrow \sigma^{\nu_1} e_1$, with ν_1 as in (3.7) (not applicable to the quantity e_1^2 within $\eta_1 := \sqrt{1 - e_1^2}$),
- BK-Rule 5: $\frac{1}{\eta^2} \rightsquigarrow \left(\frac{1}{\eta^2} - 1\right) \sigma^2 + 1$,
- BK-Rule 6: $\eta_1 \rightsquigarrow (\eta_1 - 1) \sigma^{2\nu_1} + 1$,
- BK-Rule 7: $\delta L^\lambda \rightsquigarrow \sigma^{l\nu} \delta L^\lambda$ with $l = \begin{cases} \lambda, & \text{if } \delta L^\lambda \text{ comes from } \mathcal{H}_1, \\ \lambda - 1, & \text{if } \delta L^\lambda \text{ comes from } \mathcal{H}_0, \end{cases} \lambda \in \mathbb{N} \setminus \{0\}$.

Since $\sigma = 1$, the above substitutions affect the structure of the series only at the formal level, and can be substituted directly into the original Hamiltonian, whereby they propagate at subsequent normalization steps once these steps are organized in successive powers σ , σ^2 , etc., of the book-keeping symbol. The BK-Rules 1 to 7 above are justified on physical ground as well as on motives of algorithmic convenience. In particular:

- BK-Rule 1 implies that, despite the use of closed-form formulas, the basic small quantity in powers of which the series are organized is the eccentricity of the test particle.

- BK-Rule 3 implies that a factor μ in front of a series term should be treated as of comparable order of smallness as a term of order e^ν , with ν given by (3.7). Similarly, BK-Rule 4 implies that a term containing a factor e_1 raised to some power should be treated as of comparable order of smallness with a term e_1^ν raised to the same power. Note that the eccentricity e is a quantity variable in time, so that to compute the exponents ν , ν_1 we need to use, for any examined trajectory, a reference value e_* yielding an estimate of the overall level of eccentricity all along the orbital evolution for that trajectory. Note that, by standard secular theory we have $e(t) = e_* + \mathcal{O}(\mu)$ if e_* is close to the mean eccentricity (see also discussion at the introduction). Note finally that we obtain exponents

$\nu, \nu_1 \geq 1$ in the typical case in which $e > \mu$ and $e \geq e_1$. These inequalities arise naturally in the case of small bodies in highly eccentric orbits perturbed by some planet of, say, our solar system, which are the cases of main interest in applying the present method (see, nevertheless, Remark 3.2.4 on the treatment of cases where the above conditions are not met).

- BK-Rule 7 stems from the estimate $\delta L = \mathcal{O}(\delta a) = \mathcal{O}(\mu)$ holding for the oscillations in semi-major axis of trajectories far from mean-motion resonances (as already pointed out in the latter case, instead, we have in general $\delta L = \mathcal{O}(\delta a) = \mathcal{O}(\mu^{1/2})$ and the corresponding rule has to be adapted accordingly). The lowering of the book-keeping power by one for within H_0 is introduced for reasons of algorithmic convenience, i.e., in order to maintain $n_*\delta L$ in the kernel of the homological equation.

- BK-Rules 5 and 6 imply just a partition of the unity aiming at keeping the perturbative scheme in closed-form while splitting the corresponding expressions (involving η and η_1 respectively) in two parts, of orders $\mathcal{O}(1)$ and $\mathcal{O}(e^2)$, or $\mathcal{O}(e_1^2)$.

Book-keeping: Poisson structure

Some of the formulas listed at the beginning of the subsection imply differentiation with respect to e through the corresponding partial derivatives in (3.27), (3.28), thus yielding a lowering of the power of the eccentricity in some terms arising through Poisson brackets at consecutive steps of perturbation theory. To account for this fact, similarly as in [11] we introduce the use of the book-keeping symbol σ in the formulas of the Poisson algebra as follows: first, we re-write the derivatives with respect to the angles ℓ, g, h, M_1 as

$$\frac{dF}{d\ell} = \frac{\partial F}{\partial f} \frac{\partial f}{\partial \ell} \frac{a_1(1 - e_1\sigma^{\nu_1} \cos E_1)}{\|r_1\|}, \quad (3.44)$$

$$\frac{dF}{dg} = \frac{\partial F}{\partial g} \frac{a_1(1 - e_1\sigma^{\nu_1} \cos E_1)}{\|r_1\|}, \quad (3.45)$$

$$\frac{dF}{dh} = \frac{\partial F}{\partial h} \frac{a_1(1 - e_1\sigma^{\nu_1} \cos E_1)}{\|r_1\|}, \quad (3.46)$$

$$\frac{dF}{dM_1} = \left(\frac{\partial F}{\partial E_1} + \frac{\partial F}{\partial \|r_1\|} \frac{d\|r_1\|}{dE_1} + \frac{\partial F}{\partial \phi_1} \sigma^{-\nu_1} \right) \frac{dE_1}{dM_1} - \frac{\partial F}{\partial \phi_1} \sigma^{-\nu_1}, \quad (3.47)$$

and with respect to the actions $\delta L, G$ as

$$\frac{dF}{d\delta L} = \frac{\partial F}{\partial f} \frac{\partial f}{\partial \delta L} + \frac{\partial F}{\partial \delta L} + \frac{\partial F}{\partial e} \frac{\partial e}{\partial \delta L} \sigma^{-1} + \frac{\partial F}{\partial \eta} \frac{\partial \eta}{\partial \delta L}, \quad (3.48)$$

$$\frac{dF}{dG} = \frac{\partial F}{\partial f} \frac{\partial f}{\partial G} + \frac{\partial F}{\partial e} \frac{\partial e}{\partial G} \sigma^{-1} + \frac{\partial F}{\partial \eta} \frac{\partial \eta}{\partial G} + \frac{\partial F}{\partial \iota_c} \frac{\partial \iota_c}{\partial G} + \frac{\partial F}{\partial \iota_s} \frac{\partial \iota_s}{\partial G}. \quad (3.49)$$

Note that in (3.47) use was made of the identity $\phi_1 = e_1 \sin E_1$ (Kepler's equation). Finally, we revise formulas (3.31), (3.32), (3.34)–(3.43), attributing a book-

keeping to all factors involving the eccentricity function η as

$$\frac{\partial f}{\partial \ell} = 1 + \frac{2e \cos f}{\eta^3} \sigma + \left(\frac{1}{\eta^3} - 1 + \frac{e^2 \cos^2 f}{\eta^3} \right) \sigma^2, \quad (3.50)$$

$$\frac{d \|r_1\|}{dE_1} = a_1 e_1 \sigma^{\nu_1} \sin E_1 \quad (3.51)$$

$$\frac{\partial f}{\partial \delta L} = \frac{1}{L_*} \left(\frac{2 \sin f}{e} \sigma^{-1} + \frac{\sin(2f)}{2} \right) + \mathcal{O}(\delta L \sigma^\nu), \quad (3.52)$$

$$\frac{\partial e}{\partial \delta L} = \frac{1}{L_*} \left(\frac{1}{e} \sigma^{-1} + \frac{\eta^2 - 1}{e} \sigma \right) + \mathcal{O}(\delta L \sigma^\nu), \quad (3.53)$$

$$\frac{\partial \eta}{\partial \delta L} = -\frac{1}{L_*} \left(1 + (\eta - 1) \sigma^2 \right) + \mathcal{O}(\delta L \sigma^\nu), \quad (3.54)$$

$$\begin{aligned} \frac{\partial f}{\partial G} = & -\frac{1}{L_*} \left(\frac{2 \sin f}{e} \sigma^{-1} + \frac{\sin(2f)}{2} + \frac{2 \sin f}{e} \left(\frac{1}{\eta} - 1 \right) \sigma \right. \\ & \left. + \frac{\sin 2f}{2} \left(\frac{1}{\eta} - 1 \right) \sigma^2 \right) + \mathcal{O}(\delta L \sigma^\nu), \end{aligned} \quad (3.55)$$

$$\frac{\partial e}{\partial G} = -\frac{1}{L_*} \left(\frac{1}{e} \sigma^{-1} + \frac{\eta - 1}{e} \sigma \right) + \mathcal{O}(\delta L \sigma^\nu), \quad (3.56)$$

$$\frac{\partial \eta}{\partial G} = \frac{1}{L_*} + \mathcal{O}(\delta L \sigma^\nu), \quad (3.57)$$

$$\frac{\partial \iota_c}{\partial G} = -\frac{\iota_c}{L_*} \left(1 + \left(\frac{1}{\eta} - 1 \right) \sigma^2 \right) + \mathcal{O}(\delta L \sigma^\nu), \quad (3.58)$$

$$\frac{\partial \iota_s}{\partial G} = -\frac{1 - \iota_s^2}{L_* \iota_s} \left(1 + \left(\frac{1}{\eta} - 1 \right) \sigma^2 \right) + \mathcal{O}(\delta L \sigma^\nu), \quad (3.59)$$

$$\frac{\partial \iota_c}{\partial H} = \frac{1}{L_*} \left(1 + \left(\frac{1}{\eta} - 1 \right) \sigma^2 \right) + \mathcal{O}(\delta L \sigma^\nu), \quad (3.60)$$

$$\frac{\partial \iota_s}{\partial H} = -\frac{\iota_c}{L_* \iota_s} \left(1 + \left(\frac{1}{\eta} - 1 \right) \sigma^2 \right) + \mathcal{O}(\delta L \sigma^\nu). \quad (3.61)$$

Remark 3.2.4. The *small eccentricity problem* consists of the fact that the above-proposed book-keeping rules are not applicable in the case $0 < e_* \lesssim \mu < e_1$, since, by (3.7), the exponents ν, ν_1 would be smaller than unity. The simple solution of rounding these exponents to 1, while maintaining the same book-keeping rules as above, fails, since, at any given normalization order r , the presence of $\sigma^{-1}, \sigma^{-\nu_1}$ terms in the formulas of the Poisson algebra leads to the generation of terms of order *lower than* r in the normal form's remainder. Notwithstanding our focus on a method dealing with large eccentricity orbits (for which the problem does not appear), we discuss below a variant of the main algorithm that deals with trajectories in the case $\nu = 1$, i.e., when $e_* \lesssim \mu$.

3.2.4 Iterative normalization algorithm

Preliminary step: Hamiltonian preparation

After implementing BK-Rules 1 to 7 the Hamiltonian (3.19) resumes the form:

$$\mathcal{H} = n_*\delta L + n_1 J_1 + \sum_{s \in \mathbb{Z}^4} q_s(\delta L, e, \eta, \iota_c, \iota_s; \mu, L_*, a_1, e_1, \eta_1) \cos(s_1 f + s_2 g + s_3 h + s_4 E_1) \sigma_s \quad (3.62)$$

where $\sigma_s \in \{\sigma^v, \sigma^{v+1}, \dots\}$ and, by D'Alembert rules, only cosines and real coefficients q_s appear (invariance under simultaneous change of sign of all angles). Setting $\mathcal{L}_0 = n_*\delta L + n_1 J_1$, for obtaining a closed-form normalization algorithm it turns out convenient to re-express the Hamiltonian according to

$$\mathcal{H} = \mathcal{L}_0 + (\mathcal{H} - \mathcal{L}_0) \frac{a_1(1 - e_1 \sigma^{v_1} \cos E_1)}{\|r_1\|}. \quad (3.63)$$

The Hamiltonian (3.63) resumes the form:

$$\mathcal{H} = \mathcal{H}^{(0)} = \mathcal{L}_0 + \mathcal{R}_v^{(0)}, \quad (3.64)$$

where

$$\begin{aligned} \mathcal{R}_v^{(0)} = \sum_{l \geq v} \mathcal{R}_{v,l}^{(0)} = \sum_{l \geq v} \frac{a_1}{\|r_1\|} & \left(\sum_{p \in \mathbb{Z}^2} q'_{l,p} \cos(p_1 g + p_2 h) \right. \\ & \left. + \sum_{\substack{s \in \mathbb{Z}^4 \\ (s_1, s_4) \neq (0,0)}} q''_{l,s} \cos(s_1 f + s_2 g + s_3 h + s_4 E_1) \right) \sigma^l; \quad (3.65) \end{aligned}$$

We call $\mathcal{R}_v^{(0)}$ the *remainder* at the zero-th normalization step (i.e. in the original Hamiltonian). The terms $\mathcal{R}_{v,l}^{(0)}$ contain terms of book-keeping order σ^l , with $l \geq v$.

Step 1: normalization of the σ^v -terms

For a suitable generating function $\chi_v^{(1)}$ to be determined in a while, we rely to the Lie series operator (1.39) under the flow of such map introduced as

$$\begin{aligned} \exp\left(\mathcal{L}_{\chi_v^{(1)}}\right) : C^\omega(\mathbb{T}^4 \times D) & \longrightarrow C^\omega(\mathbb{T}^4 \times D) \\ \exp\left(\mathcal{L}_{\chi_v^{(1)}}\right) & = \sum_{n \geq 0} \frac{1}{n!} \mathcal{L}_{\chi_v^{(1)}}^n = \mathbb{I} + \mathcal{L}_{\chi_v^{(1)}} + \frac{1}{2} \mathcal{L}_{\chi_v^{(1)}} \circ \mathcal{L}_{\chi_v^{(1)}} + \dots \end{aligned} \quad (3.66)$$

where the Lie derivative $\mathcal{L}_{\chi_v^{(1)}} \cdot$ is given by (1.22).

Applying (3.66) to (3.63) we get the transformed Hamiltonian

$$\mathcal{H}^{(1)} = \mathcal{L}_0 + \mathcal{R}_v^{(0)} + \{\mathcal{L}_0, \chi_v^{(1)}\} + \{\mathcal{R}_v^{(0)}, \chi_v^{(1)}\} + \frac{1}{2} \{\{\mathcal{H}, \chi_v^{(1)}\}, \chi_v^{(1)}\} + \dots, \quad (3.67)$$

in which, with the usual abuse of notation, we still indicate with $\ell, g, h, M_1, \delta L, G, H, J_1$ the new canonical variables given by the inverse transformation

$$\exp\left(\mathcal{L}_{\chi_v^{(1)}}\right)^{-1} = \exp\left(\mathcal{L}_{-\chi_v^{(1)}}\right). \quad (3.68)$$

Our scope will be to define the Lie generating function $\chi_v^{(1)}$ in such a way that, after implementing the transformation (3.67), $\mathcal{H}^{(1)}$ contains no terms depending on the angles f and E_1 at order σ^v . The required generating function $\chi_v^{(1)}$ is computed as an outcome of the following.

Proposition 3.2.1. *Define $\chi_v^{(1)}$ as*

$$\begin{aligned} \chi_v^{(1)} = & \frac{\phi_1}{n_1} \sigma^{v+v_1} \sum_{p \in \mathbb{Z}^2} q'_{v,p} \cos(p_1 g + p_2 h) \\ & + \sigma^v \sum_{\substack{s \in \mathbb{Z}^4 \\ (s_1, s_4) \neq (0,0)}} \frac{q''_{v,s}}{s_1 n_* + s_4 n_1} \sin(s_1 f + s_2 g + s_3 h + s_4 E_1). \end{aligned} \quad (3.69)$$

Then, it holds that

$$\{\mathcal{L}_0, \chi_v^{(1)}\} + \mathcal{R}_{v,v}^{(0)} = \mathcal{L}_v^{(1)} + \mathcal{O}\left(\sigma^{v+1}\right), \quad (3.70)$$

where

$$\mathcal{L}_v^{(1)} = \sigma^v \sum_p q'_{v,p} \cos(p_1 g + p_2 h). \quad (3.71)$$

Furthermore, the function $\mathcal{H}^{(1)}$ as computed by (3.67) takes the form

$$\mathcal{H}^{(1)} = \mathcal{L}_0 + \mathcal{L}_v^{(1)} + \mathcal{R}^{(1)}, \quad (3.72)$$

where the remainder $\mathcal{R}^{(1)}$ is $\mathcal{O}(\sigma^{v+1}) \forall v \geq 1$ independently of the value of v_1 .

Proof. Setting

$$\begin{aligned} \chi_v^{(1)}(f, g, h, E_1, \phi_1, \delta L, e, \eta, \iota_c, \iota_s) = & \sigma^v \left(\phi_1 \sigma^{v_1} \sum_{p \in \mathbb{Z}^2} \hat{q}'_{v,p}(\delta L, e, \eta, \iota_c, \iota_s) \times \right. \\ & \left. \cos(p_1 g + p_2 h) + \sum_{\substack{s \in \mathbb{Z}^4 \\ (s_1, s_4) \neq (0,0)}} \hat{q}''_{v,s}(\delta L, e, \eta, \iota_c, \iota_s) \sin(s_1 f + s_2 g + s_3 h + s_4 E_1) \right), \end{aligned}$$

and recalling the chain rules (3.44), (3.47) and (3.50), (3.51), (3.33), we find

$$\begin{aligned} \{\mathcal{L}_0, \chi_v^{(1)}\} + \mathcal{R}_{v,v}^{(0)} = & -n_* \left(1 + \frac{2e \cos f}{\eta^3} \sigma + \left(\frac{1}{\eta^3} - 1 + \frac{e^2 \cos^2 f}{\eta^3} \right) \sigma^2 \right) \\ & \frac{a_1(1 - e_1 \sigma^{v_1} \cos E_1)}{\|r_1\|} \sigma^v \sum_{(s_1, s_4) \neq (0,0)} s_1 \hat{q}_{v,s}'' \cos(s_1 f + s_2 g + s_3 h + s_4 E_1) \\ & - n_1 \frac{a_1}{\|r_1\|} \sigma^v \left(\sum_{(s_1, s_4) \neq (0,0)} s_4 \hat{q}_{v,s}'' \cos(s_1 f + s_2 g + s_3 h + s_4 E_1) \right. \\ & \left. + \sum_p \hat{q}'_{v,p} \cos(p_1 g + p_2 h) \right) + n_1 \sigma^v \sum_p \hat{q}'_{v,p} \cos(p_1 g + p_2 h) \\ & + \sigma^v \frac{a_1}{\|r_1\|} \left(\sum_p q'_{v,p} \cos(p_1 g + p_2 h) + \sum_{(s_1, s_4) \neq (0,0)} q''_{v,s} \cos(s_1 f + s_2 g + s_3 h + s_4 E_1) \right). \end{aligned}$$

Requiring that no trigonometric terms depending on f, E_1 be present at order σ^v then leads to

$$\begin{aligned} \hat{q}_{v,s}'' &= \frac{q''_{v,s}}{s_1 n_* + s_4 n_1}, \quad s \in \mathbb{Z}^4: (s_1, s_4) \neq (0, 0), \\ \hat{q}'_{v,p} &= \frac{q'_{v,p}}{n_1}, \quad p \in \mathbb{Z}^2, \end{aligned}$$

which implies (3.69). At order σ^v we then obtain immediately the formula

$$\mathcal{L}_v^{(1)} = \sigma^v \sum_p q'_{v,p} \cos(p_1 g + p_2 h).$$

We now consider the function $\mathcal{H}^{(1)}$ computed by replacing (3.69) into (3.67). The function $\mathcal{H}^{(1)}$ can be decomposed as in (3.72). We shall demonstrate that the remainder $\mathcal{R}^{(1)}$ contains no terms of order lower than σ^{v+1} . To this end, it suffices to show that

$$\{\mathcal{R}_v^{(0)}, \chi_v^{(1)}\} = \mathcal{O}(\sigma^{2v}), \quad \frac{1}{n!} \underbrace{\{\dots \{\{\mathcal{H}, \chi_v^{(1)}\}, \chi_v^{(1)}\}, \dots, \chi_v^{(1)}\}}_{n \geq 2} = \mathcal{O}(\sigma^{n(v-1)+2}), \quad (3.73)$$

since $n(v-1) + 2 > v$, for all $n \geq 2, v \geq 1$.

The term $\mathcal{R}_v^{(0)}$ contains terms of order equal to or larger than σ^v , while $\chi_v^{(1)}$ contains only terms of order σ^v . Thus, except for the Poisson bracket $\{\mathcal{L}_0, \chi_v^{(1)}\}$, which only contributes to the secular terms $\mathcal{L}_v^{(1)}$ due to (3.70), the first Poisson bracket in (3.73) contains prefactors of order σ^{2v} or higher, while the second contains prefactors σ^{nv} or higher. However, the exponent of σ in these brackets can be *lowered* due to the negative powers introduced in the book-keeping formulas in the following three classes of factors:

- (i) partial derivatives with respect to the eccentricity in (3.48), (3.49) (carrying σ^{-1}) multiplied by corresponding formulae (3.53), (3.56) (another σ^{-1}), hence a total of σ^{-2} ;
- (ii) differentiations (3.52), (3.55) involving f (weighting σ^{-1}) again in (3.48), (3.49), thus a pre-factor σ^{-1} ;
- (iii) partial derivatives with respect to ϕ_1 in (3.47) ($\sigma^{-\nu_1}$, $\nu_1 \geq 1$), thus a prefactor at least σ^{-1} .

As regards (iii) ϕ_1 shows up in the numerator of $\chi_v^{(1)}$ accompanied by a prefactor $\sigma^{\nu+\nu_1}$ (equation (3.69)), thus the negative powers $\sigma^{-\nu_1}$ are canceled by the positive powers σ^{ν_1} , implying no dependence of the minimum order of the remainder on ν_1 .

As regards (i), we first note that $\chi_v^{(1)}$ has no explicit dependence on e , but only an implicit dependence through η , which in the closed-form context is treated as an independent symbol. This follows from the fact that $\chi^{(1)}$ stems from balancing the coefficients of $\mathcal{R}_{\nu,\nu}^{(0)}$. The latter term contains a pre-factor μ , which is already $\mathcal{O}(\sigma^\nu)$, thus it cannot contain any further factors produced by any explicit power of e . In view of the above, setting $\partial\chi^{(1)}/\partial e = 0$, we find that for any $F \in C^\infty(\mathbb{T}^4 \times D)$ the expression in $\{F, \chi_v^{(1)}\}$ pertaining (i) can be factored out as

$$\{F, \chi_v^{(1)}\}_{(i)} = -\frac{\partial F}{\partial e} \sigma^{-1} \left(\frac{\partial f}{\partial \ell} \frac{\partial e}{\partial \delta L} \frac{\partial \chi_v^{(1)}}{\partial f} + \frac{\partial e}{\partial G} \frac{\partial \chi_v^{(1)}}{\partial g} \right). \quad (3.74)$$

We now have the following lemma:

Lemma 3.2.1. *For every term in the Hamiltonian (3.63) of the form*

$$q_s(\|r_1\|, \delta L, \eta, \iota_c, \iota_s; \mu, L_*, a_1, e_1, \eta_1) \cos(s_1 f + s_2 g + s_3 h + s_4 E_1) \sigma_s, \quad (3.75)$$

i.e., explicitly independent on e , we have $s_1 = s_2$.

Proof. This is a consequence of D'Alembert rules. Using modified Delaunay angular elements λ, γ, ζ in (1.66), as well as the formulas $f = \ell + 2e \sin \ell + \mathcal{O}(e^2)$, $e\eta(e)^{-2\alpha} = e + \alpha e^3 + \mathcal{O}(e^5)$, $\alpha \in \mathbb{N}$, we find that, after expanding in the eccentricity e , (3.75) should give the terms

$$q_s \cos(s_1(\lambda + \gamma) + s_2(\zeta - \gamma) - s_3\zeta + s_4 E_1) \sigma_s + \mathcal{O}(e). \quad (3.76)$$

However, according to the D'Alembert rules, in a generic trigonometric monomial of the form

$$b_w(\|r_1\|, \delta L, \eta, \iota_c, \iota_s; \mu, L_*, a_1, e_1, \eta_1) e^l \sigma^l \cos(w_1 \lambda + w_2 \gamma + w_3 \zeta + w_4 E_1) \sigma_w, \quad (3.77)$$

$l \in \mathbb{N}$, appearing after expanding \mathcal{H} in the eccentricities e, e_1 , we necessarily have that $l - |w_2|$ must be non-negative and even. Since for any closed-form term in the Hamiltonian, explicitly independent of e , the lowermost term in e produced after the expansion satisfies $l = 0$, we necessarily have $w_2 = 0$, that is $s_1 = s_2$. \square

In view, now, of (3.69), the relation $s_1 = s_2$ implies $\partial\chi_v^{(1)}/\partial f = \partial\chi_v^{(1)}/\partial g$. Therefore, making use of (3.50), (3.53) and (3.56), the equation (3.74) translates into

$$\{F, \chi_v^{(1)}\}_{(i)} = -\frac{\partial F}{\partial e} \sigma^{-1} \frac{\partial \chi_v^{(1)}}{\partial f} \left(\frac{\sigma^{-1}}{L_* e} - \frac{\sigma^{-1}}{L_* e} + \mathcal{O}(\sigma^0) \right) = -\frac{\partial F}{\partial e} \sigma^{-1} \frac{\partial \chi_v^{(1)}}{\partial f} \mathcal{O}(\sigma^0).$$

It follows that for any of the functions $F = \mathcal{R}_v^{(0)}, \{\mathcal{H}, \chi_v^{(1)}\}, \{\{\mathcal{H}, \chi_v^{(1)}\}, \chi_v^{(1)}\}, \dots$, terms produced by derivatives of the type (i) in (3.67) are subject to a lowering of the exponent of σ per Poisson bracket only by a factor σ^{-1} , instead of σ^{-2} . In particular, in the case $F = \mathcal{R}_{v,v}^{(0)}$ (as well as for any other closed-form function explicitly independent on the eccentricity) we have that (3.74) is identically vanishing.

As regards (ii), we find that for any $F_1, F_2 \in C^\infty(\mathbb{T}^4 \times D)$, the derivative $\partial f/\partial \delta L$ (equation (3.52)) participates in the Poisson bracket $\{F_1, F_2\}$ only through the combination

$$\frac{\partial f}{\partial \ell} \frac{\partial f}{\partial \delta L} \left(\frac{\partial F_1}{\partial f} \frac{\partial F_2}{\partial f} - \frac{\partial F_1}{\partial f} \frac{\partial F_2}{\partial f} \right) = 0. \quad (3.78)$$

On the other hand, the derivative $\partial f/\partial G$ (3.55) participates in the same Poisson bracket through the combination

$$\frac{\partial f}{\partial G} \left(\frac{\partial F_1}{\partial g} \frac{\partial F_2}{\partial f} - \frac{\partial F_1}{\partial f} \frac{\partial F_2}{\partial g} \right) \quad (3.79)$$

which, by Lemma 3.2.1, is also equal to zero for $F_1 = \mathcal{R}_{v,v}^{(0)}$ (or any other term $\mathcal{O}(\sigma^{\nu+1})$ in \mathcal{H} not depending explicitly on e), and $F_2 = \chi_v^{(1)}$.

In conclusion, returning to (3.73), and taking all the above deductions into account, we arrive at the expressions

$$\{\mathcal{R}_v^{(0)}, \chi_v^{(1)}\} = \{\mathcal{R}_{v,v}^{(0)}, \chi_v^{(1)}\} + \left\{ \sum_{l \geq \nu+1} \mathcal{R}_{v,l}^{(0)}, \chi_v^{(1)} \right\} = \mathcal{O}(\sigma^{\nu+\nu}) + \mathcal{O}(\sigma^{\nu+1+\nu-1}) = \mathcal{O}(\sigma^{2\nu})$$

and similarly,

$$\begin{aligned} \frac{1}{2} \{\{\mathcal{H}, \chi_v^{(1)}\}, \chi_v^{(1)}\} &= \frac{1}{2} \{\{\mathcal{Z}_0, \chi_v^{(1)}\}, \chi_v^{(1)}\} + \frac{1}{2} \{\{\mathcal{R}_v^{(0)}, \chi_v^{(1)}\}, \chi_v^{(1)}\} \\ &= \mathcal{O}(\sigma^{2\nu}) + \mathcal{O}(\sigma^{3\nu-1}) = \mathcal{O}(\sigma^{2\nu}), \end{aligned}$$

since $\{\mathcal{Z}_0, \chi_v^{(1)}\}$ satisfies Lemma 3.2.1. We then have $\{\mathcal{Z}_0, \chi_v^{(1)}\} = \mathcal{Z}_v^{(1)} - \mathcal{R}_{v,v}^{(0)} + \mathcal{O}(\sigma^{\nu+1})$, with $\mathcal{Z}_v^{(1)}$ independent on f, g, e . Proceeding by induction

$$\begin{aligned} \frac{1}{n!} \{ \dots \underbrace{\{\{\mathcal{Z}_0 + \mathcal{R}_v^{(0)}, \chi_v^{(1)}\}, \chi_v^{(1)}\}, \dots, \chi_v^{(1)}\}}_{n \geq 3} &= \mathcal{O}(\sigma^{\min\{n\nu - (n-2), (n+1)\nu - (n-1)\}}) \\ &= \mathcal{O}(\sigma^{n(\nu-1)+2}) \end{aligned}$$

which concludes the proof of the proposition. \square

By Proposition 3.2.1, computing all Poisson brackets in (3.67), substituting $\phi_1 = e_1 \sin E_1$ where appropriate, and multiplying all terms missing a factor $1/\|r_1\|$ with the factor $a_1(1 - \sigma^{\nu_1} e_1 \cos(E_1))/\|r_1\|$ (equal to 1), the remainder $\mathcal{R}_{\nu+1}^{(1)}$ resumes the standard form

$$\mathcal{R}_{\nu+1}^{(1)} = \sum_{l \geq \nu+1} \mathcal{R}_{\nu+1,l}^{(1)} = \sum_{l \geq \nu+1} \sum_{\lambda \geq 1} \frac{a_1}{\|r_1\|^\lambda} \sum_{s \in \mathbb{Z}^4} d_{l,\lambda,s}^{(1)} \cos(s_1 f + s_2 g + s_3 h + s_4 E_1) \sigma^l, \quad (3.80)$$

where the coefficients $d_{l,\lambda,s}^{(1)}$ satisfy the relations

$$\begin{aligned} d_{l,\lambda,s}^{(1)} &= d_{l,\lambda,s}^{(1)}(\delta L, e, \eta, \iota_c, \iota_s; \mu, L_*, a_1, e_1, \eta_1) \\ &= \begin{cases} d'_{l,\lambda,p}{}^{(1)}, & s_1 = s_4 = 0, (s_2, s_3) = p, \\ d''_{l,\lambda,s}{}^{(1)}, & (s_1, s_4) \neq (0, 0), \end{cases} \in \mathbb{R}. \end{aligned}$$

These last algebraic operations conclude the first normalization step.

Loop: normalization of the $\sigma^{\nu+j-1}$ -terms

The procedure followed in the first step can be repeated iteratively in order to normalize consecutively terms of order $\sigma^{\nu+j-1}$, with each time an $\mathcal{O}(\sigma^{\nu+j})$ remainder, for $\nu, j > 1$. As anticipated in Remark 3.2.4, the iterative procedure described below fails in the case $\nu = 1$ at step $j = 2$, so an adjustment (involving one more iteration) is required, as discussed later on below.

The j -th normalization step is carried out as follows from the next proposition.

Proposition 3.2.2. *Assume $\nu \geq 2$, $\nu_1 \geq 1$. Assume that the Hamiltonian before the j -th normalization step has the form:*

$$\mathcal{H}^{(j-1)} = \mathcal{I}_0 + \sum_{l=1}^{j-1} \mathcal{I}_{\nu+l-1}^{(l)} + \mathcal{R}_{\nu+j-1}^{(j-1)} \quad (3.81)$$

where

$$\mathcal{I}_{\nu+l-1}^{(l)} = \sigma^{\nu+l-1} \sum_{\lambda \geq 1} \sum_{p \in \mathbb{Z}^2} \zeta_{\nu+l-1,\lambda,p}^{(l)} \cos(p_1 g + p_2 h). \quad (3.82)$$

$$\begin{aligned} \mathcal{R}_{\nu+j-1}^{(j-1)} &= \sum_{l \geq \nu+j-1} \mathcal{R}_{\nu+j-1,l}^{(j-1)} = \sum_{l \geq \nu+j-1} \sum_{\lambda \geq 1} \frac{a_1}{\|r_1\|^\lambda} \left(\sum_{p \in \mathbb{Z}^2} d'_{l,\lambda,p}{}^{(j-1)} \cos(p_1 g + p_2 h) \right. \\ &\quad \left. + \sum_{\substack{s \in \mathbb{Z}^4 \\ (s_1, s_4) \neq (0,0)}} d''_{l,\lambda,s}{}^{(j-1)} \cos(s_1 f + s_2 g + s_3 h + s_4 E_1) \right) \sigma^l, \quad (3.83) \end{aligned}$$

for some real coefficients $\zeta_{v+l-1,\lambda,p}^{(l)}$, $d'_{l,\lambda,p}^{(j-1)}$, $d''_{l,\lambda,s}^{(j-1)}$ specified at previous steps, where

$$\zeta_{v,\lambda,p}^{(1)} = \begin{cases} q'_{v,p}, & \lambda = 1 \\ 0, & \lambda > 1 \end{cases}$$

by (3.71).

Define the j -th step Lie generating function $\chi_{v+j-1}^{(j)}$ as

$$\begin{aligned} \chi_{v+j-1}^{(j)} &= \frac{\phi_1}{n_1} \sigma^{v+j-1+v_1} \sum_{\lambda \geq 1} \sum_{\psi=1}^{\lambda} \frac{1}{a_1^{\psi-1} \|r_1\|^{\lambda-\psi}} \sum_{p \in \mathbb{Z}^2} d'_{v+j-1,\lambda,p}^{(j-1)} \cos(p_1 g + p_2 h) \\ &+ \sigma^{v+j-1} \sum_{\lambda \geq 1} \frac{1}{\|r_1\|^{\lambda-1}} \sum_{\substack{s \in \mathbb{Z}^4 \\ (s_1, s_4) \neq (0,0)}} \frac{d''_{v+j-1,\lambda,s}^{(j-1)}}{s_1 n_* + s_4 n_1} \sin(s_1 f + s_2 g + s_3 h + s_4 E_1). \end{aligned} \quad (3.84)$$

Then, the Hamiltonian $\mathcal{H}^{(j)}$ produced by the Lie operation $\mathcal{H}^{(j)} = \exp\left(\mathcal{L}_{\chi_{v+j-1}^{(j)}}\right) \mathcal{H}^{(j-1)}$ has the form

$$\mathcal{H}^{(j)} = \exp\left(\mathcal{L}_{\chi_{v+j-1}^{(j)}}\right) \mathcal{H}^{(j-1)} = \mathcal{F}_0 + \sum_{l=1}^j \mathcal{F}_{v+l-1}^{(l)} + \mathcal{R}_{v+j}^{(j)}, \quad (3.85)$$

where

$$\mathcal{F}_{v+j-1}^{(j)} = \sigma^{v+j-1} \sum_{\lambda \geq 1} \sum_{p \in \mathbb{Z}^2} \zeta_{v+j-1,\lambda,p}^{(j)} \cos(p_1 g + p_2 h) \quad (3.86)$$

with

$$\zeta_{v+j-1,\lambda,p}^{(j)} = \frac{1}{a_1^{\lambda-1}} d'_{v+j-1,\lambda,p}^{(j-1)}, \quad (3.87)$$

and

$$\begin{aligned} \mathcal{R}_{v+j}^{(j)} &= \sum_{l \geq v+j} \mathcal{R}_{v+j,l}^{(j)} = \sum_{l \geq v+j} \sum_{\lambda \geq 1} \frac{a_1}{\|r_1\|^\lambda} \left(\sum_{p \in \mathbb{Z}^2} d'_{l,\lambda,p}^{(j)} \cos(p_1 g + p_2 h) \right. \\ &\quad \left. + \sum_{\substack{s \in \mathbb{Z}^4 \\ (s_1, s_4) \neq (0,0)}} d''_{l,\lambda,s}^{(j)} \cos(s_1 f + s_2 g + s_3 h + s_4 E_1) \right) \sigma^l, \end{aligned} \quad (3.88)$$

with real coefficients $d'_{l,\lambda,p}^{(j)}$, $d''_{l,\lambda,s}^{(j)}$ computed from the known coefficients $\zeta_{v+l-1,\lambda,p}^{(l)}$ ($l = 1, \dots, j-1$), $d'_{l,\lambda,p}^{(j-1)}$, $d''_{l,\lambda,s}^{(j-1)}$.

Proof. We repeat the strategy of Proposition 3.2.1 and look for a generating Hamiltonian this time dependent on $\|r_1\|$:

$$\begin{aligned} & \chi_{v+j-1}^{(j)}(f, g, h, E_1, \phi_1, \|r_1\|, \delta L, e, \eta, \iota_c, \iota_s) \\ &= \sigma^{v+j-1} \left(\phi_1 \sigma^{v_1} \sum_{\lambda \geq 1} \sum_{p \in \mathbb{Z}^2} \hat{d}_{v+j-1, \lambda, p}^{(j-1)}(\|r_1\|, \delta L, e, \eta, \iota_c, \iota_s) \cos(p_1 g + p_2 h) \right. \\ & \quad \left. + \sum_{\lambda \geq 1} \sum_{\substack{s \in \mathbb{Z}^4 \\ (s_1, s_4) \neq (0, 0)}} \hat{d}_{v+j-1, \lambda, s}^{(j-1)} \sin(s_1 + s_2 g + s_3 h + s_4 E_1) \right). \end{aligned}$$

Requiring $\{\mathcal{L}_0, \chi_{v+j-1}^{(j)}\} + \mathcal{R}_{v+j-1, v+j-1}^{(j-1)}$ to be $O(\sigma^{v+j})$ in fast angles we come up with

$$\begin{aligned} & -n_* \hat{d}_{v+j-1, \lambda, s}^{(j-1)} s_1 - n_1 \hat{d}_{v+j-1, \lambda, s}^{(j-1)} s_4 + \frac{1}{\|r_1\|^{\lambda-1}} \hat{d}_{v+j-1, \lambda, s}^{(j-1)} = 0, \\ & -n_1 \frac{a_1}{\|r_1\|} \hat{d}_{v+j-1, \lambda, p}^{(j-1)} + n_1 \hat{d}_{v+j-1, \lambda, p}^{(j-1)} + \frac{a_1}{\|r_1\|^\lambda} \hat{d}_{v+j-1, \lambda, p}^{(j-1)} = \frac{1}{a_1^{\lambda-1}} \hat{d}_{v+j-1, \lambda, p}^{(j-1)}, \end{aligned}$$

that is, for $\lambda \geq 1$,

$$\begin{aligned} \hat{d}_{v+j-1, \lambda, s}^{(j-1)} &= \frac{1}{\|r_1\|^{\lambda-1}} \frac{\hat{d}_{v+j-1, \lambda, s}^{(j-1)}}{s_1 n_* + s_4 n_1}, \quad s \in \mathbb{Z}^4: (s_1, s_4) \neq (0, 0), \\ \hat{d}_{v+j-1, \lambda, p}^{(j-1)} &= \frac{1}{a_1^{\lambda-1}} \frac{\hat{d}_{v+j-1, \lambda, p}^{(j-1)}}{n_1} \sum_{\psi=0}^{\lambda-1} \left(\frac{a_1}{\|r_1\|} \right)^\psi = \frac{\hat{d}_{v+j-1, \lambda, p}^{(j-1)}}{n_1} \sum_{\psi=1}^{\lambda} \frac{1}{a_1^{\psi-1} \|r_1\|^{\lambda-\psi}}, \quad p \in \mathbb{Z}^2, \end{aligned}$$

which proves (3.84), and new accumulated addenda in normal form

$$\mathcal{L}_{v+j-1}^{(j)} = \sigma^{v+j-1} \sum_{\lambda \geq 1} \frac{1}{a_1^{\lambda-1}} \sum_p \hat{d}_{v+j-1, \lambda, p}^{(j-1)} \cos(p_1 g + p_2 h).$$

which proves (3.87). It remains to demonstrate that the expression (3.88) is $O(\sigma^{v+j})$. The proof is done by induction: for $j = 2$ we get

$$\begin{aligned} \mathcal{H}^{(2)} &= \mathcal{L}_0 + \mathcal{L}_v^{(1)} + \mathcal{L}_{v+1}^{(2)} + O(\sigma^{v+2}) + \sum_{l \geq v+2} \mathcal{R}_{v+1, l}^{(1)} + \{\mathcal{L}_v^{(1)}, \chi_{v+1}^{(2)}\} \\ &+ \{\mathcal{R}_{v+1}^{(1)}, \chi_{v+1}^{(2)}\} + \dots + \sum_{n \geq 2} \frac{1}{n!} \underbrace{\{\dots \{\{\mathcal{H}^{(1)}, \chi_{v+1}^{(2)}\}, \chi_{v+1}^{(2)}\}, \dots, \chi_{v+1}^{(2)}\}}_n. \quad (3.89) \end{aligned}$$

Similarly as in Proposition 3.2.1, a lowering of the book-keeping exponents in a Poisson bracket of the form $\{F, \chi_{v+1}^{(2)}\}$ can occur through derivatives of the form

The case $\nu = 1$

Coming to $\nu = 1$, one realizes that (3.89) produces same order σ^2 non-normalized terms via $\{\mathcal{R}_2^{(1)}, \chi_2^{(2)}\}$ and $\{\dots \{\{\mathcal{L}_0 + \mathcal{R}_2^{(1)}, \chi_2^{(2)}\}, \chi_2^{(2)}\}, \dots, \chi_2^{(2)}\}$, namely the resulting remainder is $\mathcal{R}_2^{(2)}$, so the scheme in Proposition 3.2.2 is not directly applicable beyond $j = 1$. Despite this, it is worth noticing that if we manage to get rid of these spurious terms, by performing, for instance, an extra normalization II, such that the new outcome returns $\mathcal{R}^{(II)} = \mathcal{R}_3^{(II)}$, then the algorithm (3.85) will work for $j \geq 3$ upon restarting the recursion from iteration II in place of 2. This is precisely the claim we are about to show to complete the treatment. Let us write (3.89) as $\mathcal{H}^{(2)} = \mathcal{L}_0 + \mathcal{L}_1^{(1)} + \mathcal{L}_2^{(2)} + \mathcal{R}_2^{(2)}$. Introduce the extra second normalization II based on Proposition 3.2.2 targeted to $\mathcal{R}_{2,2}^{(2)}$ with generating function $\chi_2^{(II)}$. Then we have the following.

Proposition 3.2.3. *For $\nu = 1$ and any $\nu_1 \geq 1$,*

$$\mathcal{H}^{(II)} = \exp\left(\mathcal{L}_{\chi_2^{(II)}}\right) \mathcal{H}^{(2)} = \mathcal{L}_0 + \mathcal{L}_1^{(1)} + \mathcal{L}_2^{(2)} + \mathcal{L}_2^{(II)} + \mathcal{R}_3^{(II)}. \quad (3.92)$$

Moreover the loop composed by (3.85)–(3.88) in Proposition 3.2.2 holds true for any $j \geq 4$ under the modifications

$$\mathcal{H}^{(3)} = \exp\left(\mathcal{L}_{\chi_3^{(3)}}\right) \mathcal{H}^{(II)} = \mathcal{L}_0 + \mathcal{L}_1^{(1)} + \mathcal{L}_2^{(2)} + \mathcal{L}_2^{(II)} + \mathcal{L}_3^{(3)} + \mathcal{R}_4^{(3)}, \quad (3.93)$$

$$\mathcal{H}^{(j)} = \exp\left(\mathcal{L}_{\chi_j^{(j)}}\right) \mathcal{H}^{(j-1)} = \mathcal{L}_0 + \sum_{l=1}^j \mathcal{L}_l^{(l)} + \mathcal{L}_2^{(II)} + \mathcal{R}_{j+1}^{(j)}. \quad (3.94)$$

Proof. We begin with a necessary generalization of Lemma 3.2.1.

Lemma 3.2.2. *Given $F_1, F_2 \in C^\omega(\mathbb{T} \times D)$ trigonometric monomials of the form (3.75), or equivalently in terms of the sine, fulfilling the property of Lemma 3.2.1, addenda of the same type in the Lie series transformation applied to F_1 with respect to F_2 preserve such property.*

Proof. Since $\exp(\mathcal{L}_{F_2})F_1$ involves the computation of Poisson brackets of functions explicitly independent on e , we have that (3.90), with F_1, F_2 in place of $F, \chi_{\nu+1}^{(2)}$, is identically null, as well as (3.79) because $\partial F_1/\partial f = \partial F_1/\partial g$, $\partial F_2/\partial f = \partial F_2/\partial g$ by assumption. Thus, the bracket $\{F_1, F_2\}$ in the Lie series either does not introduce any eccentricity dependence at all, or only at numerator through (3.50) multiplied by $\cos f$ or $\cos^2 f$; therefore its derivatives contain products of cosines (sines) whose coefficients are independent on e like

$$\mathcal{G}_1(s_1f + s_2g + s_3h + s_4E_1)\mathcal{G}_2(u_1f + u_2g + u_3h + u_4E_1), \quad \mathcal{G}_1, \mathcal{G}_2 = \cos, \sin.$$

The arguments are now either summed or subtracted, hence they clearly satisfy the property concerned. By cascade reasoning for further nested brackets we conclude. \square

Remark 3.2.5. A straightforward use of the lemma in conjunction with formulae (3.78), (3.79), (3.90) ($\chi_{\nu+1}^{(2)}$ replaced by generic differentiable function) reveal that any transformed Hamiltonian $\mathcal{H}^{(j)}$ and corresponding generating function $\chi_{\nu+j-1}^{(j)}$ encountered are regular at $e = 0$ in agreement with D'Alembert rules, i.e. they never depend on negative powers of e . Furthermore, every time one of the two entries of $\{\cdot, \cdot\}$ does not depend on e , the upshot due to item (i) in the proof of Proposition 3.2.1, as soon as non-zero, is diminished by σ^{-1} instead of σ^{-2} .

We consider step II:

$$\begin{aligned} \mathcal{H}^{(\text{II})} = & \mathcal{F}_0 + \mathcal{F}_1^{(1)} + \mathcal{F}_2^{(2)} + \mathcal{F}_2^{(\text{II})} + \mathcal{O}(\sigma^3) + \sum_{l \geq 3} \mathcal{R}_{2,l}^{(2)} + \{\mathcal{F}_1^{(1)}, \chi_2^{(\text{II})}\} + \{\mathcal{F}_2^{(2)}, \chi_2^{(\text{II})}\} \\ & + \{\mathcal{R}_{2,2}^{(2)}, \chi_2^{(\text{II})}\} + \dots + \sum_{n \geq 2} \frac{1}{n!} \underbrace{\{\dots \{\{\mathcal{H}^{(2)}, \chi_2^{(\text{II})}\}, \chi_2^{(\text{II})}\}, \dots, \chi_2^{(\text{II})}\}}_n. \end{aligned} \quad (3.95)$$

The analysis of the contributions reports these deductions, by which (3.92) follows.

- $\{\mathcal{F}_1^{(1)}, \chi_2^{(\text{II})}\} = \mathcal{O}(\sigma^3)$ because $\mathcal{F}_1^{(1)}$ is independent on f, g, e .
- $\{\mathcal{F}_2^{(2)}, \chi_2^{(\text{II})}\} = \mathcal{O}(\sigma^4)$ because $\mathcal{F}_2^{(2)}$ and $\chi_2^{(\text{II})}$ fulfil Lemma 3.2.2. Indeed, $\mathcal{R}_{2,2}^{(1)}$ depends on e at most linearly by book-keeping rules, so it does $\chi_2^{(2)}$ by construction. At this point we show that for eccentricity dependent terms stemming from $\mathcal{R}_{2,2}^{(1)}$ (or equivalently $\chi_2^{(2)}$) $d_{2,\lambda,p}^{(1)} = 0$.

Lemma 3.2.3. *Every trigonometric monomial in $\mathcal{R}_{2,2}^{(1)}$ explicitly dependent on e carries the dependence on at least one of the two fast anomalies f, E_1 as well, namely corresponding coefficients in (3.80) are $d_{2,\lambda,s}^{(1)} = d_{2,\lambda,s'}^{(1)}$ (s_1, s_4) $\neq (0, 0)$.*

Proof. By Proposition 3.2.1, Lemma 3.2.1 and 3.2.2, the substitution $\phi_1 = e_1 \sin E_1$ and the formulas listed in §3.2.3, we take out of (3.67) the order σ^2 remainder and it is not restrictive to assume $\nu_1 = 1$ in order to include also the $e_1 \cos E_1$ dependent term in (3.70):

$$\begin{aligned} \mathcal{R}_{2,2}^{(1)} = & \mathcal{R}_{1,2}^{(0)} + \frac{a_1}{\|r_1\|} \left(n_* \left(e_1 \cos E_1 - \frac{2e \cos f}{\eta^3} \right) \sigma \frac{\partial \chi_1^{(1)}}{\partial f} + \frac{\partial \mathcal{R}_{1,1}^{(0)}}{\partial f} \frac{\partial \chi_1^{(1)}}{\partial \delta L} \right. \\ & \left. - \frac{\partial \mathcal{R}_{1,1}^{(0)}}{\partial \delta L} \frac{\partial \chi_1^{(1)}}{\partial f} - \frac{1}{L_*} \frac{\partial \chi_1^{(1)}}{\partial \iota_c} \left(\iota_c \frac{\partial \mathcal{R}_{1,1}^{(0)}}{\partial f} - \frac{\partial \mathcal{R}_{1,1}^{(0)}}{\partial h} \right) \right) \\ & + \frac{1}{L_*} \frac{\partial \mathcal{R}_{1,1}^{(0)}}{\partial \iota_c} \left(\iota_c \frac{\partial \chi_1^{(1)}}{\partial f} - \frac{\partial \chi_1^{(1)}}{\partial h} \right) - \frac{2 \sin f}{L_* e} \sigma^{-1} \frac{\partial \chi_1^{(1)}}{\partial f} \left(\frac{\partial \mathcal{R}_{1,2}^{(0)}}{\partial g} - \frac{\partial \mathcal{R}_{1,2}^{(0)}}{\partial f} \right) \\ & - \frac{a_1}{2} \left\{ \frac{1}{\|r_1\|} \left(n_* \left(1 + \frac{2e \cos f}{\eta^3} \right) \frac{\partial \chi_1^{(1)}}{\partial f} + n_1 \frac{\partial \chi_1^{(1)}}{\partial E_1} \right), \chi_1^{(1)} \right\}_2, \end{aligned}$$

where $\{\cdot, \cdot\}_2$ indicates that we retain only σ^2 quantities after the operation (in virtue of Lemma 3.2.2 and Remark 3.2.5, inductions derived to demonstrate Proposition 3.2.1 are a coarser bound and no other parts of order σ^2 come out). Plugging in (3.69) and (3.65) for $l = 1, 2$ and taking into account Lemma 3.2.1, upon simplifications the contributions involving e result in

$$\mathcal{R}_{1,2e}^{(0)} - \frac{a_1 e n_*}{\eta^3 \|r_1\|} \sigma^2 \sum_{(s_1, s_4) \neq (0,0)} \frac{s_1 q''_{1,s}}{s_1 n_* + s_4 n_1} (\cos((1 - s_1)f - s_1 g - s_3 h - s_4 E_1) + \cos((1 + s_1)f + s_1 g + s_3 h + s_4 E_1)), \quad (3.96)$$

where

$$\mathcal{R}_{1,2e}^{(0)} = \frac{a_1}{\|r_1\|} \sigma^2 \sum_{s \in \mathbb{Z}^4} q_{2,s} \cos(s_1 f + s_2 g + s_3 h + s_4 E_1), \quad q_{2,s} = e \bar{q}_{2,s}. \quad (3.97)$$

We employ now all D'Alembert rules to show that only the harmonics of interest can exist.

Following the same argument as in Lemma 3.2.1, let us write the cosine input of (3.97) using modified Delaunay angles (1.66) also for \mathcal{P}_1 in relation to corresponding orbital elements (3.3) (subscript '1'):

$$s_1 \lambda + (s_1 - s_2) \gamma + (s_2 - s_3) \zeta + s_4 \lambda_1 + (s_4 - s_5) \gamma_1 + (s_5 - s_6) \zeta_1, \quad s_l \in \mathbb{Z},$$

in which $\gamma_1 = \zeta_1 = 0$. For the elimination of the apparent singularity at $e = 0$, we must have $1 - |s_1 + s_2| \geq 0$ and even, hence $s_2 = s_1 \pm 1$. Then, since $\mathcal{R}_{1,2e}^{(0)}$ is independent on e_1 by book-keeping setting, analogously we must end up with $s_4 = s_5$. Regarding instead the regularity at $i_1 = 0$, because of the absence of i_1 we must conclude that $0 - |s_5 - s_6| \in 2\mathbb{N}$, namely $s_5 = s_6$. At this stage, we invoke the invariance under rotation around the Z axis, which prescribes

$$s_1 - s_1 + s_2 - s_2 + s_3 + s_4 - s_4 + s_5 - s_5 + s_6 = s_3 + s_6 = 0,$$

and summing up this implies $s_3 = -s_4$. Ultimately, concerning the inclination, we must ensure that $l - |s_2 - s_3| \in 2\mathbb{N}$, with l even as well again being i_1 not involved, thus $s_2 = s_3 \pm 2n$, $n \leq l/2$ natural number. Putting all together we arrive at

$$s_1 f + s_2 g + s_3 h + s_4 E_1 \implies s_1 f + (s_1 \pm 1)g + (s_1 \mp 2n \pm 1)h + (\pm 2n \mp 1 - s_1)E_1,$$

which always depends on at least one among f, E_1 since the coefficients $s_1, \pm 2n \mp 1 - s_1$ never vanish simultaneously.

By means of an identical reasoning and given the preservation of D'Alembert rules under $\exp\left(\mathcal{L}_{\chi_1^{(1)}}\right)$, we achieve the same outcome for the remaining part of (3.96) after replacing $s_1 \mapsto 1 \pm s_1$, indeed we find

$$(1 \pm s_1) + (1 \pm s_1 \pm 1)g + (1 \pm s_1 \mp 2n \pm 1)h + (\pm 2n \mp 1 - 1 \mp s_1)E_1,$$

and no solutions to $1 \pm s_1 = 0, \pm 2n \mp 1 - 1 \mp s_1 = 0$. \square

Given that the order 2 normal form is sourced from the part of $\mathcal{R}_{2,2}^{(1)}$ explicitly independent on fast angles, it turns out that it is free of e . Finally, $\mathcal{R}_{2,2}^{(2)}$ is free of e too, being generated by terms in $\{\mathcal{R}_{2,2}^{(1)}, \chi_2^{(2)}\}$ and $\{\dots \{\{\mathcal{Z}_0 + \mathcal{R}_{2,2}^{(1)}, \chi_2^{(2)}\}, \chi_2^{(2)}\}, \dots, \chi_2^{(2)}\}$ subjected to computation (i) of Proposition 3.2.1 (Remark 3.2.5). Again by construction, the same applies to $\chi_2^{(\text{II})}$.

- $\{\mathcal{R}_2^{(2)}, \chi_2^{(\text{II})}\} = \mathcal{O}(\sigma^4)$ by Remark 3.2.5.
- $\frac{1}{n!} \underbrace{\{\dots \{\{\mathcal{H}^{(2)}, \chi_2^{(\text{II})}\}, \chi_2^{(\text{II})}\}, \dots, \chi_2^{(\text{II})}\}}_{n \geq 2} = \mathcal{O}(\sigma^4)$ consequently.

In order to conclude, we just need to check that the next step gives rise to an $\mathcal{O}(\sigma^4)$ perturbation and the cycle of normalizations can restart for $j \geq 4$ in light of the bounds on σ from (3.91) at the end of the proof of Proposition 3.2.2. Upon repeating the usual argument, it is easy to see that the only bracket worth investigating is $\{\mathcal{Z}_2^{(\text{II})}, \chi_3^{(3)}\}$, that is, nevertheless, $\mathcal{O}(\sigma^4)$ because $\mathcal{Z}_2^{(\text{II})}$ is made out of $\mathcal{R}_{2,2}^{(2)}$ independent on e . \square

Remark 3.2.6. By the above argument it is immediate to realize that even $p_2 \equiv 0$ in (3.69) and (3.65) for $l = \nu$, so $q'_{\nu,p} = 0$ for all $p \neq (0, 0)$.

Remark 3.2.7. The content of Lemma 3.2.3 comes from a obvious physical intuition: since the potential due to the secondary experienced by the particle depends on their mutual position, which is determined by f and E_1 , the unnormalized short-effect harmonics in the remainder depend necessarily on one of the two anomalies or both.

Serving as an example, a detailed demonstration of the normalization procedure exposed in the present section for a simple model, containing just few terms of the disturbing function, is presented in Appendix D.

3.3 Numerical tests

3.3.1 Computer-algebraic implementation of the normalization algorithm

Implementing the above normalization procedure, e.g. by use of a Computer Algebra System (CAS), requires working with a finite truncation of the initial Hamiltonian model (3.11). To this end, the disturbing function (3.13) multiplied by μ can be re-arranged as

$$\mu \mathcal{H}_1 = -\frac{\mathcal{G}m_0\mu}{\|R\|} \sum_{\kappa_1=0}^{\infty} \sum_{\substack{\kappa_2=0 \\ \kappa_2 \neq 1}}^{\infty} \sum_{\kappa_3=0}^{\infty} \tilde{h}_{\kappa_1, \kappa_2, \kappa_3} \mu^{\kappa_1} \left(\frac{2r_1 \cdot R}{\|R\|^2} \right)^{\kappa_2} \left(\frac{\|r_1\|}{\|R\|} \right)^{2\kappa_3}, \quad (3.98)$$

where $\tilde{h}_{\kappa_1, \kappa_2, \kappa_3}$ are real coefficients derived from the coefficients of (3.13). A convenient truncation of (3.98) stems from defining two separate truncation orders in powers of μ (truncation order k_μ), and in powers of $\|r_1\| / \|R\|$ (multipole truncation order k_{mp}), through the formula

$$\mathcal{H}_1^{\leq k_\mu, k_{\text{mp}}} = -\frac{\mathcal{G}m_0\mu}{\|R\|} \sum_{\kappa_1=0}^{k_\mu-1} \sum_{\kappa_2=0, \kappa \neq 1}^{k_{\text{mp}}} \sum_{\kappa_3=0}^{\lfloor k_{\text{mp}}/2 \rfloor} \tilde{h}_{\kappa_1, \kappa_2, \kappa_3} \mu^{\kappa_1} \left(\frac{2r_1 \cdot R}{\|R\|^2} \right)^{\kappa_2} \left(\frac{\|r_1\|}{\|R\|} \right)^{2\kappa_3}, \quad (3.99)$$

where $\lfloor \cdot \rfloor$ is the integer part function. Working with the truncated Hamiltonian $\mathcal{H}^{\leq k_\mu, k_{\text{mp}}} = \mathcal{H}_0 + \mathcal{H}_1^{\leq k_\mu, k_{\text{mp}}}$, we then obtain a sequence of secular models $\mathcal{F}^{(j)}$, $j = 1, 2, \dots$, where j denotes the normalization step, computed via the formula

$$\mathcal{F}^{(j)} = \mathcal{F}_0 + \sum_{l=1}^j \mathcal{F}_{\nu+l-1}^{(l)}. \quad (3.100)$$

In particular, we implement the following steps of the CAS algorithm:

- (i) for a fixed value of μ , choose values for k_μ, k_{mp} , perform the corresponding expansions of the Hamiltonian as in (3.98) and compute the truncated model $\mathcal{H}^{\leq k_\mu, k_{\text{mp}}}$;
- (ii) choose the reference values of a_* and e_* ;
- (iii) pass to variables $(f, g, h, E_1, \delta L, e, \eta, \iota_c, \iota_s, J_1)$ and parameters L_*, e_1, a_1, η_1 on the basis of the selected a_* ;
- (iv) compute ν and ν_1 (equation (3.7));
- (v) set the appropriate book-keeping weights following the rules in §3.2.3 and expand correspondingly the Hamiltonian in δL up to $\sigma^{\nu k_\mu}$;
- (vi) drop constants, perform the identity operation (3.63), discard book-keeping powers larger than νk_μ and introduce n_* ;
- (vii) if $\nu > 1$, compute the generating function (3.69) as well as the first-normalized Hamiltonian $\mathcal{H}^{(1)}$ by the Lie series operation (3.66) truncated at the maximum book-keeping order $N_{\text{bk}} \leq \nu k_\mu$; if $\nu = 1$, compute $\mathcal{H}^{(1)}$ (always truncated to the book-keeping order N_{bk}) via the procedure in the dedicated paragraph of §3.2.4;
- (viii) compute the successive normalizations $\mathcal{H}^{(j)}$, truncated at book-keeping order N_{bk} via the procedure of §3.2.4 in the third paragraph, up to a maximum normalization order $\nu + j_{\text{max}} - 1 < N_{\text{bk}}$, $j_{\text{max}} \leq \nu(k_\mu - 1)$; this allows us to obtain truncated Hamiltonian models containing a finite number of normal form terms as well as a finite number of terms provided by the truncated remainder.

Serving as additional support, the above road-map is structured as a pseudo-code in Appendix E.

In the CAS implementation of the above algorithm we work in WOLFRAM MATHEMATICA 12 with numerical coefficients, substituting all constants with their corresponding numerical values. Several types of numerical tests of the precision of the method can be carried out as exemplified in the sequel.

3.3.2 Semi-analytic orbit propagations in the Sun-Jupiter R3BP

For all numerical tests below we refer to the Sun-Jupiter one ($\mu = 9.5364 \cdot 10^{-4}$). We employ Earth-orbit based units, such that $\mathcal{G}m_0 = 4\pi^2 \text{ AU}^3/\text{y}^2$, $a_1 = 5.2044 \text{ AU}$, so that Jupiter's period is $T_1 = 11.86 \text{ y}$. Jupiter's mean motion is $n_1 = 2\pi/T_1$, and eccentricity either $e_1 = 0.0489$ (ER3BP) or $e_1 = 0$ (CR3BP), used throughout all computations.

In all tests below, a particle's orbit is defined by providing the initial conditions $a(0), e(0), i(0)$ ($a(0), e(0)$ in the planar case), complemented by $f(0) = g(0) = h(0) = 0$ ($f(0) = g(0) = 0$ in the planar case).

Our basic proof of the efficiency of the normalization method in the framework of the ER3BP is given by comparing the short-period oscillations of the orbital elements $a(t), e(t), i(t), g(t), h(t)$, as found by two different methods.

Direct Cartesian propagation: the initial conditions

$$z(0) := (a(0), e(0), i(0), f(0), g(0), h(0))$$

are mapped into initial conditions for the Cartesian canonical positions and conjugate momenta $(X(0), Y(0), Z(0), P_X(0), P_Y(0), P_Z(0))$. Using Hamilton's equations with the full Hamiltonian (3.1) (setting also $J_1(0) = 0, M_1(0) = 0$), we obtain the numerical evolution $(X(t), Y(t), Z(t), P_X(t), P_Y(t), P_Z(t))$, which can be transformed to element evolution

$$z(t) = (a(t), e(t), i(t), f(t), g(t), h(t)) .$$

Semi-analytical propagation: following the implementation of the normalization algorithm as described in the previous subsection, the initial osculating element state vector $z(0)$ is transformed into an initial condition for the corresponding 'mean element' state vector $\xi^{(j)}(z(0))$, i.e., the element vector corresponding to the new canonical variables conjugated to the original ones after j near-identity normalizing transformations. This is computed by the Lie series composition formula truncated at book-keeping order N_{bk} :

$$\xi^{(j)}(z) = \left(\exp \left(\mathcal{L}_{-\chi_v^{(1)}} \right) \circ \exp \left(\mathcal{L}_{-\chi_{v+1}^{(2)}} \right) \circ \dots \circ \exp \left(\mathcal{L}_{-\chi_{v+j-1}^{(j)}} \right) z \right)^{\leq N_{\text{bk}}} , \quad (3.101)$$

using (3.68) for the inverse series. We then obtain the evolution of the mean element vector $\xi^{(j)}(t)$ through numerical integration of the *secular* equations of motion.

$$\dot{\xi}^{(j)} = \mathbb{J}\nabla \mathcal{Z}^{(j)}(\xi^{(j)}) \quad (3.102)$$

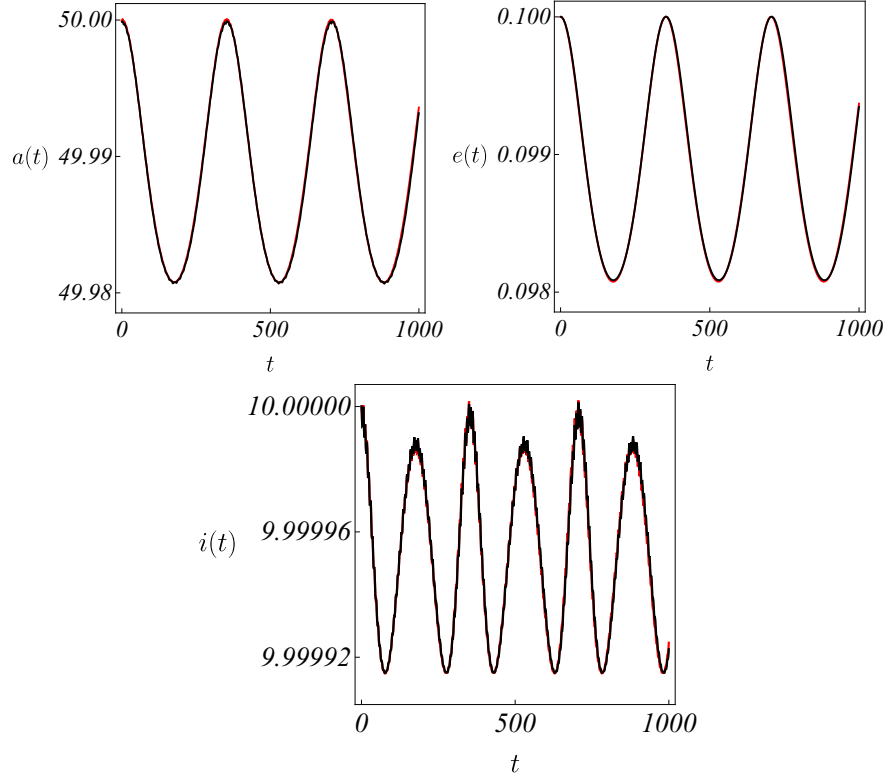


Figure 3.2: First example (ER3BP). Data: $a_* = 50$ AU, $e_* = 0.1$ ($\nu = 3$), $i(0) = 10^\circ$, $k_\mu = k_{\text{mp}} = 2$. Black curves represent semi-analytic time variations (our method), while red curves stand for Cartesian series.

This can be back-transformed to yield the evolution of the osculating element vector $z(t)$ using the truncated Lie series composition formula

$$z(\xi^{(j)}) = \left(\exp \left(\mathcal{L}_{\chi_{v+j-1}}^{(j)} \right) \circ \exp \left(\mathcal{L}_{\chi_{v+j-2}}^{(j-1)} \right) \circ \dots \circ \exp \left(\mathcal{L}_{\chi_v}^{(1)} \right) \xi^{(j)} \right)^{\leq N_{\text{bk}}} . \quad (3.103)$$

Note that both the direct and inverse transformations (Eqs.(3.101) and (3.103)), as well as Hamilton's secular equations (3.102), can be computed in closed form, using the Poisson algebra rules of §3.2.3. We then call semi-analytic the evolution of the element vector $z(t)$ obtained via the formula

$$z(t) = z(\xi^{(j)}(t)) . \quad (3.104)$$

Fig. 3.2 and 3.3 show the comparison between the Cartesian and the semi-analytical propagation of the elements in “easy” cases, where, for instance in the former, the particle departs from initial conditions $a(0) = 50$ AU, with a relatively low value of the eccentricity $e(0) = 0.1$ and inclination $i(0) = 10^\circ$. In this case, the distance ratio $\|r_1\| / \|R\|$ is small (about 10^{-1}), a fact implying that the quadrupolar expansion ($k_{\text{mp}} = 2$) suffices to have obtained a relative error of about 0.1% in the representation of the Hamiltonian perturbation \mathcal{H}_1 . Going to higher multipoles is straightforward, albeit with a significant computational

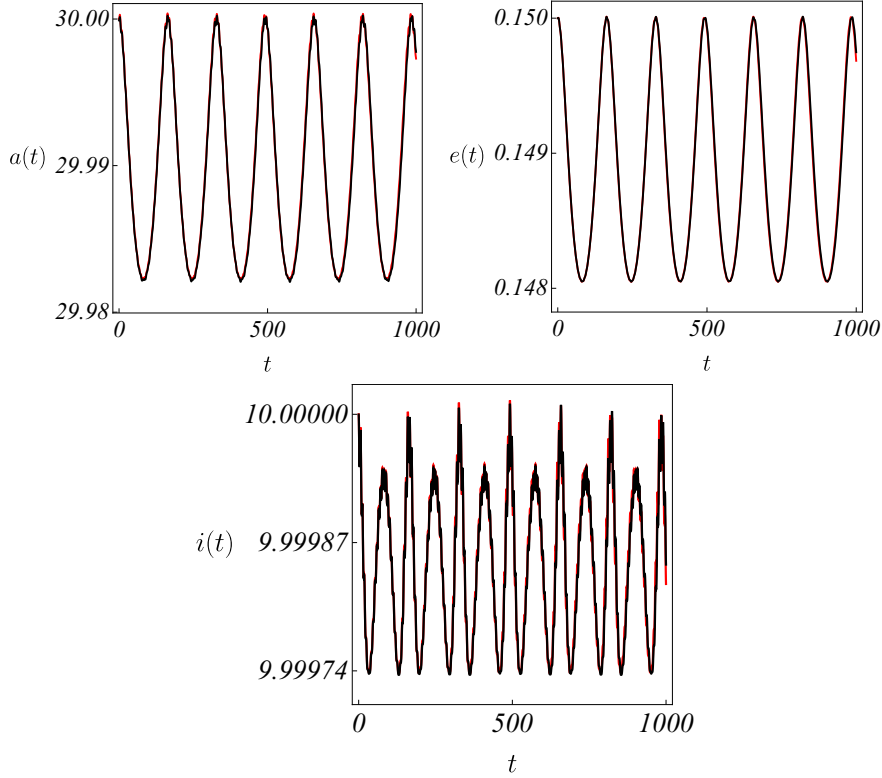


Figure 3.3: Second example (ER3BP). Data: $a_* = 30$ AU, $e_* = 0.15$ ($\nu = 4$), $i(0) = 10^\circ$, $k_\mu = k_{\text{mp}} = 2$. Same color conventions of Fig. 3.2.

cost as the number of terms in the Hamiltonian grows significantly. On the other hand, even with low-order truncations of the Hamiltonian we achieve to have an accurate semi-analytical representation of the $O(\mu)$ short-period oscillations in all three “action-like” elements (semi-major axis, eccentricity, inclination). Most notably, keeping $a(0)$ the same but changing the eccentricity to $e(0) = 0.7$, i.e., beyond the Laplace value, yields an orbit whose pericenter is at $\|R_p\| = 15$ AU, implying a distance ratio $\|r_1\| / \|R\| \approx 0.3$ (Fig. 3.4). This time, an octupole truncation ($k_{\text{mp}} = 3$) is required to produce an approximation of the Hamiltonian model at the level of a relative error of 0.1%. Still, however, as shown in Fig. 3.4 the semi-analytical propagation of the orbit is able to track the fully numerical one with an error which does not exceed 0.2% even close to the orbit’s pericentric passages.

Finally, we provide further time series examples in the case of the planar CR3BP in Fig. 3.5, 3.6, 3.7. The simpler model allows to carry out more computationally demanding performances. The agreements, indeed, reached in Fig. 3.5-3.6 (including an example for the angle $g(t)$ in the former) are obtained for $j_{\text{max}} = 6$ and $j_{\text{max}} = 10$ normalization steps respectively (see also Fig. 4.5 in §4.4.1), which are more than those employed in the elliptic case (respectively, $j_{\text{max}} = 3, 4, 4$). Moreover in Fig. 3.7, an octupole expansion is not good enough to cope with a distance ratio $\|r_1\| / \|R\| \approx 0.7$ and a pericentric distance $\|R_p\| = 7.2$ AU. Thus, a larger value $k_{\text{mp}} = 5$ allows us to improve considerably the degree of accuracy. More details in this regard are addressed

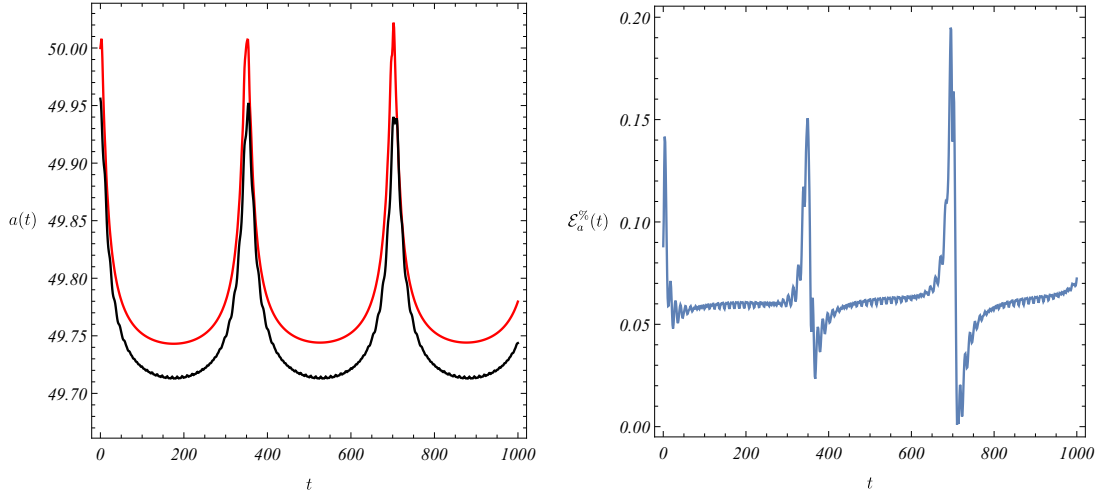


Figure 3.4: Third example (ER3BP). Data: $a_* = 50$ AU, $e_* = 0.7$ ($\nu = 20$), $i(0) = 20^\circ$, $k_\mu = 2$, $k_{\text{mp}} = 3$. On the left, the black curve represents the semi-analytic time variation of the semi-major axis (our method) versus the one found by propagation of the Cartesian equations of motion (red). The right panel shows the evolution of the corresponding percent relative error $\mathcal{E}_a^{\%}$.

in §4.4.1.

A summary of the number of terms in the final truncated generating function, normalized Hamiltonian and remainder for each example of Fig. 3.2-3.7 is provided in Table 3.1.

In the above examples, the maximum number of normalization steps j_{max} at which the secular Hamiltonian is computed was set correspondingly to the best achievable match. As discussed in the next chapter, an estimate of the *minimum possible* error in the semi-analytic propagation of the trajectories requires computing first the so-called *optimal* number of normalizations j_{opt} (or equivalently *optimal* normalization order $\nu + j_{\text{opt}} - 1$) as a function of the reference values (a_* , e_*) within a model given by a preset fixed multipole truncation order. Owing to the fact that the same divisors appear in the ER3BP and in

Ex.	$(N_{\text{bk}}, j_{\text{max}}, k_{\text{mp}})$	$\# \left(\mathcal{X}_{\nu+j_{\text{max}}-1}^{(j_{\text{max}})} \right)$	$\# \left(\mathcal{L}_{\nu+j_{\text{max}}-1}^{(j_{\text{max}})} \right)$	$\# \left(\mathcal{R}_{\nu+j_{\text{max}}}^{(j_{\text{max}})} \right)$
1 (Fig. 3.2)	(6, 3, 2)	179	18	418
2 (Fig. 3.3)	(8, 4, 2)	330	19	1111
3 (Fig. 3.4)	(24, 4, 3)	936	18	1842
4 (Fig. 3.5)	(16, 6, 3)	204	72	543
5 (Fig. 3.6)	(20, 10, 3)	618	126	726
6 (Fig. 3.7)	(9, 6, 5)	2127	140	3514

Table 3.1: Computational details of the normalization for the examples in Fig. 3.2-3.7 ($\#(\cdot)$ denotes the number of terms contained).

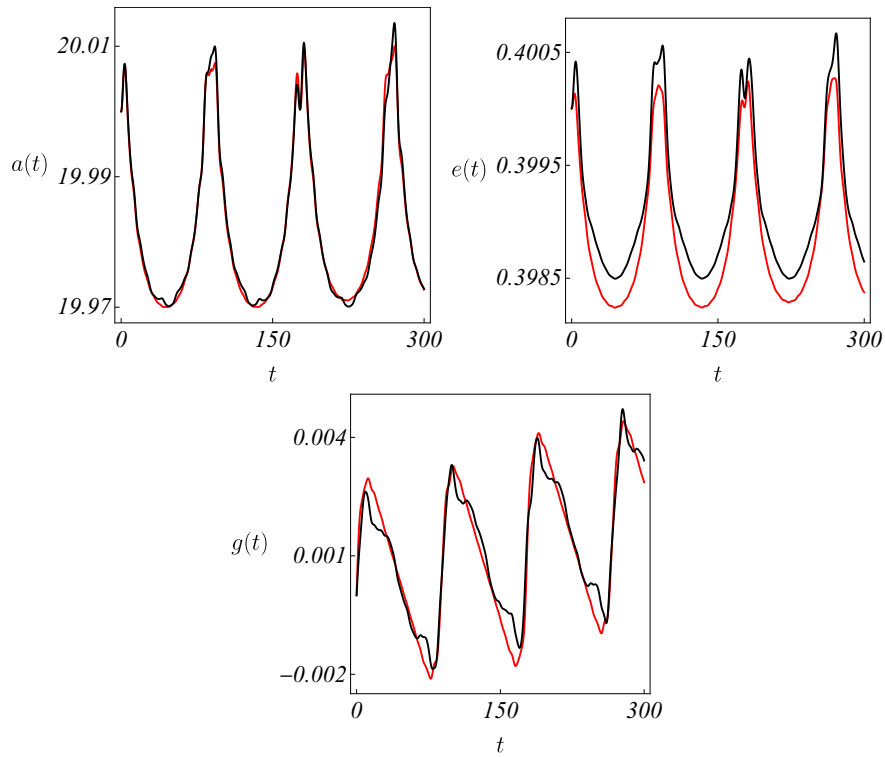


Figure 3.5: Fourth example (planar CR3BP). Data: $a_* = 20$ AU, $e_* = 0.4$ ($\nu = 8$), $k_\mu = 2$, $k_{mp} = 3$. Black curves: semi-analytic. Red curves: Cartesian.

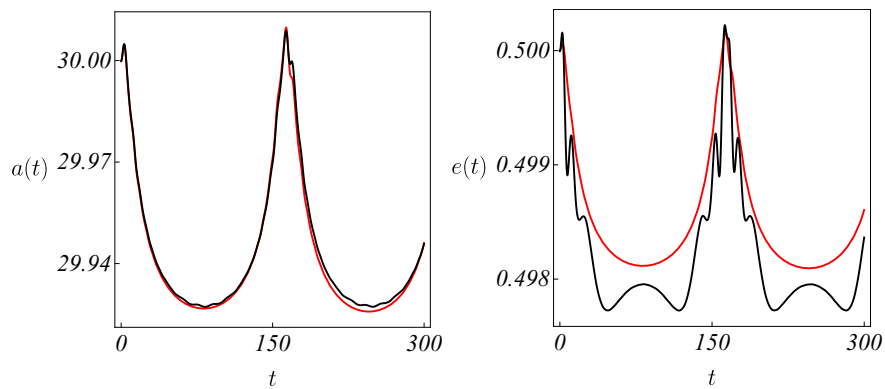


Figure 3.6: Fifth example (planar CR3BP): $a_* = 30$ AU, $e_* = 0.5$ ($\nu = 10$), $k_\mu = 2$, $k_{mp} = 3$. Black curves: semi-analytic. Red curves: Cartesian.

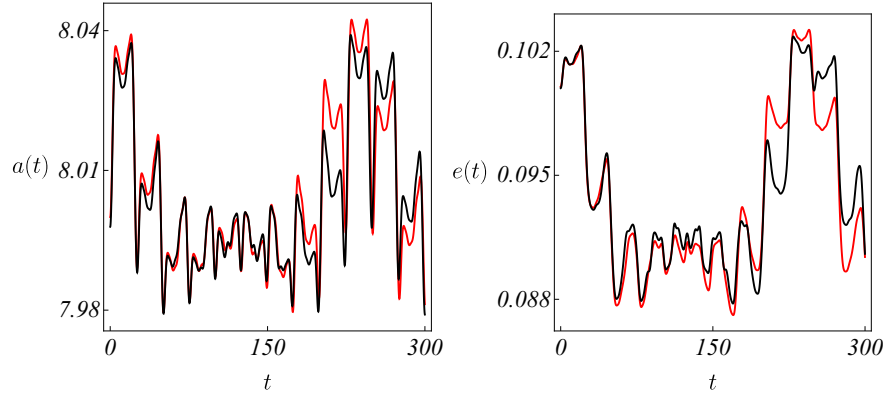


Figure 3.7: Sixth example (planar CR3BP): $a_* = 8$ AU, $e_* = 0.1$ ($\nu = 3$), $k_\mu = 3$, $k_{\text{mp}} = 5$. Black curves: semi-analytic. Red curves: Cartesian.

the CR3BP, we verify with numerical examples that the error analysis yields essentially identical results in either case. However, the computation of the optimal normalization is easier to perform in the CR3BP, owing to the considerably smaller number of terms produced in the CAS computation of the normal form. Such reduction of the operational cost, especially in the planar restriction, is due, in particular, to the following:

- The dependence on M_1 becomes explicit ($M_1 = E_1$ in (3.2)), while $a_1 = \|r_1\|$. As a consequence, $\phi_1 = 0$.
- No terms involving (h, H) appear in the disturbing function, thus l_c, l_s are discarded (planar case).
- No terms requiring a book-keeping in terms of the exponent ν_1 appear, hence, only ν is defined, as in (3.7).
- $d_{l,\lambda,p}^{(j)} = 0$ for every j, l, λ, p in (3.88), (3.84), and consequently $p_1 = p_2 \equiv 0$ in (3.86). This is due to the fact that the expression (3.16) reduces to

$$r_1 \cdot R = \|r_1\| \|R\| \cos(f + g - M_1), \quad (3.105)$$

which always depends on the difference $g - M_1$ by D'Alembert rules. This implies that, unlike the ER3BP, the action G (and the corresponding eccentricity e) are integrals of the secular Hamiltonian.

- As a consequence no lower or equal book-keeping order terms appear in any Poisson bracket of the first normalization step in the case $\nu = 1$. Hence Proposition 3.2.3 is redundant.

Hence, in the next chapter we turn our attention to a detailed study of the application of closed-form theory to this latter model.

NUMERICAL DETECTION OF THE SECULAR STABILITY DOMAIN IN THE SUN-JUPITER SYSTEM

In this chapter we first discuss the usage of numerical techniques capable to quantify the degree of orbital instability on either short- or long-term time scales in the R3BP, taking as example the Sun-Jupiter system. The numerical stability maps allow to obtain insights on the geometry of the projected phase space (orbital elements' space). We then return to the central goal of the dissertation: we employ the semi-analytic machinery of Chapter 3 in order to characterize, within the same portrait, a particular domain of initial conditions leading to motions which exhibit no instabilities caused by short-period interactions with Jupiter. This is called hereafter *the domain of secular motions*. We then explore how the closed-form technique to produce a secular normal form can be exploited in order to develop a reliable criterion by which the border of the domain of secular motion can be computed semi-analytically. The main findings of the present chapter are hinted in [89] and can be thoroughly consulted in [91].

4.1 State of the art on stability analysis and purposes

The secular (long-term) behavior of the planetary orbits with one massive central body and $N - 1$ less massive bodies is a central question in the framework of the N -body problem. Already in the R3BP, although simpler in its analytical formulation, the question of long-term orbital stability remains a long-standing and complex problem.

The question can be classically formulated basically in the following manner: given a certain semi-major axis for the particle, and fixing the angles at a certain value, what is the critical eccentricity that separates the domains of

long-term stable and unstable motion?

This problem has been addressed by different methods. The coarsest criterion one can think of is the *pericenter/apocenter crossing* method: whenever Jupiter's radius crosses the particle's radius of pericenter (for external motions) or radius of apocenter (for internal motions) the secular evolution is interrupted due to close encounters of the test particle with the planet. However, by numerical evidence, this condition seems to be inaccurate: as shown below, on one hand there exist strips of stable orbits intersecting one of the two apsides in the (a, e) plane, while off these strips, on the other hand, the apse curves overestimate the domain of regular orbits.

A more refined way to investigate stability is the so-called *Hill stability criterion*: an initial condition is said to be stable if its Jacobi constant $C_J > C_{J_{L_1}}$, where $C_{J_{L_1}}$ is the value acquired at the Lagrangian point L_1 . This is based on the fact that the particle will then be trapped within a zero-velocity region that excludes the position of the secondary. The particle's trajectory cannot cross the orbit of the perturber and will therefore remain bounded. While such a condition is sufficient for stability, it is not necessary: there exist solutions which do not comply with this inequality, but are nevertheless stable, at least for times of the order of the age of the Solar System [34].

An estimate of different nature, this time of orbital instability, is the *resonance overlap criterion*, based on the work of Chirikov [15] and Wisdom [105]: it asserts that global chaos (and therefore orbital instability) is triggered by the overlap of adjacent mean-motion resonances. Based on what is known nowadays as the Second Fundamental Model for Resonance [44], for an inner particle Wisdom proposed the empirical law

$$a_{\text{crit}} = a_1 \left(1 - 1.3 \left(\frac{m_1}{m_0} \right)^{\frac{2}{7}} \right) \quad (4.1)$$

for the critical semi-major axis leading to overlap. Various adjustments to (4.1) and revisitations of the criterion have been examined so far (see e.g. [87] and references therein).

Recently, Laskar and collaborators [22, 55, 84, 85] have presented another heuristic criterion for the secular stability, with applicability in extrasolar planetary environments. According to the so-called *Angular Momentum Deficit* (AMD) criterion, a system of bodies is AMD-stable if its total angular momentum restricts the amplitude of the secular oscillations in the bodies' orbital eccentricities and inclinations in such a way as to protect the bodies from close encounters, where the AMD is defined as the difference between the norm of the angular momentum of a coplanar and circular system with the same semi-major axis values and the norm of the angular momentum. Nonetheless, there are numerical indications that the AMD criterion has some limitations too as regards its applicability [38, 39, 63].

Finally, it is worth recalling that the above strategies pay less attention to the outermost zones of the Solar System as compared to the innermost ones.

In order to set up a new limit as regards the separation between stable and

unstable orbits, whose distinction will be made precise in the treatment below, we need an accurate representation of the domains of different regimes of motion, with emphasis on trajectories larger than Jupiter's. In the following we present high-resolution stability maps in the semi-major axis-eccentricity coordinates obtained via numerical integrations complemented by the regularization technique constructed in Chapter 2 when useful. The resulting cartographies portray short- and long-time values of the well-known chaos indicator named Fast Lyapunov Indicator [56].

Subsequently, subsets of the boundary separating strong from weak chaos captured by these images are compared to their equivalent produced this time using a coarser technique to represent instability: the particle's sudden semi-major axis jump in finite time. This is displayed using plots with a binary input (0 or 1) based on the exceeding of a chosen percentage of the moving average along the integration. Notwithstanding its crudity and evident limitations, the good match in the results proves its reliability as a simpler alternative for a preliminary stability analysis.

Along with the indicator, a distribution of corresponding "blowup" times and consequent minimum distances from the planet is provided as well.

After displaying a detailed cartography of the domain of order and chaos using the above numerical chaos indicators, we then return to our central question posed above: can we invoke, instead, a semi-analytic criterion allowing to efficiently separate the domain of long-term stable from unstable motion? Our basic result in the present chapter is that such a criterion can be obtained on the basis of the closed-form technique of derivation of a secular normal form exposed in Chapter 3.

A relevant outcome of the analysis of the behavior of the remainder obtained by the closed-form method stems from an estimation of the optimal number of normalization steps j_{opt} , where the remainder becomes of order $\nu + j_{\text{opt}} - 1$ in the book-keeping parameter, with $j_{\text{opt}} \leq \nu(k_\mu - 1)$. The value of j_{opt} is defined as the one where the error bound $\mathcal{E}^{(j)}(a_*, e_*) = \sum_{\nu+j \leq l \leq \nu k_{\mu,s}} |d_{l,s}^{(j)}| \geq \left\| \mathcal{R}_{\nu+j}^{(j)} \right\|_\infty = \sup |\mathcal{R}_{\nu+j}^{(j)}|$ becomes minimum, with $\mathcal{R}_{\nu+j}^{(j)} = \mathcal{O}(\sigma^{\nu+j})$ and $d_{l,s}^{(j)}$ as in (3.6) after j normalization steps. As typical in perturbation theory, the value of j_{opt} depends on the chosen reference values (a_*, e_*) . With the methods of Chapter 3, one can then obtain a map of the size of the optimal remainder as a function of (a_*, e_*) in the semi-plane $a > a_1$. Using this information, we compute the limiting locus uniting all points in (a_*, e_*) such that the normal form computation yields no improvement with increasing number of normalization steps, i.e., where $j_{\text{opt}} = 1$. Comparing with the above numerical stability maps, one sees that, the limiting locus found semi-analytically essentially coincides with the numerical (FLI map) limit where no harmonic in the Hamiltonian associated with one of the exterior mean-motion resonances affects the dynamics. As a consequence, all motions in the sub-domain of the plane (a_*, e_*) below the limiting locus are stable in the *secular* sense, i.e., protected against instabilities caused by short-period resonant effects. For this reason, we identify this locus as the border of the domain of secular motions and substantiate the fact that its semi-analytical

computation (through the normal forms) yields results in precise agreement with those found by the heuristic definition of the same border via the fully numerical (FLI) computation of stability maps.

4.2 Preliminaries on chaos indicators

4.2.1 Variational dynamics

The rate of growth of exponential separation of two trajectories starting at close initial points (§1.1.2), can be quantified looking at the rate of change of tangent vectors along the flow. For this purpose, instead of working only with the system (1.1), we pass to the variational dynamics governed by (1.4) multiplied by an initial tangent vector v_0 . Given a real phase space D and introducing the *tangent map*

$$\begin{aligned} T\Phi(t, x): T_x D &\longrightarrow T_{\Phi(t, x)} D \\ v_0 &\longmapsto v_t = D\Phi(t, x)v_0 \end{aligned} \quad (4.2)$$

the evolution $v_t := v(t)$ of $v_0 := v(0)$ is determined according to the variational equation

$$\dot{v} = DX(\Phi(t, x))v . \quad (4.3)$$

Similarly to (1.3), from(4.3) we have the simple estimate

$$\|v(t)\| \leq \alpha(t) \|v(0)\| , \quad (4.4)$$

where $\alpha(t) \leq e^{\Lambda|t|}$, $\Lambda > 0$. We have that $\alpha(t) \sim e^{\Lambda|t|}$ for chaotic trajectories. The variational dynamics allows to define quantities which characterize the asymptotic growth of the length of tangent vectors.

Definition 4.2.1. Let $v(t)$ be the solution of (4.3) with initial conditions x_0, v_0 . The *characteristic Lyapunov exponent* (CLE) of an initial condition x_0 and initial tangent vector v_0 is the limit

$$\chi(x_0, v_0) = \lim_{t \rightarrow \infty} \frac{\ln \|v(t)\|}{t} . \quad (4.5)$$

The anticipated well-definedness of (4.5) descends from a classic theorem in multiplicative ergodic theory.

Theorem 4.2.1 (OSELEDETS'S THEOREM). *Let \mathcal{M} be a probability measure on $D \subseteq \mathbb{R}^d$. $\chi(x_0, v_0)$ is a real number $\forall v_0 \in T_{x_0}D$, $v_0 \neq 0$, and for \mathcal{M} -almost every $x_0 \in D$. Moreover:*

- (i) *the CLE is a constant of motion for (4.3);*
- (ii) *if c is an equilibrium point and $\lim_{t \rightarrow \infty} \Phi(t, x_0) = c$, then, called $L(x) := \{\chi(x, v_0) : v_0 \in T_x D\}$, $L(x_0) = L(c)$;*
- (iii) *$L(x_0)$ for any x_0 is discrete with at most d different elements and for \mathcal{M} -almost all $v_0 \in T_{x_0}D$ $\chi(x_0, v_0) = \max L(x_0)$.*

The third property of Theorem 4.2.1 has important consequences for actual computations: a random choice of the initial tangent vector provides the largest characteristic Lyapunov exponent, that we denote henceforth by χ_L . For further readings on the computations of Lyapunov characteristic exponents, refer to [7].

4.2.2 Finite time chaos indicators

About the necessity to find numerical approximations of the flow of (1.1), we point out the following elementary facts:

- initial data of real systems are affected by errors, so we need to compute the time evolution of a set of “compatible” initial conditions;
- there are strong limitations in terms of reliability of the approximate solution when the dynamics separates exponentially the orbits.

We thereby overcome these inconveniences by making use of suitable chaos indicators inspired by χ_L . Clearly, chaotic orbits are detected by $\chi_L > 0$, hence $T_L = 1/\chi_L$, called *Lyapunov time*, represents the time scale needed to observe the exponential separation: $\|v(t)\| \sim \|v(0)\| e^{t/T_L}$. This suggests to construct *finite time chaos indicators*, so they can be practically computed.

We outline in the following some of the most popular indicators, belonging to the family of the so-called Fast Lyapunov Indicators originally introduced by Froeschlé et al. [30] and further developed in Guzzo et al. [43, 56].

Definition 4.2.2. For $\tau > 0$ the *Fast Lyapunov Indicator* is defined as the quantity

$$\text{FLI}(x_0, v_0; \tau) = \max_{t \in [0, \tau]} \ln \|v(t)\| . \quad (4.6)$$

Furthermore, given $e_j(t)$ time evolution of $\mathcal{B} = \{e_j(0)\}_{j=1, \dots, d}$ orthonormal basis of \mathbb{R}^d , the *Fast Lyapunov Indicator of the Basis* \mathcal{B} is

$$\text{FLIB}(x, \mathcal{B}; \tau) = \max_{t \in [0, \tau]} \max_{j=1, \dots, d} \|e_j(t)\| , \quad (4.7)$$

while the *Finite Time Lyapunov Exponent* is the number

$$\text{FTLE}(x; \tau) = \frac{1}{\tau} \max_{e_j(0) \in \mathcal{B}} \frac{\|D\Phi(\tau, x)e_j(0)\|}{\|e_j(0)\|} . \quad (4.8)$$

Remark 4.2.1. As expected, these numbers are theoretically consistent, because

- $\text{FLI} \approx \text{FLIB} \approx \text{FTLE}$,
- $\chi(x_0, v_0) = \lim_{\tau \rightarrow +\infty} \frac{\text{FLI}(x_0, v_0; \tau)}{\tau}$.

Hence, in virtue of Theorem 4.2.1, $\text{FLI} \propto \chi_L$.

Chaos can be driven by several dynamical instabilities, e.g. close encounters or resonances. In [40], based on a previous study developed in [41], a slightly modified definition of (4.6) is proposed in order to select only the chaos due to close encounters. This is done by introducing a *window function* (like the Hanning window) whose effect is that of filtering out all the contributions to the indicator that are not due to close encounters. As an alternative to such approach, we address the same matter in §4.3.1 by proposing an equivalent method based on the behavior of the time series of the particle's semi-major axis.

4.3 FLI cartographies of the Sun-Jupiter planar CR3BP

Let us consider the Hamiltonian (1.74) for

$$\mu \equiv \mu_J = 9.536433730801362 \cdot 10^{-4} \quad (4.9)$$

written in inertial barycentric orbital elements using (1.59) via the relations (1.60) and (1.61). We set the particle's initial angles so that the motion develops on the x - y plane and it starts either from the apocenter or the pericenter, namely $i(0) = \Omega(0) = 0$, $M(0) = \pi$ or 0 plus $\omega(0) = \pi$. Then we let $a(0)$ and $e(0)$ vary in the ranges $[0.4, 16]$ AU (from Mercury's to slightly less than Uranus's distance), suitably rescaled by $a_1 \equiv a_J = \|r_J\| = 5.2044$ AU, and $[0, 0.9]$ respectively.

Given these premises, we compute the indicator (4.6) on a refined grid of the (a, e) plane, in which, making use of the decimal logarithm for convenience, we filter out values of FLI larger than a reasonable threshold¹, say 10. This means that we cut out tangent vectors that has roughly grown more than a factor of 10^{10} . Furthermore, in order to pinpoint different types of emerging structures, we conduct a short- and long-time numerical experiment, viz. we set the maximum integration time $\tau = 50T_J$ and $\tau = 1000T_J$ where $T_1 \equiv T_J = 11.86$ y is Jupiter's mean orbital period opportunely converted in adimensionalized CR3BP units (i.e. equal to 2π).

Regarding the choice of v_0 , we remark that for chaotic orbits the time evolution of the FLI is approximately linear, while for regular orbits is approximately logarithmic; this fact is independent of the choice of the initial tangent vector as illustrated in §4.2, unless the initial tangent vector has null components on some special directions, such as the expanding directions of the tangent space, thence we expect chaotic orbits having a higher value of the FLI for the same initial tangent vector. Hereby $v_0 = 1/2(1, 1, 1, 1, 1, 1)$.

Figure 4.1 shows the apocentric and pericentric short-term FLI stability maps in question. We can observe how regions of regular (or weakly chaotic) orbits permeate the whole phase space, even above the line of pericenter crossing. In particular, for large values of the semi-major axis and correspondingly

¹Equivalently, one can modify Definition 4.2.2 by rescaling (4.6) by $\|v_0\|$ in the argument of the logarithm, as originally done in [56].

increasing eccentricities, a wide set of regular orbits emerges in the diagram. These are clearly protected from collisions and we will address them from now on as the “lower regularity region” (blue low part of the (a, e) plane). In the sequel the lower regularity region will be precisely the target of the closed-form perturbation theory approach presented in Chapter 3. Its boundary has a fractal shape whose form becomes clearer increasing the integration time, as displayed in Fig. 4.2. This highly complicates its characterization, especially from an analytical viewpoint.

The aforementioned criteria in §4.1, then, turn out to be quite inaccurate to ensure stability everywhere in the phase space: visibly, it is worth noticing for example that the line of pericenter significantly overestimates the boundary of the lower regularity region. Also, mean-motion resonances are depicted as spikes penetrating the deep blue region of the stability map.

We also observe in the same plot intricate arch-like structures created by the projected manifolds of the unstable orbits of various hyperbolic sets, like periodic orbits existing at each mean-motion resonance (the so-called “arches of chaos” according to [101], which we partially resume later in Chapter 5).

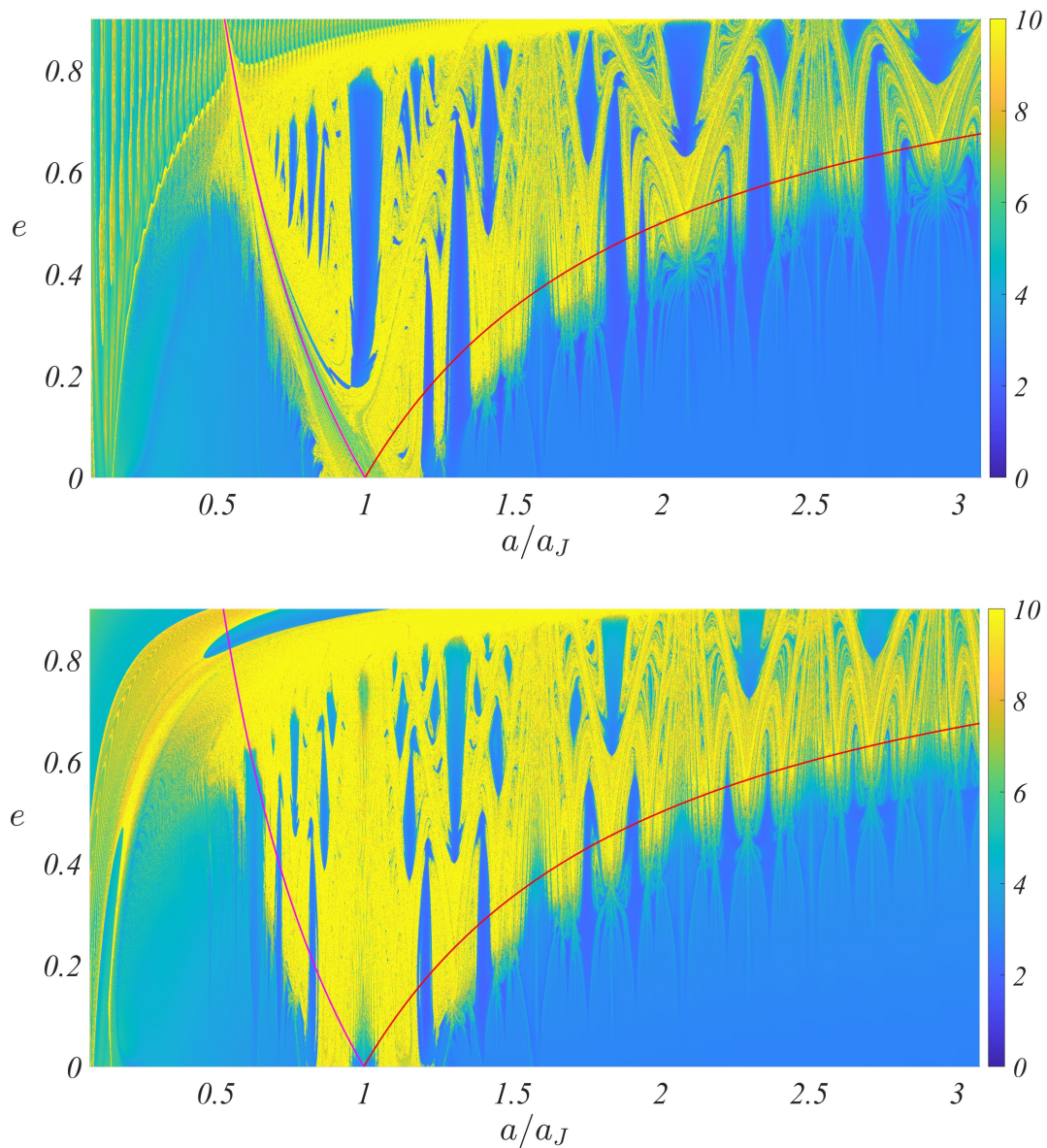


Figure 4.1: Short-period FLI cartographies of the Sun-Jupiter planar CR3BP computed over a grid of 300×900 initial data. The two curves represent the loci of points $\|r_J\| = a(1 - e)$ (red line for $a/a_J > 1$) and $\|r_J\| = a(1 + e)$ (magenta line for $a/a_J < 1$). **Top panel:** apocentric section ($M(0) = \pi$). **Bottom panel:** pericentric section ($M(0) = 0$).

4.3.1 The semi-major axis's maximum variation indicator

Increasing the exposition time τ for $M(0) = \pi$ we get the top panel of Fig. 4.2: the arches in the chaotic zones fade away, but in return we can better appreciate the contour of the lower regularity region, resembling a Cantor set pattern; in particular, the magnification in the left bottom panel highlights its sharpness.

Such behavior of the boundary is qualitatively already captured by the distribution in phase space of suddenly destabilized orbits, as close encounter

ones: in the bottom panels of Fig. 4.2 we confront a zoomed-in detail of the FLI map (left panel) with the plot of the characteristic (indicator) function of the critical set \mathcal{C} (right panel). This set is established heuristically according to an abrupt detected displacement from the short-period oscillations in the elements' time series along a numerical integration lasting $10^6 T_J$ with step size $\Delta t = T_J/100$, specifically looking at the semi-major axis $a(t)$. More precisely, we represent the indicator function

$$\mathbb{1}_{\mathcal{C}}(a, e) = \begin{cases} 1 & (a, e) \in \mathcal{C} \\ 0 & (a, e) \notin \mathcal{C} \end{cases}, \quad (4.10)$$

on a comparable grid of initial values $(a_0, e_0) \in [7.2, 7.5] \text{ AU} \times [0.1, 0.15]$, where

$$\mathcal{C} = \{(a_0, e_0) \mid \exists i = 1, \dots, 10^6 T_J / \Delta t \text{ s.t. } |a(i\Delta t) - \langle a \rangle_i| > 10^{-1} \langle a \rangle_i, \\ a(0) = a_0, e(0) = e_0\} \quad (4.11)$$

embodies the criterion according to which an initial semi-major axis $a(0)$ is deemed *non-regular* whenever the corresponding flow $a(t)$ deviates, in terms of relative error, more than the 10% with respect to the cumulative moving average

$$\langle a \rangle_i = \frac{1}{i+1} \sum_{j=0}^i a(j\Delta t), \quad i = 1, \dots, 10^8. \quad (4.12)$$

The time endpoint is adequately tailored in order to push the integration far enough in time, but concurrently to avoid to cope with diffusive phenomena and important accumulations of the numerical error (this thanks also to the help of regularization when pertinent), and thus to rely, for example, on symplectic schemes.

Fig. 4.2 and Fig. 4.3 show that the method discussed is compatible with the FLI representation, specifically concerning the boundary separating the regimes characterized by a marked difference in the amount of chaos. This trend is appreciable already at a lower level of resolution as in the latter of the two figures (computational details are written in the attached caption).

For orbits satisfying condition (4.11) one can wonder what is the instant at which the “blowup” of $a(t)$ occurs. Slightly better, we determine the time of minimum distance from Jupiter in a little larger time span $[0, k\Delta t] \subseteq [0, 10^6 T_J]$, $k \gtrsim i$, than the break-up moment $i\Delta t < 10^6 T_J$ at which we could stop the numerical integration for the binary diagrams. Basically, suppose that $(a_0, e_0) \in \mathcal{C}$, then we compute the time t_{\min} along the flow such that

$$t_{\min} = \arg \min_{1 \leq j \leq k} d_J(j\Delta t),$$

and $d_1 \equiv d_J$ given by (1.75).

In the top panels of Fig. 4.4 we report the histograms of times t_{\min} for all collision orbits detected with the indicator function (4.10) in Fig. 4.2. The left plot demonstrates that almost the totality of trajectories (around 95%) escapes

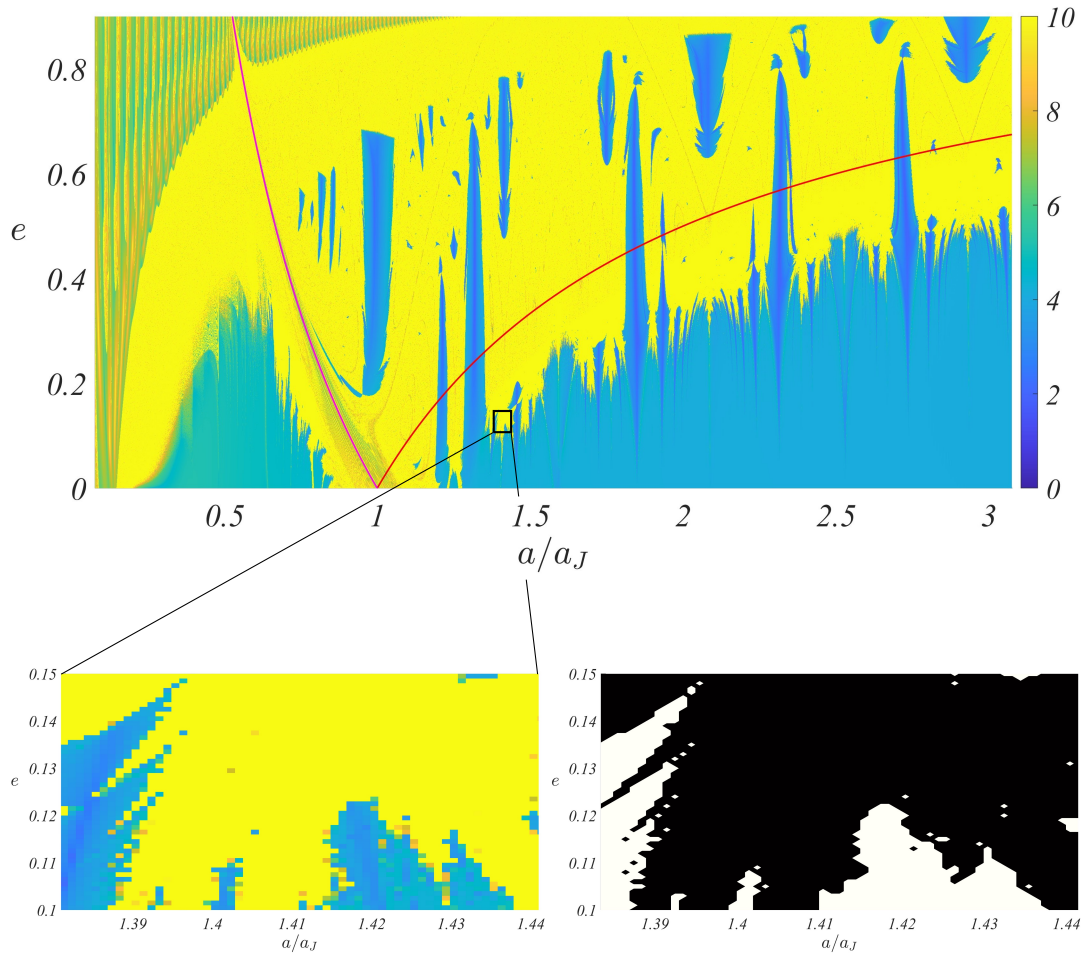


Figure 4.2: Long-period FLI cartography of the Sun-Jupiter planar CR3BP computed over a grid of 300×900 initial data and criterion (4.11) on its magnification. **Top panel:** apocentric section ($M(0) = \pi$). The two colored curves are as in Fig 4.1. **Bottom left panel:** magnification of the indicated rectangle in top panel positioned on the borderline of the lower regularity region. **Bottom right panel:** Close encounter binary plot according to (4.11) and (4.12) on the same zoomed-in image of bottom left panel discretized in 60×50 (a, e) grid points. Black pixels (■) stand for 1 in (4.10), while white ones (□) stand for 0 in (4.10).

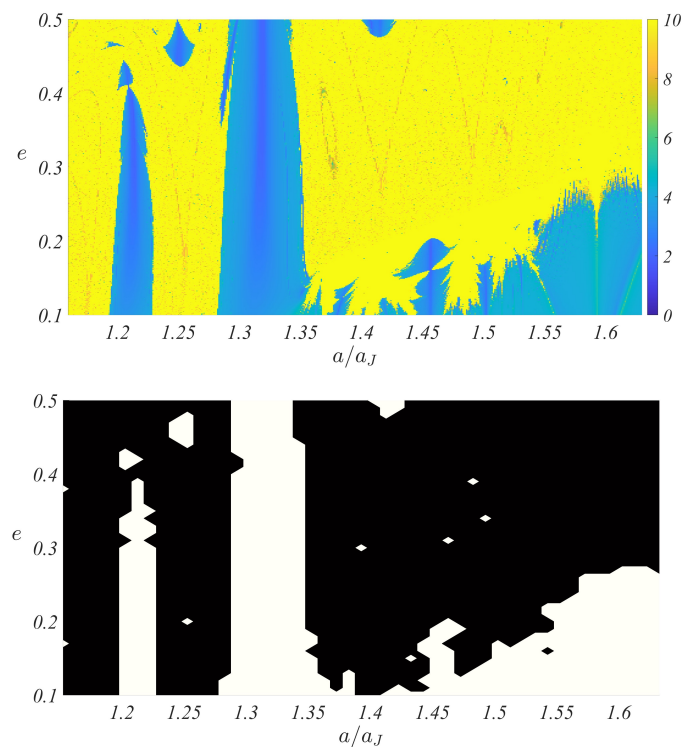


Figure 4.3: Comparison as in bottom panel of Fig. 4.2 on a larger region of the long-time FLI map. The region is 100 times larger than the magnification in Fig. 4.2, but the grid in bottom panel is kept identical to the previous one (60×50 initial data) to ease the computational effort.

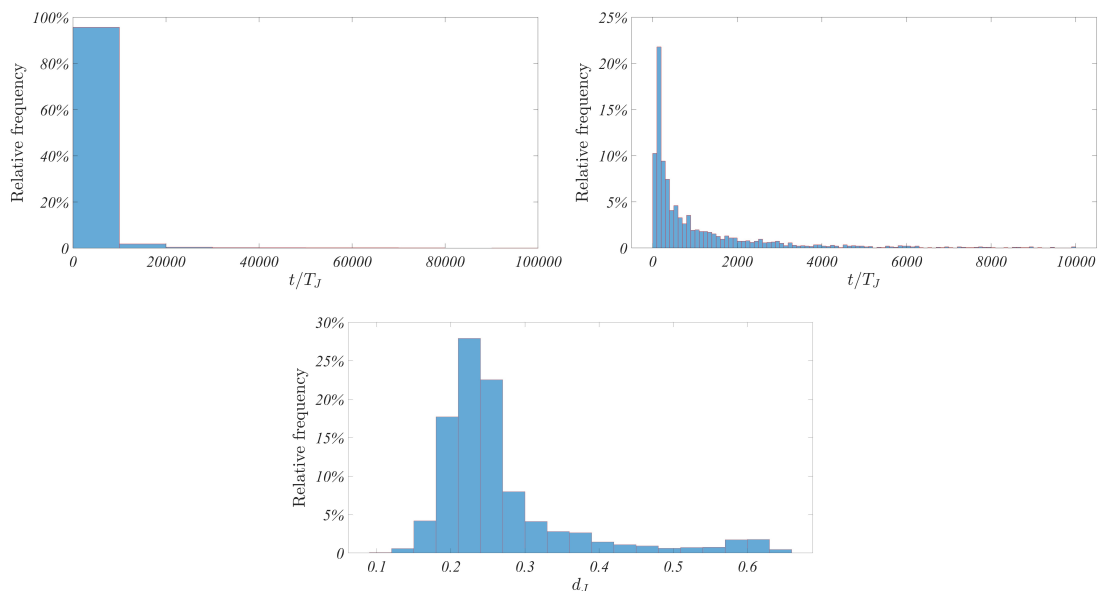


Figure 4.4: Histograms of the break-up times and corresponding distances for the binary plot in Fig. 4.2 (more refined grid of the two). **Top panels:** statistics of all break-up events t_{\min} (left) and of those happening before $10000T_J$ (right). **Bottom panel:** Relative frequency of $d_J(t_{\min})$.

within 10000 Jupiter's orbital periods and actually, from the right plot, within $4000T_J$, so of the order of 10^4 y. This hint suggests that the onset of chaos, for example due to close encounters, takes place rapidly and gives credit to the choice of $\tau = 1000T_J \approx 10^4$ y for the second proposed FLI cartography.

We complete the discussion with the bottom panel of Fig. 4.4: the average distance from the planet at which we record t_{\min} , that is the mean of $d_J(t_{\min})$, is about 0.26 (in physical units equal to $0.26a_J = 1.35$ AU) and almost all the trajectories lie in the range $[0.15, 0.4]$ (or $[0.78, 2.08]$ AU). Such finding confirms that instability can be experienced abruptly by an outer asteroid way before than Jupiter's Hill sphere, whose radius reads

$$\rho_{\text{Hill}_J} \approx a_J \sqrt[3]{\frac{\mu_J}{3}} = 0.361 \text{ AU} . \quad (4.13)$$

This, combined with the above observation, can lead groups of distant small objects to destabilize soon.

4.4 Semi-analytical determination of the domain of secular motions

4.4.1 Order and size of the optimal remainder in the planar CR3BP

As already stressed in §3.3.2, the computations in the planar CR3BP are short enough to allow for a specification of the optimal normalization order in the closed-form algorithm outlined in the previous chapter. Owing to the above, we are able to make normal form computations in a grid of points in the plane (a_*, e_*) up to a sufficiently high normalization order so that the asymptotic character of the series computed by the algorithm of Section 3.2 can show up. Fig. 4.5 shows an example of the behavior of the size of the remainder as a function of the number of normalization steps j . We introduce an estimate of the size of the series' remainder after j normalization steps via the upper norm bound

$$\mathcal{E}^{(j)} = \sum_{l=v+j}^{vk_\mu} \sum_{s \in \mathbb{Z}^3} |d_{l,s}^{(j)}| \geq \left\| \mathcal{R}_{v+j}^{(j)} \right\|_\infty , \quad j = 1, \dots, v(k_\mu - 1) , \quad (4.14)$$

where $\|\cdot\|_\infty$ denotes the sup norm. Plotting $\mathcal{E}^{(j)}$ against the number of normalization steps j allows then to estimate the error committed at any step (size of the remainder). Figure 4.5 yields examples of such computation for the experiments seen before. The relevant fact is that, looking at the top left panel of the figure, there is an optimal number of normalization steps ($j = j_{\text{opt}} = 6$) where the estimate $\mathcal{E}^{(j)}$ of the remainder size yields a global minimum.

Fig. 4.5 allows to gain some insight into the question of the dependence of the optimal number of normalization steps j_{opt} on the parameters (a_*, e_*) . The most relevant remark concerns the dependence of the behavior of the curve

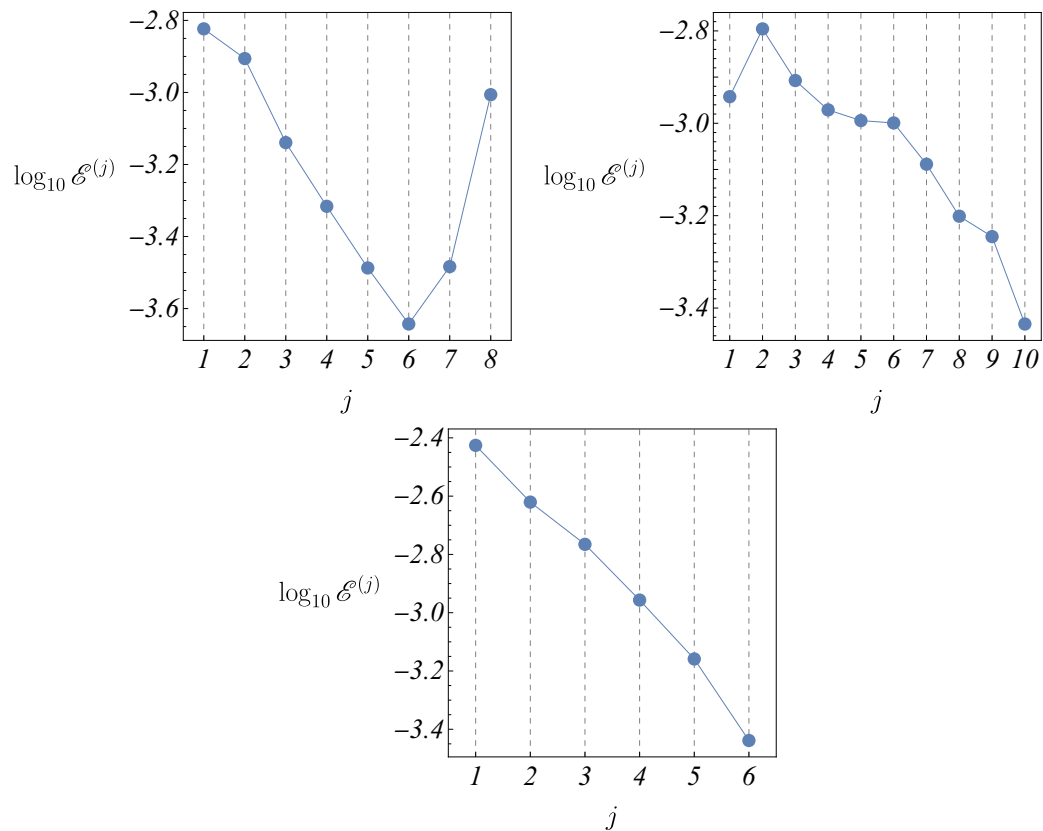


Figure 4.5: Trend of the size of the remainder for the three examples in the planar CR3BP of §3.3.2. **Top left panel:** example of Fig. 3.5. **Top right panel:** example of Fig. 3.6. **Bottom panel:** example of Fig. 3.7. The estimate $\mathcal{E}^{(j)}$ is depicted in semi-logarithmic scale for $1 \leq j \leq \nu(k_\mu - 1)$ accordingly to the data of each case.

$\mathcal{E}^{(j)}$ (versus j) on how close to the “hierarchical” regime the trajectory with reference values (a_*, e_*) is. As a measure of the hierarchical character of an orbit we adopt either the ratio of the semi-major axes a_1/a_* , or of the pericentric distances $\|r_1\|/\|R_p\| = a_1(1 - e_1)/(a_*(1 - e_*)) = a_1/(a_*(1 - e_*))$. Top right panel ($a_* = 30$ AU, $e_* = 0.5$) implies a pericentric distance ratio $\|r_1\|/\|R_p\| \approx 0.3$ smaller than the one of the example in the top left panel ($\|r_1\|/\|R_p\| \approx 0.4$). We observe that the optimal number of normalization steps in the former case satisfies $j_{opt} = 10$, i.e., it is larger than in the latter case. The bottom panel shows, instead, an example of orbit far from the hierarchical limit, satisfying the estimate $\|r_1\|/\|R_p\| \approx 0.7$. As seen before, in this case a higher order multipole ($k_{mp} = 5$) is required to obtain a precise truncated Hamiltonian model for this orbit. We note, however, that the normalization procedure performs well, producing a decreasing remainder as a function of j up to the point where it is arrested, i.e. $j = 6 = \nu(k_\mu - 1)$. We find numerically that this performance is deteriorated as we gradually approach the condition $\|r_1\|/\|R\| = 1$, beyond which the multipole expansion of the Hamiltonian is no longer convergent.

4.4.2 Semi-analytical determination of the domain of secular motions

The results shown in the previous subsection refer to isolated examples of orbits, with initial conditions in the deep blue regions of Fig. 4.1, or the corresponding regions in the domain of secular motion for values of a beyond the limits of Fig. 4.1, treated within various multipole truncation orders as well as different choices of the number of normalization steps, searching each time to arrive at the best approximating secular model given computational restrictions. In the present subsection, we aim to investigate the behavior of the remainder in a closed-form normalization with uniform choice of all truncation orders of the problem, but performed, instead, in a fine grid (100×20) of reference values in the plane (a_*, e_*) . To this end, we set $k_\mu = 2$ (second order in the mass parameter), and fix $k_{mp} = 3$ (octupole approximation). The latter choice, imposed by computational restrictions, yields an initial model whose error with respect to the full Hamiltonian becomes of the order of 1% only for $a_* > 2a_1$. However, for reasons explained below, a computation within the framework of the octupole approximation becomes relevant to the problem addressed in the sequel also in the range $1.5a_1 < a_* < 2a_1$, while higher multipoles are required to address still smaller values of a_* .

The result of the above computation is summarized in Fig. 4.6: the left panel shows in logarithmic color scale the size of the remainder, estimated by the value of $\mathcal{E}^{(n)}(a_*, e_*)$ computed as in (4.14), corresponding to each point in the plane (a_*, e_*) , where the number of normalization steps is set as $n = \min\{\nu(k_\mu - 1), 7\} = \min\{\nu, 7\}$. The maximum value $n = 7$ is, again, imposed by computational restrictions, and it implies that n varies with e_* up to about $e_* = 0.37$.

The relevant information in Fig. 4.6 is provided by the black curve, which corresponds to the iso-contour $\mathcal{E}^{(n)}(a_*, e_*) = 10^{-2}$. Since in the original Hamil-

tonian we have the estimate $\mathcal{E}^{(0)}(a, e) := \mathcal{H}_1^{k_\mu, k_{\text{mp}}} = \mathcal{O}(10^{-2})$ (equation (3.99)), the black curve provides a rough estimate of the limiting border dividing the plane (a_*, e_*) in two domains: in the one below the black curve the progressive elimination of the fast angles by the iterative normalization steps leads to a secular model whose remainder decreases with the number of normalization steps j at least up to $j = n$.

A physical interpretation of the border approximated through the iso-contour $\mathcal{E}^{(n)}(a_*, e_*) = 10^{-2}$ can be given through a comparison with a numerical stability map obtained, e.g. Fig. 4.1, as in the right panel of Fig. 4.6. As already observed according to the FLI color map, deep blue colors indicate the most regular orbits (termed lower regularity region), and light yellow the most chaotic ones. Superposed to the FLI cartography are three curves:

- (i) the perihelion crossing curve (red), that yields the locus of values satisfying the condition $a(1 - e) = \|r_J\| = a_J$ (circular case), that is the points where the pericenter of the test particle's orbit comes at distance equal to the radius of Jupiter's orbit;
- (ii) the Hill limit [87] described in §4.1 (brown) is based on the Jacobi constant relationship $C_J(a, e) = C_{J_{L_1}}$ written as function of the orbital elements, recalling that $C_{J_{L_1}}$ is its value at the Lagrangian point L_1 ;
- (iii) the iso-contour $\mathcal{E}^{(n)}(a, e) = 10^{-2}$ (black, same as in the left panel of Fig. 4.6).

Of the above three curves, the perihelion crossing curve is analogous, in the R3BP, of Laskar's Angular Momentum Deficit criterion (§4.1) used to separate systems protected from perihelia crossings in the case of the full planetary three-body problem. As indicated by the FLI cartography data, Hill's curve gives an overall better approximation separating the domain of strong chaos (yellow) from the domain of regular or weakly-chaotic orbits (all blue nuances). This is expected, since the Hill's curve separates orbits for which Jupiter's gravitational effect becomes (at least temporarily) dominant from those for which it does not. Nevertheless, through the FLI cartography we note the presence of a large domain between the curves (ii) and (iii), where the trajectories, while protected from close encounters, are subject to the long term effects on dynamics produced by resonant multiplets associated with the mean-motion resonances of the problem (the most important of which are marked in the figure). Note that in the octupole approximation, the Hamiltonian contains harmonics including all combinations of the fast angles of the form $\cos(s_1 f + s_2(g - M_1))$, with

$$\begin{aligned} (s_1, s_2) = & (1, 3), (2, 3), (3, 3), (4, 3), (5, 3), (6, 3), (7, 3), \\ & (1, 2), (2, 2), (3, 2), (4, 2), (5, 2), (1, 1), (2, 1), (3, 1), (4, 1), (5, 1), \\ & (1, -1), (2, -1), (3, -1), (1, -2), (1, -3), \end{aligned}$$

thus including all harmonics associated with the mean-motion resonances detected in the FLI cartography of Fig. 4.6 for $a > 1.5a_J$. Through the closed-form

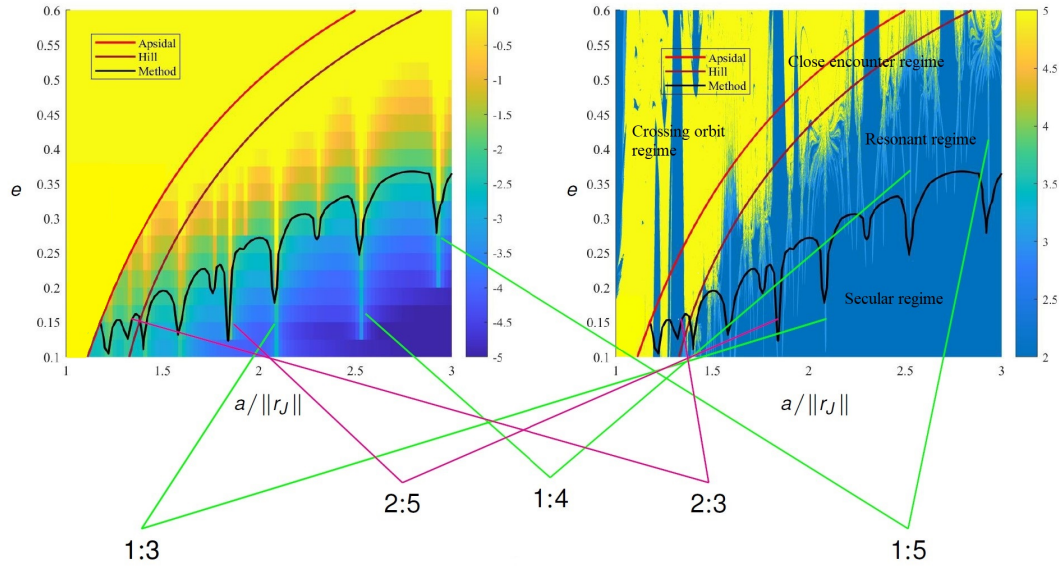


Figure 4.6: Size of the remainder vs. short-period FLI map for the Sun-Jupiter planar CR3BP in the semi-plane $a/a_J > 1$. **Left panel:** computation of $\log_{10} \mathcal{E}^{(n)}$, $n = \min\{\nu, 7\}$, $k_{\text{mp}} = 3$, over a 100×20 (a, e) grid. For every $e = e_*$, n different normalizations are executed and then evaluated for each $a = a_*$. **Right panel:** apocentric short-period ($50T_J$) FLI map (top panel of Fig. 4.1). As indicated, the three curves represent, respectively, the line of constant pericenter of the particle's trajectory equal to the radius of Jupiter's orbit $\|r_J\| = a_J$ (red), Hill's stability criterion (brown) and the iso-level $\mathcal{E}^{(n)} = 1\%$ (black). Each region enclosed by two consecutive above curves is labeled with the corresponding regime of motion. The main mean-motion resonances are reported below the pictures.

normalization (equations (3.69) and (3.84)) we then obtain small divisors in the series at every value of the semi-major axis a_* for which one of the resonant combinations $s_1 n_* - s_2 n_J$ ($n_J = 2\pi/T_J$) takes a value near zero. All these incidences lead to Arnold tongue-like spikes pointing downwards in the curve (iii), marking the failure of the approximation of the orbits based on a *non-resonant* normal form construction. On the other hand, we observe that, for any value of a_* there is a threshold value of the eccentricity $e_{*,s}$, such that, for $e_* < e_{*,s}$ no visible effects of the harmonics associated with mean-motion resonances are visible in the FLI cartography. This implies that the secular models constructed by eliminating all harmonics involving the fast angles of the problem describe with good precision the dynamics in this domain, which, for this reason, was called the *domain of secular motions*. In physical terms, the domain of secular motions corresponds to initial conditions for which the gravitational perturbation of Jupiter is only felt in the “Laplacian” meaning, i.e., as a mass distributed along a ring coinciding with Jupiter’s orbit. The curve (iii) then yields the limit of this domain, which, as found by the FLI cartography, is well distinct from the limit of the Hill domain.

The overall situation can therefore be summarized with the identification of four regimes of motion (specified in the FLI chart of Fig. 4.6):

- the *crossing orbit regime* (above curve (i));
- the *close encounter regime* (between curves (i) and (ii));
- the *resonant regime* (between curves (ii) and (iii));
- the *secular regime* (below curve (iii)).

MANIFOLDS IN THE SOLAR SYSTEM: AN APPLICATION TO THE L_4/L_5 ASYMMETRY OF TROJAN ASTEROIDS

We have already mentioned that, far from the domain of secular motions, the dynamics can be strongly influenced by the manifolds of unstable periodic orbits formed at one or more mean-motion resonances with the primary perturber. The present chapter deals with the exploration of the heteroclinic dynamics of the neighborhood of the short-term co-orbital resonance in the Sun-Jupiter system. We present ongoing results partly contained in [90].

5.1 On Trojan asteroids and the asymmetry problem

As introduced in §1.3.3, Jupiter's Trojans are a group of asteroids located in the vicinity of Jupiter's Lagrangian points L_4 and L_5 . Their tadpole orbits are relatively stable and in 1 : 1 mean-motion resonance with Jupiter and are characterized by an oscillation of the mean longitude difference $\lambda - \lambda_J$ (the label J stands for "Jupiter"). The Trojan swarms are divided into two groups: the Greeks, orbiting the L_4 point, and the genuine Trojans, orbiting L_5 . The first asteroid was spotted in 1906, later designated as (588) *Achilles* and was found orbiting L_5 . The same year a second body, (617) *Patroclus*, was found in L_5 . Since then, a continuous increasing number of asteroids have been discovered and, as instruments improved, the rate of discovery has grown rapidly: by November 2022 there are 7964 known Jupiter's Trojans at L_4 and 4226 at L_5 [14].

Two theories have been proposed about the origin of Trojans: one is based on the growing mass of Jupiter during the formation of the Solar System [65], while the other hypothesizes the capture of present Trojans in the planetary migration process that happens after the protoplanetary phase [70]. The former suffers from a lack of a satisfactory explanation for the very large orbital inclinations of some Trojans; the latter, based on the *Nice model* [35, 70, 103], solves the issue by successfully reproducing the distribution of observed Trojans by nu-

merical simulations. Recently, a modified Nice model with a “jumping Jupiter” was proposed [75] leading to further refinements of the previous theory.

As regards the size of the stability region of these bodies, analytic theories based on the analysis of the remainder of the corresponding constructed normal form are available. Stability of specific Trojans is then obtained by applying Nekhoroshev’s theorem [27, 33] or Kolmogorov’s normal form and KAM theory [31]. These studies show limitations as the smallness of the estimated stability region or simplicity of the model considered (typically the R3BP without for example Saturn’s perturbation).

Another approach is based on numerical analysis and is the one leading to a prolific literature, like [25, 59, 68, 88]. By integrating the equations of motion of the outer Solar System model or the Sun–Jupiter–Saturn system, these studies try to identify the boundary of the stability region within a fixed integration time, in a similar fashion to what proposed herein in Chapter 4.

A curious dynamical feature of Jovian Trojans is the observed *asymmetry* between the populations in L_4 and L_5 . Not only does the leading swarm have about 30–40% more asteroids than the trailing region, but there are also significant differences in the distribution of inclinations: while the physical properties are nearly identical (with some variations in size between the families of L_4 and the agglomerations of L_5), on average the L_4 region has objects slightly less inclined. A statistical graphic recap of these peculiarities is proposed in Fig. 5.1 taken from [97] (see references therein for further insights).

The birth of this asymmetry is still nowadays not completely clear and remains an open problem. Dynamical studies of the Trojan region show the same resonance structure and stability limits in both Lagrange points, even when considering the perturbations of additional planets [65, 88]. The Nice model itself predicts similar populations in both equilateral Lagrange points, so it seems that even under the most complex scenarios both L_4 and L_5 are dynamically equivalent. However, recently Hou et. al. in [46] have shown that a temporary asymmetry may be obtained with the same initial conditions in both tadpole regions, however such disparity is short-lived and cannot at present account for the observed inequality. Later on, the same authors have studied the problem including also the giant planets’ migration [47] and have discussed several mechanisms that can cause asymmetries. Their findings demonstrate that the crucial ones are the short time scale for the spatial asymmetry when Jupiter and Saturn are in resonance, the changing orbits of Jupiter and Saturn and the chaotic nature of Trojan orbits. Lastly, the thermal Yarkovsky effect is also found to be able to cause dynamical differences to the two swarms [102], but generally they are too small to be practically observed [46].

About observations, it is interesting to mention that historically the truthfulness of differences in numbers of bodies in the two groups was strongly questioned. The asymmetry was usually considered as due to observational selection effects before being officially confirmed. For more details, the interested reader can refer to [97] and references therein contained.

Following the aforementioned works, Trojans could have formed in distant regions and been subsequently captured into co-orbital motion with Jupiter

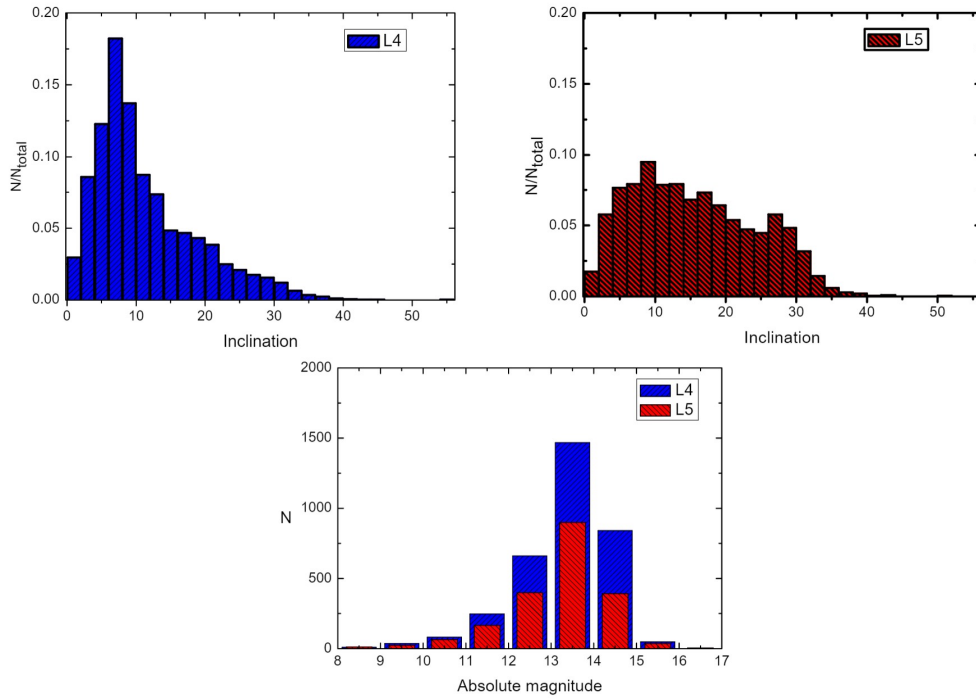


Figure 5.1: Distribution of Trojans and their inclinations in the L_4/L_5 swarms from [97]. **Top panel:** number of objects according to their observed absolute magnitude. **Bottom panels:** relative frequency for the inclination distributions.

during the time when the giant planets migrated by depleting neighboring planetesimals. The capture was possible during a short period of time, just after Jupiter and Saturn crossed their mutual 1 : 2 resonance, when the dynamics of the Trojan region was completely chaotic.

Adopting this scenario, we introduce another idea concerning the formation of the asymmetry by asking this simple question: could such asymmetry be manifold driven? If yes, to what extent? Starting with the non-migratory case, we consider the pair of sets

$$W_{L_4}^s(PL_3) \cap (W^u(PL_1) \cup W^u(PL_2)) \text{ vs. } W_{L_5}^s(PL_3) \cap (W^u(PL_1) \cup W^u(PL_2)) ,$$

where $W_{L_i}^s(PL_3)$ denotes the branch of $W^s(PL_3)$ surrounding the co-orbital L_i region for positive times, with $i = 4, 5$. We illustrate that these pairwise compared intersections are unevenly distributed in a suitable Poincaré section, both in terms of location and their cardinality. Moreover, we provide numerical experiments suggesting that particles from the outer region approach the 1 : 1 zone preferably through L_4 over L_5 . Finally, we pass to the time-varying case by injecting Jupiter's migration according to a simple exponential law. A direct computation shows that around L_4 and L_5 the non-autonomous resulting Hamiltonian is a non-increasing function in time. This can locally translate into a growth of the stability regions around the equilateral points, so that ultimately a small fraction of objects may have non-zero probability to be trapped inside newly generated invariant tori and, because of the dominance of L_4 , may trigger the asymmetry.

5.2 Heteroclinic dynamics at co-orbital resonance

5.2.1 On the computation of invariant manifolds

In Chapter 1 we have already listed the main concepts about hyperbolic dynamics and some interesting features in connection to the collinear points of the CR3BP. By means of Floquet's theory recalled in §1.1.3, we hereinafter stick to the 2 d.o.f. case and describe below the adopted iterative procedure to numerically identify periodic orbits stemming from L_i (PL_i , like the Lyapunov orbits depicted in Fig. 1.10), $i = 1, 2, 3$, as fixed points of a Poincaré map. Then, using the corresponding Floquet multipliers, we can easily propagate $W^s(PL_i)$, $W^u(PL_i)$.

Let us begin by specifying the reference Poincaré section Σ and map Ψ . Since the existence of the Jacobi integral constrains the Cartesian synodic flow $(x(t), y(t), p_x(t), p_y(t))$ to belong to a three-dimensional hypersurface in the phase space, we can determine a two-dimensional subset $\Sigma^2 \subset \mathbb{R}^4$ by imposing one more constraint. A straightforward possibility consists in considering a pericentric section, i.e. a point on Σ satisfies $M = 0$ (for orbits of instantaneous elliptic character). We are left with the parametrization of the surface of section, that shall be taken as a coordinate plane whose abscissa and ordinate are played by a pair of canonical variables for an accurate inspection of the dynamics. We are definitely interested in the evolution of the angle $\lambda - \lambda_J = \ell + g - \ell_J$ (by (1.62), (3.3)), which on Σ simply reads $g - \ell_J$. So, in the inertial frame $OXYZ$, we define a canonical transformation using a generating function of the second kind (ending part of §1.2.3)

$$F(\ell, g, \ell_J, I_1, I_2, I_3) = (g - \ell_J)I_1 + \ell I_2 + \ell_J I_3 \quad (5.1)$$

so that

$$\begin{aligned} \varphi_1 &= \frac{\partial F}{\partial I_1} = g - \ell_J, & G &= \frac{\partial F}{\partial g} = I_1, \\ \varphi_2 &= \frac{\partial F}{\partial I_2} = \ell, & L &= \frac{\partial F}{\partial \ell} = I_2, \\ \varphi_3 &= \frac{\partial F}{\partial I_3} = \ell_J, & I_J &= \frac{\partial F}{\partial \ell_J} = I_3 - I_1, \end{aligned} \quad (5.2)$$

which allows us to pass from Delaunay coordinates $(\ell, g, \ell_J, L, G, I_J)$, where I_J is the dummy action conjugated to Jupiter's anomaly $\ell_J = M_J = t$ (units according to $n_J = a_J = 1$), to $(\varphi_1, \varphi_2, \varphi_3, I_1, I_2, I_3)$ by trivial inversion of the expressions pertaining the actions.

The Jacobi integral (1.76) in the planar case becomes, in terms of the variables

(5.2), a function $E_J(\varphi_1, \varphi_2, I_1, I_2)$ and on the section Σ it takes the form

$$E_J|_{\Sigma} = \frac{I_1^2}{2\varrho_p^2} - I_1 - \frac{1 - \mu_J}{\sqrt{(\varrho_p \cos \varphi_1 + \mu_J)^2 + \varrho_p^2 \sin^2 \varphi_1}} - \frac{\mu_J}{\sqrt{(\varrho_p \cos \varphi_1 - 1 + \mu_J)^2 + \varrho_p^2 \sin^2 \varphi_1}}, \quad (5.3)$$

where $\varrho_p(I_1, I_2) = a(1 - e)$ is the radius of perihelion and μ_J is numerically given by (4.9). Notice that neither f nor $\dot{\varrho}$, with $\varrho = \|(x, y)\|$, shows up in (5.3) being vanishing on Σ .

Hence, for a fixed value $\bar{E}_J \in \mathbb{R}$ of (5.3),

$$\Sigma = \{(\varphi_1, \varphi_2, I_1, I_2): \varphi_1 \in \mathbb{T}, I_1 > 0, \varphi_2 = 0, E_J(\varphi_1, \varphi_2, I_1, I_2) = \bar{E}_J\}, \quad (5.4)$$

with associated map $\Psi: \Sigma \rightarrow \Sigma$ such that the flow crosses Σ transversely “on the same side” (§1.1.3).

Remark 5.2.1. The equation involving E_J in (5.4) to be solved for I_2 admits a unique acceptable solution (e.g. with $e < 1$).

In practice, the return map Ψ is established as follows.

- (i) Given \bar{E}_J , we pick an initial condition $(\varphi_1(0), \varphi_2(0), I_1(0), I_2(0)) \in \Sigma$, relate it to orbital elements $a(0), e(0), \omega(0), f(0) = 0$ via (3.3), convert them to $(X(0), Y(0), \dot{X}(0), \dot{Y}(0)) = (x(0), y(0), p_x(0), p_y(0))$ by (1.59) and linked formulae.
- (ii) We propagate the orbit by integrating the Cartesian vector field generated by the 2D version of (1.74) until it returns on Σ . To ensure the appropriateness of the crossing, we choose the criterion of the radial velocity at the perihelion passage, namely we determine $\varrho\dot{\varrho} = xp_x + yp_y$ throughout the numerical integration and every time such quantity changes in sign from a negative to a positive value forward in time (conversely from a positive to a negative value backward in time), we record a section crossing. Then we refine the step size and localize the intersection $(x(t^*), y(t^*), p_x(t^*), p_y(t^*))$ on Σ in such a way that $\dot{\varrho}(t^*) = 0$. Notice that this method permits to discard aphelion passages and really hit Σ from the same direction; variants, like just marking any change in sign coupled with $\ddot{\varrho}(t^*) > 0$ ($\varrho(t_*) = \varrho_p$), would create issues especially in the vicinity of Jupiter or in case of time reversal.
- (iii) By rotating $(x(t^*), y(t^*), p_x(t^*), p_y(t^*))$ of $\ell_J(t^*) = t^*$ to obtain $(X(t^*), Y(t^*), \dot{X}(t^*), \dot{Y}(t^*))$ and back-transforming to corresponding orbital elements, we calculate $(\varphi_1(t^*), \varphi_2(t^*), I_1(t^*), I_2(t^*)) \in \Sigma$ from (5.2).

Examples of Poincaré sections constructed as above are reported in Fig. 5.2 (details in the caption).

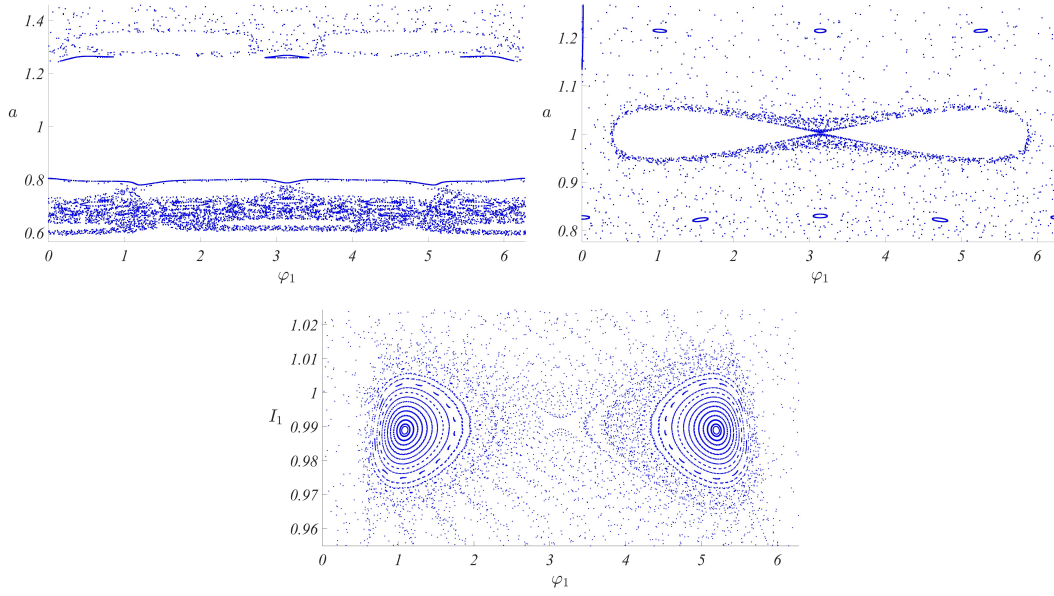


Figure 5.2: Poincaré sections Σ of the Sun-Jupiter planar CR3BP for increasing \bar{E}_J . The plots represent consecutive iterations of Ψ over a total integration time of $1000T_J$ ($T_J = 2\pi$). **Top left panel:** $\bar{E}_J = \bar{E}_{J_{L_1}}$. **Top right panel:** $\bar{E}_J = \bar{E}_{J_{L_3}}$. In both panels we use $a = I_2^2/(1 - \mu_J)$ in place of I_1 to have an approximate distance measure of the width of the forbidden region $\mathbb{R}^2 \setminus \mathcal{A}(\bar{E}_J)$ located in the center of the diagrams (see §1.3.3, Fig. 1.9). On the right, we can recognize the birth of the Lagrangian point L_3 exactly on the cusp of the eight-shaped curve. **Bottom panel:** (φ_1, I_1) section for $\bar{E}_J = -1.49 > \bar{E}_{J_{L_4}}$ (the motion is permitted everywhere on Σ).

We can now readily find the fixed points of Ψ , i.e. the periodic orbits of period equal to the return time to Σ . Nevertheless, we may be interested in finding periodic orbits associated with longer periods, say corresponding to two or more returns on Σ , but this does not alter the general argument that follows upon a simple redefinition of the Poincaré map as Ψ^n , $|n| \geq 2$, like (1.2). This, for instance, will be the case of PL_1, PL_2 with $n = 2$ for high values of \bar{E}_J and in proximity of the planet (with possible intervention of the regularization). We want to solve $(\bar{\varphi}_1, 0, \bar{I}_1, I_2(\bar{E}_J)) = \Psi(\bar{\varphi}_1, 0, \bar{I}_1, I_2(\bar{E}_J))$, i.e.

$$\begin{cases} \bar{\varphi}_1 = \Psi_1(\bar{\varphi}_1, \bar{I}_1) \\ \bar{I}_1 = \Psi_3(\bar{\varphi}_1, \bar{I}_1) \end{cases}, \quad (5.5)$$

$\Psi = (\Psi_1, 0, \Psi_3, I_2(\bar{E}_J))$. Define $F_1(\varphi_1, I_1) := \Psi_1(\varphi_1, I_1) - \varphi_1$, $F_2(\varphi_1, I_1) := \Psi_3(\varphi_1, I_1) - I_1$. The problem turns into looking for the zeroes of $F = (F_1, F_2)$. By means of a multivariate Newton-Raphson's method, starting with a "good"¹

¹Technically, in the basin of attraction of the targeted fixed point and away from the critical points of F . See the beginning of §5.2.2 for a couple of strategies on the identification of a successful initial guess in a concrete case.

seed $(\varphi_1^{(0)}, I_1^{(0)})$ the algorithm reads

$$\begin{pmatrix} \varphi_1^{(k+1)} \\ I_1^{(k+1)} \end{pmatrix} = \begin{pmatrix} \varphi_1^{(k)} \\ I_1^{(k)} \end{pmatrix} - \begin{pmatrix} \frac{\partial F_1}{\partial \varphi_1}(\varphi_1^{(k)}, I_1^{(k)}) & \frac{\partial F_1}{\partial I_1}(\varphi_1^{(k)}, I_1^{(k)}) \\ \frac{\partial F_2}{\partial \varphi_1}(\varphi_1^{(k)}, I_1^{(k)}) & \frac{\partial F_2}{\partial I_1}(\varphi_1^{(k)}, I_1^{(k)}) \end{pmatrix}^{-1} \begin{pmatrix} F_1(\varphi_1^{(k)}, I_1^{(k)}) \\ F_2(\varphi_1^{(k)}, I_1^{(k)}) \end{pmatrix}, \quad (5.6)$$

which has to be iterated for $k \geq 1$ until the convergence is reached (typically based on a desired tolerance on the residual). Note that, by Remark 1.2.3, the Jacobian matrix $D(\Psi_1, \Psi_3)(\varphi_1^{(k)}, I_1^{(k)})$ computed at every iterative step is symplectic (determinant equal to 1). As regards the computation of partial derivatives of F_1, F_2 , we rely on a central discrete finite difference approximation:

$$\frac{F_1(\varphi_1 + h, I_1) - F_1(\varphi_1 - h, I_1)}{2h} = \frac{\partial F_1}{\partial \varphi_1}(\varphi_1, I_1) + \mathcal{O}(h^2) \quad (5.7)$$

and analogously for the rest. The error committed depends on the small increment $h > 0$ (opportunistically tuned as explained in Remark 5.2.2).

Finally, once we have reached $(\bar{\varphi}_1, \bar{I}_1)$, we compute the eigenvalues of the linearization $D\Psi(\bar{\varphi}_1, 0, \bar{I}_1, I_2(\bar{E}_j))$ and, thanks to Proposition 1.1.2, we immediately have the Floquet multipliers of the monodromy matrix associated to the periodic orbit. For equilibrium points (or periodic orbits stemming from them) of hyperbolic character (like the collinear Lagrangian points, see §1.3.3) we then have the expanding/contracting direction on the plane (φ_1, I_1) along which we can propagate the stable/unstable corresponding invariant manifolds. By Theorem 1.1.3, we commence with a linear approximation of the manifolds near the equilibrium point and subsequently iterate the Poincaré map to produce their global structure on Σ .

Remark 5.2.2. In practical computations, we select h in order to minimize the bound of the quadratic error out of the Taylor expansion in (5.7) coupled with the round-off coming from working with a finite precision arithmetic. This is a standard approach in numerical analysis. Assume h is an infinite precision real number. Denote by $\tilde{\mathcal{F}}$ the floating point representation of a quantity \mathcal{F} with machine precision ϵ , namely $\tilde{\mathcal{F}} = \mathcal{F}(1 + \delta_{\mathcal{F}})$, with $|\delta_{\mathcal{F}}| \leq \epsilon$. Setting the left-hand side of (5.7) equal to $\tilde{\mathcal{F}}$, we have

$$|\mathcal{F} - \tilde{\mathcal{F}}| = \left| \frac{F_1(\varphi_1 - h, I_1)\delta_{F_1(\varphi_1-h, I_1)} - F_1(\varphi_1 + h, I_1)\delta_{F_1(\varphi_1+h, I_1)}}{2h} \right| \leq \frac{C\epsilon}{h},$$

with $C := \max_{\phi \in [\varphi_1-h, \varphi_1+h]} F_1(\phi, I_1)$. Therefore we can estimate the total error as

$$\left| \frac{\partial F_1}{\partial \varphi_1} - \tilde{\mathcal{F}} \right| = \left| \frac{\partial F_1}{\partial \varphi_1} - \mathcal{F} + \mathcal{F} - \tilde{\mathcal{F}} \right| \leq C'h^2 + \frac{C\epsilon}{h}, \quad (5.8)$$

in which C' is another constant related to $\partial^3 F_1 / \partial \varphi_1^3$ coming from the truncation error. The optimal h_{\min} is found as the solution of

$$\frac{d}{dh} \left(C'h^2 + \frac{C\epsilon}{h} \right) = 0,$$

that is $h_{\min} \approx \sqrt[3]{\epsilon}$. For double precision calculations $\epsilon \sim 10^{-16}$, thus $h_{\min} \sim 10^{-5}$.

5.2.2 The stable manifold of PL_3

For the motives stated at the end of §5.1, it is worth investigating the geometric features of $W^s(PL_3) \cap \Sigma$. We accomplish so by implementing the procedure exposed in the previous subsection, and also using the FLI method discussed in Chapter 4. We also complement the figures with a representation of $W^s(PL_3)$ overlapped to the pericentric short-period FLI cartography on the (a, e) plane reported in Fig. 4.1 (bottom panel).

For a given $\bar{E}_J \gtrsim \bar{E}_{J_{L_3}}$, the seed $(\varphi_1^{(0)}, I_1^{(0)})$ for (5.6) is computed using standard techniques for partially hyperbolic Lagrangian points:

- As already seen, taking advantage of the existence of Lyapunov orbits for continuous values in a small right neighborhood of $\bar{E}_{J_{L_3}}$, we start with the equilibrium point L_3 (which lies on Σ , cf. Fig. 5.2) and use the datum as initial guess for the algorithm when the energy is slightly increased, say $\bar{E}_{J_{L_3}} + \delta$, $\delta \approx 10^{-4}$. We repeat the reasoning up to \bar{E}_J , possibly tuning δ in order to achieve convergence every time.
- Especially when the above process is not accurate enough to keep going on, we perform the linearization around the last candidate we have found. We reduce ourselves to the center space, calculate the initial conditions for the linearized orbit and use them as new seed for the algorithm in the non-linear problem. Such conditions produce an orbit close enough to PL_3 , but we can even further refine our guess with the aid of the shooting method for boundary value problems to improve its closeness and resume with the iterations.
- Having managed to get a pair of fixed points corresponding to two values of the Jacobi integral, we can pass to the recursion for the next increment $\bar{E}_J + \delta$ using as guess the extrapolation from the previous computed values $(\bar{\varphi}_1, \bar{I}_1)$ for lower energies. In this way we build up the *characteristic curves* $\bar{\varphi}_1 = \bar{\varphi}_1(\bar{E}_J)$, $\bar{I}_1 = \bar{I}_1(\bar{E}_J)$. An example of such functions is shown in Fig. 5.3.

In Fig. 5.4 (top panels) we can appreciate the complexity of the manifold as it approaches the fixed point. The repeated folds and lobes (the so-called *homoclinic tangle*) are a consequence of Proposition 1.2.1 for Hamiltonian systems, besides the fact that the manifold spreads throughout the phase space without self-intersections (see §1.1.4). In the FLI chart we can also retrieve more information on the global structure of W^s , as well as regarding other regimes of motion, e.g. the domain of quasi-satellite objects, in deep blue on the left side (and right side by periodicity) of the plot.

Let us consider now the points of $W^s(PL_3) \cap \Sigma$ computed as above for several values of \bar{E}_J . We retain those points belonging also to the pericentric (a, e) section in the orbital elements' space of Chapter 4 (which are also characterized

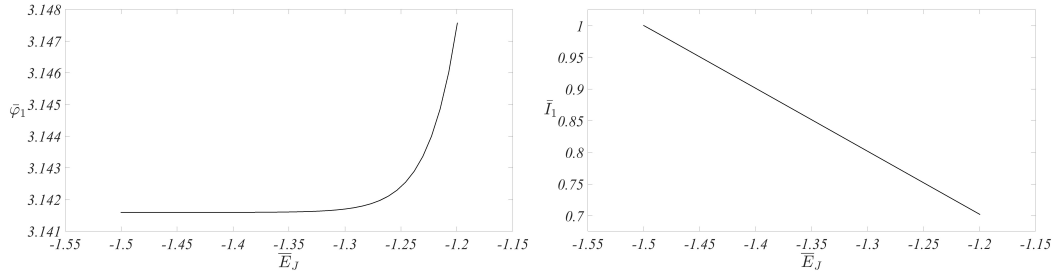


Figure 5.3: Characteristic curves of PL_3 as functions of the Jacobi integral. Here $\bar{E}_J \in [-1.5003768, -1.1995236]$, with $-1.5003768 \gtrsim \bar{E}_{J_{L_3}}$. **Left panel:** $\bar{\varphi}_1(\bar{E}_J)$. **Right panel:** $\bar{I}_1(\bar{E}_J)$.

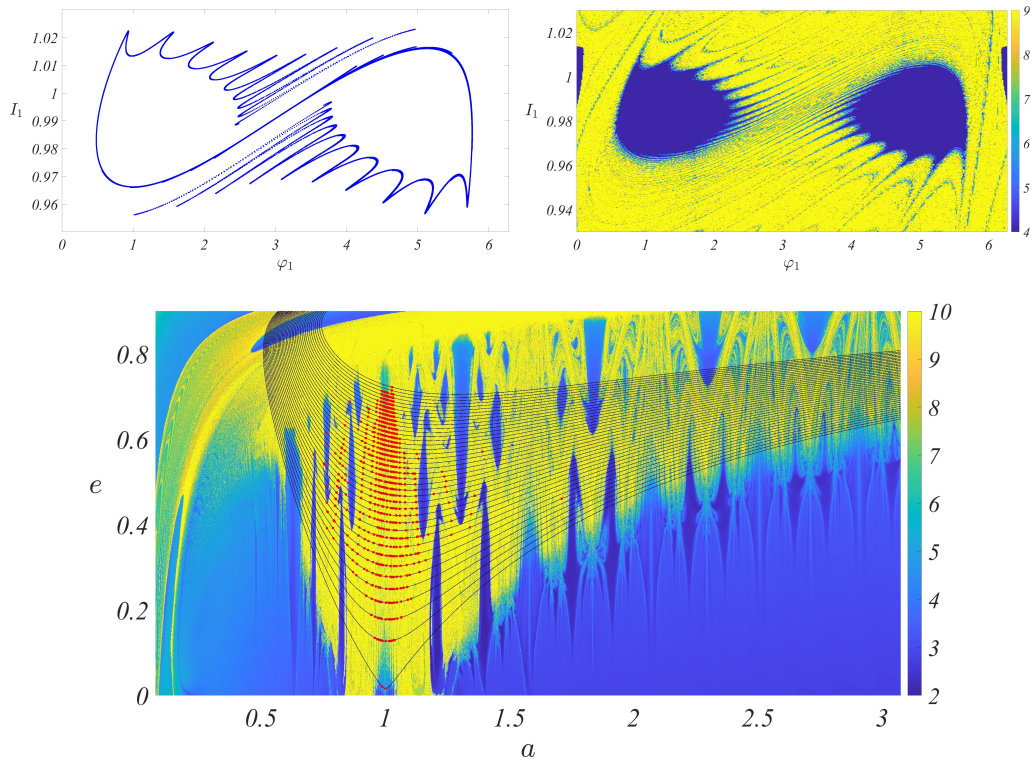


Figure 5.4: Representations of $W^s(PL_3)$ in the Sun-Jupiter-asteroid system on the (φ_1, I_1) and (a, e) planes. **Top left panel:** $\bar{E}_J = -1.4926626$, $|n| = 14$ (backward) iterations of the Poincaré map Ψ . **Top right panel:** short-time FLI map (integration time $t = 50T_J$) over a 500×500 $(\varphi_1(0), I_1(0))$ grid of initial conditions for $\bar{E}_J = -1.4849484$. **Bottom panel:** points of $W^s(PL_3)$ (red dots) for 40 values of \bar{E}_J in the same range of Fig. 5.3 (black thin iso-lines) lying on the pericentric FLI cartography of bottom panel of Fig. 4.1.

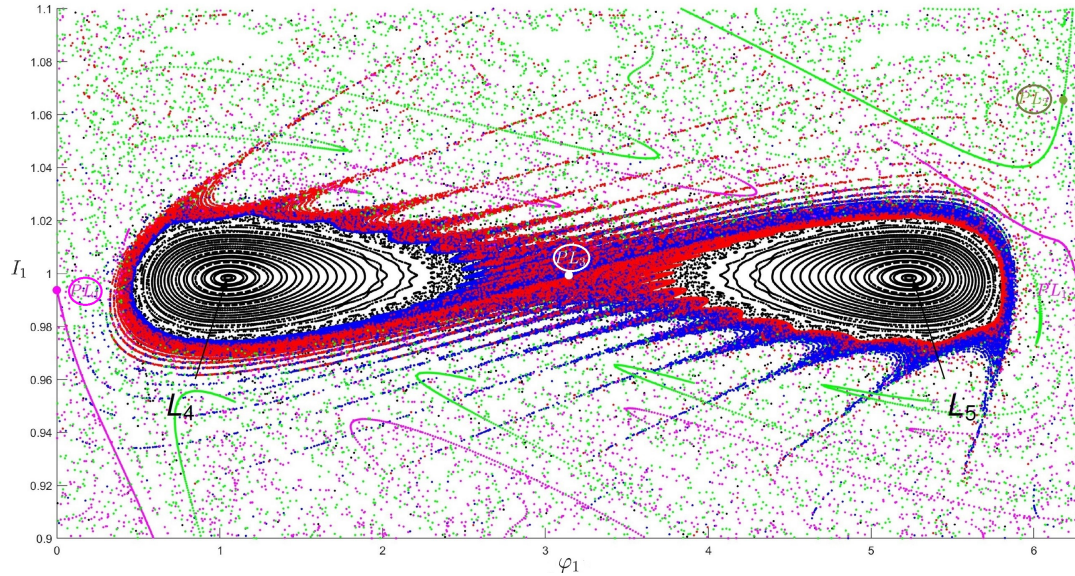


Figure 5.5: Poincaré section Σ of the heteroclinic connections between $W^s(PL_3)$ and $W^u(PL_1), W^u(PL_2)$ in the surroundings of L_4/L_5 for $\bar{E}_J = -1.4989 > \bar{E}_{J_{L_4}}$. Color code: blue for $W^s_{L_4}(PL_3)$, red for $W^s_{L_5}(PL_3)$, magenta for $W^u(PL_1)$, green for $W^u(PL_2)$ and corresponding dotted periodic orbits (except PL_3 in white), with circled labels. The black curves represent the local phase portrait around the equilateral Lagrangian points.

by $g(0) = \pi$). The result emerges in the bottom panel of Fig. 5.4: the points are placed on the level curves $E_J = \bar{E}_J$ and some of them tend to vaguely distribute along the “arches of chaos” mentioned in §4.3. Such evidence leads us to infer that these structures are actually due to the interplay of many invariant sets (the stable manifolds of several unstable periodic orbits, including $W^s(PL_3)$) that can dynamically communicate in a non-trivial manner throughout the Solar System. With this in hand, we discuss relevant heteroclinic points of $W^s(PL_3)$ in relation to Trojan dynamics.

5.2.3 The asymmetric distribution of heteroclinic intersections

If we keep iterating the Poincaré map producing $W^s(PL_3)$, the lobes of the manifold arrive at a particular configuration consisting in *rays* associated to high-order resonances (Fig. 5.5). The rays are subject to intersect unstable manifolds of other unstable periodic orbits, like the prominent ones $W^u(PL_1), W^u(PL_2)$. The collocation and number of these connections on Σ close to PL_3 govern the heteroclinic dynamics nearby the co-orbital L_4/L_5 regions.

Referring to Fig. 5.5, we discern two opposite subsets denoted by $W^s_{L_4}(PL_3), W^s_{L_5}(PL_3) \subset W^s(PL_3)$ s.t. $W^s_{L_4}|_{\Sigma}$ and $W^s_{L_5}(PL_3)|_{\Sigma}$ meet at $(\bar{\varphi}_{1_{PL_3}}, \bar{I}_{1_{PL_3}})$ and their local counterparts $W^s_{L_4,loc}, W^s_{L_5,loc}$ extend towards respectively L_4, L_5 for backward times (blue and red dots in the figure). The key observation is the following: the visible intersections between $W^s_{L_4}$ (blue rays in the lower part) and $W^u(PL_1) \cup W^u(PL_2)$ (“interrupted” magenta and green lines) are asym-

metrically positioned when compared to the intersections between $W_{L_5}^s$ (red rays in the upper part) and $W^u(PL_1) \cup W^u(PL_2)$. This behavior affects the respective number of such connections too and persists independently on $\bar{E}_J > \bar{E}_{J_{L_4}}$.

We now examine whether manifold-driven particles coming far from Jupiter (say along $W^u(PL_2)$) have different probability of being transported around the L_4 1 : 1 region rather than L_5 , due to the above mentioned asymmetric web of heteroclinic connections with $W^s(PL_3)$.

Figure 5.6-5.7 show the stable invariant manifolds $W^s(PL_3)$ for \bar{E}_J larger than in Fig 5.5. Looking at the topmost left panel of Fig. 5.6, we already note that for higher values of the Jacobi integral

- the $W^s(PL_3)$ rays arise earlier in the propagation (for instance the points of $W_{L_4}^s$ in blue remain in the upper part of the coordinate plane during the whole propagation stopped at time $\approx 14T_J$);
- the areas corresponding to the co-orbital resonance shrink together with a slight downward displacement (recognizable on the I_1 axis);
- other stability islands composed by invariant tori appear. This helps in excluding uninteresting parts of Σ to the manifold-guided initial conditions to run.

Passing to the right panel, at time $t = 0$ we consider a small neighborhood of initial conditions $\mathcal{D} \subset \Sigma$ centered at $(\bar{\varphi}_{1_{PL_2}}, \bar{I}_{1_{PL_2}})$ (green square). Then we produce the images $\Psi^t(\mathcal{D})$ for integers $t = 1, \dots, 100$, leading to the subsequent plots of Fig. 5.6 continuing in Fig. 5.7 obtained for the number of iterations t indicated. Initially, \mathcal{D} stretches approximately following $W^u(PL_2)$ (diagrams for $t = 2, 5, 10$), then tend to distribute evenly outside the stable islands (diagrams for $t = 15, 20$) until they escape (diagrams for $t = 50, 100$). For each section, we report on the right the statistics of the current objects entering pre-assigned ellipses (cyan colored) centered at L_4, L_5 and enclosing the corresponding local phase portrait. Remarkably, at the beginning L_4 entirely dominates over L_5 , in the sense that out of the total number of particles approaching the two circled regions, the flow transfers particles only inside the one of L_4 before starting to equalize the distributions for longer times.

We now refine the choice of initial conditions to make the above experiments more meaningful, as a scenario of particles coming from *outside* the co-orbital resonance, in order to mimic a temporary trapping of the Trojan particles to the L_4/L_5 regions. To this end, instead of taking \mathcal{D} directly on Σ , we consider orbits with initial conditions far from Jupiter, taken *transverse to the stable tube manifold* of the Lyapunov orbit PL_2 . Such particles reach the L_2 *bottleneck* in the positive sense of time, and then can approach the L_4/L_5 neighborhood and remain there for finite times.

Specifically, we carry out these two steps:

- (i) exploiting its intrinsic instability, we backward integrate the PL_2 orbit up to $10T_J$ (≈ 100 y), time at which more or less the semi-major axis stabilizes (up to 8-10 AU);

- (ii) we extract 10000 initial data transverse and sufficiently close to $W^s(PL_2)$ in Cartesian variables as $x_{PL_2}(-10T_J) + \varepsilon$, $y_{PL_2}(-10T_J)$, $p_{x_{PL_2}}(-10T_J)$ by varying $\varepsilon \in [-10^{-3}, 10^{-3}]$ plus $p_{y_{PL_2}}(-10T_J)$ given by the constraint $E_J = \bar{E}_J$.

If we re-perform now the Poincaré map iterations, the situation does not substantially change (Fig. 5.8): the dominance of L_4 for the transported bodies establishes at $t = 7$, slightly delayed with respect to the set \mathcal{D} .

It is worth mentioning the short time scale needed for these objects to visit the portion of Σ at interest before escaping: roughly of the order of 1000 y (since on average the sample orbits take one Jupiter's period to return to Σ , that is ~ 10 y in physical units).

5.3 Non-stationary case: Jupiter's migration

The short time span, the prevailing character of L_4 as opposed to L_5 , as the entry point of temporary captures, and, finally, the enlargement of the L_4/L_5 zones as \bar{E}_J decreases are the three key ingredients for the formulation of a possible asymmetric trapping mechanism discussed in the present section.

We have seen that orbits with initial conditions in the proximity of (albeit not exactly on) the stable tube manifold of PL_2 can be rapidly transferred from a region far from Jupiter (e.g. intersecting the orbit of Saturn) all the way through the L_2 bottleneck, eventually reaching one of the domains around L_4 or L_5 through the tube manifolds of the point L_3 . We have seen also that the entry probability is not symmetric as regards L_4 and L_5 . We now examine the consequences of assuming, in addition to the above, that during the phase of inflow of particles to the Trojan region Jupiter simultaneously *migrates* (as e.g. in the Nice model, see Fig. 5.9 (schematic)).

5.3.1 Extension of the model

A natural adjustment to the Hamiltonian (1.74) to take into account the migratory motion, consists in passing to physical units and working with a time-dependent planar CR3BP in which we insert a law $a_J = a_J(t)$ mimicking the migration phase. For the purposes of the present study, we adopt a simple model for the migration law (see, e.g., [47]):

$$a_J(t) = a_{J,0} e^{-t/T}, \quad t \in [0, t_{\text{mig}}], \quad (5.9)$$

with $a_{J,0} > a_J(t_{\text{mig}})$ the initial value determined on the basis of, say, the present semi-major axis $a_J(t_{\text{mig}})$ (= 5.2044 AU) and the migration rate time T .

We then consider the Hamiltonian

$$\mathcal{H}_{\text{mig}}(x, y, p_x, p_y, t) = \frac{p_x^2 + p_y^2}{2} - n_J(t)(xp_y - yp_x) - \frac{\mathcal{G}m_\odot}{\sqrt{(x + \mu_J a_J(t))^2 + y^2}} - \frac{\mathcal{G}m_J}{\sqrt{(x - (1 - \mu_J) a_J(t))^2 + y^2}}, \quad (5.10)$$

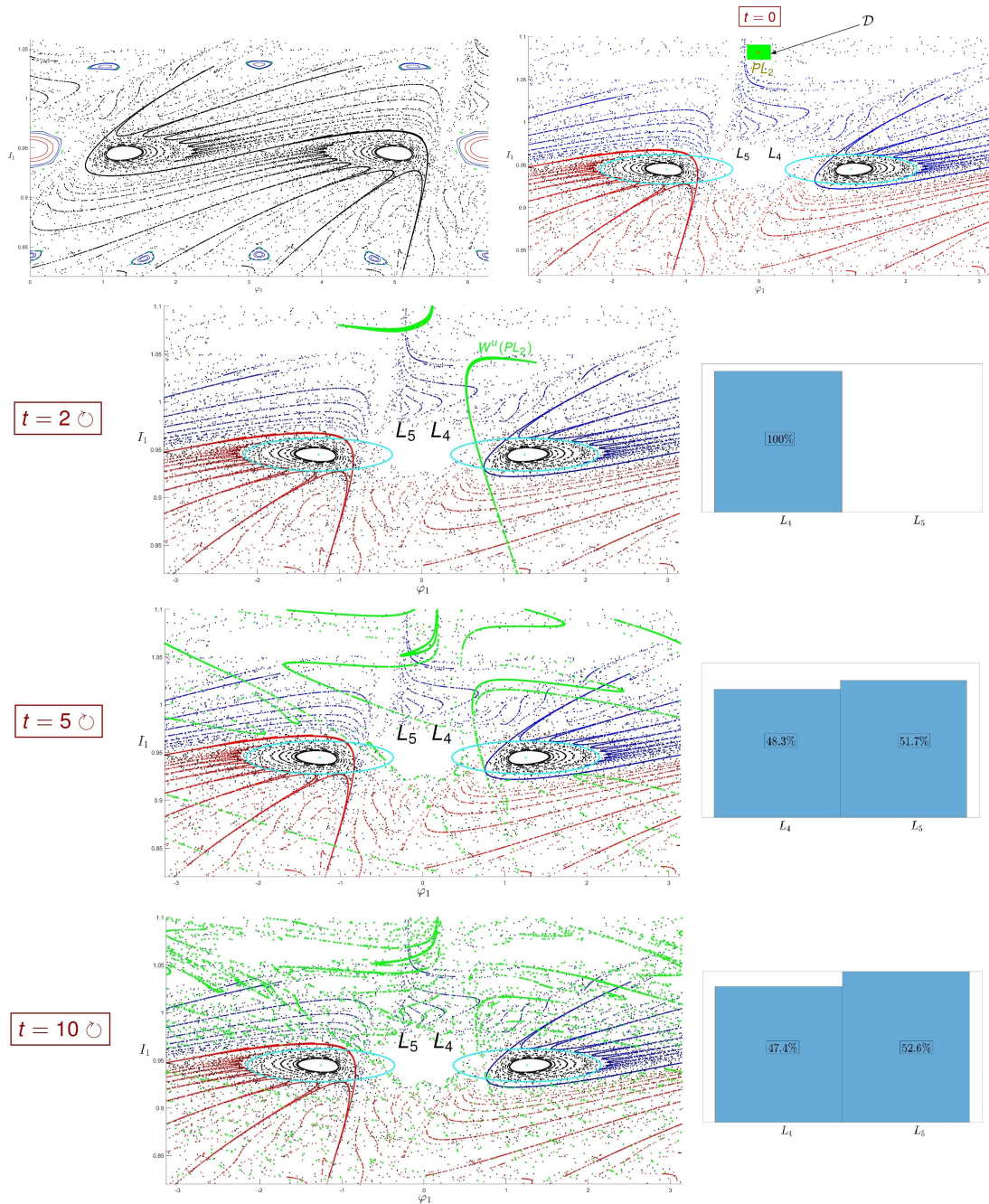


Figure 5.6: Poincaré map iterations of a neighborhood of PL_2 (green dots) for $\bar{E}_J = -1.4464$ (larger than the value of Fig. 5.5). For visual clarity, the diagrams are shifted by $-\pi$ in the angular coordinate ($\varphi_1 \in [-\pi, \pi]$). **Topmost left panel:** Manifold rays and stability islands. **Topmost right panel:** initial square-shaped neighborhood \mathcal{D} of PL_2 (discretized as 300×300 sample points) and L_4/L_5 reference ellipses. **Aligned bottom panels:** Evolution of $\Psi^t(\mathcal{D})$ for the alongside specified number of returns t (symbol \cup) together with the corresponding percentage histogram (on the right) representing $N_{L_4}/(N_{L_4} + N_{L_5})$ and $N_{L_5}/(N_{L_4} + N_{L_5})$; N_{L_i} , $i = 4, 5$, being the counted number of points inside the L_i ellipse at the present iteration. The sequence of images continues in Fig. 5.7.

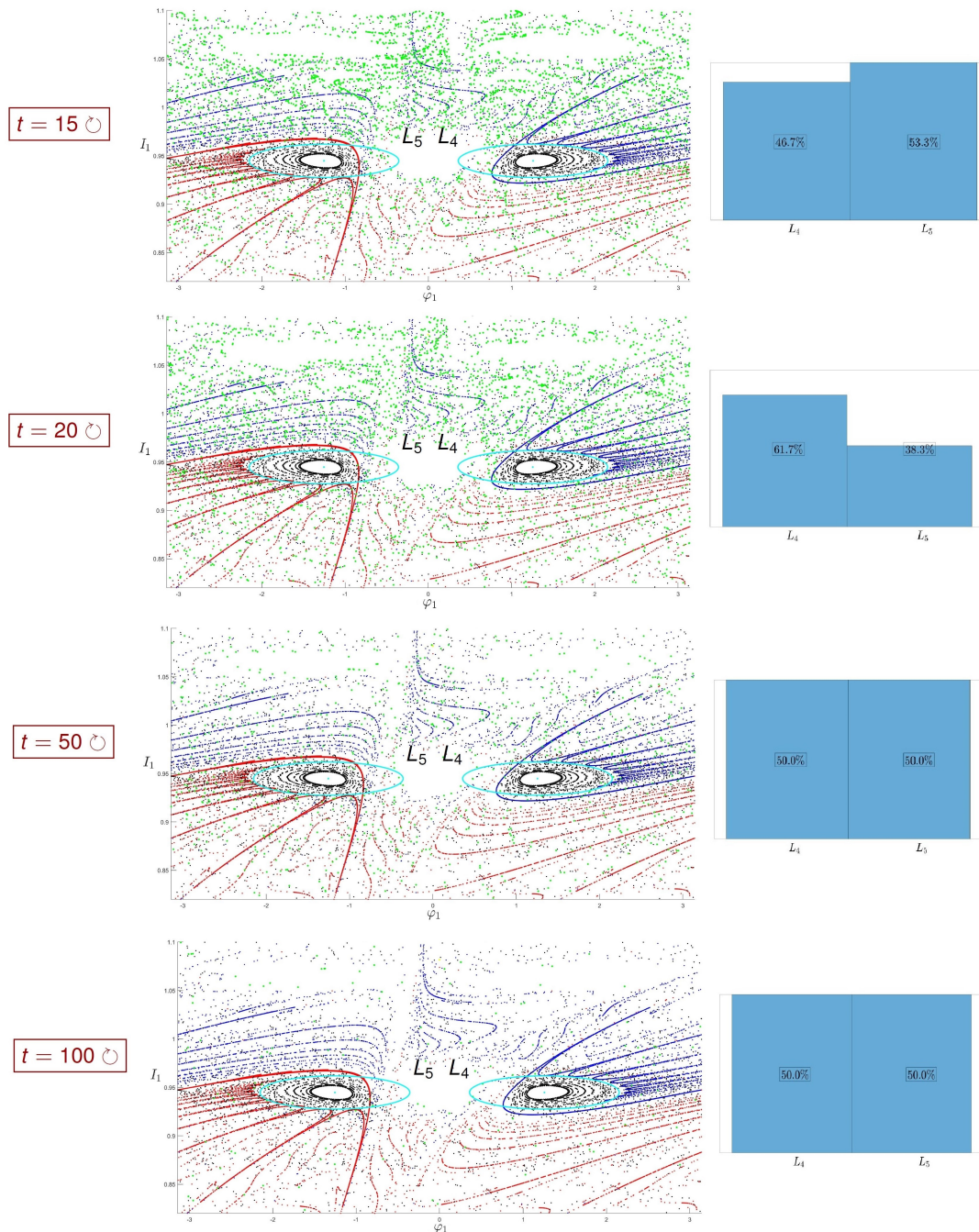


Figure 5.7: Continuation of the Poincaré map iterations of Fig. 5.6.

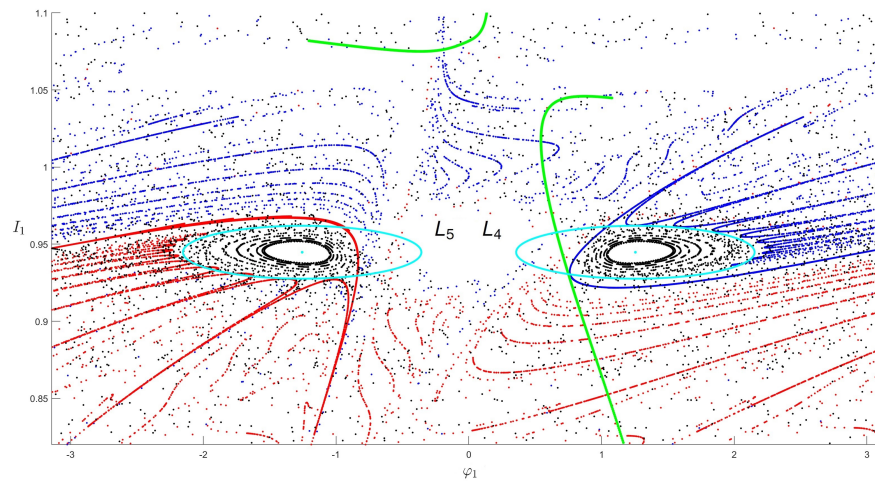


Figure 5.8: Poincaré section as in Fig. 5.6-5.7 after 7 returns \cup for initial data close and transverse to $W^s(PL_2)$ (mapped to the green elongated sets resembling branches of $W^u(PL_2)$).

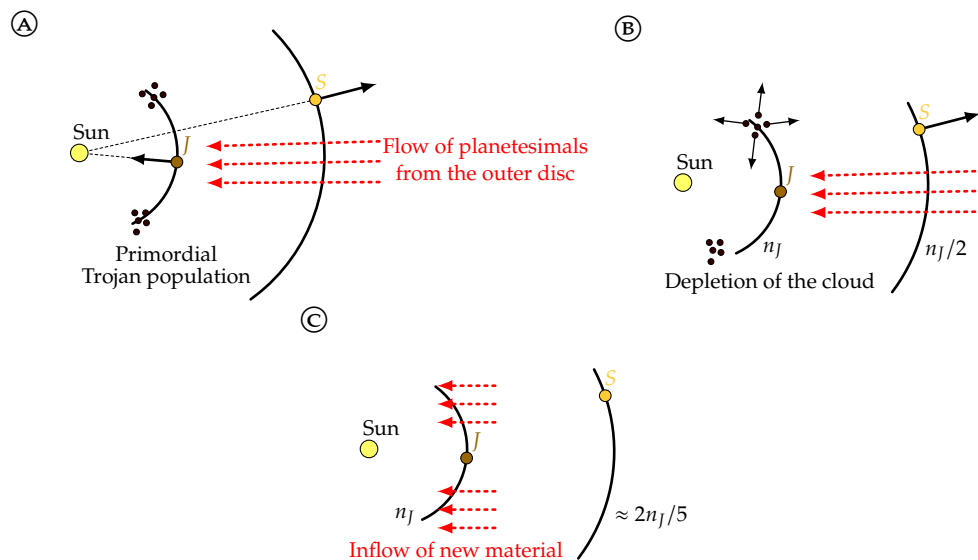


Figure 5.9: Sketch of the Trojan dynamics during the giant planets' migration phase. J and S stand for Jupiter and Saturn respectively.

where m_\odot is the solar mass and the mean motion of Jupiter is set equal to $n_J(t) = \sqrt{\mathcal{G}(m_\odot + m_J)}a_J(t)^{-3/2}$.

We have the following.

Proposition 5.3.1. *For any $t \in [0, t_{\text{mig}}]$ and $p_x, p_y \in \mathbb{R}$, the Hamiltonian (5.10) with (5.9) is a strictly decreasing function of time in the strip $(x, y) \in]-\mu_J a_J, (1 - \mu_J) a_J[\times \mathbb{R}$.*

Proof. Computing the total time derivative of \mathcal{H}_{mig} yields

$$\begin{aligned} \frac{d\mathcal{H}_{\text{mig}}}{dt} = \frac{\partial\mathcal{H}_{\text{mig}}}{\partial t} = & -\dot{n}_J(xp_y - yp_x) + \frac{\mathcal{G}m_\odot(x + \mu_J a_J)\mu_J \dot{a}_J}{((x + \mu_J a_J)^2 + y^2)^{3/2}} \\ & - \frac{\mathcal{G}m_J(x - (1 - \mu_J)a_J)(1 - \mu_J)\dot{a}_J}{((x - (1 - \mu_J)a_J)^2 + y^2)^{3/2}}. \end{aligned}$$

Since $\dot{a}_J = -a_{J,0}e^{-t/T}/T < 0$, the angular momentum $(xp_y - yp_x) = G > 0$ and

$$\dot{n}_J = -\frac{3}{2}\sqrt{\mathcal{G}(m_\odot + m_J)a_J^{-5/2}}\dot{a}_J > 0,$$

we have that always $-\dot{n}_J(xp_y - yp_x) < 0$. Hence, for $-\mu_J a_J < x < (1 - \mu_J)a_J$ the remaining two quantities of \mathcal{H}_{mig} are negative. \square

5.3.2 Trapping of particles at L_4/L_5

In light of Proposition 5.3.1, at $t = t_{\text{mig}}$ in neighborhoods of L_4, L_5 the Hamiltonian \mathcal{H}_{mig} is lower than its value at $t = 0$. This is a necessary condition to have the same outcome for the current Jacobi integral of the system, since $\forall t$

$$E_J = \frac{\mathcal{H}_{\text{mig}}}{n_J^2 a_J^2} = \frac{\mathcal{H}_{\text{mig}}}{\mathcal{G}(m_\odot + m_J)} a_J, \quad (5.11)$$

and one easily realizes that a necessary condition for $\dot{E}_J < 0$ is $\dot{\mathcal{H}}_{\text{mig}} < 0$.

We are interested in selecting appropriate initial conditions that lead to $\dot{E}_J < 0$ over time. For such initial conditions, we have $E_J(t_{\text{mig}}) < E_J(0)$, implying an enlargement of the stable L_4/L_5 Trojan regions (in view of what discussed in 5.2.3). Then, assuming an adiabatic capture scenario [103], incoming objects to the L_4/L_5 region can be trapped. A schematic illustration of such a scenario is provided in Fig. 5.10: the image is obtained as a superposition of the plot in Fig. 5.6 for 2 Poincaré map iterations and the local phase portrait on Σ computed separately for a lower value of \bar{E}_J . We can see that now the flow of particles (green) can hypothetically access the L_4 region and be captured in the resonance.

Fig. 5.11 shows the results of a numerical (non-schematic) evolution of the trajectories under the Jupiter-migrating Hamiltonian model (5.10). We consider the same $N = 10000$ transverse initial conditions in a tubular neighborhood of $W^s(PL_2)$ of Fig. 5.8 described at the end of §5.2.3. Then we propagate their flow according to (5.10) for two values of the migration rate T and migration

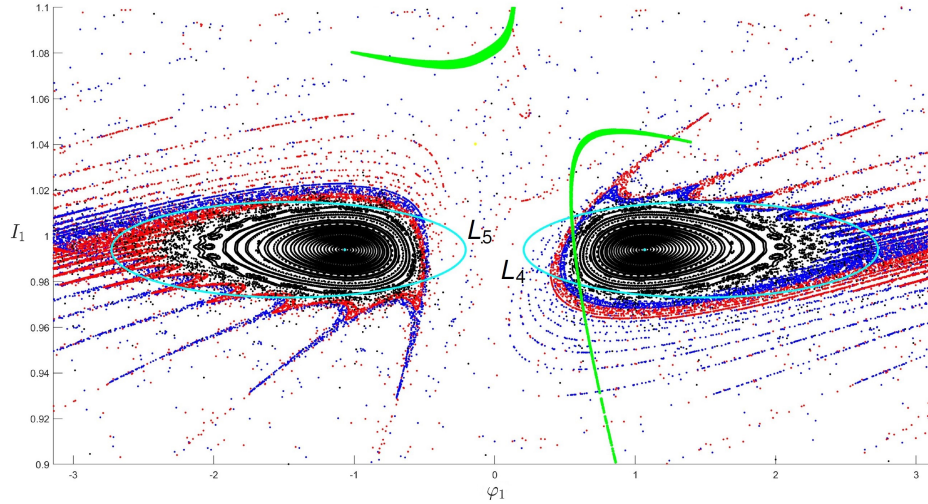


Figure 5.10: Illustration of a hypothetical proposed trapping mechanism in the Trojan regions (details in the text). The two separated sections are computed for $\bar{E}_J = -1.4948$ (rays and invariant curves) and $\bar{E}_J = -1.4464$ (green flow from Fig. 5.6).

time t_{mig} . As a last step, we count the number of particles N_{L_4} , N_{L_5} inside corresponding moving “resonant-like” rectangles

$$(\lambda - \lambda_J, a) \in \mathcal{R} \times]a_J(1 - \sqrt{\mu_J}), a_J(1 + \sqrt{\mu_J})[,$$

with $\mathcal{R} =]\pi/6, \pi/2[$ for L_4 and $\mathcal{R} =]3\pi/2, 11\pi/6[$ for L_5 , at every time step (expressed as a fraction of Jupiter’s initial period). Remarkably, we always observe the persistence of a preferential inflow from L_4 at the very beginning of the simulation, as found in absence of migration. However, we also observe the persistence of the asymmetries for a time up to 350 y, with most trapped particles migrating to L_5 at the time $t_1 \approx 150y$, and a statically significant residual returning preferentially at L_4 at the time $t_2 \approx 300$ y.

Comparing with Fig. 5.6-5.7, we see that with Jupiter migrating we reach to prolong the time scales for which significant L_4/L_5 asymmetries are observed in the temporarily trapped particles by about an order of magnitude. Scenarios with more detailed migration models $a_J(t)$, as well as more realistic initial conditions for the particles, are under investigation.

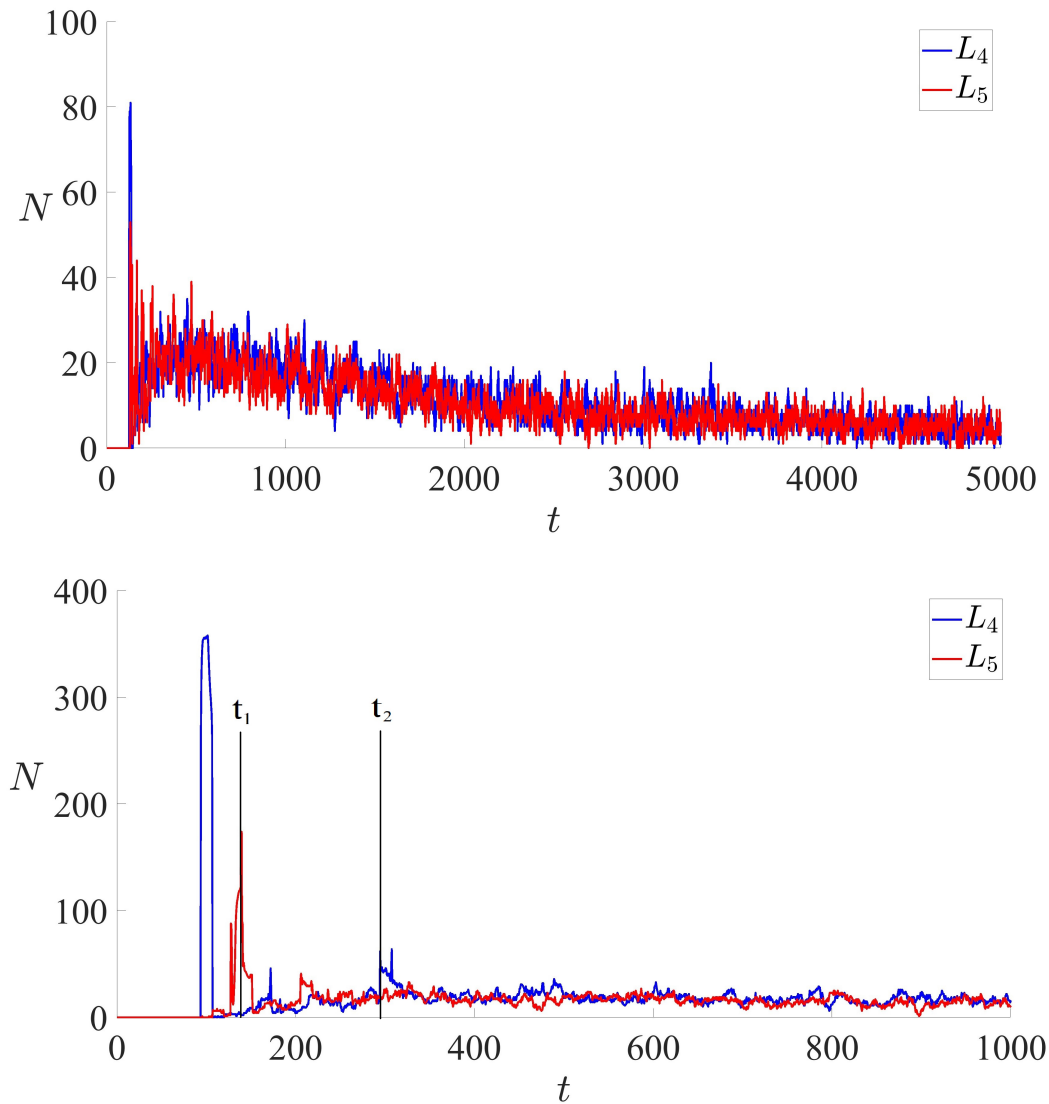


Figure 5.11: Temporary number of bodies inside the L_4/L_5 resonant-like domain during Jupiter's migration (blue and red respectively). The data inside the two regions are sampled at every $\Delta t = T_J(0)/1000 \approx 0.01$ y in both cases. **Top panel:** statistic with $T = 10^5$ y for $t_{\text{mig}} = 5000$ y. **Bottom panel:** statistic with $T = 10^4$ y for $t_{\text{mig}} = 1000$ y (in the plot, $t_1 = 139$ y, $t_2 = 294$ y).

SUMMARY OF NEW RESULTS AND PERSPECTIVES

A summary of what was accomplished in the present thesis is the following.

In Chapter 2 we obtained the regularized (locally to either the primary or the secondary) KS Hamiltonian of the ER3BP in a similar (albeit not equal) manner as in the CR3BP, namely by extending the (already) augmented phase space and arriving at a projection of the solutions in terms of the redundant variables equivalent to a symplectic reduction of the phase space through the bilinear form constraint. This was carried out starting from the Lagrangian setting, which allows a simpler mathematical derivation and compensates for the lack of an immediate regularizing canonical transformation. Eventually, we conducted numerical experiments demonstrating the efficiency of the method in a neighborhood of the collision singularity.

In Chapter 3 we developed the formal aspects of a relegation-free closed form method, which relies on the use of a “book-keeping” parameter to simultaneously account for all small quantities of the problem as they appear not only in the Hamiltonian and Lie generating functions, but also in the closed-form version of all formulas involved in the Poisson algebra between the Delaunay canonical variables of the problem. A rigorous demonstration of the consistency of the method was then given through three propositions, which also establish the explicit formulas for the implementation of one iterative step of the closed-form normalization algorithm. Successively, we gave numerical examples of the implementation and precision of the algorithm in the spatial elliptic, as well as in the planar circular R3BP, examining, also numerically, the method’s convergence properties. The effect of choosing different truncation orders (in powers of the mass parameter μ or in the multipole expansion) was discussed, along with several simplifications to the normalization procedure which hold in the circular case. The essentially asymptotic character of the series was established through numerical examples, showing the existence of an optimal number of normalization steps, after which the size of the remainder becomes the minimum possible.

In Chapter 4 we analyzed a key aspect of the above presented method, that is the possibility to exploit the behavior of the size of the remainder as a function

of the number of normalizing steps in order to obtain a clear separation of two well-distinct domains, as also identified by purely numerical (FLI cartography) means: specifically one, called the *domain of secular motions*, corresponding to the domain where the harmonics in the Hamiltonian associated with resonant combinations of the fast angles (anomalies) of the problem produce no dynamical effect on the orbits visible at the level of the FLI cartography. From the semi-analytical point of view, this turns to be the domain where a non-resonant construction as the one proposed in the previous chapter produces no (nearly-) resonant divisors up to the optimal normalization step. As a consequence, only the angles associated with the motions of the perihelion and of the line of nodes survive in the final normal form. We showed numerically how to use the information on the size of the normal form remainder in order to determine semi-analytically the border of the domain of secular motions in the case of the Sun-Jupiter system. We gave evidence that this border is well distinct from the border of the domains defined either by the Hill stability or by the perihelion crossing criterion. In addition, using an empiric method based on the maximum acceptable semi-major axis' variation at every integration step, we also provided a characterization of the fractal boundary below the pericenter crossing curve resulting from the long-term FLI map.

Finally, in Chapter 5, we examined numerically a case far from the domain of secular motions, namely the heteroclinic dynamics between the stable manifolds of the family of horizontal Lyapunov orbits around the Lagrangian point L_3 with the unstable manifolds emanating from the family of horizontal Lyapunov orbits around the Lagrangian collinear point L_1 and L_2 . We discussed possible correlations between the resulting asymmetric distribution of the heteroclinic connections between the opposite branches of the PL_3 stable manifold with the unstable manifolds of PL_1 and PL_2 with the L_4/L_5 asymmetry problem of the Trojan asteroids. In particular, we find that distant bodies entering from the L_2 bottleneck are transferred primarily towards the L_4 co-orbital region rather than L_5 . This phenomenon persists in a more realistic model in which Jupiter migrates, where, in addition, the times for which statistically important differences between the L_4/L_5 number of temporarily captured particles are observed are prolonged.

The above results open some possibilities for future developments and extensions:

- (i) in Chapter 2, the application of the KS regularization to the more general RNBP, in particular regarding its numerical performances making use of other iterative schemes (e.g. Taylor-based or symplectic methods);
- (ii) in Chapter 3, a straightforward extension of the algorithm that accounts for specific mean-motion resonances, to address for example high-dimensional phenomena like orbital diffusion in asteroid dynamics. Note that the most severe convergence issues with the relegation algorithm also occur close to low-order mean-motion resonances, thus it would be of interest to compare the present method with the relegation method in

such cases. Another interesting application of the method would concern the regimes of the so-called *Lunar problem* or *comet problem* [66], in which one can arrange the Hamiltonian function in such a way that the Keplerian term and the term related to the (fictitious) action conjugate to the eccentric anomaly of the primaries appear at different orders (and this prevents the occurrence of resonances, see [54, 80–82]);

- (iii) in Chapter 4, the convergence properties of the above algorithm with a higher order multipole expansion, especially in the vicinity of Jupiter;
- (iv) in Chapter 5, an accurate verification of the theory constructed following the conclusive steps therein listed, particularly with numerical experiments starting with large sets of initial particles (so to allow the definition of L_4/L_5 entrance probabilities) stepwise suitably modified in order to simulate a constant flow of new material coming from the outside of the system.

As a final conclusion, the above and other examples demonstrate that the dynamics of the R3BP, although extremely classical and old as a topic, still exhibits prospects for a variety of new results, as well as an arena for the development of new methods of interest, not only mathematical but also as regards important open problems in the general area of Celestial Mechanics.

DERIVATION OF THE f -DEPENDENT ELLIPTIC RESTRICTED THREE-BODY PROBLEM HAMILTONIAN IN THE ROTATING-PULSATING FRAME

Contrary to the CR3BP, in the ER3BP the primary and the secondary rotate non-uniformly around their common center of mass and have constantly varying relative distance. Consider then the equivalent frame $Oxyz$ of the synodic frame in §1.3.3 that at the same time and for any instant

- (i) pulsates in order to rescale lengths by a factor $1/\varrho(f(t))$, where

$$\varrho(f) = \frac{1 - e_1^2}{1 + e_1 \cos f} \quad (\text{A.1})$$

obtained by (1.54) according to units and notations of §2.3.1,

- (ii) rotates by $f(t)$, thus with non-constant angular speed \dot{f} ,

in such a way that \mathcal{P}_0 and \mathcal{P}_1 appear at rest and their inter-distance $\overline{\mathcal{P}_0\mathcal{P}_1}$ is equal to 1, thus the name *rotating-pulsating reference frame*.

The two prescriptions translate mathematically in the application of a rotation matrix $\mathcal{R}(f) \in SO(3)$ and the scaling factor $\varrho(f)$ to a vector $r = (x, y, z) \in \mathbb{R}^3$ in $Oxyz$ to retrieve a barycentric vector $R = (X, Y, Z) \in \mathbb{R}^3$ in the inertial frame $OXYZ$:

$$R = \varrho(f)\mathcal{R}(f)r, \quad (\text{A.2})$$

where

$$\mathcal{R}(f) = \begin{pmatrix} \cos f & -\sin f & 0 \\ \sin f & \cos f & 0 \\ 0 & 0 & 1 \end{pmatrix}, \quad (\text{A.3})$$

thereby $\mathcal{P}_0(-\mu, 0, 0)$, $\mathcal{P}_1(1 - \mu, 0, 0)$ in the new frame.

A.1 Time-dependent Lagrangian

This section is devoted to sum up the main calculations resulting from the application of (A.2) to the Lagrangian

$$L_I(R, \dot{R}) = \frac{1}{2} \|\dot{R}\|^2 + \frac{1-\mu}{\|R - R_0\|} + \frac{\mu}{\|R - R_1\|} \quad (\text{A.4})$$

being R_0, R_1 inertial locations of $\mathcal{P}_0, \mathcal{P}_1$ respectively, whose orbital plane coincide with the X-Y plane.

Proposition A.1.1. *The Lagrange's function (A.4) in the rotating-pulsating reference frame takes the form*

$$L_{RP}(x, y, z, \dot{x}, \dot{y}, \dot{z}, t) = \frac{1}{2} \varrho^2 (\dot{x}^2 + \dot{y}^2 + \dot{z}^2) + \sqrt{1 - e_1^2} (x\dot{y} - \dot{x}y) - \frac{1}{\varrho} \mathcal{U}(x, y, z, t), \quad (\text{A.5})$$

where

$$\mathcal{U}(x, y, z, t) = \mathcal{V}(x, y, z) - \frac{1}{2} (x^2 + y^2 - z^2 e_1 \cos f), \quad \mathcal{V}(x, y, z) = -\frac{1-\mu}{d_0} - \frac{\mu}{d_1}, \quad (\text{A.6})$$

is the scaled effective potential, in which d_0, d_1 are expressed by (1.75).

The proof of the statement consists in some algebra; before going through the main steps, there is a couple of relationships of the Kepler's problem which are needed next, especially the former will be necessary later to pass from t to f as new independent variable.

Lemma A.1.1. *The time derivative of the true anomaly f and the second time derivative of the mutual distance ϱ for the motion of the primaries in the ER3BP satisfy respectively*

$$\dot{f} = \frac{\sqrt{1 - e_1^2}}{\varrho^2}, \quad (\text{A.7})$$

$$\ddot{\varrho} = \frac{1 - e_1^2}{\varrho^3} - \frac{1}{\varrho^2}. \quad (\text{A.8})$$

Proof. Setting $f = 0$ and $f = \pi$ in (1.54) for the radii of pericenter ϱ_p and apocenter ϱ_a respectively and combining with $\varrho_p + \varrho_a = 2a_1 = 2$, it gives, recalling that $\mathcal{G}(m_0 + m_1) = a_1 = 1$,

$$\mathcal{M}_Z = \sqrt{1 - e_1^2},$$

for \mathcal{M}_Z from (1.51); equivalently this descends immediately from the G De-launay element's expression in (3.3) with $\|\mathcal{M}\| = \mathcal{M}_Z$ due to the choice of the inertial frame. From the expression of the angular momentum in polar coordinates

$$M_Z = \varrho^2 \dot{f}$$

(A.7) follows.

About the second equality, by twice differentiation of $\varrho = \varrho(t)$ and applying the chain rule we end up with (the superscript indicates differentiation with respect to the argument)

$$\dot{\varrho} = \varrho'(f)\dot{f}, \quad \ddot{\varrho} = \varrho''(f)\dot{f}^2 + \varrho'(f)\ddot{f}.$$

Now replacing (A.7)

$$\begin{aligned} \ddot{\varrho} &= \varrho'' \frac{1 - e_1^2}{\varrho^4} + \varrho' \frac{d}{dt} \left(\frac{\sqrt{1 - e_1^2}}{\varrho^2} \right) \\ &= \varrho'' \frac{1 - e_1^2}{\varrho^4} - (\varrho')^2 \frac{2\sqrt{1 - e_1^2}}{\varrho^3} \frac{\sqrt{1 - e_1^2}}{\varrho^2} \\ &= \frac{1 - e_1^2}{\varrho^4} \left(\varrho'' - \frac{2(\varrho')^2}{\varrho} \right), \end{aligned}$$

let us explicit ϱ' and ϱ'' in terms of ϱ :

$$\varrho' = \frac{(1 - e_1^2)e_1 \sin f}{(1 + e_1 \cos f)^2} = \frac{\varrho e_1 \sin f}{1 + e_1 \cos f},$$

$$\begin{aligned} \varrho'' &= \frac{(1 - e_1^2)e_1 \cos f (1 + e_1 \cos f) + 2e_1 \sin f (1 - e_1^2)e_1 \sin f}{(1 + e_1 \cos f)^3} \\ &= \frac{(1 - e_1^2)(e_1 \cos f + e_1^2 \cos^2 f + 2e_1^2 \sin^2 f)}{(1 + e_1 \cos f)^3} \\ &= \frac{\varrho e_1 (e_1 + \cos f + e_1 \sin^2 f)}{(1 + e_1 \cos f)^2}. \end{aligned}$$

Coming back to $\ddot{\varrho}$, after the substitution

$$\begin{aligned} \ddot{\varrho} &= \frac{1 - e_1^2}{\varrho^3} \left(\frac{e_1^2 + e_1 \cos f + e_1^2 \sin^2 f}{(1 + e_1 \cos f)^2} - \frac{2e_1^2 \sin^2 f}{(1 + e_1 \cos f)^2} \right) = \frac{(1 - e_1^2)e_1 \cos f}{\varrho^3(1 + e_1 \cos f)} \\ &= \frac{e_1 \cos f}{\varrho^2}, \end{aligned}$$

we are left with, from (1.54),

$$e_1 \cos f = \frac{1 - e_1^2}{\varrho} - 1 \implies \ddot{\varrho} = \frac{1 - e_1^2}{\varrho^3} - \frac{1}{\varrho^2}.$$

□

At this point the proof of Proposition A.1.1 is ready to be exposed.

Proof of Proposition A.1.1. Consider the Lagrangian (A.4) and perform the transformation (A.2) term by term.

- *Kinetic energy contribution:*

$$\dot{X}^2 + \dot{Y}^2 + \dot{Z}^2 = \dot{R} \cdot \dot{R} = \frac{d}{dt}(\varrho(f)\mathcal{R}(f)r) \cdot \frac{d}{dt}(\varrho(f)\mathcal{R}(f)r) ,$$

from which

$$\begin{aligned} \|\dot{R}\|^2 &= (\varrho' \dot{f} \mathcal{R}r + \varrho \dot{f} \mathcal{R}'r + \varrho \mathcal{R}\dot{r}) \cdot (\varrho' \dot{f} \mathcal{R}r + \varrho \dot{f} \mathcal{R}'r + \varrho \mathcal{R}\dot{r}) \\ &= (\varrho')^2 \dot{f}^2 \mathcal{R}r \cdot \mathcal{R}r + \varrho^2 \dot{f}^2 \mathcal{R}'r \cdot \mathcal{R}'r + \varrho^2 \mathcal{R}\dot{r} \cdot \mathcal{R}\dot{r} + 2\varrho' \varrho \dot{f}^2 \mathcal{R}r \cdot \mathcal{R}'r \\ &\quad + 2\varrho' \varrho \dot{f} \mathcal{R}r \cdot \mathcal{R}\dot{r} + 2\dot{f} \varrho^2 \mathcal{R}'r \cdot \mathcal{R}r \end{aligned}$$

and

$$\mathcal{R}'(f) = \begin{pmatrix} -\sin f & -\cos f & 0 \\ \cos f & -\sin f & 0 \\ 0 & 0 & 0 \end{pmatrix}$$

is a skew-symmetric matrix which is no more orthogonal; however

$$(\mathcal{R}')^T \mathcal{R}' = \begin{pmatrix} 1 & 0 & 0 \\ 0 & 1 & 0 \\ 0 & 0 & 0 \end{pmatrix} ,$$

so handling each dot product separately using the equalities

$$\begin{aligned} \mathcal{R}r \cdot \mathcal{R}r &= \|r\|^2 & \mathcal{R}'r \cdot \mathcal{R}'r &= x^2 + y^2 \\ \mathcal{R}\dot{r} \cdot \mathcal{R}\dot{r} &= \|\dot{r}\|^2 & \mathcal{R}r \cdot \mathcal{R}\dot{r} &= r \cdot \dot{r} \\ \mathcal{R}r \cdot \mathcal{R}'r &= 0 & \mathcal{R}'r \cdot \mathcal{R}\dot{r} &= x\dot{y} - \dot{x}y \end{aligned} ,$$

it turns out that, upon simplifications and rearrangements,

$$\begin{aligned} \|\dot{R}\|^2 &= \dot{f}^2((\varrho')^2 \|r\|^2 + \varrho^2(x^2 + y^2)) + \varrho^2 \|\dot{r}\|^2 + 2\varrho' \varrho \dot{f} r \cdot \dot{r} \\ &\quad + 2\dot{f} \varrho^2(x\dot{y} - \dot{x}y) . \end{aligned}$$

- *Potential energy contribution:*

$$\begin{aligned} -\frac{1-\mu}{\|R-R_0\|} - \frac{\mu}{\|R-R_1\|} &= -\frac{1-\mu}{\|\varrho \mathcal{R}(r-r_0)\|} - \frac{\mu}{\|\varrho \mathcal{R}(r-r_1)\|} \\ &= -\frac{1-\mu}{\varrho d_0} - \frac{\mu}{\varrho d_1} , \end{aligned}$$

r_0, r_1 corresponding vectors in $Oxyz$ of R_0, R_1 .

Assembling the two parts, the transformed Lagrangian reads

$$\begin{aligned} L_{RP} &= \frac{1}{2}(\dot{f}^2((\varrho')^2 \|r\|^2 + \varrho^2(x^2 + y^2)) + \varrho^2 \|\dot{r}\|^2 \\ &\quad + 2\varrho' \varrho \dot{f} r \cdot \dot{r} + 2\dot{f} \varrho^2(x\dot{y} - \dot{x}y)) - \frac{1}{\varrho} \mathcal{V} , \end{aligned}$$

that yet can be considerably simplified using Lemma A.1.1 and the identity

$$\frac{d}{dt}(\varrho\dot{\varrho}\|r\|^2) = \dot{\varrho}^2\|r\|^2 + \varrho\ddot{\varrho}\|r\|^2 + 2\varrho\dot{\varrho}r \cdot \dot{r}.$$

This can be cleverly inserted in the expression above of L_{RP} , since

$$\dot{f}^2(\varrho')^2\|r\|^2 + 2\varrho\varrho'f r \cdot \dot{r} = \frac{d}{dt}(\varrho\dot{\varrho}\|r\|^2) - \varrho\ddot{\varrho}\|r\|^2,$$

therefore by substitution

$$\begin{aligned} L_{RP} = \frac{1}{2}(\varrho^2\|\dot{r}\|^2 + 2\dot{f}\varrho^2(xy - \dot{x}y) + \dot{f}^2\varrho^2(x^2 + y^2) - \varrho\ddot{\varrho}\|r\|^2) \\ + \frac{d}{dt}\left(\frac{1}{2}\varrho\dot{\varrho}\|r\|^2\right) - \frac{1}{\varrho}\mathcal{V}. \end{aligned}$$

Now, using (A.7) and (A.8),

$$\dot{f}^2\varrho^2 - \varrho\ddot{\varrho} = \frac{1}{\varrho}$$

and again (A.7) for \dot{f} one derives

$$L_{RP} = \frac{1}{2}\left(\varrho^2\|\dot{r}\|^2 + 2\sqrt{1 - e_1^2}(xy - \dot{x}y) + \frac{1}{\varrho}(x^2 + y^2) - \frac{1}{\varrho}e_1z^2 \cos f\right) - \frac{1}{\varrho}\mathcal{V},$$

in which the term $d(1/2\varrho\dot{\varrho}\|r\|^2)/dt$ can be discarded by gauge transformation invariance of Lagrangians; so upon rearrangements

$$\begin{aligned} L_{RP}(x, y, z, \dot{x}, \dot{y}, \dot{z}, t) = \frac{1}{2}\varrho^2(\dot{x}^2 + \dot{y}^2 + \dot{z}^2) + \sqrt{1 - e^2}(xy - \dot{x}y) \\ + \frac{1}{\varrho}\left(\frac{1}{2}(x^2 + y^2 - z^2e_1 \cos f) + \frac{1 - \mu}{d_0} + \frac{\mu}{d_1}\right). \end{aligned}$$

□

The consequent equations of motion produced by (A.5) can be written as

$$\begin{cases} 2\varrho\dot{\varrho}\dot{x} + \varrho^2\ddot{x} - 2\sqrt{1 - e_1^2}\dot{y} + \frac{1}{\varrho}\frac{\partial\mathcal{U}}{\partial x} = 0 \\ 2\varrho\dot{\varrho}\dot{y} + \varrho^2\ddot{y} + 2\sqrt{1 - e_1^2}\dot{x} + \frac{1}{\varrho}\frac{\partial\mathcal{U}}{\partial y} = 0 \\ 2\varrho\dot{\varrho}\dot{z} + \varrho^2\ddot{z} + \frac{1}{\varrho}\frac{\partial\mathcal{U}}{\partial z} = 0 \end{cases} \quad (\text{A.9})$$

It is quite straightforward to realize that the equilibrium points of this system are situated exactly at the same positions as in the circular problem, since after setting $\dot{x} = \dot{y} = \dot{z} = \ddot{x} = \ddot{y} = \ddot{z} = 0$ one is left with

$$\nabla\mathcal{U} = \left(\frac{\partial\mathcal{U}}{\partial x}, \frac{\partial\mathcal{U}}{\partial y}, \frac{\partial\mathcal{U}}{\partial z}\right) = 0,$$

admitting the same known five equilibrium configurations which do not depend on e_1 . The study of their stability is not nevertheless the same, especially because of the dependence of the linearizing coefficients on the eccentricity (see e.g. [13]). In particular, a numerical procedure based on Floquet theory (see [21]) provides the domain of the linear stability in the parameter plane (μ, e_1) for the equilateral equilibria:

- at $\mu = 0.028$ there is linear instability for any value of e_1 ;
- at $\mu = 0.038$ there is instability also for $e_1 = 0$, while e_1 can have a stabilizing effect up to $\mu = 0.047$.

The collinear points are always unstable, as in the circular case, for any value of (μ, e_1) . Lastly, as regards the existence and stability of periodic orbits in the ER3BP, the problem is yet to be fully explored. Families of periodic motions similar to those of the CR3BP have been found around the collinear points [76]. In [19] and references therein contained the reader can find a good summary of the main contributions existing in the literature on this subject.

A.2 The true anomaly as independent variable

Owing to the fact that $\dot{f} > 0 \forall t \in \mathbb{R}$ by (A.7), the dependence $f = f(t)$ is invertible and thus f can be made as new independent variable in (A.5) to finally get (2.3). We achieve this task by operating on the equations (A.9).

Proposition A.2.1. *The Lagrange's equations (A.9) with f as independent variable read*

$$\begin{cases} x'' = 2y' - \frac{1}{1 + e_1 \cos f} \left(\frac{\partial \mathcal{V}}{\partial x} - x \right) \\ y'' = -2x' - \frac{1}{1 + e_1 \cos f} \left(\frac{\partial \mathcal{V}}{\partial x} - y \right) \\ z'' = -\frac{1}{1 + e_1 \cos f} \left(\frac{\partial \mathcal{V}}{\partial z} + ze_1 \cos f \right) \end{cases} . \quad (\text{A.10})$$

where the superscript indicates differentiation w.r.t. f .

Proof. Starting from the equations in vector form

$$\varrho^2 \ddot{r} + 2\varrho \dot{\varrho} \dot{r} - 2\sqrt{1 - e_1^2} (\dot{y}, -\dot{x}, 0) + \frac{1}{\varrho} (\nabla \mathcal{U} - (x, y, -ze_1 \cos f)) = 0 ,$$

consider $r(t) = r(f(t))$. Then

$$\dot{r} = \dot{f} r' , \quad \ddot{r} = \dot{f}^2 r'' + \ddot{f} r' ,$$

and replacing back

$$\varrho^2 \dot{f}^2 r'' + (\varrho^2 \ddot{f} + 2\varrho \dot{\varrho} \dot{f}) r' - 2\sqrt{1 - e_1^2} \dot{f} (y', -x', 0) + \frac{1}{\varrho} (\nabla \mathcal{U} - (x, y, -ze_1 \cos f)) = 0 .$$

Recognize now that $\varrho^2 \ddot{f} + 2\varrho \dot{\varrho} \dot{f} = d(\varrho^2 \dot{f})/dt = 0$, as $\varrho^2 \dot{f}$ is the magnitude of the \mathcal{P}_0 - \mathcal{P}_1 angular momentum, and with the help of (A.7) and (A.1) one arrives at

$$r'' - 2(\dot{y}, -\dot{x}, 0) + \frac{1}{1 + e_1 \cos f} (\nabla \mathcal{U} - (x, y, -ze_1 \cos f)) = 0 ,$$

which is equivalent to the system (A.10). □

The related Lagrangian (2.3) is thereby easily deduced, as well as the Hamiltonian (2.2) via Legendre transform after introducing the momenta

$$p_x = \frac{\partial L}{\partial x'} = x' - y , \quad p_y = \frac{\partial L}{\partial y'} = y' + x , \quad p_z = \frac{\partial L}{\partial z'} = z' .$$



COMPUTATION OF POISSON BRACKET'S INTERMEDIATE DERIVATIVES

Derivatives (3.31)–(3.43) are computed combining adequately definitions (3.3), the polar relationship (3.15), including its alternative expression involving the eccentric anomaly E given by (1.56), $\|r_1\|$ again via (1.56), Kepler's equation (1.57) for ℓ and M_1 and the trigonometric equalities (1.55). Equation (3.31) comes from $\|R\|(E)$ and $\|R\|(f)$ by total differentiation with respect to ℓ :

$$\frac{d}{d\ell} \|R\| \stackrel{(1.56)}{=} \frac{\partial \|R\|}{\partial E} \frac{\partial E}{\partial \ell} = \frac{ae \sin E}{1 - e \cos E} \stackrel{(3.15)}{=} \frac{\partial \|R\|}{\partial f} \frac{\partial f}{\partial \ell} = \frac{a\eta^2 e \sin f}{(1 + e \cos f)^2} \frac{\partial f}{\partial \ell},$$

since a, e do not depend on ℓ , where $\partial E/\partial \ell$ is deduced from (1.57) making use of the derivative of inverse functions ($\partial \ell/\partial E \neq 0$ is ensured). Thus the result by (1.55).

Equations (3.32), (3.33) are straightforward to obtain by ordinary differentiation and the inverse derivative once again of $dM_1/dE_1 \neq 0$ from (1.57) for M_1 :

$$\frac{dE_1}{dM_1} = \frac{1}{1 - e_1 \cos E_1} = \frac{a_1}{\|r_1\|}.$$

Solving for e in (3.3) and partially differentiating, we immediately have (3.35) and (3.38), from which (3.36), (3.39) as

$$\frac{\partial \eta}{\partial \delta L} = -\frac{e}{\eta} \frac{\partial e}{\partial \delta L} = -\frac{\eta}{L}, \quad \frac{\partial \eta}{\partial G} = -\frac{e}{\eta} \frac{\partial e}{\partial G} = \frac{1}{L}.$$

The true anomaly derivatives with respect to the actions are slightly more elaborated. Employing (1.55),

$$-\sin f \frac{\partial f}{\partial \delta L} = \frac{\partial}{\partial \delta L} \cos f = \frac{\partial}{\partial e} \left(\frac{\cos E - e}{1 - e \cos E} \right) \frac{\partial e}{\partial \delta L} + \frac{\partial}{\partial E} \left(\frac{\cos E - e}{1 - e \cos E} \right) \frac{\partial E}{\partial \delta L},$$

that leads upon simplifications to

$$\frac{\partial f}{\partial \delta L} = \frac{\sin f}{eL} + \frac{1 + e \cos f}{\eta} \frac{\partial E}{\partial \delta L};$$

finally we explicit $\partial E / \partial \delta L$ exploiting the corresponding Kepler equation (1.57) and the inter-independence $\ell, \delta L$ by conjugacy:

$$0 = \frac{d}{d\delta L}(E - e \sin E) = \frac{\partial E}{\partial \delta L} - \frac{\partial e}{\partial \delta L} \sin E - e \cos E \frac{\partial E}{\partial \delta L} \implies \frac{\partial E}{\partial \delta L} = \frac{\eta \sin f}{eL},$$

thereby (3.34).

The relation for $\partial f / \partial G$ is found precisely in the same manner, so one finds out

$$\frac{\partial f}{\partial G} = -\frac{\sin f}{\eta eL} + \frac{1 + e \cos f}{\eta} \frac{\partial E}{\partial G}, \quad \frac{\partial E}{\partial G} = -\frac{\sin f}{eL},$$

that is (3.37).

Finally, derivatives (3.40), (3.42) involving $\iota_c = \cos i$ easily follow again by partial differentiation in (3.3) with respect to G and H respectively; while for those containing $\iota_s = \sin i$ we can rely, for example, to the identity $\sin^2 i + \cos^2 i = 1$:

$$0 = 2 \sin i \frac{\partial \iota_s}{\partial G} + 2 \cos i \frac{\partial \iota_c}{\partial G}$$

and consequently (3.41) provided $\sin i \neq 0$, as well as (3.43) repeating the same argument with the variable H .



EXAMPLE OF NORMALIZATION FOR A μ^2 QUADRUPOLE EXPANSION

Consider the following toy model Hamiltonian with $k_\mu = k_{\text{mp}} = \nu = 2$, $\nu_1 = 1$, according to conventions introduced in §3.2.4:

$$\mathcal{H}^{(0)} = \mathcal{L}_0 + \mathcal{R}_{2,2}^{(0)} + \mathcal{R}_{2,3}^{(0)} + \mathcal{R}_{2,4}^{(0)},$$

where

$$\begin{aligned} \mathcal{R}_{2,2}^{(0)} = \sigma^2 \left(& - \frac{3a_1^3 \mathcal{G}^4 \mu m_0^4 \iota_c^2 \cos(2(E_1 - f - g - h))}{16L_*^6 \|r_1\|} \right. \\ & - \frac{3a_1^3 \mathcal{G}^4 \mu m_0^4 \iota_c^2 \cos(2(E_1 + f + g - h))}{16L_*^6 \|r_1\|} - \frac{3a_1^3 \mathcal{G}^4 \mu m_0^4 \iota_c \cos(2(E_1 - f - g - h))}{8L_*^6 \|r_1\|} \\ & + \frac{3a_1^3 \mathcal{G}^4 \mu m_0^4 \iota_c \cos(2(E_1 + f + g - h))}{8L_*^6 \|r_1\|} + \frac{3a_1^3 \mathcal{G}^4 \mu m_0^4 \iota_c^2 \cos(2(E_1 - h))}{8L_*^6 \|r_1\|} \\ & + \frac{3a_1^3 \mathcal{G}^4 \mu m_0^4 \iota_c^2 \cos(2(f + g))}{8L_*^6 \|r_1\|} - \frac{3a_1^3 \mathcal{G}^4 \mu m_0^4 \iota_c^2}{8L_*^6 \|r_1\|} - \frac{3a_1^3 \mathcal{G}^4 \mu m_0^4 \cos(2(E_1 - f - g - h))}{16L_*^6 \|r_1\|} \\ & - \frac{3a_1^3 \mathcal{G}^4 \mu m_0^4 \cos(2(E_1 + f + g - h))}{16L_*^6 \|r_1\|} - \frac{3a_1^3 \mathcal{G}^4 \mu m_0^4 \cos(2(E_1 - h))}{8L_*^6 \|r_1\|} \\ & \left. - \frac{3a_1^3 \mathcal{G}^4 \mu m_0^4 \cos(2(f + g))}{8L_*^6 \|r_1\|} + \frac{a_1^3 \mathcal{G}^4 \mu m_0^4}{8L_*^6 \|r_1\|} - \frac{3a_1 \delta L^2 \mathcal{G}^2 m_0^2}{2L_*^4 \|r_1\|} - \frac{a_1 \mathcal{G}^2 \mu m_0^2}{L_*^2 \|r_1\|} \right). \end{aligned}$$

The first step $j = 1$ of the method aims to normalize $\mathcal{R}_{2,2}^{(0)}$ via (3.70) solved by

$$\begin{aligned} \chi_2^{(1)} = & \sigma^3 \left(\frac{3\mathcal{G}^4 \mu a_1^2 \iota_c^2 \phi_1 n_*^2 m_0^4}{8n_1 L_*^6 (n_1^2 - n_*^2)} - \frac{\mathcal{G}^4 \mu a_1^2 \phi_1 n_*^2 m_0^4}{8n_1 L_*^6 (n_1^2 - n_*^2)} \right. \\ & - \frac{3\mathcal{G}^4 \mu a_1^2 n_1 \iota_c^2 \phi_1 m_0^4}{8L_*^6 (n_1^2 - n_*^2)} + \frac{\mathcal{G}^4 \mu a_1^2 n_1 \phi_1 m_0^4}{8L_*^6 (n_1^2 - n_*^2)} + \frac{\mathcal{G}^2 \mu \phi_1 n_*^2 m_0^2}{n_1 L_*^2 (n_1^2 - n_*^2)} \\ & \left. + \frac{3\mathcal{G}^2 \delta L^2 \phi_1 n_*^2 m_0^2}{2n_1 L_*^4 (n_1^2 - n_*^2)} - \frac{\mathcal{G}^2 \mu n_1 \phi_1 m_0^2}{L_*^2 (n_1^2 - n_*^2)} - \frac{3\mathcal{G}^2 \delta L^2 n_1 \phi_1 m_0^2}{2L_*^4 (n_1^2 - n_*^2)} \right) \\ & + \sigma^2 \left(- \frac{3\mathcal{G}^4 \mu \sin(2(E_1 - h)) a_1^2 \iota_c^2 n_*^2 m_0^4}{16n_1 L_*^6 (n_1^2 - n_*^2)} + \frac{3\mathcal{G}^4 \mu \sin(2(E_1 - h)) a_1^2 n_*^2 m_0^4}{16n_1 L_*^6 (n_1^2 - n_*^2)} \right. \\ & + \frac{3\mathcal{G}^4 \mu \sin(2(f + g)) a_1^2 n_* m_0^4}{16L_*^6 (n_1^2 - n_*^2)} - \frac{3\mathcal{G}^4 \mu \sin(2(-f - g - h + E_1)) a_1^2 n_* m_0^4}{32L_*^6 (n_1^2 - n_*^2)} \\ & + \frac{3\mathcal{G}^4 \mu \sin(2(f + g - h + E_1)) a_1^2 n_* m_0^4}{32L_*^6 (n_1^2 - n_*^2)} - \frac{3\mathcal{G}^4 \mu \sin(2(f + g)) a_1^2 \iota_c^2 n_* m_0^4}{16L_*^6 (n_1^2 - n_*^2)} \\ & - \frac{3\mathcal{G}^4 \mu \sin(2(-f - g - h + E_1)) a_1^2 \iota_c^2 n_* m_0^4}{32L_*^6 (n_1^2 - n_*^2)} + \frac{3\mathcal{G}^4 \mu \sin(2(f + g - h + E_1)) a_1^2 \iota_c^2 n_* m_0^4}{32L_*^6 (n_1^2 - n_*^2)} \\ & - \frac{3\mathcal{G}^4 \mu \sin(2(-f - g - h + E_1)) a_1^2 \iota_c n_* m_0^4}{16L_*^6 (n_1^2 - n_*^2)} - \frac{3\mathcal{G}^4 \mu \sin(2(f + g - h + E_1)) a_1^2 \iota_c n_* m_0^4}{16L_*^6 (n_1^2 - n_*^2)} \\ & + \frac{3\mathcal{G}^4 \mu \sin(2(E_1 - h)) a_1^2 n_1 \iota_c^2 m_0^4}{16L_*^6 (n_1^2 - n_*^2)} - \frac{3\mathcal{G}^4 \mu \sin(2(-f - g - h + E_1)) a_1^2 n_1 \iota_c^2 m_0^4}{32L_*^6 (n_1^2 - n_*^2)} \\ & - \frac{3\mathcal{G}^4 \mu \sin(2(f + g - h + E_1)) a_1^2 n_1 \iota_c^2 m_0^4}{32L_*^6 (n_1^2 - n_*^2)} - \frac{3\mathcal{G}^4 \mu \sin(2(E_1 - h)) a_1^2 n_1 m_0^4}{16L_*^6 (n_1^2 - n_*^2)} \\ & - \frac{3\mathcal{G}^4 \mu \sin(2(-f - g - h + E_1)) a_1^2 n_1 m_0^4}{32L_*^6 (n_1^2 - n_*^2)} - \frac{3\mathcal{G}^4 \mu \sin(2(f + g - h + E_1)) a_1^2 n_1 m_0^4}{32L_*^6 (n_1^2 - n_*^2)} \\ & - \frac{3\mathcal{G}^4 \mu \sin(2(-f - g - h + E_1)) a_1^2 n_1 \iota_c m_0^4}{16L_*^6 (n_1^2 - n_*^2)} + \frac{3\mathcal{G}^4 \mu \sin(2(f + g - h + E_1)) a_1^2 n_1 \iota_c m_0^4}{16L_*^6 (n_1^2 - n_*^2)} \\ & \left. - \frac{3\mathcal{G}^4 \mu \sin(2(f + g)) a_1^2 n_1^2 m_0^4}{16L_*^6 n_* (n_1^2 - n_*^2)} + \frac{3\mathcal{G}^4 \mu \sin(2(f + g)) a_1^2 n_1^2 \iota_c^2 m_0^4}{16L_*^6 n_* (n_1^2 - n_*^2)} \right), \end{aligned}$$

so that the new truncated Hamiltonian becomes

$$\mathcal{H}^{(1)} = \mathcal{L}_0 + \mathcal{L}_2^{(1)} + \mathcal{R}_{3,3}^{(1)} + \mathcal{R}_{3,4}^{(1)},$$

with

$$\mathcal{L}_2^{(1)} = \sigma^2 \left(- \frac{3a_1^2 \mathcal{G}^4 \mu m_0^4 \iota_c^2}{8L_*^6} + \frac{a_1^2 \mathcal{G}^4 \mu m_0^4}{8L_*^6} - \frac{3\delta L^2 \mathcal{G}^2 m_0^2}{2L_*^4} - \frac{\mathcal{G}^2 \mu m_0^2}{L_*^2} \right)$$

and

$$\begin{aligned}
\mathcal{R}_{3,3}^{(1)} = & \sigma^3 \left(- \frac{3e\mathcal{G}^4 \mu \cos(f + 2g + 2h - 2E_1) a_1^3 t_c^2 n_* m_0^4}{8\eta^3 \|r_1\| L_*^6 (2n_1 - 2n_*)} \right. \\
& - \frac{3e\mathcal{G}^4 \mu \cos(3f + 2g + 2h - 2E_1) a_1^3 t_c^2 n_* m_0^4}{8\eta^3 \|r_1\| L_*^6 (2n_1 - 2n_*)} + \frac{3\mathcal{G}^4 \mu \cos(2f + 2g + 2h - 3E_1) a_1^3 e_1 t_c^2 n_* m_0^4}{16 \|r_1\| L_*^6 (2n_1 - 2n_*)} \\
& + \frac{3\mathcal{G}^4 \mu \cos(2f + 2g + 2h - E_1) a_1^3 e_1 t_c^2 n_* m_0^4}{16 \|r_1\| L_*^6 (2n_1 - 2n_*)} - \frac{3e\mathcal{G}^4 \mu \cos(f + 2g + 2h - 2E_1) a_1^3 t_c n_* m_0^4}{4\eta^3 \|r_1\| L_*^6 (2n_1 - 2n_*)} \\
& - \frac{3e\mathcal{G}^4 \mu \cos(3f + 2g + 2h - 2E_1) a_1^3 t_c n_* m_0^4}{4\eta^3 \|r_1\| L_*^6 (2n_1 - 2n_*)} + \frac{3\mathcal{G}^4 \mu \cos(2f + 2g + 2h - 3E_1) a_1^3 e_1 t_c n_* m_0^4}{8 \|r_1\| L_*^6 (2n_1 - 2n_*)} \\
& + \frac{3\mathcal{G}^4 \mu \cos(2f + 2g + 2h - E_1) a_1^3 e_1 t_c n_* m_0^4}{8 \|r_1\| L_*^6 (2n_1 - 2n_*)} - \frac{3e\mathcal{G}^4 \mu \cos(f + 2g + 2h - 2E_1) a_1^3 n_* m_0^4}{8\eta^3 \|r_1\| L_*^6 (2n_1 - 2n_*)} \\
& - \frac{3e\mathcal{G}^4 \mu \cos(3f + 2g + 2h - 2E_1) a_1^3 n_* m_0^4}{8\eta^3 \|r_1\| L_*^6 (2n_1 - 2n_*)} + \frac{3\mathcal{G}^4 \mu \cos(2f + 2g + 2h - 3E_1) a_1^3 e_1 n_* m_0^4}{16 \|r_1\| L_*^6 (2n_1 - 2n_*)} \\
& + \frac{3\mathcal{G}^4 \mu \cos(2f + 2g + 2h - E_1) a_1^3 e_1 n_* m_0^4}{16 \|r_1\| L_*^6 (2n_1 - 2n_*)} + \frac{3e\mathcal{G}^4 \mu \cos(f + 2g - 2h + 2E_1) a_1^3 t_c^2 n_* m_0^4}{8\eta^3 \|r_1\| L_*^6 (2n_1 + 2n_*)} \\
& + \frac{3e\mathcal{G}^4 \mu \cos(3f + 2g - 2h + 2E_1) a_1^3 t_c^2 n_* m_0^4}{8\eta^3 \|r_1\| L_*^6 (2n_1 + 2n_*)} - \frac{3\mathcal{G}^4 \mu \cos(2f + 2g - 2h + E_1) a_1^3 e_1 t_c^2 n_* m_0^4}{16 \|r_1\| L_*^6 (2n_1 + 2n_*)} \\
& - \frac{3\mathcal{G}^4 \mu \cos(2f + 2g - 2h + 3E_1) a_1^3 e_1 t_c^2 n_* m_0^4}{16 \|r_1\| L_*^6 (2n_1 + 2n_*)} - \frac{3e\mathcal{G}^4 \mu \cos(f + 2g - 2h + 2E_1) a_1^3 t_c n_* m_0^4}{4\eta^3 \|r_1\| L_*^6 (2n_1 + 2n_*)} \\
& - \frac{3e\mathcal{G}^4 \mu \cos(3f + 2g - 2h + 2E_1) a_1^3 t_c n_* m_0^4}{4\eta^3 \|r_1\| L_*^6 (2n_1 + 2n_*)} + \frac{3\mathcal{G}^4 \mu \cos(2f + 2g - 2h + E_1) a_1^3 e_1 t_c n_* m_0^4}{8 \|r_1\| L_*^6 (2n_1 + 2n_*)} \\
& + \frac{3\mathcal{G}^4 \mu \cos(2f + 2g - 2h + 3E_1) a_1^3 e_1 t_c n_* m_0^4}{8 \|r_1\| L_*^6 (2n_1 + 2n_*)} + \frac{3e\mathcal{G}^4 \mu \cos(f + 2g - 2h + 2E_1) a_1^3 n_* m_0^4}{8\eta^3 \|r_1\| L_*^6 (2n_1 + 2n_*)} \\
& + \frac{3e\mathcal{G}^4 \mu \cos(3f + 2g - 2h + 2E_1) a_1^3 n_* m_0^4}{8\eta^3 \|r_1\| L_*^6 (2n_1 + 2n_*)} - \frac{3\mathcal{G}^4 \mu \cos(2f + 2g - 2h + E_1) a_1^3 e_1 n_* m_0^4}{16 \|r_1\| L_*^6 (2n_1 + 2n_*)} \\
& - \frac{3\mathcal{G}^4 \mu \cos(2f + 2g - 2h + 3E_1) a_1^3 e_1 n_* m_0^4}{16 \|r_1\| L_*^6 (2n_1 + 2n_*)} - \frac{9e\mathcal{G}^4 \mu \cos(f) a_1^3 t_c^2 m_0^4}{8 \|r_1\| L_*^6} \\
& + \frac{9e\mathcal{G}^4 \mu \cos(f + 2g) a_1^3 t_c^2 m_0^4}{16 \|r_1\| L_*^6} - \frac{3e\mathcal{G}^4 \mu \cos(f + 2g) a_1^3 t_c^2 m_0^4}{8\eta^3 \|r_1\| L_*^6} \\
& + \frac{9e\mathcal{G}^4 \mu \cos(3f + 2g) a_1^3 t_c^2 m_0^4}{16 \|r_1\| L_*^6} - \frac{3e\mathcal{G}^4 \mu \cos(3f + 2g) a_1^3 t_c^2 m_0^4}{8\eta^3 \|r_1\| L_*^6} \\
& + \frac{9e\mathcal{G}^4 \mu \cos(f + 2h - 2E_1) a_1^3 t_c^2 m_0^4}{16 \|r_1\| L_*^6} - \frac{9e\mathcal{G}^4 \mu \cos(f + 2g + 2h - 2E_1) a_1^3 t_c^2 m_0^4}{32 \|r_1\| L_*^6} \\
& - \frac{9e\mathcal{G}^4 \mu \cos(3f + 2g + 2h - 2E_1) a_1^3 t_c^2 m_0^4}{32 \|r_1\| L_*^6} + \frac{9e\mathcal{G}^4 \mu \cos(f - 2h + 2E_1) a_1^3 t_c^2 m_0^4}{16 \|r_1\| L_*^6} \\
& - \frac{9e\mathcal{G}^4 \mu \cos(f + 2g - 2h + 2E_1) a_1^3 t_c^2 m_0^4}{32 \|r_1\| L_*^6} - \frac{9e\mathcal{G}^4 \mu \cos(3f + 2g - 2h + 2E_1) a_1^3 t_c^2 m_0^4}{32 \|r_1\| L_*^6} \\
& - \frac{3\mathcal{G}^4 \mu \cos(2h - 3E_1) a_1^3 e_1 t_c^2 m_0^4}{16 \|r_1\| L_*^6} + \frac{3\mathcal{G}^4 \mu \cos(2f + 2g + 2h - 3E_1) a_1^3 e_1 t_c^2 m_0^4}{32 \|r_1\| L_*^6}
\end{aligned}$$

$$\begin{aligned}
& - \frac{3\mathcal{G}^4 \mu \cos(2f + 2g - E_1) a_1^3 e_1 t_c^2 m_0^4}{8 \|r_1\| L_*^6} - \frac{15\mathcal{G}^4 \mu \cos(2h - E_1) a_1^3 e_1 t_c^2 m_0^4}{16 \|r_1\| L_*^6} \\
& + \frac{15\mathcal{G}^4 \mu \cos(2f + 2g + 2h - E_1) a_1^3 e_1 t_c^2 m_0^4}{32 \|r_1\| L_*^6} + \frac{9\mathcal{G}^4 \mu \cos(E_1) a_1^3 e_1 t_c^2 m_0^4}{8 \|r_1\| L_*^6} \\
& - \frac{3\mathcal{G}^4 \mu \cos(2f + 2g + E_1) a_1^3 e_1 t_c^2 m_0^4}{8 \|r_1\| L_*^6} + \frac{15\mathcal{G}^4 \mu \cos(2f + 2g - 2h + E_1) a_1^3 e_1 t_c^2 m_0^4}{32 \|r_1\| L_*^6} \\
& + \frac{3\mathcal{G}^4 \mu \cos(2f + 2g - 2h + 3E_1) a_1^3 e_1 t_c^2 m_0^4}{32 \|r_1\| L_*^6} - \frac{9e\mathcal{G}^4 \mu \cos(f + 2g + 2h - 2E_1) a_1^3 t_c m_0^4}{16 \|r_1\| L_*^6} \\
& - \frac{9e\mathcal{G}^4 \mu \cos(3f + 2g + 2h - 2E_1) a_1^3 t_c m_0^4}{16 \|r_1\| L_*^6} + \frac{9e\mathcal{G}^4 \mu \cos(f + 2g - 2h + 2E_1) a_1^3 t_c m_0^4}{16 \|r_1\| L_*^6} \\
& + \frac{9e\mathcal{G}^4 \mu \cos(3f + 2g - 2h + 2E_1) a_1^3 t_c m_0^4}{16 \|r_1\| L_*^6} + \frac{3\mathcal{G}^4 \mu \cos(2f + 2g + 2h - 3E_1) a_1^3 e_1 t_c m_0^4}{16 \|r_1\| L_*^6} \\
& + \frac{15\mathcal{G}^4 \mu \cos(2f + 2g + 2h - E_1) a_1^3 e_1 t_c m_0^4}{16 \|r_1\| L_*^6} - \frac{15\mathcal{G}^4 \mu \cos(2f + 2g - 2h + E_1) a_1^3 e_1 t_c m_0^4}{16 \|r_1\| L_*^6} \\
& - \frac{3\mathcal{G}^4 \mu \cos(2f + 2g - 2h + 3E_1) a_1^3 e_1 t_c m_0^4}{16 \|r_1\| L_*^6} + \frac{3e\mathcal{G}^4 \mu \cos(f) a_1^3 m_0^4}{8 \|r_1\| L_*^6} \\
& - \frac{9e\mathcal{G}^4 \mu \cos(f + 2g) a_1^3 m_0^4}{16 \|r_1\| L_*^6} + \frac{3e\mathcal{G}^4 \mu \cos(f + 2g) a_1^3 m_0^4}{8\eta^3 \|r_1\| L_*^6} \\
& - \frac{9e\mathcal{G}^4 \mu \cos(3f + 2g) a_1^3 m_0^4}{16 \|r_1\| L_*^6} + \frac{3e\mathcal{G}^4 \mu \cos(3f + 2g) a_1^3 m_0^4}{8\eta^3 \|r_1\| L_*^6} \\
& - \frac{9e\mathcal{G}^4 \mu \cos(f + 2h - 2E_1) a_1^3 m_0^4}{16 \|r_1\| L_*^6} - \frac{9e\mathcal{G}^4 \mu \cos(f + 2g + 2h - 2E_1) a_1^3 m_0^4}{32 \|r_1\| L_*^6} \\
& - \frac{9e\mathcal{G}^4 \mu \cos(3f + 2g + 2h - 2E_1) a_1^3 m_0^4}{32 \|r_1\| L_*^6} - \frac{9e\mathcal{G}^4 \mu \cos(f - 2h + 2E_1) a_1^3 m_0^4}{16 \|r_1\| L_*^6} \\
& - \frac{9e\mathcal{G}^4 \mu \cos(f + 2g - 2h + 2E_1) a_1^3 m_0^4}{32 \|r_1\| L_*^6} - \frac{9e\mathcal{G}^4 \mu \cos(3f + 2g - 2h + 2E_1) a_1^3 m_0^4}{32 \|r_1\| L_*^6} \\
& + \frac{3\mathcal{G}^4 \mu \cos(2h - 3E_1) a_1^3 e_1 m_0^4}{16 \|r_1\| L_*^6} + \frac{3\mathcal{G}^4 \mu \cos(2f + 2g + 2h - 3E_1) a_1^3 e_1 m_0^4}{32 \|r_1\| L_*^6} \\
& + \frac{3\mathcal{G}^4 \mu \cos(2f + 2g - E_1) a_1^3 e_1 m_0^4}{8 \|r_1\| L_*^6} + \frac{15\mathcal{G}^4 \mu \cos(2h - E_1) a_1^3 e_1 m_0^4}{16 \|r_1\| L_*^6} \\
& + \frac{15\mathcal{G}^4 \mu \cos(2f + 2g + 2h - E_1) a_1^3 e_1 m_0^4}{32 \|r_1\| L_*^6} - \frac{3\mathcal{G}^4 \mu \cos(E_1) a_1^3 e_1 m_0^4}{8 \|r_1\| L_*^6} \\
& + \frac{3\mathcal{G}^4 \mu \cos(2f + 2g + E_1) a_1^3 e_1 m_0^4}{8 \|r_1\| L_*^6} + \frac{15\mathcal{G}^4 \mu \cos(2f + 2g - 2h + E_1) a_1^3 e_1 m_0^4}{32 \|r_1\| L_*^6} \\
& + \frac{3\mathcal{G}^4 \mu \cos(2f + 2g - 2h + 3E_1) a_1^3 e_1 m_0^4}{32 \|r_1\| L_*^6} - \frac{e\mathcal{G}^2 \mu \cos(f) a_1 m_0^2}{\|r_1\| L_*^2} \\
& + \frac{\mathcal{G}^2 \mu \cos(E_1) a_1 e_1 m_0^2}{\|r_1\| L_*^2} + \frac{3\mathcal{G}^2 \delta L^2 \cos(E_1) a_1 e_1 m_0^2}{2 \|r_1\| L_*^4} \Big).
\end{aligned}$$

Next, we move on with the second and last iteration $j = 2$ targeted to $\mathcal{R}_{3,3}^{(1)}$:

$$\mathcal{H}^{(2)} = \mathcal{L}_0 + \mathcal{L}_2^{(1)} + \mathcal{L}_3^{(2)} + \mathcal{R}_{4,4}^{(2)},$$

in which $\chi_3^{(2)}$ is omitted for brevity and

$$\mathcal{L}_3^{(2)} = 0$$

as expected, being $\mathcal{R}_{3,3}^{(1)}$ solely made up of harmonics containing fast angles.



NORMALIZATION ALGORITHM AS PSEUDO-CODE

```
1: function TRIGPOL( $F$ )                                ▶ Write  $F$  as trigonometric polynomial  $\mathcal{F}$ 
2:   return  $\mathcal{F}$ 
3: end function

4: function COEFFICIENT( $F, x, N$ )                      ▶ Extract coefficient  $F_N$  of  $x^N$  from  $F$ 
5:   return  $F_N$ 
6: end function

7: function EXPAND( $F, x, x_0, N$ )                      ▶ Give power expansion  $\mathcal{F}_N$  of  $F$  w.r.t.  $x$ 
8:   return  $\mathcal{F}_N$                                      around  $x_0$  up to  $(x - x_0)^N$ 
9: end function
```

Require: $F = \sum_n(\cdot)\epsilon^n$ as \mathcal{F} in cosines only

```
10: procedure CHI( $F, \epsilon, N, N_1$ )                       ▶ Compute  $\chi_N^{(\cdot)}$  from  $F$  with b.-k.  $\epsilon$ 
11:    $F_{\text{norm}} = F - (F \leftarrow 1/\|r_1\|^l = 0)$           ( $\epsilon^{N_1}$  for  $\phi_1$ )
12:    $F_{\text{norm}} = \text{TRIGPOL}(\text{COEFFICIENT}(F_{\text{norm}}, \epsilon, N)\epsilon^N)$ 
13:    $\chi_N^{(\cdot)} = 0$ 
14:   for  $\mathcal{T} = (\cdot)\|r_1\|^{-\lambda} \in F_{\text{norm}}$  do
15:     if  $\mathcal{T}$  depends explicitly on  $f \vee E_1$  then
16:        $\mathcal{T}_{\chi_N^{(\cdot)}} = \|r_1\|^{1-\lambda} \text{TRIGPOL}(\mathcal{T}\|r_1\|^\lambda/a_1) \leftarrow \cos(\cdot) = \sin(\cdot)/(s_1 n_* + s_4 n_1)$ 
17:     else
18:        $\mathcal{T}_{\chi_N^{(\cdot)}} = \epsilon^{N_1} \phi_1/n_1 \text{TRIGPOL}(\mathcal{T}\|r_1\|^\lambda/a_1) \sum_{l=1}^\lambda a_1^{1-l} \|r_1\|^{l-\lambda}$ 
19:     end if
20:      $\chi_N^{(\cdot)} \leftarrow \chi_N^{(\cdot)} + \mathcal{T}_{\chi_N^{(\cdot)}}$ 
21:   end for
22:   return  $\chi_N^{(\cdot)}$ 
23: end procedure
```

Require: $F_1, F_2 = \sum_n(\cdot)\epsilon^n$

24: **procedure** POISSON($F_1, F_2, \epsilon, \tau, N_1$) ▷ Compute $\{F_1, F_2\}$ up to ϵ^τ terms
 25: $\mathcal{E}_1 = \{n : F_1 = \sum_n(\cdot)\epsilon^n, (\cdot) \neq 0\}$
 26: $\mathcal{E}_2 = \{n : F_2 = \sum_n(\cdot)\epsilon^n, (\cdot) \neq 0\}$
 27: **for** $j_1 \in \mathcal{E}_1$ **do**
 28: **for** $j_2 \in \mathcal{E}_2$ & $j_2 \leq \tau - j_1$ **do**
 29: $\{F_1, F_2\} = 0$
 30: $F_{1_{j_1}} = \text{COEFFICIENT}(F_1, \epsilon, j_1)$
 31: $F_{2_{j_2}} = \text{COEFFICIENT}(F_2, \epsilon, j_2)$
 32: Compute $\{F_{1_{j_1}} \epsilon^{j_1}, F_{2_{j_2}} \epsilon^{j_2}\}$ by BK and $1/\|r_1\|$ dep. eqns. in §3.2.3
 33: $\{F_1, F_2\} \leftarrow \{F_1, F_2\} + \{F_{1_{j_1}} \epsilon^{j_1}, F_{2_{j_2}} \epsilon^{j_2}\}$
 34: **end for**
 35: **end for**
 36: **for all** $n > \tau$ **do**
 37: $\{F_1, F_2\} \leftarrow (\cdot)\epsilon^n = 0$
 38: **end for**
 39: $\{F_1, F_2\} = \text{TRIGPOL}(\{F_1, F_2\})$
 40: **return** $\{F_1, F_2\}$
 41: **end procedure**

Require: $F_1, F_2 = \sum_n(\cdot)\epsilon^n$

42: **procedure** EXPLIE($F_1, F_2, \epsilon, \tau, N_1$) ▷ Compute $\exp(\mathcal{L}_{F_2}) F_1$ up to ϵ^τ terms
 43: $\{F_1, F_2\} = \text{POISSON}(F_1, F_2, \epsilon, \tau, N_1)$
 44: $\exp(\mathcal{L}_{F_2}) F_1 = F_1 + \{F_1, F_2\}$
 45: **for** $j \leftarrow 2$ to τ **do**
 46: $\{F_1, F_2\} = \text{POISSON}(\{F_1, F_2\}, F_2 \leftarrow \phi_1 = e_1 \sin E_1, \epsilon, \tau, N_1)/j$
 47: $\exp(\mathcal{L}_{F_2}) F_1 = \exp(\mathcal{L}_{F_2}) F_1 + \{F_1, F_2\}$
 48: $j \leftarrow j + 1$
 49: **end for**
 50: **for all** $n > \tau$ **do**
 51: $\exp(\mathcal{L}_{F_2}) F_1 \leftarrow (\cdot)\epsilon^n = 0$
 52: **end for**
 53: $\exp(\mathcal{L}_{F_2}) F_1 = \text{TRIGPOL}(\exp(\mathcal{L}_{F_2}) F_1)$
 54: **return** $\exp(\mathcal{L}_{F_2}) F_1$
 55: **end procedure**

Require: $\mu < 1$; $n_1, a_1 > 0, \mathcal{G}m_0 > 0$; $a_* > 0$; $e_* \in]0, 1[$, $e_1 \in [0, 1[$, $e_* < 1 - a_1(1 + e_1)/a_*$; $k_\mu > 1$; $k_{\text{mp}} \geq 1$

56: **procedure** METHODR3BP($\mu, n_1, a_1, e_1, \mathcal{G}m_0, a_*, e_*, k_\mu, k_{\text{mp}}$) ▷ Main routine
 57: $\mathcal{H} \leftarrow \rho \|r_1\| / \|R\|, \rho r_1 \cdot R / \|R\|^2, \mu\sigma$ from Equation (3.9)
 58: $\mathcal{H} = \text{EXPAND}(\text{EXPAND}(\mathcal{H}, \rho, 0, k_{\text{mp}}), \sigma, 0, k_\mu)$
 59: $v = \lceil \log_{10} \mu / \log_{10} e_* \rceil, v_1 = \lceil \log_{10} e_1 / \log_{10} e_* \rceil$
 60: $\mathcal{H} \leftarrow \rho = 1, \sigma = \sigma^v$
 61: $\mathcal{H} \leftarrow$ Eqs. (3.14), (3.15), (3.16), $e = e\sigma, e_1 = e_1\sigma^{v_1}, \sqrt{1 - e_l^2} = \eta_l, l = -, 1$
 62: $\mathcal{H} \leftarrow a = (L_* + \delta L \sigma^v)^2 / (\mathcal{G}m_0)$

```

63:   $\mathcal{H} = \text{EXPAND}(\mathcal{H}, \delta L, 0, k_\mu)$  and Poisson structure in §3.2.3
64:   $\mathcal{H}_0 \leftarrow \sigma = \sigma^{-\nu}$ 
65:   $\mathcal{H} \leftarrow -(\mathcal{G}m_0)^2/(2L_*^2) = 0, (\mathcal{G}m_0)^2/L_*^3 = n_*$ 
66:   $\mathcal{L}_0 = n_*\delta L + n_1 J_1$ 
67:   $\mathcal{H} = \text{TRIGPOL}((\mathcal{H} - \mathcal{L}_0)a_1(1 - \sigma^{\nu_1}e_1 \cos E_1)/\|r_1\| + \mathcal{L}_0)$ 
68:  for all  $n > \nu k_\mu$  do
69:     $\mathcal{H} \leftarrow (\cdot)\sigma^n = 0$ 
70:  end for
71:   $\mathcal{H}^{(0)} = \mathcal{H}$ 
72:  if  $\nu \neq 1$  then
73:     $\mathcal{J} = \{1, \dots, \nu(k_\mu - 1)\}$ 
74:  else
75:     $\mathcal{J} = \{1, 2, \text{II}, 3, \dots, \nu(k_\mu - 1)\}$ 
76:  end if
77:  for  $j \in \mathcal{J}$  do
78:     $\chi_{\nu+j-1}^{(j)} = \text{CHI}(\mathcal{H}^{(j-1)}, \sigma, \nu + j - 1, \nu_1)$ 
79:     $\mathcal{H}^{(j)} = \text{EXPLIE}(\mathcal{H}^{(j-1)}, \chi_{\nu+j-1}^{(j)}, \sigma, \nu k_\mu - 1 + \nu_1, \nu_1) \leftarrow \phi_1 = e_1 \sin E_1$ 
80:     $\mathcal{H}^{(j)} = \text{TRIGPOL}(\mathcal{H}^{(j)})$ 
81:     $j \leftarrow j + 1$ 
82:  end for
83:  return  $\mathcal{H}^{(\nu(k_\mu-1))}$ 
84: end procedure

```

BIBLIOGRAPHY

- [1] NASA - National Aeronautics and Space Administration. *Planetary Fact Sheet - the NSSDCA - NASA*. URL: <https://nssdc.gsfc.nasa.gov/planetary/factsheet/>.
- [2] R.F. Arenstorf. "Regularization theory for the elliptic restricted three body problem". In: *Journal of Differential Equations* 6.3 (1969), pp. 420–451.
- [3] V. I. Arnol'd. "A theorem of Liouville concerning integrable problems of dynamics". In: *Sibirskii Matematicheskii Zhurnal* 4.2 (1963), pp. 471–474.
- [4] V. I. Arnol'd. "Instability of dynamical systems with several degrees of freedom". In: *Hamiltonian Dynamical Systems*. CRC Press, 2020, pp. 633–637.
- [5] V. I. Arnold. "Proof of a theorem of AN Kolmogorov on the invariance of quasi-periodic motions under small perturbations of the Hamiltonian". In: *Russ. Math. Surv* 18.5 (1963), pp. 9–36.
- [6] J. Banks et al. "On Devaney's definition of chaos". In: *The American mathematical monthly* 99.4 (1992), pp. 332–334.
- [7] G. Benettin et al. "Lyapunov characteristic exponents for smooth dynamical systems and for Hamiltonian systems; a method for computing all of them. Part 1: Theory". In: *Meccanica* 15.1 (1980), pp. 9–20.
- [8] G. D. Birkhoff. "The restricted problem of three bodies". In: *Rendiconti del Circolo Matematico di Palermo (1884-1940)* 39.1 (1915), p. 265.
- [9] F. Cardin and M. Guzzo. "Integrability of close encounters in the spatial restricted three-body problem". In: *Communications in Contemporary Mathematics* 24.06 (2022), p. 2150040.
- [10] A. Carusi, L. Kresák, and G. B. Valsecchi. "Conservation of the Tisserand parameter at close encounters of interplanetary objects with Jupiter". In: *Earth, Moon, and Planets* 68.1 (1995), pp. 71–94.

- [11] I. Cavallari and C. Efthymiopoulos. "Closed-form perturbation theory in the restricted three-body problem without relegation". In: *Celestial Mechanics and Dynamical Astronomy* 134.2 (2022), pp. 1–36.
- [12] M. Ceccaroni, F. Biscani, and J. Biggs. "Analytical method for perturbed frozen orbit around an asteroid in highly inhomogeneous gravitational fields: a first approach". In: *Solar System Research* 48.1 (2014), pp. 33–47.
- [13] A. Celletti. *Stability and chaos in celestial mechanics*. Springer Science & Business Media, 2010.
- [14] IAU - Minor Planet Center. *List of Jupiter Trojans*. URL: <https://minor-planetcenter.net//iau/lists/JupiterTrojans.html>.
- [15] B. V. Chirikov. "A universal instability of many-dimensional oscillator systems". In: *Physics reports* 52.5 (1979), pp. 263–379.
- [16] B. V. Chirikov. *Research concerning the theory of non-linear resonance and stochasticity*. Tech. rep. CM-P00100691, 1971.
- [17] E. A. Coddington and N. Levinson. *Theory of ordinary differential equations*. Tata McGraw-Hill Education, 1955.
- [18] C. C. Conley. "Low energy transit orbits in the restricted three-body problems". In: *SIAM Journal on Applied Mathematics* 16.4 (1968), pp. 732–746.
- [19] J. M. Cors, C. Pinyol, and J. Soler. "Periodic solutions in the spatial elliptic restricted three-body problem". In: *Physica D: Nonlinear Phenomena* 154.3-4 (2001), pp. 195–206.
- [20] J. M. A. Danby. "Fundamentals of celestial mechanics, /Willmann-Bell, 1988". In: *The Observatory* 109 (1989), p. 211.
- [21] J. M. A. Danby. "Stability of the triangular points in the elliptic restricted problem of three bodies". In: *The Astronomical Journal* 69 (1964), p. 165.
- [22] J. B. Delisle, A. C. M. Correia, and J. Laskar. "Stability of resonant configurations during the migration of planets and constraints on disk-planet interactions". In: *Astronomy & Astrophysics* 579 (2015), A128.
- [23] A. Deprit. "Canonical transformations depending on a small parameter". In: *Celestial mechanics* 1.1 (1969), pp. 12–30.
- [24] A. Deprit, J. F. Palacián, and E. Deprit. "The relegation algorithm". In: *Celestial Mechanics and Dynamical Astronomy* 79.3 (2001), pp. 157–182.
- [25] R. Dvorak and R. Schwarz. "On the stability regions of the Trojan asteroids". In: *Celestial Mechanics and Dynamical Astronomy* 92.1 (2005), pp. 19–28.
- [26] C. Efthymiopoulos. "Canonical perturbation theory; stability and diffusion in Hamiltonian systems: applications in dynamical astronomy". In: *Workshop series of the Asociación Argentina de Astronomía*. Vol. 3. 2011, pp. 3–146.

- [27] C. Efthymiopoulos and Z. Sándor. “Optimized Nekhoroshev stability estimates for the Trojan asteroids with a symplectic mapping model of co-orbital motion”. In: *Monthly Notices of the Royal Astronomical Society* 364.1 (2005), pp. 253–271.
- [28] S. R. Finch. *Mathematical constants*. Cambridge university press, 2003.
- [29] G. Floquet. “Sur les équations différentielles linéaires à coefficients périodiques”. In: *Annales scientifiques de l’École normale supérieure*. Vol. 12. 1883, pp. 47–88.
- [30] C. Froeschlé, E. Lega, and R. Gonczi. “Fast Lyapunov indicators. Application to asteroidal motion”. In: *Celestial Mechanics and Dynamical Astronomy* 67.1 (1997), pp. 41–62.
- [31] F. Gabern, A. Jorba, and U. Locatelli. “On the construction of the Kolmogorov normal form for the Trojan asteroids”. In: *Nonlinearity* 18.4 (2005), p. 1705.
- [32] A. Giorgilli. *Notes on Hamiltonian Dynamical Systems*. Vol. 102. Cambridge University Press, 2022.
- [33] A. Giorgilli and C. Skokos. “On the stability of the Trojan asteroids.” In: *Astronomy and Astrophysics* 317 (1997), pp. 254–261.
- [34] B. Gladman. “Dynamics of systems of two close planets”. In: *Icarus* 106.1 (1993), pp. 247–263.
- [35] R. Gomes et al. “Origin of the cataclysmic Late Heavy Bombardment period of the terrestrial planets”. In: *Nature* 435.7041 (2005), pp. 466–469.
- [36] G. Gómez. *Dynamics and mission design near libration points: fundamentals—the case of collinear libration points*. Vol. 1. World Scientific, 2001.
- [37] W. Gröbner. *Die Lie-reihen und ihre Anwendungen*. Vol. 3. Deutscher Verlag der Wissenschaften, 1967.
- [38] G. F. Gronchi and A. Milani. “Proper elements for Earth-crossing asteroids”. In: *Icarus* 152.1 (2001), pp. 58–69.
- [39] G. F. Gronchi and C. Tardioli. “The evolution of the orbit distance in the double averaged restricted 3-body problem with crossing singularities”. In: *arXiv preprint arXiv:1206.2584* (2012).
- [40] M. Guzzo and E. Lega. “A study of the past dynamics of comet 67P/Churyumov-Gerasimenko with fast Lyapunov indicators”. In: *Astronomy & Astrophysics* 579 (2015), A79.
- [41] M. Guzzo and E. Lega. “Evolution of the tangent vectors and localization of the stable and unstable manifolds of hyperbolic orbits by Fast Lyapunov Indicators”. In: *SIAM Journal on Applied Mathematics* 74.4 (2014), pp. 1058–1086.
- [42] M. Guzzo and E. Lega. “Scenarios for the dynamics of comet 67P/Churyumov–Gerasimenko over the past 500 kyr”. In: *Monthly Notices of the Royal Astronomical Society* 469.Suppl_2 (2017), S321–S328.

- [43] M. Guzzo, E. Lega, and C. Froeschlé. "On the numerical detection of the effective stability of chaotic motions in quasi-integrable systems". In: *Physica D: Nonlinear Phenomena* 163.1-2 (2002), pp. 1–25.
- [44] J. Henrard and A. Lemaître. "A second fundamental model for resonance". In: *Celestial mechanics* 30.2 (1983), pp. 197–218.
- [45] G. Hori. "Theory of general perturbation with unspecified canonical variable". In: *Publications of the Astronomical Society of Japan* 18 (1966), p. 287.
- [46] X. Hou, D. J. Scheeres, and L. Liu. "Dynamics of the Jupiter Trojans with Saturn's perturbation in the present configuration of the two planets". In: *Celestial Mechanics and Dynamical Astronomy* 119.2 (2014), pp. 119–142.
- [47] X. Hou, D. J. Scheeres, and L. Liu. "Dynamics of the Jupiter Trojans with Saturn's perturbation when the two planets are in migration". In: *Celestial Mechanics and Dynamical Astronomy* 125.4 (2016), pp. 451–484.
- [48] A. Hurwitz. "Über die Zahlentheorie der Quaternionen". In: *Math. Werke* 2 (1933), pp. 303–330.
- [49] R. Jost. "Winkel- und Wirkungsvariable für allgemeine mechanische Systeme". In: *Helvetica Physica Acta* 41.6-7 (1968), pp. 965–968.
- [50] A. N. Kolmogorov. "On preservation of conditionally periodic motions under small variations of the Hamiltonian function". In: *Dokl. Akad. Nauk SSSR*. Vol. 98. 4. 1954, pp. 527–530.
- [51] P. Kustaanheimo. "Spinor regularisation of the Kepler motion". In: *Annales Universitatis Turkuensis A* 73, 1-7 73 (1964), pp. 1–7.
- [52] P. Kustaanheimo and E. L. Stiefel. "Perturbation theory of Kepler motion based on spinor regularization". In: *J. für die Reine und Angewandte Mathematik* 218 (1965), pp. 204-219–569.
- [53] M. Lara, J. F. San Juan, and L. M. López-Ochoa. "Averaging tesseral effects: closed form relegation versus expansions of elliptic motion". In: *Mathematical Problems in Engineering* 2013 (2013).
- [54] M. Lara et al. "Analytical theory for spacecraft motion about Mercury". In: *Acta Astronautica* 66.7-8 (2010), pp. 1022–1038.
- [55] J. Laskar and A. C. Petit. "AMD-stability and the classification of planetary systems". In: *Astronomy & Astrophysics* 605 (2017), A72.
- [56] E. Lega, M. Guzzo, and C. Froeschlé. "Theory and applications of the Fast Lyapunov Indicator (FLI) method". In: *Chaos Detection and Predictability*. Springer, 2016, pp. 35–54.
- [57] T. Levi-Civita. "Sur la régularisation qualitative du problème restreint des trois corps". In: *Acta Math.* 30 (1906), pp. 305–327.
- [58] H. F. Levison, E. M. Shoemaker, and C. S. Shoemaker. "Dynamical evolution of Jupiter's Trojan asteroids". In: *Nature* 385.6611 (1997), pp. 42–44.

- [59] H. F. Levison, E. M. Shoemaker, and C. S. Shoemaker. "The long-term dynamical stability of Jupiter's Trojan asteroids". In: *Nature* 385.42-44 (1997), p. 223.
- [60] A. J. Lichtenberg and M. A. Leiberman. "Applied mathematical sciences". In: *Regular and Chaotic Dynamics, 2nd ed.* (Springer-Verlag, New York, NY, 1992) 38 (1992), p. 49.
- [61] H. A. Luther. "An explicit sixth-order Runge-Kutta formula". In: *Mathematics of Computation* 22.102 (1968), pp. 434–436.
- [62] B. Mahajan, S. R. Vadali, and K. T. Alfriend. "Exact Delaunay normalization of the perturbed Keplerian Hamiltonian with tesseral harmonics". In: *Celestial Mechanics and Dynamical Astronomy* 130.3 (2018), pp. 1–25.
- [63] S. Marò and G. F. Gronchi. "Long term dynamics for the restricted N-body problem with mean motion resonances and crossing singularities". In: *SIAM Journal on Applied Dynamical Systems* 17.2 (2018), pp. 1786–1815.
- [64] J. Marsden and A. Weinstein. "Reduction of symplectic manifolds with symmetry". In: *Reports on mathematical physics* 5.1 (1974), pp. 121–130.
- [65] F. Marzari et al. "Origin and evolution of Trojan asteroids". In: *Asteroids III* 1 (2002), pp. 725–738.
- [66] K. R. Meyer. *Periodic solutions of the N-body problem*. Vol. 1719. Springer Science & Business Media, 1999.
- [67] K. R. Meyer. "Symmetries and integrals in mechanics". In: *Dynamical systems*. Elsevier, 1973, pp. 259–272.
- [68] A. Milani. "The Trojan asteroid belt: proper elements, stability, chaos and families". In: *Celestial Mechanics and Dynamical Astronomy* 57.1 (1993), pp. 59–94.
- [69] A. Morbidelli. *Modern celestial mechanics: aspects of solar system dynamics*. 2002.
- [70] A. Morbidelli et al. "Chaotic capture of Jupiter's Trojan asteroids in the early Solar System". In: *Nature* 435.7041 (2005), pp. 462–465.
- [71] J. Moser. "Dynamical Systems, past and present". In: *Proc. Int. Congress of Math.* Vol. 1. 1998, pp. 381–402.
- [72] J. Moser. "On invariant curves of area-preserving mappings of an annulus". In: *Nachr. Akad. Wiss. Göttingen, II* (1962), pp. 1–20.
- [73] C. D. Murray and S. F. Dermott. *Solar system dynamics*. Cambridge university press, 1999.
- [74] N. N. Nekhoroshev. "An exponential estimate of the time of stability of nearly-integrable Hamiltonian systems". In: *Russian Mathematical Surveys* 32.6 (1977), p. 1.
- [75] D. Nesvorný, D. Vokrouhlický, and A. Morbidelli. "Capture of Trojans by jumping Jupiter". In: *The Astrophysical Journal* 768.1 (2013), p. 45.

- [76] R. I. Paez and M. Guzzo. “Transits close to the Lagrangian solutions L_1 , L_2 in the elliptic restricted three-body problem”. In: *Nonlinearity* 34.9 (2021), p. 6417.
- [77] P. Painlevé. *Leçons sur la théorie analytique des équations différentielles, Professées à Stockholm, 1895*. Librairie Scientifique A. Hermann et Fils, 1897.
- [78] J. F. Palacián. “Normal forms for perturbed Keplerian systems”. In: *Journal of Differential Equations* 180.2 (2002), pp. 471–519.
- [79] J. F. Palacián. “Teoría del satélite artificial: armónicos teserales y su relegación mediante simplificaciones algebraicas”. PhD thesis. Universidad de Zaragoza, 1992.
- [80] J. F. Palacián, J. Vanegas, and P. Yanguas. “Compact normalisations in the elliptic restricted three body problem”. In: *Astrophysics and Space Science* 362 (2017), pp. 1–17.
- [81] J. F. Palacián and P. Yanguas. “From the circular to the spatial elliptic restricted three-body problem”. In: *Celestial Mechanics and Dynamical Astronomy* 95 (2006), pp. 81–99.
- [82] J. F. Palacián et al. “Searching for periodic orbits of the spatial elliptic restricted three-body problem by double averaging”. In: *Physica D: Nonlinear Phenomena* 213.1 (2006), pp. 15–24.
- [83] L. Perko. *Differential equations and dynamical systems*. Vol. 7. Springer Science & Business Media, 2013.
- [84] A. C. Petit, J. Laskar, and G. Boué. “AMD-stability in the presence of first-order mean motion resonances”. In: *Astronomy & Astrophysics* 607 (2017), A35.
- [85] A. C. Petit, J. Laskar, and G. Boué. “Hill stability in the AMD framework”. In: *Astronomy & Astrophysics* 617 (2018), A93.
- [86] H. Poincaré. *Les méthodes nouvelles de la mécanique céleste: Méthodes de MM. Newcomb, Gyldén, Linstadt et Bohlin*. Vol. 2. Gauthier-Villars et fils, imprimeurs-libraires, 1893.
- [87] X. S. Ramos, J. A. Correa-Otto, and C. Beauge. “The resonance overlap and Hill stability criteria revisited”. In: *Celestial Mechanics and Dynamical Astronomy* 123.4 (2015), pp. 453–479.
- [88] P. Robutel and F. Gabern. “The resonant structure of Jupiter’s Trojan asteroids–I. Long-term stability and diffusion”. In: *Monthly Notices of the Royal Astronomical Society* 372.4 (2006), pp. 1463–1482.
- [89] M. Rossi and C. Efthymiopoulos. “Characterization of the stability for trajectories exterior to Jupiter in the restricted three-body problem via closed-form perturbation theory”. In: *Proceedings of the International Astronomical Union* 15.S364 (2021), pp. 232–238.
- [90] M. Rossi and C. Efthymiopoulos. “Manifolds in the Solar System: an application to the L_4/L_5 asymmetry of Trojan asteroids”. In: *N.A.* In preparation (2023).

- [91] M. Rossi and C. Efthymiopoulos. “Relegation-free closed-form perturbation theory and the domain of secular motions in the Restricted 3-Body Problem”. In: *arXiv preprint arXiv:2301.03070* (2023).
- [92] M. Rossi and M. Guzzo. “A Hamiltonian revisitation of the Kustaanheimo-Stiefel regularization of the elliptic restricted three-body problem”. In: *arXiv preprint arXiv:2206.07022* (2022).
- [93] D. G. Saari. “A global existence theorem for the four-body problem of Newtonian mechanics”. In: *Journal of Differential Equations* 26.1 (1977), pp. 80–111.
- [94] M. Sansottera and M. Ceccaroni. “Rigorous estimates for the relegation algorithm”. In: *Celestial Mechanics and Dynamical Astronomy* 127.1 (2017), pp. 1–18.
- [95] W. Scheibner. “Satz aus der Störungstheorie. (Auszug aus einem Schreiben an den Herausgeber).” In: *N.A.* (1866).
- [96] A. M. Segerman and S. L. Coffey. “An analytical theory for tesseral gravitational harmonics”. In: *Celestial Mechanics and Dynamical Astronomy* 76.3 (2000), pp. 139–156.
- [97] I. G. Slyusarev. “Asymmetry between the L4 and L5 swarms of Jupiter Trojans”. In: *44th Annual Lunar and Planetary Science Conference*. 1719. 2013, p. 2223.
- [98] E. Stiefel et al. *Methods of regularization for computing orbits in Celestial Mechanics*. Vol. 769. National Aeronautics and Space Administration, 1967.
- [99] V. Szebehely. *Theory of orbits: the restricted problem of three bodies*. Tech. rep. Yale univ. New Haven CT, 1967.
- [100] V. Szebehely and G. E. O. Giacaglia. “On the elliptic restricted problem of three bodies”. In: *The Astronomical Journal* 69 (1964), p. 230.
- [101] N. Todorović, D. Wu, and A. J. Rosengren. “The arches of chaos in the Solar System”. In: *Science advances* 6.48 (2020), eabd1313.
- [102] K. Tsiganis, H. Varvoglis, and R. Dvorak. “Chaotic diffusion and effective stability of Jupiter Trojans”. In: *Celestial Mechanics and Dynamical Astronomy* 92.1 (2005), pp. 71–87.
- [103] K. Tsiganis et al. “Origin of the orbital architecture of the giant planets of the Solar System”. In: *Nature* 435.7041 (2005), pp. 459–461.
- [104] J. Waldvogel. “Die Verallgemeinerung der Birkhoff-regularisierung für das räumliche Dreikörperproblem”. PhD thesis. ETH Zurich, 1966.
- [105] J. Wisdom. “The resonance overlap criterion and the onset of stochastic behavior in the restricted three-body problem”. In: *The Astronomical Journal* 85 (1980), pp. 1122–1133.
- [106] Z. Xia. “The existence of noncollision singularities in the n-body problem”. In: *Annals of Mathematics* 135.3 (1992), pp. 411–468.

- [107] J. Xue. "Non-collision singularities in a planar 4-body problem". In: *Acta Mathematica* 224.2 (2020), pp. 253–388.
- [108] H. von Zeipel. *Sur les singularités du probleme des n corps*. Almqvist & Wiksell, 1908.
- [109] L. Zhao. "Kustaanheimo-Stiefel regularization and the quadrupolar conjugacy". In: *Regular and Chaotic Dynamics* 20.1 (2015), pp. 19–36.

ACKNOWLEDGEMENTS

It is very hard for me to put into words my gratitude to the people who have left their mark on this journey, because all of them, whatever the way and the context, have truly made the difference.

How could I not begin with my dear ones? No good can come without sacrifice, true. But the role of luck in life achievements is far greater than we usually want to admit, and my family is definitely part of it. My thankfulness for their unconditional support, for their quiet and constant acting “behind the scenes”, will never be enough.

A very special thank goes to my supervisor, Prof. Christos Efthymiopoulos. His scientific enthusiasm, his brilliance, his big-picture vision and his countless teachings have been pure gold to me, a source of inspiration and passion that I will treasure forever. Equally importantly, I still feel flattered that he believed in me at the very beginning of this path, in a moment of uncertainty in which I first doubted myself. Finally, besides his guidance during my Ph.D. work, I would like to thank him as a friend, for the good (and also less good) times spent together. His personality with “non-zero eccentricity” (I am being nerdy, I know) was certainly a cure against boredom.

There are many other people wandering around the “Torre Archimede” building to whom I would like to express deep gratitude: among all, my former advisor, Prof. Massimiliano Guzzo, for having kept active the scientific collaboration started at the end of my Master’s Degree, for his wise pieces of advice and his valuable contribution to this accomplishment; the Coordinator of the Ph.D. Program, Prof. Giovanni Colombo, for his commendable efforts in making the Doctoral School in Mathematics a more enjoyable experience for everyone; Prof. Carlo Mariconda, for having nurtured my interest in teaching by introducing me to the fascinating world of the educational innovation; the whole technical and administration staff of the Department, particularly the Secretary of the Ph.D. Course Mrs. Loretta Dalla Costa and Mrs. Marinella Boischio, who were often a safe shelter from the bureaucratic storm.

I would also like to thank the referees of my thesis, Prof. Elena Lega and Prof. Jesús Francisco Palacián, for their careful reading of the manuscript with constructive comments.

I am thankful to Prof. Kleomenis Tsiganis, Prof. George Voyatzis and Dr. Ioannis Gkolias for having welcomed me in their research group during

my stay in Thessaloniki (about which I acknowledge the “Fondazione Aldo Gini” for the financial aid). In particular, I am grateful to Prof. Tsiganis for the interesting discussions and his precious suggestions regarding the future developments of the present work. Thanks to Ioannis and Michalis also for their amazing hospitality and the excellent crash course in Greek (especially culinary) culture.

I warmly thank all my past and present colleagues of the 7th floor, for the friendly environment, the fun, the chats, the mutual help. In particular, thanks to Luca, Daniele, Piero and Ofelia for having put up with me in stressful moments. And I cannot forget Rita, partners in crime in this adventure, with whom I shared a lot of joys and sorrows.

Many thanks go to my friends outside the academia, because, like extras in a movie, they deserve credit too. I want to mention two of the closest ones: my mountain buddy, “compare” Eddy, and my eternal teammate, “36 sul campo” Roberto.

Last, but not least, I would like to thank one of the people I care about the most, Valentina, whose support and truths, though often uncomfortable, have been my compass in difficult times.